A Network Informed Identification of Novel Effectors of Synaptic Function

Thesis submitted in accordance with the requirements of the University of Liverpool for the degree of Doctor in Philosophy by

Bronwyn Dawson

January 2017

Acknowledgements

Firstly I would like to thank Prof. Chris Sanderson for his support and guidance throughout my PhD. I would also like to thank Dr. Jeff Barclay and the rest of red block (particularly Paul Todd) for all of their help with the worm experiments.
I would also like to thank the Wellcome Trust for funding this project.

To everyone in the Sanderson lab, thanks for making my PhD an enjoyable experience! Amy, Dave, Emily, Hanna, Jen, Joanna and Jonathan, you saved me from insanity at times. Special thanks goes to Jen, who was always there to have a gossip and solve our lab/non-lab problems, as well as give me awesome cooking tips ☺

Outside of the lab, I would like to thank Dayani, Paul, Jen and also Helen, for the fun of BiotechYes. It was such a great experience (despite staying up until 5am making presentation changes!), and I'll never forget it.

Thanks to my family, who have always supported me doing a PhD, even when I moaned about it. Especially to my eldest sister, Gwyneth, who was taken away from us far too soon, and who made me the person I am today. Last of all, a huge thanks to Dave, who came along during my PhD, and everything has been better since that first meeting. He saved me from becoming a crazy lab monster on so many occasions, and was/is always willing to eat my stress relieving bakes. Without him, I may have finished the PhD, but I'd have been far unhappier than I am today.

Contents

Abstract

Neuronal function is a highly complex process, and model organisms are required to elucidate novel pathway components that may play a role in neurological disease. High-throughput targeted RNAi screens were performed on worm strains sensitive to neuronal RNAi, in order to assess the functional consequences of changing gene expression on synaptic function, as assessed by the relative changes in sensitivity to the acetylcholinesterase inhibitor aldicarb. A one-step binary aldicarb-sensitivity protein interaction network was constructed, using all genes with a known aldicarb sensitivity phenotype as core nodes. Connectivity and betweenness to genes known to cause a change in aldicarb sensitivity was measured. 19 genes highly connected and 17 high betweenness genes displayed a change in aldicarb sensitivity, with 8 having both high betweenness and connectivity.

Previous microarray studies on the effects of sodium valproate were carried out on wild type worms (Munasinghe, 2015), and suggested that valproate could conditionally influence synaptic function at neuromuscular junctions. To investigate this relationship further genes that exhibited dose dependent changes in gene expression were identified and clustered within the one-step aldicarb betweenness network using a module prediction algorithm. Proteins within functional modules that were not previously known to exhibit aldicarb sensitivity were systematically screened, and 16 genes were shown to cause a significant change in the rate of aldicarb-induced paralysis, including sel-12 and dhhc-2, a palmitoyl-acyl transferase.

Abstract

Data from valproate dose response microarrays were re-analyzed and DAVID, Ingenuity and WebGestalt analyses were performed on the subset of genes showing valproate-induced changes in gene expression. Several known disease associations were identified, including Alzheimer's disease, epilepsy and Huntington's disease. Microarray data from other available valproate sensitivity studies were also analyzed, and the overlap in genes with the worm micro array dataset was assessed. This analysis suggests that changes in neuronal development and differentiation, Wnt signaling and cholinergic transmission may all be functionally affected by exposure to valproate.

Dhhc-2 is a member of the palmitoyl-acyl transferase family, and the rest of the family was systematically tested using aldicarb-sensitivity assays. The *dhhc-13* mutant was shown to cause hypersensitivity and the *dhhc-14* showed resistance to aldicarb, suggesting mechanisms of reciprocal conditional regulation. Hypersensitivity to aldicarb was also observed when dhhc-1 and dhhc-5 were knocked down, while *dhhc-3, -11,* and *spe-10* genetic knockdown led to resistance. The *dhhc-2* mutant and RNAi knockdown both caused enhanced paralysis when treated with 15mM valproate, suggesting a functional effect of the drug at neuromuscular junctions. A selection of human PATs were analyzed in the Y2H library screens using cytoplasmic domains of DHHC5, 5, 13 and 17. DHHC5CT, 17N and 13N revealed 11, 13 and 11 interaction partners, respectively. Membrane based Y2H library screening was also carried out, and 17 novel interaction partners of full length DHHC9 were identified, including reticulin and selenoprotein K. These screens revealed interesting novel interaction partners, which could provide new insights into the mechanisms by which PAT family members may differentially affect neuromuscular function.

Abbreviations

Aβ: Amyloid beta

ABE: Acyl-biotinyl exchange

ACh: Acetylcholine

ACOT: acyl-coA thioesterases

AD: Activation domain

AMPAR: Alpha-amino-3-hydroxy-5-methyl-4-isoxalonepropionic acid receptor

ANCL: Adult neuronal ceroid lipofuscinosis

APC: Anaphase Promoting Complex

APP: Amyloid Precursor Protein

APT: Acyl-protein thioesterases

BAAT: Bile acid CoA: amino acid N-acyltransferase

BACE2: Beta-site amyloid precursor protein-cleaving enzyme

CAMKII: Calmodulin-dependent kinase II

CDKL5: Cyclin-dependent kinase-like 5

CGC: *Caenorhabditis* genetics center

CMT2B: Charcot-Marie-Tooth disease, type 2B

CNS: Central Nervous System

CREB: C-AMP response element-binding protein

CRISPR: Clustered regularly interspaced short palindromic repeats

CSPα: Cysteine String Protein alpha

DAVID: Database for Annotation, Visualization and Integrated Discovery

DISC1: Disrupted-In-Schizophrenia-1

DB: DNA binding domain

Abbreviations

EEF1A: Elongation factor 1A

EMS: Ethyl Methyl Sulfonate

ER: Endoplasmic reticulum

ERAD: ER associated degradation

Erf2p: Effector of Ras Function 2p

FLP: FMRFamide-related peptide

FOXO: Forkhead Box O

GABA: Gamma-amino-butryic acid

GAD65: Glutamate decarboxylase

GAP-43: Growth Associated Protein 43

GO: Gene Ontology

GSEA: Gene set enrichment analysis

HDAC: Histone Deacetylase

HIC: Hypersensitivity to Inhibitors of Cholinesterase

HIP14: Huntingtin Interacting Protein 14

HIP14L: HIP14-like

HSP: Hereditary spastic paraplegia

HTT: Huntingtin

INP: Insulin-related Peptide

IPTG: Isopropyl beta-d-1-thiogalactopyranoside

KEGG: Kyoto Encyclopedia of Genes and Genomes

LAT: Linker for activation of T cells

LONP1: Lon peptidase 1

MAPK: Mitogen-activated protein kinase

MYTH: Membrane-based yeast two-hybrid

Abbreviations

NIBA: Neurodegeneration with associated brain ion accumulation

NGM: Nematode Growth Medium

NLP: Neuropeptide-like protein

NMDAR: N-methyl-D-aspartate receptor

NMJ: Neuromuscular junction

NRTK: Non-receptor tyrosine kinase

NSF: N-ethylmaleimide sensitive fusion protein

OGT: O-GlcNAc transferase

ORF: Open Reading Frame

PAT: Palmitoyl-acyl transferase

PCR: Polymerase chain reaction

PFKFB3: 6-phophofructo-2-kinase/fructose-2,6 bisphosphate, isoform 3

PICK1: Protein Interacting with C Kinase

PKA: Protein Kinase A

PM: plasma membrane

PPI: Protein-protein interaction

PPT: Protein-palmitoyl thioesterases

PSD: Postsynaptic density

RAC: Resin-assisted capture

RIC: Resistance to inhibitors of cholinesterase

ROS: Reactive oxygen species

SNAP-25: Synaptosomal-associated-protein 25kDa

SNARE: Soluble NSF attachment receptor proteins

UPS: Ubiquitin proteasome system

VPA: Sodium valproate, valproic Acid

Abbreviations

VPD: Valpromide

VGLUT: Vesicular Glutamate Transporter

XLID: X-linked Intellectual Disability

Y2H: Yeast Two-Hybrid

Chapter 1 - Introduction

1.1 Summary

Neuronal function is dependent on the appropriate conditional release and action of neurotransmitters at synaptic and motor neuron junctions. This process is highly complex, as demonstrated by the diverse array and variable prognosis and pathophysiology of early- and late-onset neuropathies. Although the fundamental processes involved in synaptic signaling are well understood, the spectrum of functional regulators, conditional dominance or the combinatorial consequence of somatic mutations affecting biological pathways, such as transcriptional regulation, post-translational modifications and the intracellular environment remain unclear. To enhance understanding of these processes, it would be difficult to begin in humans due to the comparative low percentage coverage of the functional and physical human interactome. By first elucidating candidate effectors in *C. elegans,* then extrapolating this information to predict the functional relevance of human orthologues, these candidates can then be prioritized for functionally relevant interactome studies, with the aim of providing higher network coverage of evolutionary conserved effectors of synaptic function.

This chapter will give an overview of:

- Neurotransmission
- The use of *Caenorhabditis elegans* in neurobiology
- Protein Interaction Networks
- Sodium valproate (also known as VPA or valproic acid)
- Protein palmitoylation and palmitoyl acyl transferases (PATs)
- Methods of elucidating interaction partners

1.2 History of neurotransmission research

Our general understanding of the fundamental principles of neurotransmission originated from pioneering studies by Emil du Bois Reymond, who discovered action potentials and chemical synapses (Sudhof, 2013). In the 19th Century Santiago Ramon y Cajal described the '*neuron doctrine'*, which describes the concept that the nervous system is composed of discrete individual cells (López-Muñoz & Alamo, 2009). Another key figure in defining the physiological concept of synapses was Sherrington, who in 1925 developed a theory of the action of synapses, even though the detailed structure of the synapse remained unknown until early electron microscopy studies were performed in the 1950s (Robertson, 1953) .

In 1969 Bernard Katz published a paper describing the fundamentals of neuronal transmission through detailed electrophysiological analysis (Katz, 1970). In this seminal work Katz proposed two hypotheses, the first of which was the quantal hypothesis, which described the exocytosis of neurotransmitter-filled vesicles at distinct points on the pre-synaptic membrane. Heuser and Reese elaborated on this hypothesis in 1973, showing evidence that fusion of vesicles with the active zone of the presynaptic membrane is followed by recycling of vesicles into endosomal organelles (Heuser & Reese, 1973). This hypothesis was further substantiated by electron microscopy showing synaptic vesicle fusion at the presynaptic membrane (Heuser et al., 1979)

The second hypothesis proposed by Katz was the '*calcium hypothesis*', which stated that the effect of a nerve impulse was to elicit calcium ion entry into the presynaptic terminal, leading to vesicle fusion. Katz proposed that a calcium sensor was responsible for the

triggering of fusion pore opening. Following this proposal, synaptotagmin proteins Syt1, Syt 2 and Syt 9 were all shown to bind calcium, and function as calcium sensors (J. Xu, Mashimo, & Sudhof, 2007).

In order for neurotransmitter to be released across the synaptic cleft, a fusion event must occur between the synaptic vesicle and the presynaptic membrane. This is generally thought to occur by the fusion of three soluble N-ethylmaleimide sensitive fusion (NSF) Attachment Receptor Proteins (SNARE) and SM (Sec1/Munc18-like) proteins. SNAREs consist of the V-SNARE Synaptobrevin (also known as VAMP-2), which is found on the synaptic vesicle membrane, and the t-SNAREs Synaptosomal-Associated-Protein 25kDa (SNAP-25) and syntaxin-1, located on the presynaptic membrane (Sudhof & Rizo, 2011). When fusion occurs, N to C terminal zippering of the 4 alpha helices from the three SNARE proteins occurs, two alpha helices being derived from SNAP-25 and one alpha helix being provided by synaptobrevin and syntaxin-1 respectively. This zippering causes the synaptic vesicle and pre-synaptic membranes to be brought into close proximity, leading to membrane destabilization and fusion pore formation. NSF then disassembles the assembled SNARE complex.

The formation of SNARE complexes is tightly regulated, and munc18-1 and munc13 are both known to be required for membrane fusion. Interestingly, Munc18-1 has both stimulatory and inhibitory effects on vesicle fusion, as it binds to syntaxin-1, keeping it in a closed conformation, thus preventing membrane fusion. However it is also capable of binding to the assembled SNARE complex, where it may promote vesicle fusion (Dawidowski & Cafiso, 2016).

Two chaperone systems are also involved in synaptic vesicle fusion. The first of these is the complex of cysteine string protein alpha (CSPα), Hsc70 and SGT. This complex binds to SNAP-25 on the presynaptic membrane, maintaining it in a monomeric form that is capable of forming SNARE complexes. The second chaperone system is centered around synucleins, which act to increase the rate of complex formation (Sudhof & Rizo, 2011). Mutations in synuclein have been shown to cause Parkinson's disease.

1.3 Use of *C. elegans* to study neurobiology

Sydney Brenner could be described as the godfather of *C. elegans* neurobiology as he began to study the genetics of worms as model organisms in 1963. In 1967 he carried out the first chemical mutagenesis studies on wild type worms. Using the chemical ethyl methane sulfonate (EMS) he phenotypically characterized around 100 mutants that had easily visible phenotypes (Brenner, 1974). Of particular interest were those that had uncoordinated movement, which he described as the "Unc" phenotype. These mutated genes included may genes now known to be involved in the process of neurotransmission, including *unc-30*, which controls differentiation of some GABA neurons, as well as those in neuronal path-finding, such as *unc-6*, which plays a role in axonal outgrowth.

Although Brenner's early studies were performed in *C. briggsae*, he then switched to *C. elegans,* due to its relative ease of growth and maintenance. *C. elegans* are earth dwelling microscopic self-fertilizing hermaphrodites (XX). When hatched, the worms are around 0.25mm long but grow to 1mm in length once they reach adulthood, which takes around 3 days. They are transparent, meaning that fluorescent constructs can be easily used to

investigate protein localization or dynamics. In addition, protein-protein interactions can also be studied *in vivo* (Feinberg et al., 2008). To observe worm phenotypes, such as egg laying and feeding, dissection microscopes can be used to observe phenotypic changes in worms grown in petri dishes. For higher resolution images, compound or confocal microscopes are used to achieve single-cell resolution (Corsi, Wightman, & Chalfie, 2015). Although the majority of worms are hermaphrodites, less than one percent of the population is male (XO). This allows scientists to perform genetic crosses to generate worms with genotypes of interest. The fact that 99% of the population is self-fertilizing is greatly advantageous as it means that a whole worm population can be generated from a single worm.

During development *C. elegans* go through four larval stages, known as L1, L2, L3 and L4. At the end of each stage, a new cuticle is formed and the old cuticle molts from the worm. Around 12 hours after the L4 stage of development adult worms begin to produce progeny. Egg laying continues for 2-3 days until the worms have run out of sperm. After this, progeny can only develop if they are mated with a male worm. Following the reproduction phase, wild type worms live for another 2-3 weeks under normal conditions (Corsi et al., 2015).

In 1975, dauer larva were discovered (Cassada & Russell, 1975), where *C. elegans* go into an arrested developmental stage in response to environmental stress. This is sometimes known as L2d –an alternative L3 stage. In this phase a cuticle forms around the whole of the organism, plugging the mouth so that the worm cannot feed or develop. This increases the worm's resistance to chemicals, and in this state the worm can survive for many months with no food source. Three main parameters for dauer arrest are population

density, supply of food and temperature. This phase is useful in a lab setting. For example when strains are ordered, they are often in transit for several days and hence they run out of food. However, rather than starving and dying, worms (in L1 phase) signal to become dauer. Therefore, when the worms arrive in the lab, they can be transferred to petri dishes containing bacteria. This causes the worms to molt (and lose their mouth plugs), enabling feed to resume, and development to L4 and adult worms to continue (Cassada & Russell, 1975).

C. elegans provide a simple model organism, which can be used to genetically investigate the physiological regulators of neuronal function. The *C. elegans* genome encodes around 19000 genes, and a single pair of X chromosomes. An adult hermaphrodite has 302 neurons, and forms about 2000 synapses at neuromuscular junctions (NMJ) (White, Southgate, Thomson, & Brenner, 1986), not including an additional 5000 non neuromuscular synapses (e.g. interneurons). The synaptic and gap junctions formed in worms are stereotypical from worm to worm, showing about 75% reproducibility. In 1986 electron microscopy studies generated a near complete map of the worm neuronal network, known as the connectome (White et al., 1986). However, this map was lacking in certain areas of the network, especially in ventral cord neurons. In 2011 Dmitri Chklovskii and his group published a complete map of the connectome, and this represents the first and only complete connectome in any organism (Varshney, Chen, Paniagua, Hall, & Chklovskii, 2011). This allowed them to test relationships of signal propagation to behavioural phenotypes (Varshney et al., 2011), demonstrating why *C. elegans* is an ideal model organism in which to study neurobiology.

1.4 Neurotransmitters from *C. elegans* to Humans

1.4.1 Acetylcholine

The first neurotransmitter to be discovered was acetylcholine (Ach) in 1921, and it was later shown to also act as an excitatory neurotransmitter in nematodes (del Castillo, De Mello, & Morales, 1963), although at this stage, not in *C. elegans* specifically. Excitatory cholinergic signaling facilitates many functions in *C. elegans,* from egg laying to pharyngeal pumping and defecation cycles. However, most significantly for this study is its effect on locomotion.

Acetylcholine is the primary excitatory neurotransmitter in *C. elegans* (Rand, 2007). The enzyme choline acetyltransferase (ChAT) catalyzes the synthesis of acetylcholine from choline, which is then loaded into synaptic vesicles by the Vesicular Acetylcholine Transporter (VAchT, Unc-17). One classical way to determine whether a neuron is cholinergic or not is to test for the expression of these two proteins. The lumen of the synaptic vesicle is acidic, due to the action of an ATP-dependent proton-pump, which allows VAChT to exchange protons for the acetylcholine, resulting in acetylcholine uptake into synaptic vesicles. At this point, docking, priming and release of the acetylcholine containing vesicles is very similar to that of other neurotransmitters (Rand, 2007). Following vesicle/membrane fusion, acetylcholine is released into the synaptic cleft where it binds to two main types of acetylcholine receptor – ionotropic heterotrimeric receptors that are responsive to the drug levamisole, and homomeric receptors that are insensitive to levamisole but sensitive to nicotine. Activation of these receptors leads to an influx of sodium and calcium cations, leading to depolarization of the muscle cell, and muscle contraction (Rand, 2007).

To re-set the cholinergic signal, acetylcholinesterases (AChEs) degrades acetylcholine in the synaptic cleft back into acetate and choline molecules. Four AChEs (*ace-1, ace-2, ace-3,* and *ace-4)* have been discovered in *C. elegans. Ace-1* is expressed in a few neurons, however, its predominant site of expression is in muscle cells. In contrast, motor neurons express *Ace-2*. *Ace-3* has been shown to have AChE activity but this only represents a small proportion of the AChE activity in *C. elegans.* To date, *Ace-4* has not been shown to have enzymatic activity. ((Combes, Fedon, Toutant, & Arpagaus, 2003), (Lewis, Gehman, Baer, & Jackson, 2013)), Choline then needs to be returned to the presynaptic terminal by transporters such as Choline-Transporter 1 (CHO-1), which mediates high-affinity choline uptake, and whose loss leads to a decreased acetylcholine production (Matthies, Fleming, Wilkes, & Blakely, 2006). SNF-6 has also been reported as a choline transporter, but little research has been carried out into its role in comparison to CHO-1 at the NMJ.

In humans, acetylcholine is thought to act more as a neuromodulator than a neurotransmitter in the brain (Picciotto, Higley, & Mineur, 2012), whereas in the peripheral nervous system (at NMJs) it has an excitatory role. A neuromodulator is a chemical that causes a change of state of a neuron (or group of neurons), but is not directly excitatory. Cholinergic signaling has roles in the excitability of neurons, as well as influencing synaptic transmission itself and inducing synaptic plasticity. However the machinery behind the cholinergic signaling is highly conserved. For example, the human ortholog of VAChT (also termed VAChT) was elucidated via sequence similarity to the *C. elegans* protein. This provides an excellent example of how the identification of novel effectors in *C. elegans* can provide new insight into evolutionary conserved effectors of human synaptic function.

1.4.2 GABA (gamma-amino-butyric acid)

In vertebrates, the most common inhibitory neurotransmitter is GABA. Significantly, GABA is also a vital neurotransmitter in *C. elegans,* primarily at NMJs (Jorgensen, 2005). In *C. elegans* GABA is found in 26 neurons, including D-type neurons (dorsal and ventral muscles), RME motor neurons (head muscle) as well as in the AVL and DVB motor neurons. GABA is only excitatory in the AVL/DVB motor neurons, where it controls the contraction of the enteric body muscles, enabling defecation. In other neurons, GABA acts as an inhibitory neurotransmitter.

For locomotion to occur in *C. elegans*, the dorsal and ventral longitudinal muscles must alternatively contract and relax (Jorgensen, 2005). When the dorsal muscles contract, the ventral muscles relax and vice versa. Acetylcholine release from ventral or dorsal cholinergic motor neurons causes body wall muscle contraction. Acetylcholine also stimulates GABA to be released, by either the dorsal or ventral GABA motor neurons (the opposite to where the acetylcholine was released). GABA crosses the synapse and binds to a heterodimer of Unc-49A and Unc-49B subunits (Jorgensen, 2005). This heterodimer forms a ligand activated chloride channel, and is the ortholog of vertebrate GABA-A receptors. Upon binding GABA, chloride ions are able to diffuse into the cell, leading to hyperpolarization and decreased excitability of the membrane. If the chloride ion concentration is high in the muscle, muscle contraction inhibition still occurs because the membrane voltage is clamped at that of the chloride equilibrium potential, preventing further depolarization (Jorgensen, 2005). From this it can be seen that a balance of excitatory: inhibitory Ach: GABA signaling is essential for normal locomotion. This is the

reason why worms lacking GABA "shrink" as contraction of both dorsal and ventral muscles occurs.

In vertebrates, GABA inhibition is caused by either activation of chloride channels (mediated by the GABA-A receptor), or by the combined opening of potassium and inhibiting calcium channels (mediated by the GABA-B receptor). GABAergic neurotransmission is essential for neuron synchronization in the brain, and therefore is key to neuronal communication and memory processing (Nava-Mesa, Jiménez-Díaz, Yajeya, & Navarro-Lopez, 2014).

1.4.3 Glutamate

The main excitatory neurotransmitter in humans is glutamate, which is a biological precursor of GABA (Danbolt, 2001). Glutamate is transported by Vesicular Glutamate Transporters (VGLUTs) into synaptic vesicles. At the postsynaptic zone, Postsynaptic Density (PSD)-95 anchors the glutamate receptors N-methyl-D-asparatate receptor (NMDAR) and alpha-amino-3-hydroxy-5-methyl-4-isoxalonepropionic acid receptor (AMPAR) to the surface. As described previously the balance of excitatory: inhibitory neurotransmission in *C. elegans* is required for their locomotion. Likewise, this balance is also required in humans, as imbalances have been proposed to lead to diseases such as autism spectrum disorders and schizophrenia as well as neurodegenerative disorders like Alzheimer's disease (Nava-Mesa et al., 2014).

Ionotropic glutamate receptors have also been identified in *C. elegans* neurons, for example subunits have been detected in both RIA and command interneurons (Brockie & Maricq, 2006). By mutating receptor subunits, functions of glutamatergic

neurotransmission can be elucidated. The first example of this was in *glr-1* mutants, where mutants were found to have defective long-term memory, avoidance to stimuli (such as nose-touch or octanol), and foraging behaviour (Wang GJ et al., 2010). This excitatory neurotransmission is hence also vital in worm neurons.

As well as acetylcholine, GABA and glutamate, *C. elegans* also use other chemicals as neurotransmitters, including biogenic amines, and neuropeptides. Four biogenic amines are found in *C. elegans*. These are octopamine, tyramine, dopamine and serotonin. In vertebrates other signaling amines are also produced, such as histamine and epinephrine, however, this is not the case in *C. elegans*.

1.4.4 Other Neurotransmitters in *C. elegans*

Serotonin is a conserved regulator of energy balance from invertebrates to vertebrates. Serotonin has been found to act with another biogenic amine, octopamine to control body fat loss in *C. elegans* (Noble, Stieglitz, & Srinivasan, 2013). Serotonin has also been linked to locomotion behavior, and is synthesized in neurosecretory motor neurons. Thus defects in serotonin signaling can affect the locomotive behavior of worms. In humans defects in serotoninergic neurotransmission have been linked to multiple psychological disorders, from schizophrenia to depression and anorexia nervosa (Lin, Lee, & Yang, 2014).

Octopamine is synthesized from tyramine, and has been described as the invertebrate equivalent of norepinephrine. In the octopamine biosynthesis pathway, tyrosine is firstly converted to another amine neurotransmitter, tyramine, which is then converted to

octopamine. However, tyramine and octopamine have been found to have distinct receptors, leading to the conclusion that both can act as neurotransmitters (Alkema, Hunter-Ensor, Ringstad, & Horvitz, 2005; Wragg et al., 2007).

Dopamine signaling is vital in *C. elegans* for responding to changes in environmental conditions. An important example is the response to food availability (Chase & Koelle, 2007). Dopamine signaling is induced in the presence of food, which is thought to lower their locomotion rate upon entering a food source. Interestingly the dopaminergic and octopaminergic pathways link in SIA cholinergic neurons. Upon presence of food, dopamine signaling inhibits the release of octopamine, which leads to decreased c-AMP response element-binding protein (CREB) induction. Inhibition of dopaminergic receptors causes a Resistance to Inhibitors of Cholinesterase (RIC) phenotype, making the interpretation of the aldicarb-sensitivity assays more complex (Suo & Ishiura, 2013).

There are over 100 genes in *C. elegans* (C. Li & Kim, 2008) encoding over 250 neuropeptides. These include insulin-related peptides (INPs), FMRFamide-related peptides (FLPs), and neuropeptide-like proteins (NLPs). These directly or indirectly affect synaptic function, with some being reported to act as neurotransmitters themselves. Some neuropeptides have been reported to regulate locomotion in *C. elegans,* and several neuropeptide mutants (e.g. nlp-12) have been shown to confer resistance to aldicarb, indicating a change in cholinergic or GABA signaling (Sieburth et al., 2005). Certain neuropeptides, such as flp-1 and flp-8, have also been shown to play a role in homeostasis of the excitatory: inhibitory balance at the NMJ (Stawicki, Takayanagi-Kiya, Zhou, & Jin, 2013). Thus, neuropeptide signaling is crucial for *C. elegans* locomotion and

other phenotypes such as egg laying, metabolism and their response to different environmental conditions.

1.5 Increasing Complexity of Neurotransmission

The complexity of neurotransmission increases when the effects of conditional post-translational modifications and cross talk between pathways are considered.

1.5.1 Phosphorylation

In the 1990s studies showed the effect of Protein Kinase A (PKA)-dependent phosphorylation at the presynaptic and postsynaptic terminals (Nguyen & Woo, 2003). Phosphorylation has since been shown to be critical in some forms of long-term memory and synaptic plasticity. PKA plays a role in the recruitment of synaptic vesicles to the readily releasable pool (from the reserved pool), and certain phosphoproteins are localized on synaptic vesicles. Key examples of these are synapsins (Menegon et al., 2006). Synapsin 1 and 2 normally act to tether synaptic vesicles to the actin cytoskeleton. They are phosphorylated by PKA following calcium stimulation in hippocampal neurons. This stimulation leads to an increased rate of synaptic vesicle exocytosis, as the vesicles dissociate from the actin cytoskeleton. As well as having one site for PKA phosphorylation, synapsin-1 also has two sites for calmodulin-dependent kinase II (CAMKII) phosphorylation, and all isoforms have consensus sequences to allow other kinase activity (e.g. Mitogen-activated Protein Kinase (MAPK)). In combination these facts suggest that neurotransmission and hence locomotion defects could be seen if phosphorylation pathways were altered.

1.5.2 Glycosylation

Other posttranslational modifications that increase the complexity of synaptic transmission include glycosylation. O-GlcNac–modification is the addition of one N-acetylglucosamine to serines and threonines (O-linkage) of proteins, and is also thought to be a reversible dynamic process. O-GlcNAc Transferase (OGT) and O-GlcNACases catalyze the addition and removal of O-GlcNAC, respectively (Tallent et al., 2009). O-GlcNAC, OGT and O-GlcNACases are all highly abundant in the brain, especially in the hippocampus. Furthermore, pharmacological modulation of O-GlcNAc levels has been shown to alter synaptic plasticity (Tallent et al., 2009). It has been shown that there are extensive O-GlcNAc-modifications of proteins expressed in the pre- and post-synaptic terminals. Synapsin-1 for example, has 9 sites of potential O-GlcNAC-modification. It has also been shown that in many proteins, O-GlcNAC and phosphate compete for sites on their target proteins, thus providing links to signaling pathways and conditional variation or modulation of responses. In rats, synapsin-1 has three O-GlcNAc sites, two of which are also CAMKII sites (Skorobogatko et al., 2014). Glycosylation of these sites has been reported to increase phosphorylation of synapsin-1 at serine-9 in mice, which is a site known to be phosphorylated by PKA. However phosphorylation of two other sites (MAPK and CAMKII) was also reported, increasing the complexity of regulatory crosstalk (Tallent et al., 2009).

1.5.3 Ubiquitination

There is a significant amount of evidence to demonstrate the important role of the ubiquitin proteasome system (UPS) in both pre- and post-synaptic compartments (Rinetti & Schweizer, 2010). There is a large amount of combinatorial diversity in the UPS. There are only one or two genes encoding E1 ubiquitin activating enzymes, tens of E2 ubiquitin-conjugating enzymes, but up to 1000 genes encoding E3 ubiquitin ligases, with many showing neuron specific expression (Nakayama & Nakayama, 2006). The UPS system has been shown to play a role in the formation of the presynaptic terminal, regulating both axonal growth and growth cone guidance (Rinetti & Schweizer, 2010). This role is conserved throughout evolution, as in *Apylsia*, inhibition of the proteasome leads to increased strength of neurotransmission, with an increase in the number of presynaptic boutons (Zhao, Hegde, & Martin, 2003). This has also been shown in *Drosophila melanoganster* NMJs, with the increased strength being due to an increased level of Dunc-13 (Unc-13) – the fly ortholog of human Munc13 (Speese, Trotta, Rodesch, Aravamudan, & Broadie, 2003). This change was dependent on PKA, again showing the complex effects of crosstalk between post-translational pathways. In humans, studies have been carried out in hippocampal neurons, where proteasomal inhibition for 2 hours led to an increase in the size of the recycling pool of vesicles (Willeumier, Pulst, & Schweizer, 2006). This increased pool size was dependent on neuronal activity, suggesting a regulatory role for the UPS at synapses.

In *C. elegans* the multi-subunit ubiquitin ligase Anaphase Promoting Complex (APC) has been reported to regulate the excitatory: inhibitory balance at the NMJ, as APC mutants (and knockdowns) caused hypersensitivity to aldicarb, which was rescued by APC-expression, specifically in GABA neurons, indicative of a role in GABA signaling (Kowalski et al., 2014).

1.6 Lipid Modifications – Palmitoylation

1.6.1 Palmitoylation

Lipid modification is required for the membrane localization, trafficking and function of many proteins. There are three main kinds of lipid modification; prenylation, myristoylation and palmitoylation. Prenylation is a non-reversible reaction where either 15- or 20-carbon isoprenoids are added to proteins near to the C-terminus (F. L. Zhang & Casey, 1996). Myristoylation is also non-reversible, but involves the addition of 14-carbon myristate to N-terminal glycines of target proteins (Wright, Heal, Mann, & Tate, 2010). In contrast, palmitoylation is the most common kind of lipid-modification of proteins in the brain, and classically involves the addition of the 16-carbon fatty acid palmitate to a cysteine residue on substrate proteins.

There are two types of palmitoylation reactions possible for target proteins. The less common is N-palmitoylation, where a non-reversible amide bond forms between the palmitoyl group and the target protein. The more common type is S-palmitoylation, which will be the focus of this section. S-palmitoylation (also known as S-acylation) is a reversible reaction where a thioesterase bond is formed between the cysteine residue of the target protein and palmitate.

As palmitoylation is the most prevalent post-translational lipid modification in neurons, numerous studies have uncovered several examples of palmitoylated neuronal proteins. Examples include signaling proteins (such as HRAS and RHOB), synaptic scaffolding

proteins, such as Postsynaptic Density Protein (PSD)-95, neuronal cell adhesion molecules and synaptic vesicle proteins (Fukata & Fukata, 2010). Unlike other forms of lipid modification, palmitoylation substrates tend to have multiple palmitoylated amino acids. The cysteine-string domain of CSPα, for example, is palmitoylated several times, which is essential for its function. Mutations in CSPα lead to adult neuronal ceroid lipofuscinosis (ANCL), and mutations may affect the palmitoylation of it's cysteine-string domain (Greaves et al., 2012).

Both integral membrane and cytoplasmic proteins can be palmitoylated, and there are over 200 known proteins in the palmitoylation database (known as the palmitoylome) (Sanders et al., 2015). Palmitoylation of cytoplasmic proteins can allow the protein to be anchored to membranes. This is the case for SNAP-25. Anchoring to the membrane allows SNAP-25 (with syntaxin-1) to form SNARE complexes with VAMP2 on vesicles to enable neuronal exocytosis (Greaves, Prescott, Gorleku, & Chamberlain, 2010). Interestingly both VAMP2 and syntaxin-1 have also been reported to be palmitoylated (Drisdel & Green, 2004; Veit, Becher, & Ahnert-Hilger, 2000). As both are transmembrane proteins, the role of palmitoylation cannot only be to facilitate membrane anchorage.

The reversible nature of S-palmitoylation makes it a vital modification to allow the intracellular shuttling of proteins. H- and N-Ras go through rapid palmitoylation/de-palmitoylation cycles, which causes shuttling between the Golgi apparatus and the plasma membrane (Fukata & Fukata, 2010). Their rate of shuttling determines Ras signaling, which is in turn linked to MAPK signaling, thus directly linking palmitoylation and phosphorylation pathways. Another example of shuttling is the enzyme glutamate decarboxylase (GAD65), which is responsible for the synthesis of GABA. However, there

is still much to understand about the role and conditional nature of palmitoylation in the crosstalk of the different pathways of synaptic transmission.

Palmitoylation can also change the interaction profiles of soluble proteins. Postsynaptic Density (PSD)-95 is localized at excitatory synapses, and has two N-terminal palmitoylation sites (El-Husseini et al., 2002). Palmitoylation of PSD-95 is essential for its localization at the PSD, which leads to AMPAR clustering. Therefore palmitoylation is essential for excitatory glutamatergic signaling in mammals, and has been suggested to play a role in synaptic plasticity (El-Husseini et al., 2002). PSD-95 palmitoylation is also required for the binding to cyclin-dependent kinase-like 5 (CDKL5). Inhibiting this interaction (through down regulation of CDKL5 or PSD-95 mutation) leads to an inhibition of dendritic spine formation and growth (Zhu et al., 2013).

Palmitoylation of integral membrane proteins also serves multiple purposes. For example, palmitoylation of integral membrane proteins can lead to their localization at specific subdomains of the plasma membrane, for example in lipid rafts. Non-receptor tyrosine kinases (NRTKs) and linker for activation of T cells (LATs) are both palmitoylated, and this palmitoylation allows clustering into lipid rafts. If this does not occur, T cell activation is attenuated (Guan & Fierke, 2011; Kabouridis, Magee, & Ley, 1997). The hydrophobic palmitate has also been proposed to cause a membrane tilt of the substrate integral membrane protein, which can alter the protein's interaction profile (Blaskovic, Blanc, & Van Der Goot, 2013; Joseph & Nagaraj, 1995).

1.6.2 Palmitoylation enzymes

Palmitoylation is an enzyme-mediated reaction, and the enzymes required to add palmitate to substrates are known as palmitoyl-acyl transferases (PATs). Protein-palmitoyl thioesterases (PPTs) and acyl protein thioesterases (APTs) remove the palmitate from substrates. The first PAT to be discovered was Effector of Ras Function 2p (Erf2p) in *Saccharomyces cerevisiae* (Lobo, Greentree, Linder, & Deschenes, 2002). In combination with the auxiliary protein Effector of Ras Function 4 (Erf4p), it was found to palmitoylate Ras2p at the endoplasmic reticulum (ER). The rate of Erf2p palmitoylation has been shown to be dependent on Erf4p, but no mechanism has yet been elucidated to describe this.

From this another PAT was discovered known as Akr1p, which functions independently to palmitoylate Yck2p (Roth, Feng, Chen, & Davis, 2002). By comparing Erf2p and Akr1p's sequences, a common motif was found, which contained the Asp-His-His-Cys (DHHC) domain in a 51 cysteine-rich amino acid span. Identification of this motif enabled systematic screening of yeast and other organisms for potential PATs. From this, seven family members were elucidated in *S. cerevisiae*, fifteen in *C. elegans*, twenty-two in *Drosophila melanogaster*, twenty-four in mice, and twenty-three in humans. It is not however known if all of these proteins function as active PATs (Huang et al., 2009).

Far less is understood about PPT enzymes, due to the lack of a common motif, unlike the PATs, all of which encode a DHHC domain. Palmitoyl-protein thioesterase 1 (PPT1) has been shown to de-palmitoylate substrates such as H-Ras and G-alpha subunits, and is localized in lysosomes and synaptic vesicles (Lehtovirta et al., 2001; Liu, Dudler, & Gelb, 1996). Another branch of palmitoyl thioesterases are known as acyl-protein thioesterase (APT) 1 and 2, which are localized in the cytosol. APT1 is known to de-palmitoylate

substrates such as SNAP-23, H-Ras and G protein alpha subunits. APT2 has a different substrate profile, and so far is known only to de-palmitoylate Growth Associated Protein 43 (GAP-43) (Tomatis, Trenchi, Gomez, & Daniotti, 2010). α/β-Hydrolase domain-containing protein 17 members have also been discovered, which specifically depalmitoylate PSD-95 (Yokoi et al., 2016).

1.6.3 Mechanism of PAT action

There is some debate regarding the mechanism of action of the PAT family. By studying the yeast PAT Akr1p, it was found that upon incubation with palmitate, auto-palmitoylation occurs, where a bond forms between the PAT and the palmitate group. This palmitate can be removed using the chemical hydroxylamine, suggesting a thioester bond, and mutation of the DHHC motif inhibited auto-palmitoylation as well as the trans-palmitoylation of substrate (Guan & Fierke, 2011; Mitchell, Mitchell, Ling, Budde, & Deschenes, 2010). Some of the human PAT family members have also been shown to be palmitoylated, namely DHHC9, DHHC15 and DHHC17 (Kang et al., 2008; Swarthout et al., 2005b). These studies lead to the proposal of a two-step mechanism of palmitoylation, in which a labile thioester bond is formed between the cysteine of the PAT (in the DHHC sequence) and the palmitate molecule (Figure 1.1). This palmitate is then either

hydrolyzed or transferred to the substrate at a specific cysteine residue (Guan & Fierke, 2011).

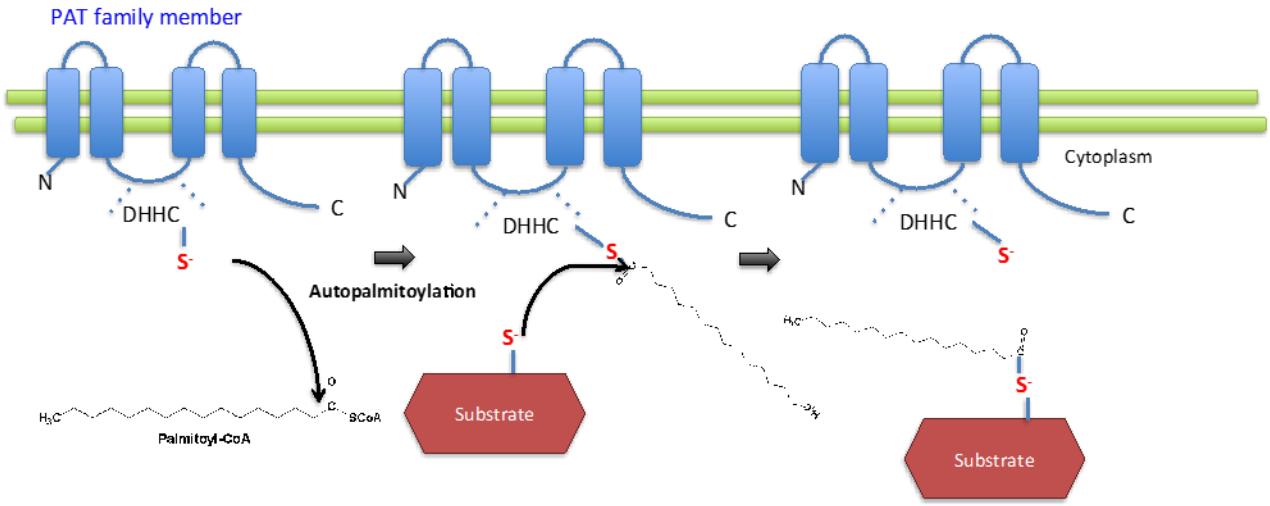

Figure 1.1 – **Proposed two-step mechanism of PAT enzymatic activity.** All PATs are transmembrane proteins. In the first step of the reaction a labile thioester bond is formed between the cysteine in the DHHC domain of the PAT and palmitoyl-CoA. This is known as autopalmitoylation. The palmitoyl group is then transferred to the substrate.

1.6.4 *C. elegans* PATs

In *C. elegans* there are fifteen PATs, predicted on the basis of containing a DHHC domain (Edmonds & Morgan, 2014). However, only five of the PATs have knock out mutants available, and few phenotypes have been seen with these mutants. For example, locomotion assays revealed that the dhhc-12 mutant has a decreased rate of locomotion, and the dhhc-14 mutant has a significant increased locomotive rate (Edmonds & Morgan, 2014). Lifespan was also analyzed in the same study, showing that dhhc-1, -9 and -14 mutants each have a reduced mean lifespan, whereas dhhc-12 and dhhc-13 mutants have an increased median lifespan, and spe-10 causing a significant increase in the maximum

lifespan (Edmonds & Morgan, 2014). However, no synaptic function assays were carried out on these mutants, and RNAi experiments revealed no other phenotypes.

1.6.5 Human PAT family

All PATs are transmembrane proteins, having between four and six transmembrane domains. Every human PAT contains the DHHC motif, located within a 51-amino acid cysteine-rich domain between two transmembrane domains. However, some other PAT family members in other organisms have differences in this motif. For example, in *S. cerevisiae*, Akr-1, Akr-2 and Pfa-5 have DHYC instead of a DHHC motif (where Y is tryptophan) (Mitchell, Vasudevan, Linder, & Deschenes, 2006). The localization of these family members varies, with some known to localize to the ER, Golgi and plasma membrane (PM).

The consensus sequence for PAT family member substrates is still not fully understood. Different PATs are known to have different substrate specificities – for example DHHC17 is known to have many substrates (Mitchell et al., 2006), whereas DHHC9 is thought to only palmitoylate H- and N-Ras (Swarthout et al., 2005b). All of the human PATs except DHHC13, DHHC23 and DHHC24 have been shown to be functional, though not all of these have been demonstrated in human systems.

The closest ortholog to the yeast Erf2 PAT is zDHHC9, which has been shown to palmitoylate N- and H-Ras. This palmitoylation only occurs when DHHC9 is bound to the auxiliary protein GCP16 (Swarthout et al., 2005b). There are 3 Ras family members, N-, H-, and K-Ras. All Ras isoforms are farnesylated in their C-termini, which allows low

affinity interactions with membranes (Eisenberg et al., 2013). H- and N-Ras are pamitolyated either once or twice on cysteine residues in the C-terminal hypervariable region. This palmitoylation enhances the membrane association of H- and N-Ras. However in this region K-Ras instead has 6 lysine residues that mediate hydrophobic interactions with membranes (Eisenberg et al., 2013).

As mentioned previously, the target proteins of many of the PATs is unknown, as for the majority of PATs there is not yet an identified consensus binding sequence, which would help the prediction of substrates. It has been shown in co-expression studies that regions outside of the DHHC cysteine rich (DHHC-CR) domain may confer specificity. For example, when the DHHC-CR domain of DHHC15 is replaced by that of DHHC3 no palmitoylation of a known DHHC3 palmitoylation substrate, SNAP23 is observed (Greaves, Gorleku, Salaun, & Chamberlain, 2010).

This theory is enhanced by two of the PATs; DHHC17, also known as Huntingtin Interacting Protein 14 (HIP14) and DHHC13 (HIP14L), both of which have N-terminal N-Ankyrin repeat domains. DHHC17 is known to interact with the neuronal protein Huntington (HTT), and when the N-terminus of DHHC17 was added to DHHC3, which does not normally show activity/interact with HTT, DHHC3 and HTT interacted (Huang et al., 2009). As well as HTT, DHHC17 has also been shown to palmitoylate other neuronal proteins, such as JNK3a2, SNAP25b and CSPα. Although zDHHC13 does not seem to palmitoylate JNK3a2, SNAP25b or CSPα, it binds all of the above proteins. Recently a sequence motif was found for DHHC13/17 substrate proteins – in symbolic form this is ΨβXXQP, where Ψ is any aliphatic amino acid, i.e. valine, isoleucine, alanine, or proline. β

indicates C-beta branched valine, isoleucine, or threonine. X indicates any amino acid (Lemonidis, Sanchez-Perez, & Chamberlain, 2015).

The algorithm known as CSS-PALM was created as a method to determine palmitoylation substrates (Zhou, Xue, Yao, & Xu, 2006). This predicts palmitoylation sites based on a clustering algorithm, where they collected experimentally verified palmitoylation sites (in version 4.0 this was 583 palmitoylation sites from 277 proteins), and grouped them into subsets based on their sequence similarity (Zhou et al., 2006). This algorithm has been shown to predict palmitoylation sites for around 1000 proteins in a short time frame (within 2 minutes). This is a useful tool in determining substrates of palmitoylation.

Many of the PATs have known cellular localization. Most of the PATs are localized at the Golgi or ER. Interestingly some PATs have specific localization profiles. For example human DHHC2 has been shown to localize to dendritic vesicles, on Rab11 positive endosomes, and DHHC8 is localized near synapses (Greaves, Carmichael, & Chamberlain, 2011; Thomas, Hayashi, Huganir, & Linden, 2013). Some DHHC family members have also been found to change their localization dependent on neuronal activity, a key example being DHHC5 (Brigidi, Santyr, Shimell, Jovellar, & Bamji, 2015). Normally DHHC5 is localized in dendritic spines, and is sequestered there by forming a complex with Fyn kinase (which phosphorylates DHHC5) and PSD-95. Upon neuronal activity, this complex is disrupted, and DHHC5 is internalized and transported to dendritic shafts, where it palmitoylates delta-catenin (Brigidi et al., 2015). Palmitoylated delta-catenin stabilizes N-cadherin at synapses, and mediates changes in dendritic spine remodeling, synapse efficacy, and thus learning and memory (Brigidi et al., 2014).

The TMD organelle predictor can also be used to predict the localization of transmembrane proteins. This prediction software uses the first two transmembrane domains to predict localization, and has an overall success rate of 82% (Sharpe, Stevens, & Munro, 2010).

1.7 Neuronal Function of PATs

There are multiple key examples of PATs playing a role in neuronal function (Fukata & Fukata, 2010). As mentioned previously, palmitoylation of PSD-95 is key for glutamatergic signaling, as well as dendritic spine formation and development. DHHC3 is localized on the Golgi membrane and has been shown to be the major PAT responsible for palmitoylating PSD-95, as well as GABA receptors at inhibitory synapses (Keller et al., 2004). However, palmitoylation of PSD-95 by DHHC2 has also been reported. DHHC2 has a very different localization to DHHC3, being predominantly restricted to dendritic spines. This palmitoylation allows dynamic changes in the palmitoylation state of PSD-95 at the synapse (Noritake et al., 2009). This suggests that multiple PATs may have similar substrate specificities, but play different roles depending on their localization.

Palmitoylation has also been implicated in various neurological diseases, and mutations in certain PATs have been proposed to be a factor in disease onset/progression.

1.8 Disease Related PATs

1.8.1 DHHC8

The most widely studied DHHC enzyme in terms of neurological disease is DHHC8. The gene encoding DHHC8 (*zDHHC8*) is located on chromosome 22 at 22q11.2. Either a 3Mb or 1.5Mb deletions have been shown to be associated with the development of schizophrenia (Mukai et al., 2004), as well as other emotional deficits and autism. Genetic deletion at this locus also leads to DiGeorge syndrome, which is associated with a 20- to 30-fold increase in the risk of the patient developing schizophrenia. Around 30% of patients with this micro-deletion develop schizophrenia. As well as this, genetic variants of zDHHC8 have also been associated with schizophrenia (Mukai et al., 2008).

DHHC8 knockout mice have been shown to exhibit a reduction in pre-pulse inhibition, a phenotype that has also been shown in some schizophrenic patients. In a mouse model, where a 1.3Mb chromosomal deficiency was created on the syntenic chromosome to 22q11.2, primary hippocampal neurons had a lower density of dendritic spines, an impairment of the growth of dendrites, and a reduced number of glutamatergic synapses (Mukai et al., 2008). All of these phenotypes were rescued by the reintroduction of DHHC8, highlighting its vital role at the synapse. However, few interaction partners and specific substrates of DHHC8 have yet been elucidated.

Protein Interacting with C Kinase (PICK1) has been shown to be a substrate of DHHC8, which is involved in cerebellar long-term synaptic depression. The palmitoylation of PICK1 is required for the induction of long-term depression. Few other substrates/interaction partners have been found for DHHC8 however, therefore, it could be playing other roles at the synapse (Thomas et al., 2013). As DHHC8 is localized at or near to all synapses, DHHC8 is a very interesting PAT to study.

Furthermore, in a recent study, a modified acyl-biotinyl exchange (ABE) technique was carried on post-mortem brains from patients suffering from schizophrenia. Samples were collected from the frontal cortex and homogenized. They found that palmitolylation was reduced by 20% in the brains of patients suffering from schizophrenia, specifically in the dorsolateral prefrontal cortex (Pinner, Tucholski, Haroutunian, McCullumsmith, & Meador-Woodruff, 2015). This effect was not seen in rats treated with anti-psychotic medication, suggesting defects in palmitoylation could be the cause or effect of schizophrenia.

1.8.2 DHHC5

DHHC5 is localized in postsynaptic compartments, and has been demonstrated to palmitoylate delta-catenin and grip-1b (Brigidi et al., 2014). In mice that are homozygous for a hypomorphic allele of zDHHC5, impaired synaptic plasticity as well as impaired performance on learning and memory tasks was observed (Y. Li et al., 2010). Genome-wide association studies have shown an association between DHHC5 and bipolar disorder and schizophrenia (Brigidi et al., 2015). As well as this, one paper lists a non-sense mutation of zDHHC5 being found in a patient diagnosed with schizophrenia (Fromer et al., 2014).

1.8.3 DHHC17 and DHHC13

Another PAT of high interest is DHHC17, which to date has been shown to palmitoylate thirteen substrates in mammals. These substrates include neuronal proteins such as synaptotagmin-1, SNAP-25, and HTT. In Huntington's disease, expansion in the

trinucleotide CAG repeat region of the HTT gene is the causative factor, which encodes a polyglutamine stretch. If a patient has more than 36 repeats of this CAG, the patient will develop Huntington's disease provided their life span is long enough. The polyglutamine stretch causes HTT to aggregate, leading to toxicity and neurodegeneration (Bates, 2003). Studies have found that in some sufferers with Huntington's disease, this polyglutamine expansion prevents its interaction with DHHC17, meaning that palmitoylation is decreased (Fukata & Fukata, 2010). This decreased palmitoylation is postulated to cause an accumulation of HTT. HTT and DHHC17 appear to have a lot of inter-regulation. For example, mutation of HTT has been shown to decrease the palmitoylation of another substrate of HIP14, SNAP-25 (Huang et al., 2011). This was corroborated in a study of a Huntington's disease mouse model (YAC128), where a reduced SNAP-25 palmitoylation was observed (Singaraja et al., 2011).

Recently, a yeast 2-hybrid (Y2H) screen was carried out to find novel interaction partners of DHHC17 (Butland et al., 2014). In this paper a Y2H library screen was carried out using a pool of three fragments of HIP14 against the human ORFeome. This screen identified 214 non-redundant proteins, 36 of which were shared with one of DHHC17's known substrates, HTT. Seventeen of these genes were known to play a role in Huntington's disease. Synaptic-related proteins were identified, and interestingly this also included K-Ras. This screen, however, was not carried out on full length DHHC17.

DHHC13 is the only other human PAT family member to have an N-ankyrin repeat domain at the N-terminus. It is ubiquitously expressed, but studies have shown it to play an important role in the central nervous system (CNS). DHHC13 has been reported to palmitoylate SNAP-25, and mutant mice develop features of Huntington's disease. Both

DHHC17 and DHHC13 interact with HTT, and when either of these PAT proteins were mutated in mice, this interaction was interrupted (Sutton et al., 2013). Both mutants displayed motor defects in climbing and learning, although some differences were seen, for example in the time of onset of the neuropathy. DHHC17 knockouts showed neuropathy from embryonic stages, whereas DHHC13 knockouts showed deficits later, when the mice were adults (Sutton et al., 2013). This shows both proteins are interesting candidates for further study.

1.8.4 DHHC9

DHHC9 is localized in the Golgi and has four transmembrane domains, with the catalytic DHHC domain located between the second and third transmembrane region. The N-, C-, and DHHC domain are all cytoplasmic (Fukata & Fukata, 2010). Mutations in zDHHC9 have been linked to X-linked intellectual disability (XLID), associated with marfonoid habitus. XLID is one of the most common causes of mental disorders, with 79 other genes being associated with XLID (Mitchell et al., 2014). Four different mutations of zDHHC9 have been found, which lead to XLID. Two are nonsense mutations, caused by a truncation or a frameshift. The other two are missense variants (Mitchell et al., 2014). As the nonsense mutations delete the catalytic domain, these mutations render DHHC9 non-functional. However the two missense mutations have been suggested to alter auto-palmitoylation of DHHC9 in different ways. Both reduce the steady state level of the DHHC9 that has been palmitoylated. The P150S mutation decreases the initial burst of palmitoylation, but the R148 increases the rate of hydrolysis of the palmitoyl-steady state substrate (Mitchell et al., 2014). Either mutation is proposed to decrease the rate of N-

and H-Ras palmitoylation. It is important to note that no mechanisms have been proven for exactly how zDHHC9 mutations functionally leads to the symptoms seen in XLID.

1.9 Problems of palmitoylation research

The progress of palmitoylation research has been slow since the discovery of Erf2. This is due to the difficulty in studying palmitoylation. Firstly there is a significant level of redundancy in the PATs – cells/tissues often express several different PATs. For example HeLa cells express 20 of the 23 PAT family members. Carrying out multiple gene knockouts is not usually realistic/feasible, hence elucidating which PAT palmitoylates which substrate in human cells is very challenging. Furthermore, carrying out *in vitro* assays is also problematic due to the low levels of PAT activity in its soluble state, and the fact that it is difficult to purify substrates without their palmitate group. Nevertheless in recent years, new techniques such as ABE and click chemistry have allowed palmitoylation to be detected more sensitively.

1.10 *C. elegans* genetic manipulation techniques

To assess if a gene has an effect on synaptic function in *C. elegans*, the gene can be disrupted via different methods – namely mutation (to generate loss of function or gain-of-function mutants), RNAi (to knock down the expression of selective gene transcripts), or the generation of transgenic constructs (to express variants of the gene of interest).

1.10.1 Microinjection

When generating transgenic constructs, microinjection is commonly used and constructs can be targeted to specific regions of the worm, dependent on the construct design. For example, the neurosensitive *Tu3311* strain was generated by injecting a construct of the *sid-1* gene fused to the pUNC-119 promoter into the worm (Calixto, Chelur, Topalidou, Chen, & Chalfie, 2010). This means that the *sid-1* gene is over-expressed in all neurons. There are many advantages of this system as fluorescent constructs can be injected in to allow visualization of the gene under a fluorescent microscope. Temperature sensitive alleles can also be used, which allows the temporal assessment of the gene's activity, which is useful when mutating the gene would cause lethality at the developmental stage. RNAi can also be performed by microinjection. However, microinjection of worms is considered difficult in comparison to other methods of genetic manipulation, and is not a viable technique to combine with high-throughput screens.

1.10.2 Mutation

For mutation screens, either forward genetic screens or reverse genetic screens can be carried out (Kutscher & Shaham, 2014). In forward genetic screens, the whole genome is mutagenized, and unknown genes are sought that have caused a change in a biological process (e.g. egg laying). A common mutagenesis agent used is EMS. This induces random genetic mutations in the *C. elegans* embryo. The worms are then genotyped to elucidate where a mutation has taken place. Stocks of these worms can then be made and stored. Other forms of forward genetics are radiation-induced and transposon-induced mutagenesis.

In reverse genetic screens, target-selected and gene-targeted mutagenesis can be performed. In target-selected mutagenesis, the whole genome is mutagenized but only a single gene is then selected for commonly by the polymerase chain reaction (PCR). In gene-targeted mutagenesis, a single gene is mutated (i.e. the rest of the worm is not mutagenized). An example of this form of mutagenesis is clustered regularly interspaced short palindromic repeats (CRISPR), which has become a widely used method of gene editing. CRISPR utilizes the Cas9 protein, which binds a single guide RNA, and cleaves DNA complementary to a 20bp region of this RNA strand, generating double strand breaks (Frøkjær-Jensen, 2013). CRISPR has been used in *C. elegans* to mutate endogenous genes to study gene function, as well as to insert fluorescent protein coding sequences into genomes to analyze the expression and localization of endogenous proteins (Katic & Grosshans, 2013; Rose et al., 2007).

The main advantage of generating mutant strains is that mutations are heritable and 100% efficient. Although RNAi can give variable results, depending on how efficiently the RNAi has been up-taken, genomic mutations tend to give more reliable results. However when a gene is essential, mutating it can lead to lethality or sterility, making it impossible to make knockout worms for these genes. Another disadvantage is that as the worm background is not neuronally sensitive, the mutation occurs throughout the entire worm. For genes that are expressed throughout the worm this can lead to phenotypes that are not due to the change of gene expression in neurons. Another point to note is that mutations may delete a locus of genes, not just the specific gene of interest. Generating mutants can also be time-consuming and laborious.

Human protein constructs can also be injected into worms, in order to analyze the effect of overexpression of toxic proteins in worms. One example of this is the transgenic worms overexpressing amyloid beta (Aβ)(McColl et al., 2012). Aβ is formed from proteolytic cleavage of amyloid precursor protein (APP), and Aβ peptide buildup is a characteristic of plaques found in several neurodegenerative diseases, the most well known being in Alzheimer's disease. Although *C. elegans* express an ortholog of APP – APL-1, an ortholog of Aβ has not been observed (due to a lack of cleavage sites for γ-secretase). The group transgenically expressed Aβ1-42 (a fragment consisting of 42 amino acids) and phenotypically characterized the worms. By overexpressing human proteins in *C. elegans*, drug screens can also be used to screen for possible therapeutics in humans. This is far simpler and more rapid than using the drugs in more complex organisms. In addition, neuroprotective compounds have also been tested in *C. elegans* screens (Chen, Barclay, Burgoyne, & Morgan, 2015). This shows the possible power of using *C. elegans* to better understand the mechanism of action of drugs with multiple effects and plausible targets.

1.10.3 RNAi

RNAi has successfully been used in *C. elegans* for many years for reverse genetic screens. It is systemic, meaning that when worms are either soaked in dsRNA or fed bacteria expressing dsRNA, the dsRNA can spread throughout the worm to take effect (Calixto et al., 2010). RNAi is also hereditary – it has been shown to last for up to 4 generations (Grishok, 2005). There are two methods of ingestion of RNAi – the first of these is soaking the worms in a solution concentrated in dsRNA. However, the more simplistic technique is the ingestion of bacteria expressing dsRNA, which is the technique focused on here.

There are two main libraries of dsRNA clones, from the Ahringer (Fraser et al., 2000; Kamath et al., 2003) and Vidal (Rual et al., 2004a) labs. The Ahringer library has 16,757 clones, and the inserts contain introns and exons between 500bp and 2.5kb. The Vidal library is smaller, with 11,511 clones, and is known as the ORFeome-RNAi v1.1 (Kamath et al., 2003; Rual et al., 2004b), as full-length open-reading frames (ORFs) are inserted into a double T7 vector. The bacterial strain HT115 is used in both libraries, which has an isopropyl beta-d-1-thiogalactopyranoside (IPTG) inducible T7 polymerase as well as having disruption of the dsRNAse RNAse III. The dsRNA construct is fused to a promoter dependent on T7 polymerase. Therefore, only when T7 polymerase is expressed will the bacteria express dsRNA, hence IPTG induces the bacterial expression of dsRNA. Feeding plates containing Nematode Growth Medium (NGM) and IPTG are poured and seeded with bacteria containing the dsRNA construct of interest. T7 polymerase is induced, leading to dsRNA production. Worms feed on the bacteria, and the dsRNA is taken up into cells. Although RNAi is systemic, some specialized machinery is required. SID-1 and SID-2 channels are independently required for the uptake of dsRNA. SID-2 channels are only expressed in the intestine apical membrane, and SID-1 is expressed at very low levels in neurons (Calixto et al., 2010).

Feeding RNAi is efficient in all cell types apart from neurons. However if dsRNA is directly injected into the neurons, the gene of interest is knocked down, indicating the process is inefficient due to the low levels of SID-1. In 2010, a strain of transgenic worms was produced that pan-neuronally expressed SID-1, under the control of the Punc-119 promoter (Calixto et al., 2010). Significantly these worms exhibited an increased efficiency of knockdown in the neurons, and also a decreased knockdown in non-neuronal tissues. Furthermore, as non-neuronal RNAi is blocked in these SID-1 strains,

neuronal phenotypes for genes that were lethal when knocked down in non-neuronal tissues, can be tested. Two of the strains they generated were *Tu3311 (Punc119-Sid-1)* and *Tu3335 (Punc119-Sid1-Lin15b)*, where Tu3335 showed the highest efficiency of RNAi. Lin15b has been previously shown to enhance RNAi in other strains (Lehner et al., 2006), but is known to affect mechanosensation, so is not always a suitable strain to use for behavioural assays.

1.11 The aldicarb-sensitivity assay to find effectors of synaptic function

To test for effectors of synaptic function, aldicarb-sensitivity assays have been carried out for many years (T R Mahoney, Luo, & Nonet, 2006). Normally at the cholinergic synapse, post calcium stimulation, acetylcholine–filled vesicles merge with the presynaptic membrane and acetylcholine diffuses across the synaptic cleft to the postsynaptic receptors. In *C. elegans* there are thought to be two types of acetylcholine-receptive postsynaptic receptors – nicotinic-sensitive and levamisole-sensitive receptors. To recycle the acetylcholine, in the synaptic cleft, acetylcholinesterase hydrolyses the acetylcholine into choline and acetate, which then are transported back into the presynaptic terminal.

Aldicarb is an acetylcholinesterase inhibitor. This means that when worms are picked onto plates containing aldicarb, it is absorbed into the worm, and acetylcholinesterase is inhibited (T R Mahoney et al., 2006). Acetylcholine builds up at cholinergic NMJ in synaptic clefts. This hyperstimulates the acetylcholine receptors on the postsynaptic membrane, leading to constant muscle contraction or paralysis. In this study, paralysis is

defined as no detectable movement when worms are touched on the head or tail with a platinum wire (Figure 1.2).

There are two previously described methods for carrying out aldicarb assays. The first of these involves "chronic" exposure to aldicarb (del Castillo et al., 1963), where L3 worms are picked onto plates containing low concentrations of aldicarb, and the number of progeny is measured. The second uses "acute" exposure, where worms are placed onto plates containing the aldicarb and the rate of paralysis is assessed. This is the more commonly used method, and was the method employed in this study.

To assess whether genetic knockdown has an effect on synaptic function, the time for aldicarb-induced paralysis to occur is measured. Figure 1.2 shows the principles of the aldicarb assay, and Figure 1.3 displays a typical graph showing results from a full time course assay. If the average paralysis is longer than that of the wild type (or control) worm, the phenotype is described as a Resistance to Inhibitors of Cholinesterase (RIC). More than 50 genes have been shown to cause this type of RIC phenotype. This could happen for many reasons. For example knocking down a gene involved in acetylcholine secretion would cause a decreased rate of acetylcholine secretion, leading to a delay in paralysis. Paralysis also could be due to a change in acetylcholine metabolism or catabolism. As *C. elegans* locomotion is dictated by contraction (cholinergic) and relaxation (GABAergic) of opposite muscles, a fault in GABA signaling could also cause a change in the rate of paralysis. This means that a decreased rate of paralysis could be due to an increase in GABAergic signaling. For example, by knocking down a gene prevented inhibition of GABA secretion.

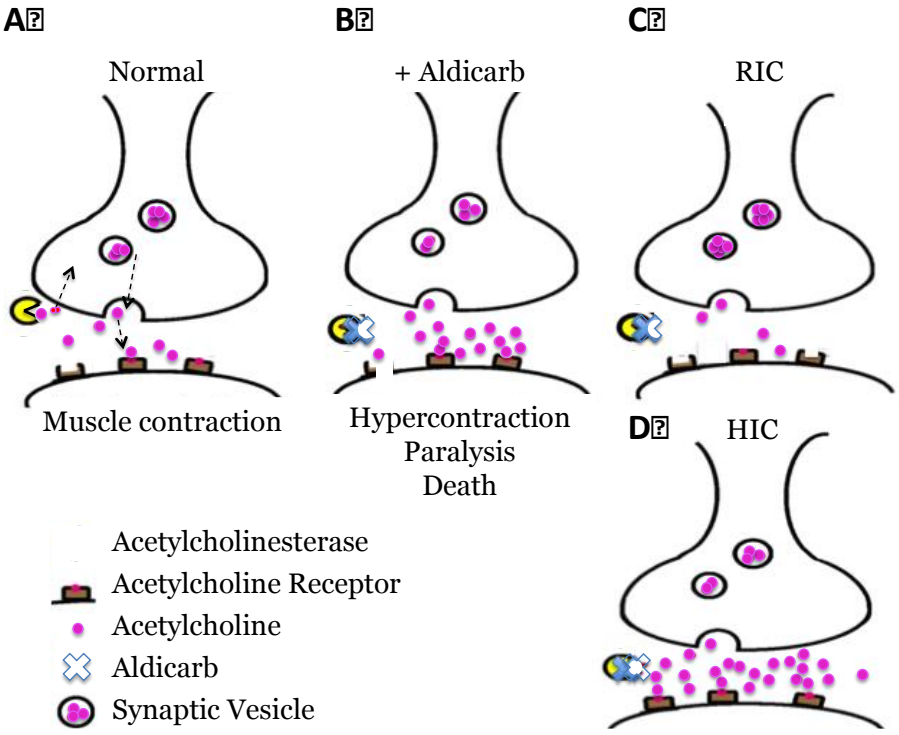

Figure 1.2 – **The principle of the aldicarb sensitivity assay at the cholinergic NMJ.** A. Under normal conditions acetylcholine is released from the pre-synaptic terminal upon calcium stimulation, travels across the synaptic cleft and binds to acetylcholine receptors on the postsynaptic membrane, inducing muscle contraction. After a certain amount of time, acetylcholinesterase degrades the acetylcholine and the choline and acetate are recycled. B. When aldicarb is absorbed into the worm, acetylcholinesterases are inhibited, meaning acetylcholine builds up in the synaptic cleft, leading to hypercontraction, paralysis and then death. C. If a gene is knocked down/mutated that decreases the secretion of acetylcholine, it will take longer for paralysis to occur, which is known as a RIC phenotype. D. If a gene is knocked down/mutated that increases the secretion of acetylcholine, paralysis will be quicker, which is known as a HIC phenotype.

If the opposite phenotype is seen, i.e. when worms paralyze quicker than the wild type worm, this is known as a Hypersensitivity to Inhibitors of Cholinesterases (HIC) phenotype. This is a less common phenotype than a RIC and could be due to increase cholinergic or decreased GABAergic signaling. For example a HIC phenotype results if

there is an increased secretion of acetylcholine or a decreased number of cholinergic receptors. A HIC phenotype can also result if GABA neurotransmission is inhibited.

Aldicarb assays can be used to better elucidate complex pathways. For example the G-

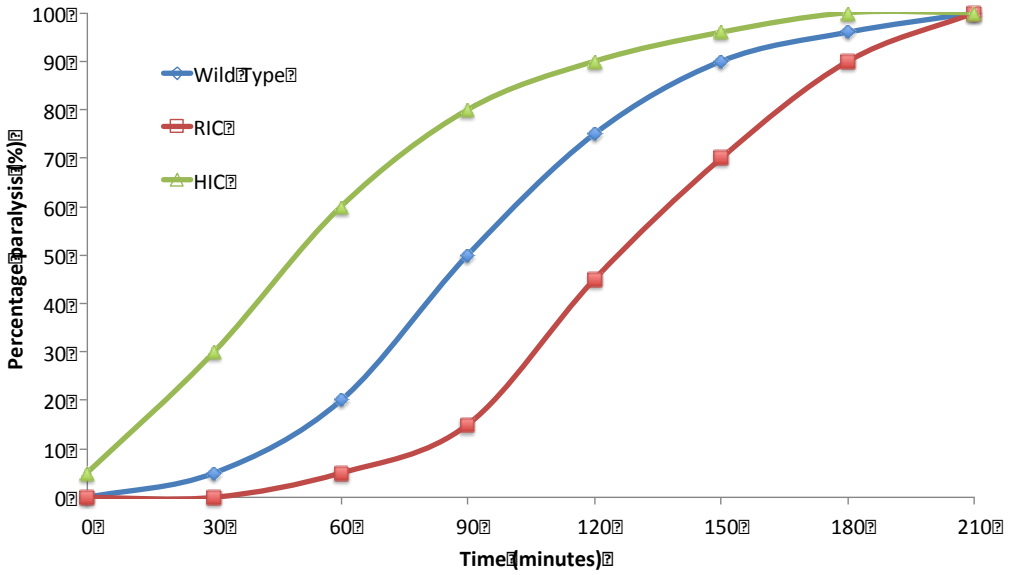

Figure 1.3 – **Graph showing typical result of aldicarb-sensitivity assay**. The numbers of paralysed worms are counted at each time point through the use of a platinum wire being pressed against the head and tail of the worms. The percentage of worms paralysed at each time point is calculated and plotted against time. If a RIC phenotype is observed, the rate of paralysis is slower than the control worm, and a shift to the right on the graph is seen (shown by the green line). If a HIC phenotype is observed, the rate of paralysis is faster than the control worm, and a shift to the left on the graph is observed (shown by the red line).

protein coupled signaling pathway is involved in acetylcholine release from ventral cord neurons – when mutated some genes in the pathway cause a strong RIC phenotype (e.g. RIC-8 and egl-3), while others cause a HIC phenotype (inhibitory factors such as DGK-1) (Rand, 2007). Aldicarb assays can be used to identify novel effectors of synaptic function. Certain mutations (e.g. *cha-1*) cause a decreased secretion of only acetylcholine, however others (such as synaptobrevin and synaptotagmin) cause a decreased secretion of all neurotransmitters (Rand, 2007). This means that following a phenotype, investigating the molecular basis to the phenotype can be complex but important. Hence by elucidating genes that cause a RIC or a HIC phenotype, complex pathways and the effects of

conditional crosstalk that underpin cholinergic/GABA/general neurotransmission might be better understood.

1.12 Advantages and Disadvantages of *C. elegans*

1.12.1 Advantages of *C. elegans*

There are many advantages to using *C. elegans* as a model organism. As mentioned previously they are easy to maintain in the lab. At room temperature, a worm grows from egg to adult in 3 days. L1 worms can also be frozen at -80^{0}C by using glycerol (Stiernagle, 2006). They can grow either on solid NGM with calcium chloride, magnesium sulphate and potassium phosphate supplementation, seeded with OP50 bacteria. If high throughput screening is required, *C. elegans* can also be grown in liquid. Both options are cost-effective, making *C. elegans* a cheap organism to maintain.

There is also a plethora of mutants/strains available via the *Caenorhabditis* Genome Centre (CGC), priced at just over £4 per strain. They are genetically tractable, and there are multiple methods of genetic manipulation including mutations, RNAi knockdowns and overexpressing constructs via microinjection. The aldicarb-assay is also a simple method to identify genes involved in synaptic function.

Importantly for systems biology, C. *elegans* have high percentage coverage of their physical and functional interactome, and they are the only organisms to have a complete connectome (Varshney et al., 2011; White et al., 1986). Furthermore, there are few ethics

regarding their use, and very high numbers of worms can be generated in a short space of time (allowing high-throughput screening).

1.12.2 Advantages of the aldicarb-sensitivity assay

The aldicarb sensitivity assay has been used for many years in the study of *C. elegans* synaptic function, and so the assay is well characterized. The endpoint of paralysis is quick to measure, and easy to see. It can also be manipulated to enable carrying out of semi high-throughput screens. Furthermore as it shows general synaptic transmission defects, it can be used as a general screen for effectors of synaptic function (Rose et al., 2007).

1.12.3 Disadvantages of *C. elegans*

Although *C. elegans* have many advantages, disadvantages must be considered prior to their usage. Firstly, as *C. elegans* are a model organism it can sometimes be difficult to determine the relevance in a human system. For this reason, other organism and/or techniques are used, if this is appropriate. It is important for this reason, to check the similarity and identity of the worm and human orthologs of interest.

There can be variability between worm plates if for example; one worm strain is faster growing than another due to the particular mutation or knockdown that occurred. If not dealt with this can also lead to starving of the quicker growing plate, or the use of immature worms for the slower growing plate. For these reasons all assays should be carried out on gravid adult hermaphrodites that are not starved or overcrowded. Furthermore, RNAi can have variable efficiency.

1.12.4 Disadvantages of the aldicarb-sensitivity assay

Although used frequently in the past, there are limitations to the aldicarb-sensitivity assay. One is the subjective nature of the experiment – it is necessary to do all of the experiments blind. This means that the person carrying out the experiment is not aware of which plate is which strain/knockdown. If a mutant is known to cause a specific phenotype that would make them obvious to the experimenter, where possible a control worm that shows the same phenotype should also be used in the assay.

Furthermore if the aldicarb assay is used following RNAi knockdown, high variancy can occur due to the variable efficiency of the RNAi, and the fact that RNAi is rarely 100% efficient. Knocking down a gene itself can cause phenotypes in the worm, such as an altered motility or locomotion. This must be kept in mind when performing the assay.

The main disadvantage of the aldicarb-sensitivity assay however, is the fact that it does not delineate why a RIC or HIC phenotype has occurred. As mentioned previously, if the mutation affects GABA, or another neurotransmitter pathway, a phenotype may also be seen. A phenotype may also result if a regulatory process has become abnormal, or the synthesis/degradation of the neurotransmitter itself has occurred. One main control used in RNAi experiments to check that RNAi has worked is to use a positive control in the aldicarb-sensitivity assay. This commonly is egl-30, which is actually an octopamine receptor, highlighting the complexity of mutants that can cause an aldicarb phenotype. For these reasons, other assays should be carried out to determine to reason behind a RIC or HIC phenotype. For example checking whether the phenotype is caused due to pre- or post-synaptic changes.

Levamisole is a cholinergic agonist, which acts by inactivating levamisole-sensitive postsynaptic acetylcholine receptors (Locke et al., 2008). If a genetic mutation has caused a RIC phenotype in response to aldicarb treatment, this phenotype could be caused by a change at the pre- or post-synaptic membranes at a cholinergic NMJ. If the gene has caused a change in the number of levamisole-sensitive receptors, this will cause a phenotype with both aldicarb and levamisole. If the gene affects acetylcholine at the presynaptic level, no difference in phenotype will be seen compared to N2 worms, when worms are treated with levamisole.

1.13 Sodium Valproate

Sodium valproate, also known as valproic acid (VPA) was first synthesized in 1882 as an analogue of valeric acid (Terbach et al., 2011). In 1962 it was found to have anticonvulsant and mood-stabilizing properties, leading it to be a prime drug for the treatment of epilepsy. Currently VPA is also used to treat some cases of bipolar disorder and neuropathic pain, as well as migraines. It has also been shown to have anti-cancer properties – for example it has been shown to enhance growth arrest and apoptosis of chronic myeloid leukemia cells (Morotti et al., 2006). Its mechanism of action is debated and many different roles have been discussed.

Due to its value in the medical field, a lot of research has been undertaken to work out the mechanism behind the drug's action. It is thought to act via the GABAergic pathway, increasing the concentration of GABA in the brain by multiple mechanisms – for example by increasing the activity of glutamate decarboxylase and inhibiting GABA

aminotransferase (Lloyd, 2013). VPA has also been proposed to inhibit voltage-gated sodium channels and T-type calcium channels (Lloyd, 2013). However many of these early studies are disputed, as they might not be valid at the levels of therapeutic doses used in humans. VPA has also been reported to decrease aspartate levels in nerve terminals in the hippocampus (Morland, Nordengen, & Gundersen, 2012). Aspartate is an excitatory transmitter, and thus decreasing the levels decreases excitatory neurotransmission.

VPA has been reported to have neuroprotective effects, due to its anti-oxidant properties (Christian et al., 2012). The term "neuroprotective" means that the drug has properties that protect nerves against damage due to reduced supply of oxygen and/or glucose. VPA has been shown to reduce brain damage in a model of cerebral ischemia in rats, via modulation of caspases (Christian et al., 2012; Ren, Leng, Jeong, Leeds, & Chuang, 2004). Treatment has also been reported to affect both neuronal plasticity and neurite outgrowth (Yuan et al., 2001). VPA has been shown to activate the ERK signaling pathway, leading to activation of MEK, c-Fos and Gap-43 (Yuan et al., 2001). Gap-43 is known to be important for neuronal plasticity, and c-Fos is used as an indirect marker for neuronal activity (Bullitt, 1990). By generating *in vitro* and *in vivo* models, VPA has been shown to promote the outgrowth of neurites, which is dependent on MEK (10, 58). VPA has also been used in combination with antipsychotic medications to treat schizophrenia (Tseng et al., 2016). Interestingly, certain proteins implicated in schizophrenia, such as Disrupted-In-Schizophrenia-1 (DISC1) and Dysbindin-1, when mutated also affect neurite outgrowth (Ma, Fei, Fu, Ren, & Wang, 2011; Miyoshi et al., 2003), suggesting neurite outgrowth is an important factor for how VPA ameliorates the symptoms of schizophrenia.

VPA has also been shown to be a histone deacetylase (HDAC) inhibitor (Göttlicher et al., 2002). This role is thought to be independent of the role VPA plays in preventing seizures, though few experiments delineating this have been carried out. Specifically VPA is a class 1 HDAC inhibitor, which causes the proteosomal degradation of HDAC2 (Kramer et al., 2003). HDAC inhibition leads to a shift towards acetylation, leading to hyper-acetylated histone cores. This regulates the expression of genes such as the transcription factor AP-1. HDAC inhibition by VPA is thought to at least partially explain the ability of VPA to induce the differentiation of certain carcinoma cells, and reduce tumour growth and metastases in animal models (Kramer et al., 2003).

Despite the benefits of VPA, it has also been shown to be teratogenic, meaning that it can be harmful to foetuses in pregnant mothers. VPA has also been shown to cause neurodevelopmental defects, such as reduced cognitive function and learning difficulties, as well as major congenital malformations such as heart abnormalities and neural tube defects (8, 58). This implies that VPA has a detrimental developmental role. Mechanisms proposed to explain this teratogenicity include VPA accumulation in the foetus, as well as VPA acting to increase the level of reactive oxygen species (ROS). In the first three months of pregnancy the foetus is able to metabolize VPA to produce ROS, but has a poor anti-oxidant defense system (Lloyd, 2013). This means ROS can damage proteins, lipids and DNA in the foetus, causing abnormalities. However other pathways have also been proposed to cause teratogenicity, such as VPA causing decreased levels of folate (Lloyd, 2013). Folate is essential for foetal development and maturation. HDAC inhibition has also been proposed to cause teratogenicity. This shows the complexity of VPA

mechanisms, and how a simpler organism needs to be used to better understand this drug's effect.

Due to the huge number of possible mechanism of how VPA treatment leads to an anti-convulsant effect, *C. elegans* have been used due to the ease of studying their neurobiology.

1.14 VPA in *C. elegans*

VPA has been studied in *C. elegans* and has been found to cause interesting phenotypes. Firstly, it has been proposed to extend *C. elegans* lifespan. 6mM VPA treatment resulted in an increase in the mean adult lifespan from 16.2 to 21.9 days (Evason, Collins, Huang, Hughes, & Kornfeld, 2008), and also reduced the age-related decline of body movement. In this paper they also used the drug valpromide (VPD), which is an aliphatic amide analogue that shares the anticonvulsant activity of VPA. However it cannot inhibit HDACs, meaning that VPD can be used to determine whether an effect is due to inhibition of HDACs. Both VPA and VPD caused the lifespan increase as well as an increase in dauer formation.

VPA has also been proposed to ameliorate dopaminergic neurodegeneration in *C. elegans*. In a worm model of Parkinson's disease, where alpha-synuclein is overexpressed, VPA attenuated degeneration of the six anterior dopaminergic neurons of the worm, increasing from 11.2% to 72% of worms exhibiting non-degenerated neurons at day 7 (Kautu, Carrasquilla, Hicks, Caldwell, & Caldwell, 2013). As in humans, they propose that VPA activates ERK-MAPK signaling, increasing the number of neurites. Knocking down

the worm ortholog of ERK, mpk-1, and its upstream regulator, mek-2, prevented this protective effect (Kautu et al., 2013). This suggests that certain roles of VPA; such as in the ERK-MAPK pathway may be conserved between species. Hence through the study of the role of VPA in *C. elegans,* more could be understood about the conserved role VPA plays at the synapse.

1.15 Protein Interaction Networks

In 1941 the theory of one gene encoding one enzyme to have one function was proposed (Beadle & Tatum, 1941). Since then this has been disproven, and it has been shown that proteins rarely act in isolation. Instead they often act as parts of complex molecular machines or pathways, and enzymes can have multiple binding partners to affect different functions in a cell.

Graph theory has been used to explain properties of protein-protein interaction (PPI) networks (Vidal, Cusick, & Barabási, 2011). Firstly PPI networks are scale-free, meaning that there are a few highly connected nodes connected to many nodes with few interaction partners. Nodes with a high number of interaction partners are known as hubs. This feature of connections between nodes is known as connectivity. PPI networks are also described, as "small-world" as the average distance between any two proteins is small. For this reason, random perturbations of genes (which are not hubs) does not greatly affect the integrity of the network, whereas mutation of hubs can disrupt the network to such a degree that the network is fragmented into smaller sub-networks (Vidal et al., 2011).

Another feature of networks is that they are modular, meaning that clusters of proteins form where there are large numbers of interactions between themselves, but they have fewer connections between the clusters. These modules can be used to uncover proteins with novel functions, by the principle of "guilt-by-association" (Oliver, 2000) – i.e. if a protein is found in a module containing proteins involved in e.g. transcription, it is likely that this protein also plays a role in this process.

As well as connectivity, another topological measure used in networks is betweenness centrality (Joy, Brock, Ingber, & Huang, 2005). Betweenness centrality is a measure of how many times a protein is found in the shortest path between two other proteins. Proteins can have high betweenness but a low connectivity, i.e. hubs do not necessarily have high betweenness values. Betweenness is a good measure of the level of control a node may have within a network. If perturbed, large effects on the integrity of networks are seen. Figure 1.4 shows a simple schematic to illustrate betweenness – protein A is in the shortest path between protein C and proteins G, F, E, D and B. However in the top panel, A has high connectivity but in the bottom panel node A forms fewer connections and thus does not have a high connectivity.

It is important to note that in the original PPI maps, neither alternatively spliced isoforms, nor post-translational modifications were considered. For a complete interaction map, these must be taken into account. An example of this is an autism spliceform network that was created, which used all clonable isoforms of autism candidate genes to find novel interaction partners. A third of the interactions found in their screens were from the non-reference isoforms of the genes (Corominas et al., 2014). Furthermore with over 200 different types of post-translational modification (Jensen, 2006), post-translational

modifications and protein-protein interactions can often be functionally linked. For example phosphorylation of one protein can modulate its binding to several other proteins. Both of these examples highlight how traditional interaction networks can be increased using extra data like isoforms.

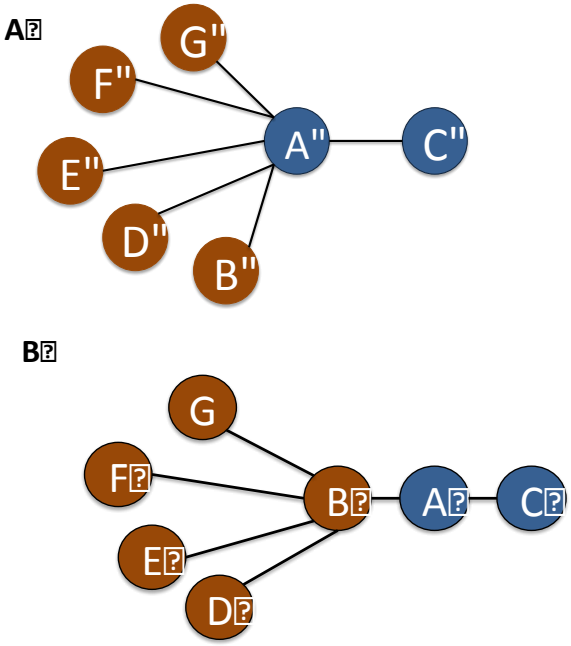

Figure 1.4 **Simple networks to show the concepts of connectivity and betweenness. A. Protein A is in the shortest path between proteins** C and proteins G, F, E, D and B. It has high connectivity (as it is connected to all six other nodes) and high betweenness. B. Although protein A is still in the shortest path between proteins C and proteins G, F, E, D and B, it is only directly connected to B and C. Thus it has a high betweenness but lower connectivity.

1.16 PPI Methods

To study the interactions of proteins, multiple techniques have been developed, some of which show direct or binary interactions, others indirect or co-complex interactions. Direct assays include yeast-two-hybrid (Y2H) assays, and protein complementation assays. Indirect assays are those such as affinity-purification mass spectrometry and co-immunoprecipitation experiments. These are described as indirect as it is not known in these assays whether a binding partner is attached directly or via another protein to the bait of interest.

1.16.1 Y2H techniques

In 1989, the Y2H system was initially published as a novel system to investigate binary PPI (Fields & Song, 1989). In the classical yeast-two-hybrid system, the bait of interest is attached via its N-terminus to the DNA binding domain (DB), and the prey via its N-terminus to the activation domain (AD) of the transcription factor Gal4 (Fields & Song, 1989). When the bait and prey interact, Gal4 becomes functionally active and reporter genes are transcribed. Examples of reporter genes are biosynthetic genes such as ADE2 and HIS3, which enable yeast to grow on plates lacking adenine and histidine, respectively, and enzymatic genes such as lacZ, which enzymatically degrades X-Gal to produce a blue pigment visible on plates. Other reporter genes such as AUR1-C, which causes the yeast to be resistant to the antibiotic aureobasidin A, have also been used and shown to cause lower background activity. Figure 1.5 shows the principle of the classical Y2H assay.

There are two general types of yeast-two-hybrid assay – targeted array based matings and library screenings. In a targeted Y2H mating assay both bait and prey genes are known and are simply screened against each other. Alternatively, library screening can be carried out in yeast to find novel interaction partners of the bait of interest. In general high complexity whole cDNA libraries are used, which contain cDNA extracted from a certain tissue/organism, e.g. foetal brain.

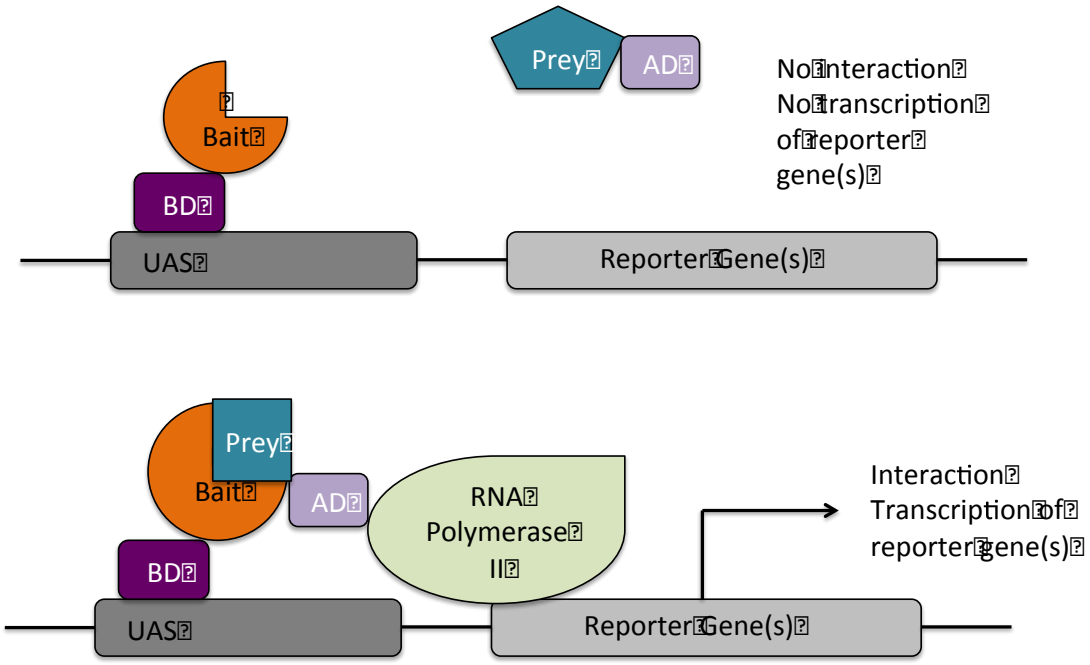

Figure 1.5 – **The molecular basis of the classic yeast two hybrid methodology.** The bait of interest is fused to the DNA binding domain (BD) and the prey to the activation domain (AD) of the Gal4 transcription factor. A. Bait and prey do not interact, meaning there is no transcription of reporter genes. This means, for example, that the yeast will not grow on media lacking adenine or histidine (the genes ADE2 and HIS3 are common reporter genes). B. The bait and prey proteins interact. The BD and AD are in close enough proximity to function as the whole transcription factor, recruiting RNA polymerase II, and transcribing reporter genes. This means that for example if ADE2 and HIS3 are two of the reporter genes transcribed, the yeast will be able to grow on plates lacking adenine and histidine, indicating an interaction has occurred.

Advantages of a targeted matrix mating approach are that the position and identity of both bait and prey is known, therefore no sequencing is needed to interpret positive interactions. This process can also be automated relatively easily. However, library screening is advantageous when novel PPI are sought, and the protocol requires little hands-on time and technical skill. Other advantages of Y2H are that is it relatively simple and easy to scale up into a high-throughput assay. It is non-biased, and is a method of detecting binary interactions. It is also far cheaper than other techniques for elucidating interaction partners, such as mass spectrometry.

One limitation of library screening however is that, as the prey binding the bait of interest is not pre-defined, colony PCR analysis must be performed, as well as sequencing in order

to determine the identity of the potential interaction partner. This makes library screening both time-consuming and expensive. Other limitations of the classic Y2H system are that as the genes are being expressed in yeast, post-translational modifications and the folding of the protein may not be the same in yeast as in humans, leading to different protein interaction profiles. Also, tagging of the proteins with bait or prey domains may lead to incorrect folding. Another limitation is that the data is qualitative, i.e. the strength of an interaction cannot be measured. Furthermore the classical system only works for soluble proteins – they must be able to reach the nucleus for an interaction to occur. Transmembrane proteins have issues as they may not be targeted to the nucleus, and so cannot activate the reporter genes, or the hydrophobic transmembrane domains may misfold preventing binding to appropriate interaction partners. This last limitation can be overcome by using a second-generation Y2H technique, known as membrane-based yeast-two hybrid (MYTH).

1.16.2 MYTH

In 2002 Igor Stagljar published a paper describing the MYTH system, which allowed the examination of full-length membrane proteins in a Y2H system (Stagljar & Fields, 2002). This system utilizes ubiquitin, which can be split into two fragments – N-terminal NubI, and C-terminal Cub domains. These two fragments can spontaneously re-associate to form pseudoubiquitin. To prevent this, NubI is mutated at isoleucine 13 to a glycine residue, making a fragment known as NubG. The Cub domain is attached via the N- or C-terminus to the membrane protein of interest – this is the bait protein in the system. The Cub domain is also fused to the reporter molecule, consisting of *E. coli* DB, LexA and

Herpes simplex AD, VP16. The prey can be cytosolic or membrane bound, and is fused to the NubG domain of ubiquitin.

Upon bait and prey interaction, the two ubiquitin fragments are brought into close enough proximity to re-associate and form pseudoubiquitin. Ubiquitin-specific proteases can then hydrolyze the amide bond between ubiquitin and the protein, leading to release of the LexA-VP16 transcription factor tag, which is then free to translocate to the nucleus, where it activates transcription of reporter genes. Like in the traditional yeast-two-hybrid, these are typically ADE2, HIS3 and lacZ. Figure 1.6 shows the principle of the MYTH system.

Advantages of the MYTH system are that it allows the screening of full-length membrane proteins. MYTH can also be used in library screens, where cDNA libraries are generated with N- or C-terminal NubG fusions. This means the MYTH is relatively easy to scale up and can be used as a discovery tool to elucidate novel interaction partners for proteins that have previously been tricky to study.

Limitations of MYTH are that the N- and/or C-terminal domain of the bait protein must be localized in the cytosol for the system to work. It is also limited to looking at binary interactions, as in most cases, an indirect interaction of bait and prey would not allow pseudoubiquitin formation, as they would not be in close enough proximity.

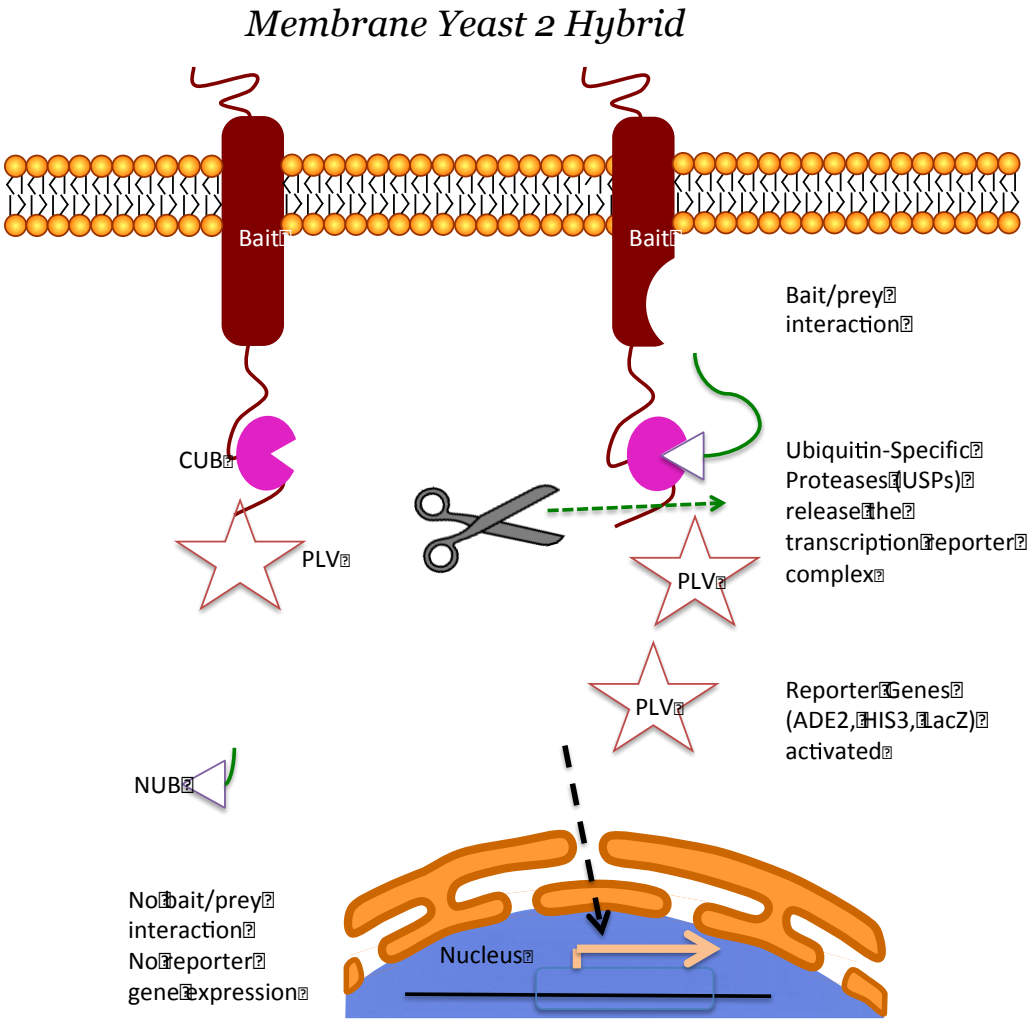

Figure 1.6 – **Membrane Based Yeast Two Hybrid concept**. The transmembrane bait protein of interest is fused to the C-terminal Cub domain of ubiquitin, which is tagged with the *E. coli* DNA binding domain (DB), LexA and the Herpes simplex activation domain (AD) known as PLV. The prey protein can be cytosolic or transmembrane and is tagged with the N-terminal Nub domain (with I13G mutation). When bait and prey interact, psedoubiquitin is formed. Ubiquitin specific proteases release the PLV, which then translocates to the nucleus to activate the transcription of reporter genes such as ADE2, HIS3 and lacZ.

The main aim of this work was to identify novel effectors of synaptic function, whose human orthologs may play a role in neurological/neurodegenerative diseases. As mentioned in 1.2.3, wild type nor worms classically hypersensitive to RNAi have neuronal sensitivity to RNAi, due to a lack of sid-1 neuronal expression (Winston, Molodowitch, & Hunter, 2002). This means that in RNAi screens previously performed (Sieburth et al., 2005), false negatives may have occurred when genes were inefficiently knocked down

in neurons. Also, expression throughout the worm could have lead to lethality, whereas specificity to neurons may prevent this phenotype. For this reason we decided to carry out high throughput aldicarb screening in the sid-1 expressing *Tu3311* strain, which displayed higher efficiency and specificity of neuronal RNAi. Gene lists to test can be generated by generating aldicarb one-step networks, and prioritizing based on connectivity and betweenness.

Previously a microarray was carried out on wild type worms following VPA treatment (Munasinghe, 2015). A bespoke clustering algorithm was used to identify genes that exhibited similar dose dependent changes in gene expression. To complement this data a one-step known RIC/HIC protein interaction network (as described in chapter 3) was generated, and sub-networks generated containing novel genes to test in the high throughput aldicarb screens. Furthermore, by looking at the human orthologs of hits from these screens, candidates can then be identified to use in yeast two-hybrid library screening, in order to identify novel interaction partners, which may themselves play a role in neurological/neurodegenerative diseases.

1.17 Aims of the study

The overall aim of the PhD work carried out were:

- To elucidate novel effectors of synaptic function in *C. elegans*
- To investigate the effect of sodium VPA on C. elegans synaptic function
- To investigate protein-protein interaction networks of human orthologs of a selection of novel synaptic effectors.

Chapter 2 – Materials and Methods

2.1 Reagents

All chemicals were obtained from Sigma-Aldrich (Poole, UK), unless otherwise stated.

2.2 Worm strains

All C. elegans strains used in this study were obtained from the CGC (University of Minnesota). These include: N2, *Tu3311 (unc119p::YFP + unc119p::Sid-1), rrf-3(NL2039), Tu3335 (lin15b X [*unc-119p::YFP + unc-119p::sid-1 + mec-6p::mec-6], *LT186 (sma-6(WK7) II), CB904 (unc-38(e264) I), MT6490 (unc-25(n2569)III), VC1433 (unc-25(ok1901)III), RB1044 (Y47H9C.2(ok990) I), VC2067 (C43H6.7(gk985) X), VC2039 (F59C6.2(gk1013) I), VC108(H32C10(gk36) IV)* and *VC918(dhhc-14(ok10232) X)*. OP50 was also obtained from the CGC.

All worms were maintained at 20^0C as previously described (Brenner, 1974). For *C. elegans* maintenance, worms were grown in 55mm petri dishes containing 10ml NGM (0.3% NaCl (w/v), 0.25% peptone (Formedium) and 2% agar (Bioagar, Biogene)). After autoclaving and immediately prior to pouring the plates, 1mM $CaCl_2$, 1mM $MgS0_4$, 5µg/ml cholesterol and 25mM KH_2PO_4 were added to the media. Detail relating to the preparation of the stock solutions is shown in Table 2.1. After pouring, plates were dried in a sterile hood, and 55µl of OP50 *E. coli* was added to each plate. These were then incubated at 37°C overnight prior to use.

	Grams/100 ml dH_2O	Sterilization Procedure	Storage	Stock Concentration
$CaCl_2$	11.09	Sterile Filter	Room Temperature	1M (in dH_2O)
$MgSO_4$	12.04	Autoclave	Room Temperature	1M (in dH_2O)
KH_2PO_4	13.61	Autoclave	Room Temperature	1M (in dH_2O)
Cholesterol	0.5 (in 100% ethanol)	Sterile Filter	4°C	5mg/ml

Table 2.1 – Chemicals required to make NGM media.

For long term storage at -80°C, a plate containing worms that had been starved for at least one day was washed with 3ml of autoclaved M9 buffer (0.3% KH_2PO_4, 0.6% Na_2HPO_4, 0.5% NaCl, 1mM $MgSO_4$ in dH_2O). 3ml of freezing buffer (0.585% NaCl, 0.68% KH_2PO_4, 30% glycerol, 3mM $MgSO_4$, in dH2O, autoclaved) was then added and 1ml aliquots of resuspended worms were then pipetted into 1.8ml cryovials and stored at -80**°C** .

2.3 RNAi feeding

Although *Tu3311 and Tu3335* strains have enhanced neuronal RNAi, optimization of previously published protocols was required to carry out optimal RNAi knockdowns (Kamath & Ahringer, 2003; Sieburth et al., 2005; Vashlishan et al., 2008).

All *E. coli* expressing the dsRNA were obtained from the *C. elegans* Vidal library (Rual, 2004) or were created and gifted by Matt Edmonds and Alan Morgan (University of Liverpool) as indicated. *E. coli* were streaked out onto Luria Broth (LB, 10% NaCl, 10% tryptone, 5% yeast extract, 10% agar) plates supplemented with 100µg/ml ampicillin. After overnight incubation at 37°C, multiple colonies were picked into 3ml Luria Broth supplemented with 100µg/ml ampicillin. Subcultures were incubated at 37**°C** with shaking overnight. Glycerols were made of all constructs by adding 80µl of 80% glycerol (w/v) to 200µl subculture. These were vortexed briefly before storing at -80**°C** .

1M IPTG stock solutions were made up in dH_2O and stored in the dark at -20°C. 6 well (Cytooone CC7672-7506) dishes were used firstly to make 4mM IPTG (Melford) feeding NGM plates, as described above in section 2.2, with the additional supplementation of 100µg/ml ampicillin and 4mM IPTG. Once dry these plates were seeded with 40µl of bacterial stock. Dishes were then left in the dark for 48 hours, before picking 2 gravid worms to each plate. After 4 days these were treated with bleach and transferred onto 48-hr seeded 55cm plates (Greiner) in triplicate (Stiernagle, 2006) to synchronize/age-match the worms.

2.4 Pharmacological Assays

1mM aldicarb (dissolved in 70% ethanol) was used for all aldicarb-sensitivity assays, and each experiment was carried out blind in triplicate. The assay was run in a similar manner to previously published protocols (Timothy R Mahoney, Luo, & Nonet, 2006). In brief, between 20-30 young gravid worms were picked from plates containing F2 non-starved worms. For full-time course assays, paralysis of worms on aldicarb plates was assessed

every 20-40 minutes, until all worms were paralyzed, as judged by prodding the head or tail with a metal wire. Prior to high throughput assays, the rate of paralysis of the control (*Tu3311* fed with L440 dsRNA-expressing bacteria) was assessed. From this an appropriate time point for the high throughput assays was chosen. For some assays, paralysis was assessed at two time points, but this made the assay slower throughput and paralysis was often found to be very similar at both time points. Therefore, unless otherwise indicated, only one time point between 100-160 minutes was used in all high throughput assays. Any worms that crawled off the plate or underwent vulval prolapse were discarded from the assay.

Other pharmacological assays performed in this study are summarized in Table 2.2. In levamisole, valproate, and drug combination assays, only paralysis were measured as described above for aldicarb assays.

Drug	Solvent	Stock Concentration	Final Concentration
Aldicarb	70% Ethanol	1M	1mM
Sodium Valproate	dH_2O	50mg/ml	15mM
Levamisole	M9 buffer	100mM	0.1mM

Table 2.2 – Concentrations and solvents used for the pharmacological agents used in *C. elegans* studies.

2.5 Statistical Analysis

For the high throughput aldicarb-sensitivity assays, the mean number of paralyzed worms for the test sample was compared against the mean number of paralyzed worms for the negative control (measured for each repeat) using an unpaired t-test. A change in the rate of paralysis was deemed to be significant if the p value was less than 0.05. To plot the increase/decrease in paralysis, the differences of the test samples against the negative control were normalized to the mean of the control and plotted as a positive/negative percentage.

2.5 Data visualization and network generation

Cytoscape is a program commonly used to visualize protein interaction networks. The free online tool also enables the integration of gene-expression data. In this study the version of Cytoscape used was either 2.8.3 or 3.2.1, as specified in the legends of the respective tables. Interaction networks are presented in the form of nodes (proteins), and edges (interactions). For the *C. elegans* networks, databases used to access primary data were Wormnet version 3 (Cho et al., 2014), the CCSB Worm Interactome 8 yeast-2-hybrid data sets (Simonis et al., 2009) and the worm version of BioGrid. Wormnet integrates data from *C. elegans* as well as known interlogs in humans, mouse, *S. cerevisiae* and *D. melanoganster.* Cytoscape was also used to calculate the connectivity and betweenness scores of nodes in selected worm sub-networks.

For the PAT interaction networks, data was integrated from BioGrid, as well as an in-house human interactome (created by Russell Hyde and Jonathan Woodsmith), which curates data from several other databases – Human Protein Reference Database (HPRD) (Keshava Prasad et al., 2009), IntAct (Kerrien et al., 2007), Molecular Interaction

Database (MINT) (Licata et al., 2012), as well as an older version of Biogrid. For fly interactions, the Drosophila Interactions Database (DroID) was used. Wormnet (Cho et al., 2014) was mined for *C. elegans* interactions. For the human PAT family, as well as BioGrid, the human CCSB (Rolland et al., 2014), Human Integrated Protein-Protein Interaction rEference (HIPPIE) (Schaefer et al., 2012) and Bioplex (Huttlin et al., 2015) were incorporated. All genetic interactions were removed, and all ID's were converted into human orthologs.

2.6 Microarray Analysis

Although the single-channel Agilent microarray was carried out in 2012 (Munasinghe, 2015), we re-analyzed the data from the array to identify sets of genes that were significantly up- or down-regulated in response to valproic acid treatment. Full detail of this analysis can be found in Chapter 4. The programming language known as R was used for the microarray analysis. R is a language widely used in data science for data analysis and visualization. The open-source language was used in the program RStudio, which is a graphical user interface that provides a simple way to develop R scripts and visualize results, such as heatmaps.

DAVID (Database for Annotation, Visualisation and Integrated Discovery) and Ingenuity Pathway Analysis were used to analyse enrichment of genes. *C. elegans* genes were also converted to their human orthologs, before inputting into the databases, as Ingenuity is not 100% compatible with worms.

2.7 Cloning of constructs

Standard gateway cloning procedures were used to clone human DHHC enzymes according to the manufacturer's instructions (Invitrogen). PCR primers were designed to amplify the gene of interest, with flanking *attB* sequences. Primers were synthesized by Life Technologies (ThermoFisher). The attB sequences used in the primer design are as follows:

Forward: gaattcacaagtttgtacaaaaaagcaggctggATG

Reverse (without a stop codon): gtcgaccactttgtacaagaaagctggGTG

This allows recombination into the pDONR223 entry vector to create a gateway-entry clone with *attL* sites. The desired gene targets were amplified from either 210ng HeLa cDNA, or from the gene of interest (in a different vector). High Fidelity Hot Start KOD polymerase (Invitrogen) was used to amplify all genes of interest.

To clone the human PAT family members, primers were designed with the attB N-terminal portion and a gene-specific 15bp region. Primers used in this study are shown in Table 2.3.

Gene Symbol	Size (bp)	Primer	Primer Sequence
ZDHHC9	1094	Forward	ATGtctgtgatggtggtgaga
		Reverse (-Stop)	cttctcagcttcagctgc
zDHHC3	899	Forward	ATGcttatccccatccac
		Reverse (-Stop)	gaccacatactggtacgg
zDHHC4	1034	Forward	ATGgactttctggtcctcttc
		Reverse (-Stop)	ttcttgtttcttcctctc
zDHHC5	2147	Forward	ATGcccgcagagtctggaaag
		Reverse (-Stop)	caccgaaatctcatagg
zDHHC7	1037	Forward	ATGcagccatcaggacacagg
		Reverse (-Stop)	cactgagaactccgggcc
zDHHC16	1131	Forward	ATGcgaggccagcggagcctg
		Reverse (-Stop)	cactgccatcacagaggc

Table 2.3 – Gene specific primer sequences for the human PAT family members successfully cloned.

Mouse PAT family members were transferred from an entry vector (PEF-BOS-HA) into the pDONR223 vector through KOD PCR, BP reactions, transformation and minipreps, as detailed in the following sections.

2.7.1 Proof-reading PCR using high-fidelity KOD enzyme

Constituents used to amplify the PAT family members and add AttB sites are shown in Table 2.4.

Reagent	Final Concentration	µl/reaction
Forward Primer (10µM)	0.5µM	0.5
Reverse Primer (10µM)	0.5µM	0.5

10 x KOD buffer	1x	2.5
MgSO4 (25mM)	15mM	1.5
dNTPs (2mM)	0.2mM	2.5
DNA / cDNA	DNA: 10ng cDNA: 200-250ng	DNA: 1 cDNA:
HSKOD	-	0.5
dH2O	-	Up to 25
Total	25ul	25

Table 2.4 - Mastermix constituents for Hotstart KOD polymerase reactions.

In the PCR machine the cycle used was:

1. 94°C for 2 minutes
2. 94°C for 30 seconds
3. 55°C/60°C/65°C/68°C for 1 minute (dependent on the melting temperature of the primers)
4. 70°C for 30 seconds per kilobase of amplified construct
5. Go to 2. 29 – 39 times. When cloning from cDNA 39 repeats were used. Otherwise 29 repeats occurred.
6. 4°C hold.

2.7.2 Gateway BP reactions

After PCR amplification to add on the *attB* sites, BP reactions were carried out using BP clonase II (Invitrogen), following the reaction scheme shown in Table 2.5

Reagent	**Volume**

PCR amplified product	2µl
pDONR223	100ng
BP Clonase/Buffer Mix	1µl
Water	Up to 5µl
Proteinase K	0.5µl

Table 2.5 – Reaction scheme for BP reaction.

PCR amplified product, pDONR223 and BP Clonase/Buffer mix were mixed in a 1.5ml eppendorf tube before incubating at 25°C for 16 hours. Following this, 0.5µl of proteinase K was added and the mixture was heated at 37**°C** to terminate the reaction.

To check the band size of PCR products, 1% agarose gels were used, where the agarose (Bioline) was melted in 0.5% TBE. After cooling slightly, Sybr-safe (Thermofisher) was added (1:20,000 dilution) to allow DNA visualization and Gels were run at 120V for 40 minutes unless otherwise specified.

2.7.3 Transformation into RecA- bacteria

Following the BP reaction, transformations were carried out into either chemically competent sliver efficiency alpha-select (Bioline), or stellar competent (Clontech) cells. 2µl of BP reaction was transformed into 25µl alpha select or stellar cells. These were incubated on ice for 30 minutes before being heat shocked at 42°C for 45 seconds. Samples were then returned to ice for 30 seconds and 250µl of SOC media was added, and samples were incubated at 37°C, 200rpm for 1hour. 200µl of samples were then spread onto LB (10% tryptone, 10% NaCl, 5% yeast extract, 10% bioagar) with the antibiotic required for construct selection. Antibiotic resistance of the vectors used in this

study are shown in Table 2.6. Plates were incubated overnight at 37°C in a static incubator.

Vector	Antibiotic
pDONR223	Spectinomycin (100ug/ml)
pGBKT7	Kanamycin (50ug/ml)
pAMBV	Kanamycin (50ug/ml)

Table 2.6 – Antibiotic resistances of vectors used.

2.7.4 Bacterial colony PCR

Following transformation, diagnostic PCRs were carried out on a selection of (5-6) colonies to ascertain that the transformation was successful and the construct was present in the bacteria. Table 2.7 shows the mastermix for diagnostic bacterial colony PCRs.

Reagent	Final Concentration	µl/reaction
Forward Primer (10µM)	0.7µM	0.7
Reverse Primer (10µM)	0.7uM	0.7
dNTPs (25mM)	0.625mM	0.25
NH4 buffer (10x)	1x	1
MgCl2 (50mM)	2.25mM	0.4
BioTaq	-	0.05

dH_2O	-	6.9

Table 2.7 – Mastermix for diagnostic bacterial colony PCR.

Samples were kept on ice during preparation. After dispensing 10µl per sample, half of each colony was picked into each tube.

The PCR cycle used when performing diagnostic PCRs is as follows:

1. 95°C for 5 minutes
2. 95°C for 1 minute
3. 55°C/60°C for 1 minute (temperature is dependent on the melting temperature of the primers used)
4. 72°C for 1 minute per kilobase of DNA to amplify
5. Go to 2. 34 times.
6. 72°C for 5 minutes
7. 15°C hold

Following PCR samples were run on 1% agarose gels. Colonies that gave rise to bands of the correct size were picked from the remaining spot on the LB plate into 9ml LB containing appropriate selection antibiotic. These were then incubated overnight at 37°C, shaking at 200rpm. The next day glycerols were made to preserve the constructs. 200µl of subculture and 80µl 80% glycerol (weight/volume) were mixed in a 1.5ml eppendorf, kept on ice for a few minutes, and then transferred to the -80°C freezer.

Minipreps (Wizard) were carried out to extract the DNA from bacteria, as described in the kit manual. Constructs were then sent to GATC Biotech for sequencing.

2.7.5 Matchmaker Gold Construct Generation using Seamless Ligation Cloning Extract

pGBKT7 is a bait vector used in the Matchmaker Gold yeast two hybrid system. To clone into this vector, primers were designed that had flanking pGBKT7 regions, as indicated below.

F: CATGGAGGCCGAATTCatg…*cDNA of interest*

R (with stop): GCAGGTCGACGGATCC…*reverse complement of gene of interest + stop codon*

The pGBKT7 vector was enzymatically cut using BamH1-HF (NEB) and EcoR1-HF (NEB), using the reaction scheme shown in Table 2.7.

Reagent	**Amount**
Uncut pGBKT7	5µg
BamH1-HF	5 units
EcoR1-HF	5 units
CutSmart Buffer	5µl
Water	Up to 50µl

Table 2.8 – Reaction scheme for enzymatic double digest of the pGBKT7 vector

Digests were incubated for 2 hours at 37°C. The enzymes were then denatured at 65°C for 20 minutes. Cut Vectors were run on a 0.8% agarose gel, then gel-extracted and purified (Qiagen).

2.7.6 SLICE extract generation

In order to clone genes into vectors that are not gateway compatible, another method was required. For this, we used a method recently developed in the Motohashi lab (Kyoto, Japan), where they were able to generate bacterial lysates that were capable of carrying out seamless ligation of an insert into an appropriately cut vector (Motohashi, 2015). This is an incredibly cheap and simple methodology, and when compared to the commercial In-fusion seamless-ligation kit, efficiencies were found to be very similar.

The SLICE extract can be created from any strain of bacteria that is RecA(-). Alpha-select cells were used in this case. On the first day 5ml of 2xLB (20% tryptone, 20% NaCl, 10% yeast extract) was inoculated with 5µl of cells, and incubated overnight at 200rpm, 37°C. The culture was then diluted with the addition of 45ml 2xLB, and poured into a 1 litre flask. This was then incubated for around 3 hours, until a 1:10 dilution of the culture gave an optical density reading of 0.3 at 600nm. Cells were harvested by centrifugation at 4300rpm for 20 minutes at 4°C. The supernatant was removed, and the pellet was re-suspended in 50ml ice-cold sterilized water. Cells were then spun down at 4300rpm, 4°C for 10 minutes. the supernatant was again discarded, and the pellet was re-suspended in 1.2ml 3% Triton X-100 (w/v), diluted in 50mM TrisHCl (pH 8.0): For 10ml: 0.5ml 1M TrisHCl, 0.3ml Triton X-100, 9.2ml dH_2O, adjusted to pH 8.0 using 5M HCl or NaOH.
This was then transferred to a 1.5ml eppendorf. The cells were incubated for 10 minutes at room temperature, then spun down at 13,000rpm, 4°C, for 5 minutes. The supernatant was transferred to a fresh eppendorf on ice. One volume of ice cold 80% glycerol was added. The lysate was aliquoted into PCR tubes (50µl per tube), before being snap frozen, and stored at -80°C

SLICE buffer was prepared as shown in Table 2.9 before being sterile filtered. The mixture was aliquoted and stored at -20°C.

Reagent	Stock Concentration	Final Concentration	Volume (ml)
Tris-HCL, pH 7.5	1M	500mM	5
MgCl2	1M	100mM	1
ATP	100mM	10mM	1
DTT	100mM	10mM	1
Water	-	-	2

Table 2.9 – SLICE buffer constituents.

2.7.7 SLICE reactions

To ligate the gene of interest to the cut pGBKT7 vector, SLICE reactions was carried out according to the reaction scheme shown in Table 2.10.

Reagent	Amount
Cut Vector	10ng
PCR amplified gene of interest	30ng
SLICE extract	1µl
SLICE buffer	1µl
Water	Up to 10µl

Table 2.10 – Reaction scheme for SLICE reaction

Reactions were placed in a 37°C heat block for 15 minutes before being transferred to ice. Transformations, diagnostic PCRs and minipreps were then carried out as previously described.

2.8 Y2H Library screening

2.8.1 Constituents/media required for screening

The media required for yeast growth and maintenance is shown in Tables 2.11 to 2.14.

YPAD (500ml)	
D-Glucose (Formedium)	10g
Bioagar (for solid, Biogene)	10g
Peptone (Formedium)	10g
Yeast Extract (Formedium)	5g
Adenine Hemisulphate	0.1g

Table 2.11 – Constituents of YPAD media

SD-X (where X represents the amino acids lacking from the medium, 500ml)	
D-Glucose	10g

Yeast Nitrogen Base without Amino Acids (Formedium)	3.35g
Bioagar (if making solid media)	10g
Appropriate amount of amino acid mixture	See Table 2.11 and 2.12

Table 2.12 – Constituents of yeast selective dropout media.

A/H/L/W/U DropOut (DO)	
Amino Acid	Grams/100L
Arginine	2
Isoleucine	3
Lysine	3
Methionine	2
Phenylalanine	5
Threonine	20
Tyrosine	3
Valine	15
Total (g/L)	0.53

Table 2.13 – Recipe for dropout salts mixture for SD media

SD – X powder mix (for 100L)				
	-L*	-W	-WL	-WLAH
Adenine Hemisulphate (A)	0.6	0.6	0.6	-
Leucine (L)	-	1.0	-	-
Histidine (H)	0.2	0.2	0.2	0.2
Uracil (U)	0.2	0.2	0.2	0.2
A/H/L/W/U DO	5.3	5.3	5.3	5.3
Total g/L	0.63	0.73	0.63	0.57

Table 2.14 – Recipe for selective media amino acid additions.

* Tryptophan (W) is added to the media after autoclaving.

Powders of the amino acids were added to falcon tubes, shielded from the light, and kept at 4°C until needed. When preparing the media, the appropriate mass of powder was added to the other constituents (Table 2.14). Bottles were then filled with 500ml water, and autoclaved.

To clone fragments of constructs, the same flanking pGBKT7 primers were used, but the gene-specific primers were designed so as to only clone the fragment needed.

2.8.2 Preparation of competent yeast cells

Constructs were transformed into the Y2HGold strain (Clontech), as per the Matchmaker gold manual, with a few adjustments. 10ml of YPAD was added to a 50ml falcon tube, and

inoculated with one colony of Y2HGold. The culture was then incubated overnight at 30^0C, shaking at 200-220rpm. 5ml of the overnight culture was then added to a further 45ml YPAD, split into two 50ml tubes, and incubated for 90 minutes at 30^0C, shaking at 200-220rpm. Cultures were centrifuged at 2300rpm for 5 minutes at room temperature. The supernatant was discarded and pellets were re-suspended in 30ml dH_2O. Tubes were then centrifuged again at 2300rpm for 5 minutes, and the supernatant was discarded and pellets were re-suspended in 1.5ml 1.1xTE/LiOAc (for 10ml, 1.1ml 10x TE buffer, 1.1ml 100mM LiOAc, 7.8ml dH_2O), and transferred to 2ml eppendorfs. Eppendorfs were centrifuged at 13000rpm for 15 seconds, and then the pellets were re-suspended in 600ul 1.1xTe/LiOAc. At this point the yeast were ready to be transformed with constructs.

2.8.3 Yeast Transformation

For each set of transformations, a negative control, empty pGBKT7 vector was also carried out to check bait toxicity. To a pre-chilled 1.5ml eppendorf 100ng plasmid DNA (sequenced gene of interest in the pGBKT7 vector, or the negative control) was added, with 5µl of 10mg/ml salmon testes DNA that had been denatured at 95°C for 5 minutes just prior to use. To each tube 50µl of the competent Y2HGold were added and mixed gently. 500µl of PEG/LiOAc (for 5ml, 1ml 50% (w/v) PEG, 1ml LiOAc, 3ml dH_2O) were then added. Samples were then incubated at 30°C for 30 minutes, before the addition of 20µl DMSO. Yeast were then heat shocked by placing them in a water bath set at 42°C for 1 hour to allow the entry of the DNA into the yeast cells. After this incubation, tubes were centrifuged at 13000rpm for 15 seconds, and pellets were re-suspended in 1ml YPAD plus (Clontech), and incubated in a 30°C incubator, shaking at 200-220rpm for 1 hour, to

allow recovery of the yeast cells. Samples were then centrifuged at 13000rpm for 15 seconds, and pellets re-suspended in 1ml 0.9% (w/v) NaCl solution.

100µl of 1/10 and 1/100 dilutions of the empty pGBKT7 transformation were spread onto 90mm –W plates. 100µl of 1/10 and 1/100 dilutions of the gene-pGBKT7 constructs were also spread onto the –W plates, as well as –W plates supplemented with X-Alpha Gal (-W/X) and plates supplemented with both X-Alpha-Gal and Aureobasidin A (-W/X/A). Table 2.15 summarizes the preparation of these two chemicals.

To proceed to the next stage, growth of yeast should occur on the –W plates, blue colonies should appear on the –W/X plates and no yeast should grow when aureobasidin A is added to the media. This is the autoactivation test. If colonies on the gene-pGBKT7 plate appear much smaller than those on the negative control plate, this indicates construct toxicity, negating its use for future experiments.

Constituent	Stock Solution	Solvent	Storage	Working Concentration
Aureobasidin A	500µg/ml	100% Ethanol	4C	200ng/ml
X-alpha-Gal	20mg/ml	Dimethylformamide	-20C	40µg/ml

Table 2.15 – Constituents required for matchmaker library screening – Aureobasidin A and X-alpha Gal. Both are added after the media has been autoclaved.

2.8.4 Matchmaker Gold Yeast Library Screening

The library was performed as described in the Matchmaker manual, with the following differences. Initially bait was grown in 5ml –W, and left shaking at 200rpm for 8 hours. At this point, a further 45ml –W was added, and transferred to a 1L flask. This was then incubated overnight at 30°C, 200rpm.

Clontech's Matchmaker normalized human brain library (Cat Number: 630479) was used to perform library screens. This was amplified in the lab by diluting 500µl of the human brain library stock to a total volume of 7.5ml. This was then pipetted equally onto 50 140mm –L plates, and incubated at 30°C for 3 days. To each plate, 4ml of liquid –L was added and the yeast scraped into a sterile conical flask. A further 1ml of the liquid –L was added to the same plate, and the rest of the yeast was scraped off. The optical density was tested (at 600nm), and glycerol was added to a final percentage of 80%. 1ml aliquots of the library were made, and then stored at -80°C.

To carry out a library screen, after the overnight amplification of bait, the culture was poured into 50ml non-skirted centrifuge tubes and centrifuged at 2300rpm for 5 minutes. The pellets were re-suspended in a combined volume of 1ml 2xYPAD (combine the pellets). An aliquot of the library was defrosted on ice, and 1ml was added to the bait re-suspension. This was then poured onto a 140mm YPAD plate, and incubated at 30°C for 5 hours.

After 5 hours, 4ml of 0.5x YPAD (supplemented with 80µg/ml kanamycin) was pipetted onto the plate, and the yeast scraped off into a sterile 15ml centrifuge tube. 1ml of YPAD was used to scrape the remainder of the yeast into the same tube. 100µl of the 5ml was used to make 1 in 10, 1 in 100, and 1 in 1000 dilutions. The remaining yeast was pipetted

equally between sixteen 140mm –WL plates with aureobasidin A. Plates were incubated for 3-5 days at 30°C. After this, the mating efficiency was calculated as follows:

Mating efficiency = 100 * (colonies on -90mm –WL plate x dilution factor*10)/(colonies on either –L or –W plate, whichever had fewer)

Colonies were picked from the –WL/Aureobasidin A plates, into 100ul 0.9% NaCl, and 2.5µl was spotted onto higher stringency –WLAH/X-alpha-Gal/Aureobasidin A plates. If possible 96 or 2x96 colonies were picked. These plates were then further incubated for 3-5 days at 30°C.

2.8.5 Diagnostic yeast colony PCR

Diagnostic yeast colony PCRs were carried out on all colonies that showed robust growth on the –WLAH/X/A plates, which also turn blue.

For the yeast colony PCR, the primers pGADT7.F and pGADT7.R were used:

pGADT7.F: cgactcactatagggcgagc

pGADT7.R: gatggtgcacgatgcacag

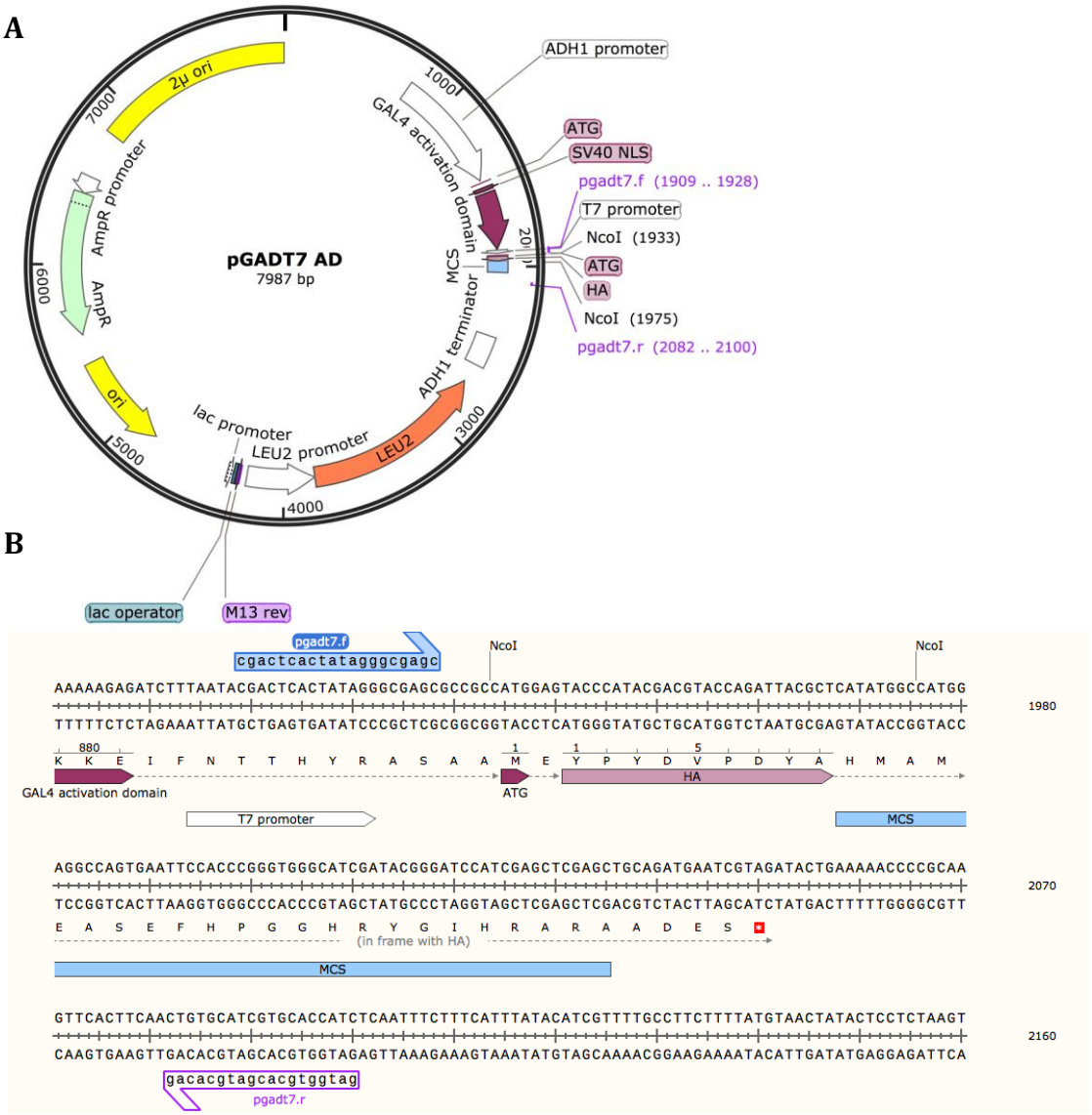

Figure 2.1 – **pGADT7 map.** A. Circular map of pGADT7, generated in Snapgene. B. Region amplified by pGADT7.f and pGADT7.r primers.

These primers amplify the prey, leaving flanking regions to allow recombination back into the pGADT7 vector in the Y187 yeast (see library gap repair section). 3µl of 20mM NaOH was pippetted into each well. Picking colonies into the solution and incubating at

room temperature for 20 minutes leads to yeast lysis. For a 96 well plate, a 120-reaction mastermix was made as shown in Table 2.16 (for one reaction).

Reagent	Start Concentration	End Concentration	Volume (µl)
pGADT7.F	10µM	0.5µM	0.75
pGADT7.R	10µM	0.5µM	0.75
dNTPs	25mM	0.42mM	0.45
$MgCl_2$	50mM	1.5mM	1.5
10 x NH_4 buffer	10x	1x	0.75
DMSO			0.3
BioTaq			0.15
dH_2O			7.35

Table 2.16 – Reaction scheme for diagnostic yeast colony PCR

12µl of mastermix was added to each 3µl of lysed yeast, sealed and run in the PCR machine on the following cycle:

1. 95°C for 5 minutes
2. 95°C for 1 minute
3. 60°C for 1 minute
4. 72°C for 3:30 minutes
5. Go to 2. 39 times
6. 72°C for 5 minutes
7. 15°C hold

1% agarose gels were then used to determine band presence.

2.8.6 Library gap repair

After amplification of interacting prey inserts, PCR products were gap repaired back into the yeast Y187 strain (Clontech). In this process the cut pGADT7 vector and the PCR fragment is transformed into the yeast. A table showing the reaction scheme for digesting pGADT7 is shown in Table 2.17.

Constituent	
Uncut pGADT7	5µg
Nco1	5 units
NEBuffer 3.1	5µl
dH_2O	Up to 50µl

Table 2.17 – Reaction scheme for Nco1 digest of pGADT7

Samples were heated at 37°C for 2 hours, then denatured at 80°C for 20 minutes. As with the pGBKT7 vector digestion, digested pGADT7 was run on a 0.6% agarose gel, then extracted and purified.

The library gap repair process is very different to the protocol recommended by Clontech, who instead carry out 96 well minipreps on colonies that grow on the –WLAH/X/A plates. The adaptation used in this study is a far cheaper and a well-established method previously used in other Y2H studies in the Sanderson lab (Markson et al., 2009).

10ml of YPAD is inoculated with Y187 yeast (that had been freshly streaked out onto YPAD plates), and incubated overnight at 30°C, shaking at 200rpm. The following day, 5ml was discarded, and 45ml YPAD added and split into two 50ml falcons. The subculture

was incubated at 30**°C** , 200rpm for 90 minutes. The Y187 was then centrifuged at 2300rpm for 5 minutes to spin down the yeast. The pellets were combined and re-suspended in 30ml dH_2O. Cultures were then centrifuged at 2300rpm for 5 minutes, and the pellet was re-suspended in 1.5ml 1.1xTe/LiOAc (Transformation solution 1, Table 2.23). The culture was then transferred to a 2ml eppendorf and centrifuged at 13000rpm for 15 seconds. The pellet was then re-suspended in the mastermix shown in Table 2.18.

Constituent	
50% PEG 3350	1110µl
1M LiOAc	167µl
10ng/ml Salmon testes DNA (denatured at 95c for 5 minutes)	40µl
pGADT7 cut with Nco1	60ng
dH_2O	170µl

Table 2.18 – Mastermix for library gap repair

The pellet was re-suspended in the mastermix then 8µl of cell re-suspension was pipetted per well in a 96 well plate. 4µl of the YCPCR products (section 2.8.4) were then added to these wells and mixed by pipetting. The plates were sealed and the following program was used on the PCR machine:

1. 30°C for 30 minutes
2. 42°C for 25 minutes
3. 30°C for 1 minute

The transformed yeast was then pipetted onto a 140mm –L agar plate to select for the prey (i.e. the interacting protein to the protein of interest). 4µl was pipetted at a time to

prevent spots from merging. Plates were then incubated for 3-5 days at 30°C, before photographing each plate and recording the number of colonies per spot.

2.8.7 Reconfirmation of prey against the original bait

After the prey has been selected for and is in the Y187 yeast, a standard yeast mating was performed to test whether the prey will bind to the bait of interest. As well as testing the prey against the bait of interest, the prey is also mated against empty-PGBKT7 (in the Y2HGold yeast strain) as a negative control. Several colonies from each spot of the library gap repair plate were picked into 25µl of dH_2O. 4ul of each re-suspension was then pipetted onto two 140mm plates containing YPAD, then left to dry. Bait (either the gene of interest or the empty vector) were then re-suspended in 500µl dH_2O, and 4µl of the re-suspension were pipetted onto each spot, so that one plate contains the mating of the gene of interest and the prey, and the other is the empty vector against the prey. Plates were then incubated for 24 hours at 30°C.

Yeast was then replicated from the YPAD plates to –WL plates using standard velvet replication procedure (Fields & Song, 1989) and -WL plates were incubated for 48 hours, and then the replication process was repeated onto –WLAH/X/A and –WLAH plates. These plates were then incubated for 1 – 2 weeks at 30**°C** , and pictures were taken every few days.

The expected results after this time are shown in Table 2.19. If colonies appear on the –WLAH/X/A plate where the bait is the empty vector, these are false positives and should not be sent for sequencing.

Genuine Positive Hit			
	Agar plate	2mm colonies?	Colour
Bait + candidate prey	-WL/X	Yes	Blue
Bait + candidate prey	-WLAH/X/AbA	Yes	Blue
Empty pGBKT7 + candidate prey	-WL/X	Yes	White
Empty pGBKT7 + candidate prey	-WLAH/X/AbA	No	N/A

False Positive			
	Agar plate	2mm colonies?	Colour
Bait + candidate prey	-WL/X	Yes	Blue
Bait + candidate prey	-WLAH/X/AbA	Yes	Blue
Empty pGBKT7 + candidate prey	-WL/X	Yes	Blue
Empty pGBKT7 + candidate prey	-WLAH/X/AbA	Yes	Blue

Table 2.19 – Summary of results expected for a positive and false positive result

Prey hits were then sent for sequencing using the pGADT7.F sequencing primer (Section 2.8.4).

2.8.8 MYTH construct generation

To use constructs in the membrane-based yeast-two-hybrid library system, the pAMBV vector was used. This is a C-terminally tagged vector.

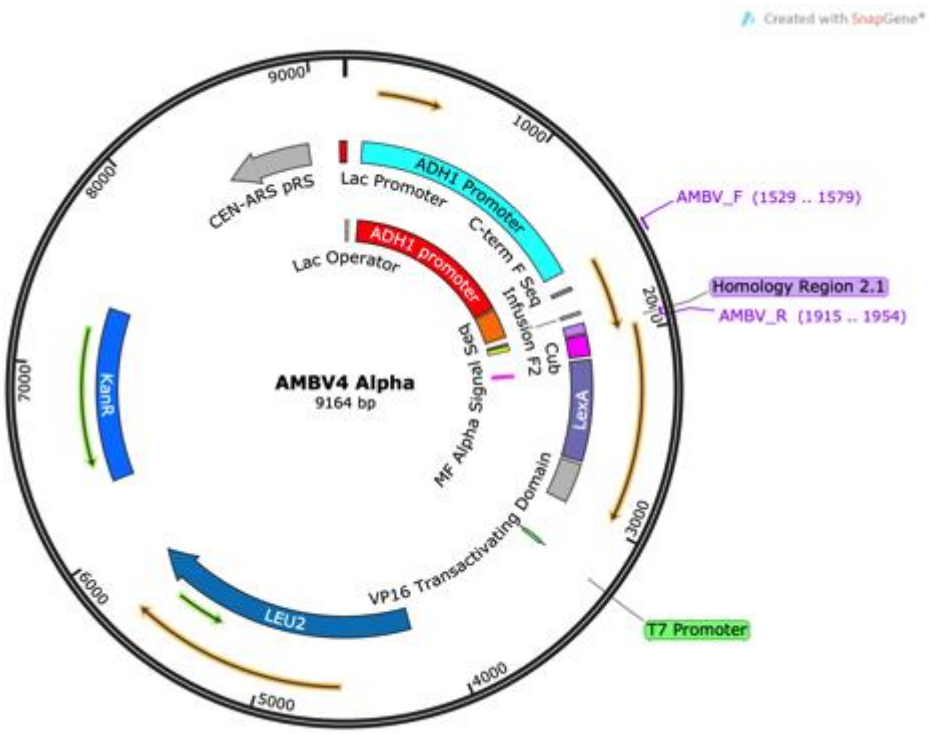

Figure 2.2 – **AMBV4 vector map generated using Snapgene.**

Primers were designed to have the following flanking regions:

Forward: tgcacaatatttcaagctataccaagcatacaatcaactccaagcaacacaATG…*cDNA of interest*

Reverse: tcgacggtatcgataagcttgatatcgaattcctgcagat…*Reverse complement of Gene of interest without stop codon*

Following the flanking regions, primers were designed to have 15bp gene specific regions of mouse PAT family members. The primers used are shown in Table 2.20.

Gene Symbol	Size (bp)	Primer	Primer Sequence
zDHHC8	2288	Forward	ATGccccgcagccccgggacg
		Reverse (-Stop)	caccgagatttcatacgt
zDHHC13	1868	Forward	ATGgagggcccgggcctgggc
		Reverse (-Stop)	tacagagcgaaggactttc
zDHHC17	1898	Forward	ATGaccaagatggcggacggc
		Reverse (-Stop)	cacaagctggtacccaga

Table 2.20 - Gene specific primer sequences for mouse DHHC family members of interest.

Following successful KOD polymerase chain reaction to add these flanking ends to cDNAs of interest, gap repairs were carried out to recombine the insert into the pAMBV vector using the yeast native recombination enzymes. For this, the pAMBV vector was digested by Nco1. Table 2.18 shows the reaction scheme. Samples were heated at 37c for 2 hours, and then Nco1 was denatured by heating the sample at 80**°C** for 20 minutes.

Constituent	
Uncut pAMBV	5µg
Nco1	5 units
Cutsmart Buffer	5µl
dH_2O	Up to 50µl

Table 2.21 – Reaction scheme for pAMBV digest

2.8.9 Gap repair of gene of interest and pAMBV into Nmy51

The yeast strain Nmy51 was used for all transformations in the MYTH system. One colony of freshly streaked out Nmy51 was inoculated in 5ml YPAD broth, and incubated overnight shaking at 200rpm, 30°C. The 5ml culture was then diluted by a further 45ml

YPAD, and transferred to two 50ml falcons. These were grown at 30**°C** , 200rpm, for a further 3 to 4 hours, until the OD was between 0.6 and 0.8.

Cultures were centrifuged at 1100g for 5 minutes, and the supernatant was discarded. Each pellet was re-suspended in 25ml dH_2O, and then centrifugation was repeated as above. Pellets were re-suspended in 1ml dH_2O.

For transformations and gap repairs, a solution containing PEG and LiOAc was required, and this transformation solution is shown in Table 2.22.

Constituent	**Volume**
50% PEG 3350	2.4ml
1M LiOAc	300µl
10ng/ml Salmon testes DNA (denatured at 95°C for 5 minutes)	50µl

Table 2.22 – Transformation solution for gap repair and transformation of baits into Nmy51

For each gap repair reaction, 100µl of the yeast cells, 300µl of the transformation solution (Table 2.22), 50fmol of PCR product and 200fmol of pAMBV vector were combined in a 1.5ml eppendorf.

Reactions were mixed and incubated at 30**°C** for 30 minutes, followed by heat shock at 42**°C** for one hour. The solutions were then centrifuged at 1100g for 5 minutes, and the pellets re-suspended in 200µl dH_2O. These were then plated onto selective –L plates, and incubated at 30°C for 2-4 days until colonies appear.

DNA was isolated from the transformants by inoculating single colonies into 4ml –L broth and incubating overnight at 200rpm, 30°C. DNA was then extracted from the subcultures using a commercial miniprep kit, following the manufacturer's instructions with one extra step, where after initial re-suspension a small volume of lime soda beads were added to the re-suspension to break yeast cell walls and enhance extraction of DNA. As these minipreps give a low yield of DNA, they were transformed back into alpha-select cells as described previously. Diagnostic PCRs, minipreps and sequencing were then carried out following successful transformation.

As these minipreps give a low yield of DNA, they were transformed back into alpha-select cells as described previously. Diagnostic PCRs, minipreps and sequencing were then carried out following successful transformation.

Once sequenced, constructs were transformed back into the Nmy51 strain. The method is the same as for gap repair, except 200fmol of the insert and vector were transformed into the yeast. Following successful transformation, several colonies were picked into 800ul –L media. These were incubated overnight at 200rpm, 30°C. 200ul 80% glycerol was then added, and the mixtures vortexed and frozen at -80°C.

2.8.10 Bait Autoactivation – NubGI Test

As with the matchmaker system, baits need to be checked for autoactivation prior to their use in a library screen. However, the autoactivation test used in MYTH is very different to that in the Matchmaker. In this system, two proteins Ost1 and Fur4 are fused to NubG and NubI fragments. NubI is the native N-terminal fragment of ubiquitin, and will

spontaneously bind Cub fragments, even if the bait and prey themselves do not interact. For a bait to pass this test (dependent on it's subcellular localization), it must interact with only the NubI constructs.

To carry out the NubGI test, the bait was freshly streaked out onto –L plates. Colonies were then picked into 5ml of –L broth, and incubated overnight at 30°C, 200rpm. 45ml of –L was added, and the culture grown until the OD was between 0.6 and 0.8. At this stage, transformation was carried out as previously. Cultures were centrifuged at 1100g for 5 minutes, and supernatant was discarded. Each pellet was re-suspended in 25ml dH_2O. Centrifugation was repeated as above, and pellets are re-suspended in 1ml dH_2O.
100µl of yeast, 300µl of transformation solution (Table 2.22), and 150ng of each of the NubGI constructs (Ost1-NubI, Ost1-NubG, Fur4-NubI, Fur4-NubG) were combined in an eppendorf. These were incubated at 30°C for 30 minutes, followed by 42**°C** for 1 hour. Samples were centrifuged at 1100g for 5 minutes, then re-suspended in 200µl dH_2O, and plated onto double selection (-WL) plates. Plates were incubated for 3-5 days, until 1-2mm colonies had grown. On –WL plates, colonies should appear when both NubG and NubI constructs have been transformed, as the plate selects for the presence (not binding) of bait and prey. Single colonies of each transformed bait and NubGI control were re-suspended in 0.9% NaCl, and ten-fold dilutions are made (0, 1:10, 1:100 and 1:1000). These were spotted onto –WL plates, as well as –WLH and –WLAH plates, which had varying concentrations of 3-aminotrizol (3AT) in the media (from 0 to 10mM 3AT). 3AT limits bait expression, and if auto-activation can be prevented by using higher concentrations of 3AT. Plates were grown for 2-4 days and assessed for growth.

2.8.11 MYTH library screening

The MYTH library system is different to that of the Matchmaker because a DNA library is transformed into the bait-transformed yeast, whereas in Matchmaker, a mating-based screen is used.

To begin, 2-3 colonies of the bait construct (in Nmy51) were inoculated into 10ml –L broth, and incubated for 8 hours, shaking at 200rpm, 30°C. The 10ml starter culture was then added to 100ml –L in a 1 litre flask, and grown overnight at 30°C, 200rpm. The next day, the optical density of the culture was measured, and the amount of culture required for 30 units calculated. This volume of culture was centrifuged at 1100g for 5 minutes. The pellet was re-suspended in 10ml pre-warmed 2 x YPAD and transferred to a 1 litre flask. The falcon tube was rinsed with a further 40ml 2xYPAD, and then another 150ml 2xYPAD was added to the flask.

Yeast were grown at 200rpm, 30°C until the OD reaches 0.6 (between 3 and 5 hours).
The two solutions are required for transformation, shown in Tables 2.23.

Once grown the yeast cultures were divided into four 50ml falcons, and centrifuged at 700g for 5 minutes. Pellets were re-suspended in 30ml dH_2O, and the centrifugation step repeated. 1ml of Transformation Solution I (Table 2.23) was then added to each tube, and the pellets re-suspended and transferred to a 1.5ml eppendorf. Yeast were then centrifuged at 1100g for 5 minutes, and re-suspended in 600µl Transformation solution I (Table 2.23).

Constituent	Volume
Transformation Solution I	
10xTE buffer	1.1ml
1M LiOAc	1.1ml
dH2O	7.8ml
Transformation Solution II	
1M LiOAc	1.5ml
10 x TE buffer	1.5ml
50% PEG	12ml

Table 2.23 Transformation solutions required for MYTH library screening

To each of four 50ml falcons, 600µl yeast cells, 2.5ml of Transformation solution II, 20µl 10mg/ml salmon testes DNA (denatured at 95c for 5 minutes), and 8µg of the foetal brain Nub-library were added. Each falcon was vortexed for 1 minute, then incubated at 30°C for 45 minutes, vortexing every 15 minutes. 160µl DMSO was then added to each tube, and incubated at 42°C for 20 minutes. Following this, samples were centrifuged at 1100g for 5 minutes, and each pellet was re-suspended in 3ml 2xYPAD. Samples were then pooled. Cultures were centrifuged at 1100g for 5 minutes, and the pellet was re-suspended in 4.9ml 0.9% NaCl. 100ul of the re-suspension was used to make 1:10, 1:100 and 1:1000 dilutions, and these dilutions were plated onto 90mm –WL plates, and grown at 30**°C** for 3-4 days.

200ul aliquots of the remaining 4.8ml cell suspension were pipetted onto –WLAH plates (with 3AT as needed), and grown for 3-5 days. If colonies grow, they were picked into 100ul 0.9% NaCl, and 2.5ul volumes were spotted onto –WLAH (with 3AT if needed) + X-

gal plates (Table 2.24). Colonies that show robust growth and turn blue can be used for further analysis.

Constituent	
-WLAH media	450ml
X-Gal (100mg/ml)	400ul
Sodium Phosphate solution (7g sodium phosphate dibasic and 3g sodium phosphate monobasic in 100ml dH2O)	50ml

Table 2.24 – Recipe for X-gal selection plates in MYTH library screening. X-gal and sodium phosphate are added after the –WLAH media has been autoclaved and cooled to around 50c.

2.8.12 Diagnostic yeast colony PCR of MYTH interaction partners

For the yeast colony PCRs of prey that underwent robust growth and turned blue on the –WLAH/X-Gal plates, the NubGX seq F and pPR3N seq R primers were used:

NubGX seq F: GTCGAAAATTCAAGACAAGG

pPR3N seq R: AAGCGTGACATAACTAATTAC

Yeast were lysed in a 96 well format by pipetting 3µl of 20mM NaOH into each well of a 96 well plate. Yeast colonies were then picked into the solution and incubated at room temperature for 20 minutes. For a 96 well plate, a 120-reaction mastermix was made. The reaction scheme is as shown in Table 2.25 (for one reaction).

Reagent	Start Concentration	End Concentration	Volume (µl)
NubGX Seq F	10µM	0.5µM	0.75
NubGX Seq R	10µM	0.5µM	0.75
dNTPs	25mM	0.42mM	0.45
MgCl2	50mM	1.5mM	1.5
10 x NH4 buffer	10x	1x	0.75
DMSO			0.3
BioTaq			0.15
dH2O			7.35

Table 2.25 – Reaction scheme for diagnostic yeast colony PCR in the MYTH library screening

12µl of mastermix was added to each 3µl of lysed yeast, sealed and run in the PCR machine on the following cycle:

1. 95°C for 5 minutes
2. 95°C for 1 minute
3. 60°C for 1 minute
4. 72°C for 3:30 minutes
5. Go to 2. 39 times
6. 72°C for 5 minutes
7. 15°C hold

1% agarose gels were then used to determine band presence.

2.8.13 Gap repair of MYTH prey yeast colony PCR fragments into the pPR3N vector

The yeast colony PCR fragments obtained as described in section 2.8.13 were then gap repaired back into the prey pPR3N vector, which had been digested with Sfi1 (Table 2.26).

Constituent	
Uncut pPR3N	5ug
Sfi1	5 units
Cutsmart Buffer (10x)	5ul
dH_2O	Up to 50ul

Table 2.26 – Digestion Reaction Scheme of the MYTH pPR3N vector

Samples were incubated for 2 hours at 50**°C** , then run on a 0.6% agarose gel and extracted as per the manufacturer's protocol.

5ml of YPAD is inoculated with a single colony of Nmy51 yeast (that had been freshly streaked out onto YPAD plates), and incubated overnight at 30°C, shaking at 200rpm. The following day, 5ml was discarded, 45ml YPAD added and the optical density was checked and diluted to 0.15. The culture was then incubated at 30°C, 200rpm for four to five hours, until the optical density reached 0.6. Once this optical density was reached, the culture was centrifuged at 700g for 5 minutes to spin down the yeast, and the pellet the re-suspended in 25ml dH_2O. The culture was then centrifuged at 2300rpm for 5 minutes, and the supernatant removed. In a 2ml tube the mastermix shown in Table 2.27 was made, which is enough for 96 reactions. The mixture was vortexed, and then used to re-suspend the pellet.

Constituent	
50% PEG 3350	1110µl
1M LiOAc	167µl
10ng/ml Salmon testes DNA (denatured at 95c for 5 minutes)	40µl
dH2O	170µl

Table 2.27 – Mastermix for library gap repair of MYTH prey fragments.

The mixture was vortexed, and then used to re-suspend the pellet.

To a 1.5ml eppendorf, 8µl of yeast per reaction was added (for 96 reactions this would be 768µl), 5ng of the original bait/reaction (for 96 reactions this would be 480ng) and 5ng of the pPR3N (digested with Sfi1). 8µl of this suspension was pipetted per well in a 96 well plate (or PCR tube). 2-4µl of the YCPCR products (section 2.8.13) were then added to these wells and mixed by pipetting. The plates were sealed and the following program was used on the PCR machine:

1. 30°C for 30 minutes
2. 42°C for 25 minutes
3. 30°C for 1 minute

The transformed yeast was then spotted onto a 140mm plate filled with solid –WL agar, 3-4µl at a time (allowing the spots to dry before spotting on top). Plates were then incubated for 3 days at 30°C, before being photographed and the number of colonies per spot recorded.

3-4 colonies of each spot were then re-suspended in 20µl dH_2O, and spotted onto –WLAH (with the 3AT concentration used in the library screen), and –WLAH/X-Gal (with the 3AT concentration used in the library screen). The plates were then incubated for 2-3 days at 30°C and pictures were taken after this time.

2.8.14 Yeast colony PCR for MYTH prey sequencing

Yeast that underwent robust growth on the –WLAH and –WLAH/X-Gal plates (section 2.8.14), and had strong yeast colony PCR bands (section 2.8.13) were picked, and re-grown for 3-4 days.

Each freshly grown colony was picked into 10ul 20mM NaOH, and incubated at 99°C for 10 minutes. The reaction scheme for the MiFi Polymerase PCR cycle is shown in Table 2.28.

Reagent	**Start Concentration**	**End Concentration**	**Volume (µl)**
NubGX Seq F	10µM	0.4µM	1.2
NubGX Seq R	10µM	0.4µM	1.2
5x Buffer	5x	1x	6
MiFi polymerase			1.2
Yeast			2
dH_2O			18.4

Table 2.28 – MiFi Polymerase PCR mastermix (for one reaction)

Samples were then run in the PCR machine on the following cycle:

1. 95°C for 2 minutes
2. 95°C for 15 seconds
3. 55°C for 15 seconds
4. 72°C for 1 minute 45 seconds
5. Back to step 2. 30 times.
6. 4°C hold.

5µl of the reaction was then run on 1% agarose gel to check for prey presence. The rest of the reaction mixture (25µl) was sent for sequencing with the NubGX seq F primer.

Chapter 3 – Elucidating novel effectors of synaptic function using connectivity and betweenness centrality

3.1 Abstract

Understanding the complex machinery underpinning synaptic function is necessary to better elucidate the pathophysiology of a wide range of neurological disorders, from autism to schizophrenia and Alzheimer's disease. *C. elegans* are an ideal model organism to use to elucidate these factors due to the high coverage of their physical and functional interactome, the relative ease of RNAi mediated knockdown of target genes and the ability to assess subtle changes in synaptic function via the aldicarb-sensitivity assay. Initially, we used two network-based criteria to identify potential novel regulators of synaptic function or plasticity, based on connectivity and betweenness scores in phenotypically defined aldicarb one-step protein interaction networks.

Many proteins in the one-step aldicarb network were found to have a high number of interaction partners that were known to cause an aldicarb phenotype, as well as having a high betweenness centrality in the aldicarb and synaptic transmission one-step network. In total 37 novel candidate proteins were common between the two methods of network analysis, with 33 and 30 nodes being identified in the connectivity and betweenness screens, respectively. Following aldicarb-sensitivity assays, a total of 28 genes were found to cause a significant change in the rate of paralysis. 8 of these were shared between the datasets, with 11 and 8 genes were elucidated to cause a significant shift in the rate of paralysis in the connectivity and betweenness screens, respectively. Nodes with human orthologs were identified and chosen for further analysis. Significantly, only the human orthologs of 7 genes found in both datasets, 1 gene found specifically in the betweenness dataset, and 4 genes found in the connectivity dataset were in the current synaptomeDB, and the majority of these proteins are predicted to

have a postsynaptic distribution. From this data a subset of potential novel regulators of synaptic efficacy were selected.

3.2 Introduction

3.2.1 Network based methods to elucidate effectors of synaptic function

As previously discussed (see Introduction), many studies into the genes affecting neuronal function have already been carried out in *C. elegans,* Large-scale RNAi screens were carried out in worms hypersensitive to RNAi, which elucidated 185 genes that decreased acetylcholine secretion, and 90 genes that regulated GABA neurotransmission (Sieburth et al., 2005; Vashlishan et al., 2008). However the worm strains used were not neuronally sensitive to RNAi due to the lack of Sid-1 expression, and thus genes expressed neuron-specifically may not have been knocked down efficiently. In addition, even if neuronal knockdown did occur, it is possible that knockdown in the muscles of the worm may counteract any phenotype, and deletion of genes with essential developmental roles may result in lethality before neuronal effects could be analyzed. For this reason we chose to perform screens in a strain of *C. elegans* with a higher neuronal sensitivity to RNAi.

To identify novel effectors without performing unbiased global RNAi screens we adopted network based approaches that offer the potential to logically prioritize candidates to be tested. Previous studies show that connectivity, betweenness and the principle of "guilt by association" are important properties in biological networks (Oliver, 2000). Therefore, the construction and analysis of functional/phenotypic networks may logically provide a mechanism of capturing as yet untested components of common phenotypic processes.

Applying the principle of guilt by association, proteins that are highly connected to proteins known to cause a RIC or HIC phenotype are more likely to also cause the same phenotype. This property is known as connectivity. Connectivity values for all nodes in the network were simply defined by how many proteins with a known aldicarb-sensitivity phenotype a currently untested protein interacts with. Another algorithm that can be used to prioritize functionally relevant proteins within a network is "betweenness centrality", which reflects how many times a given protein is in the shortest path between two other proteins. By ranking the betweenness of the one-step interacting proteins, those of higher betweenness again have the potential to have a greater functional impact, which in this study would be to cause an aldicarb phenotype when expression was suppressed.

In order to test these principles, a higher-throughout aldicarb methodology was required. Traditionally full time course aldicarb experiments are carried out. However, this approach significantly restricts the number of candidate genes/proteins that can be tested, due to the need to check the worm's paralysis every 30 minutes, and inherent day-to-day variability, meaning that comparative experiments should ideally be carried out on the same day. Therefore, to make the assay higher throughput, we experimentally defined one or two time points when any changes in aldicarb-sensitivity should be detected.

3.2.2 Aims

The aims of this chapter were to:

- Optimize the aldicarb-sensitivity assay on the neurosensitive *Tu3311* strain.

- Generate a *C. elegans* one-step network using genes already known to cause an aldicarb-sensitivity assay as the core nodes.
- Generate lists of novel proteins with highest connectivity and betweenness relative to known aldicarb-sensitivity proteins
- Carry out high-throughput aldicarb-sensitivity screens following knockdown of identified highest connectivity and betweenness genes.

3.3 Results

3.3.1 Optimization of higher-throughput aldicarb-sensitivity assays

As aldicarb-sensitivity assays are inherently subjective to significant day-to-day variability, the assay was optimized so that it could be used in a reproducible high-throughput manner, in combination with RNAi feeding.

Initially wild-type (N2) worms were tested for aldicarb-sensitivity to 1mM aldicarb, as this was the most commonly used drug concentration used in previous publications. However, in these papers large discrepancies are seen in the average times that N2 worms take to paralyze. For this reason standard assay conditions were required to limit these differences. A detailed protocol is described in the Methods section, however, in brief, drying aldicarb plates in a sterile hood for 20 minutes gave the most consistent results, and were very different from plates dried for different time periods. Furthermore, unlike some protocols, bacteria were not seeded onto plates. This meant that if worms crawled off the plate, they were discounted from the experiment. This is also the case if worms underwent vulval prolapse. The effect of storing the plates at 4°C or room

temperature overnight was also tested, as well as the age of the worms used in the experiments (data not shown). It is vital to note that all assays for one experiment were carried out on the same day – Figure 3.1 shows two aldicarb assays where N2 worms had been treated with 1mM aldicarb on separate occasions. The results reveal a large difference between the two experiments, possibly due to the age or health of the worms, or variability in the batch of the aldicarb used.

3.3.2 RNAi optimization

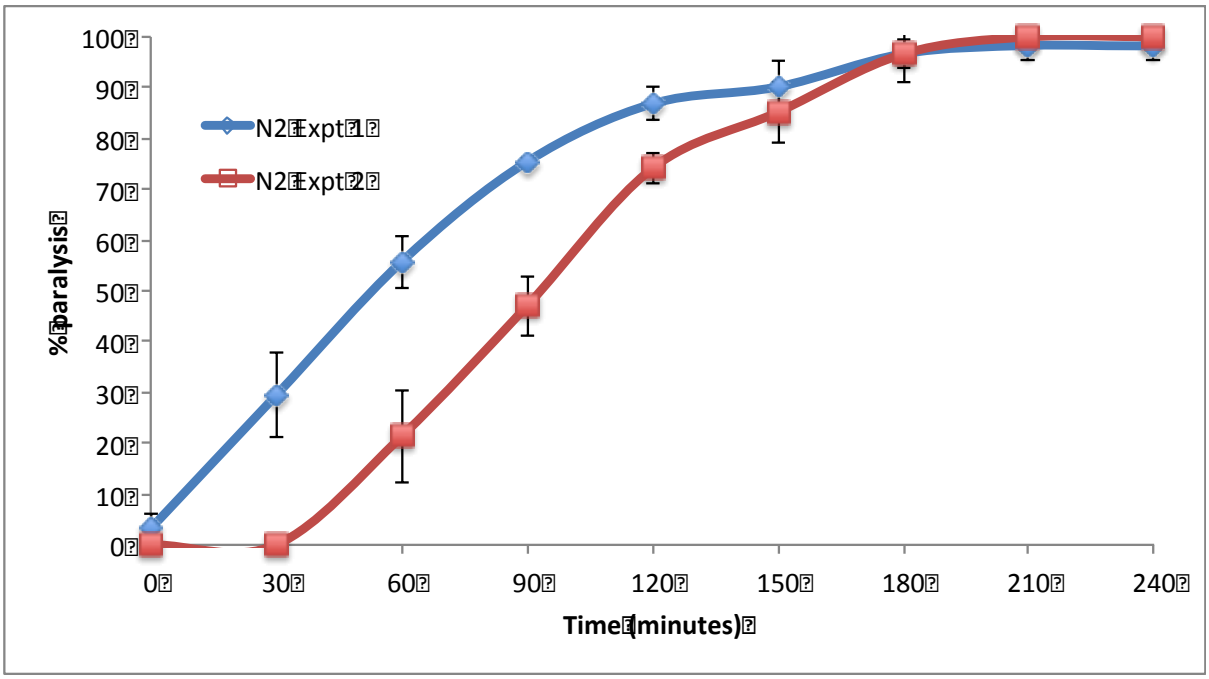

Figure 3.1 - Experiment to show day-to-day variability in aldicarb assays. In each replicate experiment 20 worms were picked onto 1mM aldicarb plates, the numbers of paralysed worms were counted every 30 minutes, and the percentage of paralysis calculated and plotted. Although efforts were made to directly replicate assay conditions significant day-to-day variability can be seen. For this reason all comparative aldicarb assays were carried out on the same day. In each case assays were performed in triplicate (N=3) and error bars represent the standard deviation.

After optimizing the aldicarb assay with wild-type worms, the Sid-1 mutant worm strains (*Tu3311* and *Tu3335*) were tested using the aldicarb assay, as these strains would be used for RNAi experiments. These strains express the double-stranded RNA channel Sid-1 under the control of the Unc-119 promoter. This ensures that Sid-1 is pan-neuronally expressed, which should enhance the uptake of dsRNA into neurons. Significantly, compared to N2 worms, both *Tu3311* and *Tu3335* showed a RIC phenotype (Figures 3.2 and 3.3). *Tu3335* is known to have an additional mutation in mec-6, which is known to cause effects on mechanosensation. For this reason there is a possibility that the mec-6

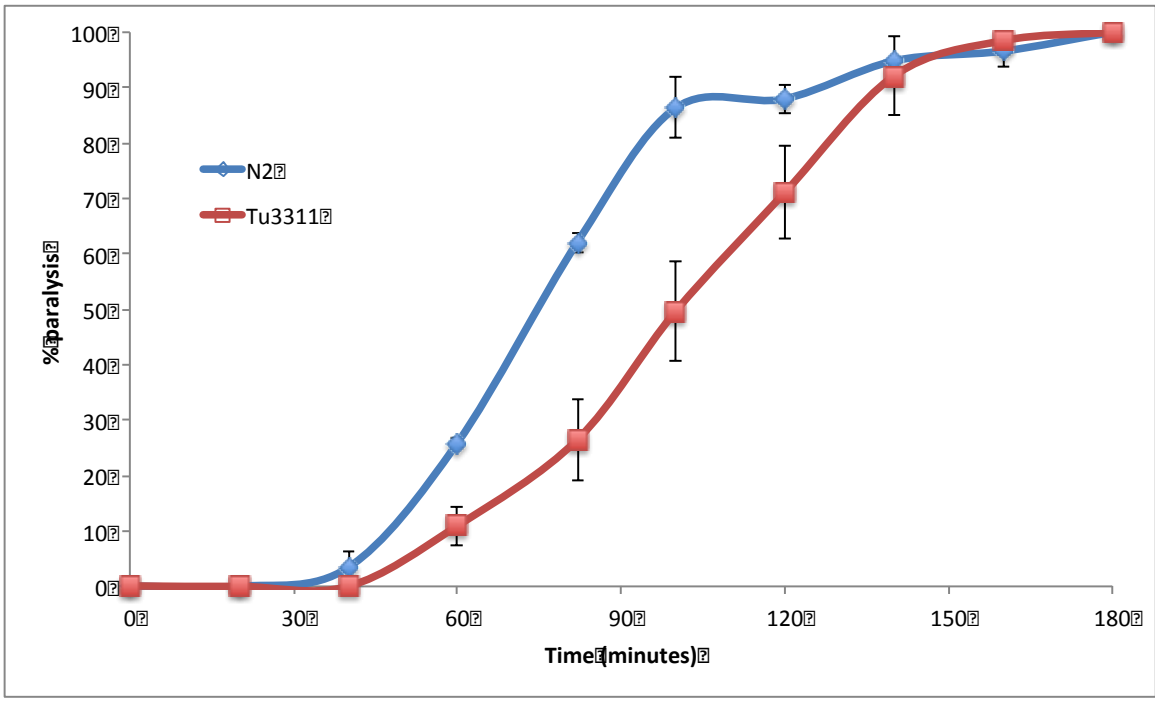

Figure 3.2 - The Tu3311 worm strain exhibits an inherent RIC phenotype compared to N2 worms. In each case, three sets of 20 worms were picked onto 1mM aldicarb plates and paralysis of worms on each plate was measured every 20 minutes. The percentage of paralyzed worms at each time point were then calculated and plotted. N=3. Error bars represent standard deviation.

mutation could interfere with changes in aldicarb-sensitivity following gene knockdown. *Tu3311* therefore was the strain selected for use in these higher throughput RNAi screens.

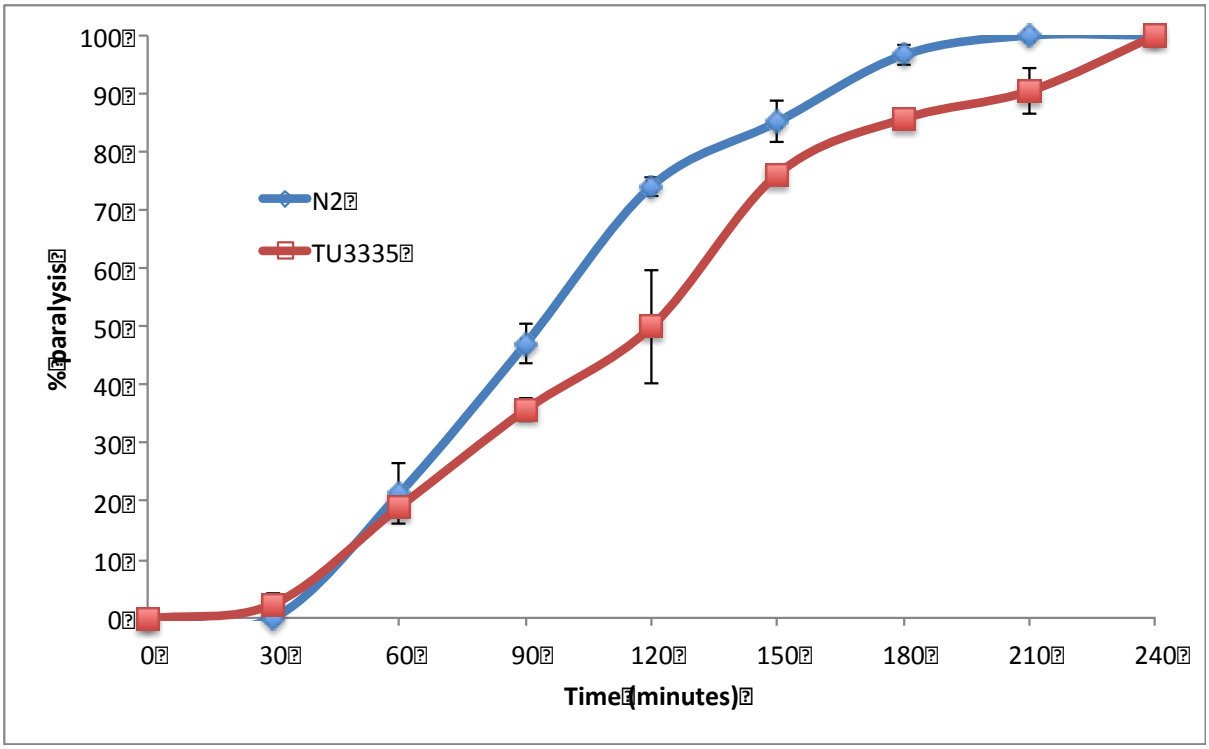

Figure 3.3 - **The Tu3335 worm strain shows a mild RIC phenotype when compared to wild type N2 worms**. Three sets of 20 worms for each strain were picked onto 1mM aldicarb plates and paralysis of worms on each plate was measured every 30 minutes. The percentage of paralyzed worms at each time point were then calculated and plotted. N=3. Error bars represent standard deviation.

As the *Tu3311* strain exhibited an inherent RIC phenotype it was important to first test whether additional RIC changes could be detected in *Tu3311* worms. To address this issue, the observed rate of paralysis in the *Tu3311* (Sid-1 mutant) strain was compared to that of the *rrf-3* mutant strain (*NL2099*), which has enhanced sensitivity of RNAi throughout the worm. There was no significant difference in rate of paralysis observed between *Tu3311* and *rrf-3*. However, *Tu3335* was found to have a slightly HIC phenotype compared to these strains (Figure 3.4). Significantly, this data suggests that there is little difference between the synaptic functions of each of the strains before RNAi knockdown.

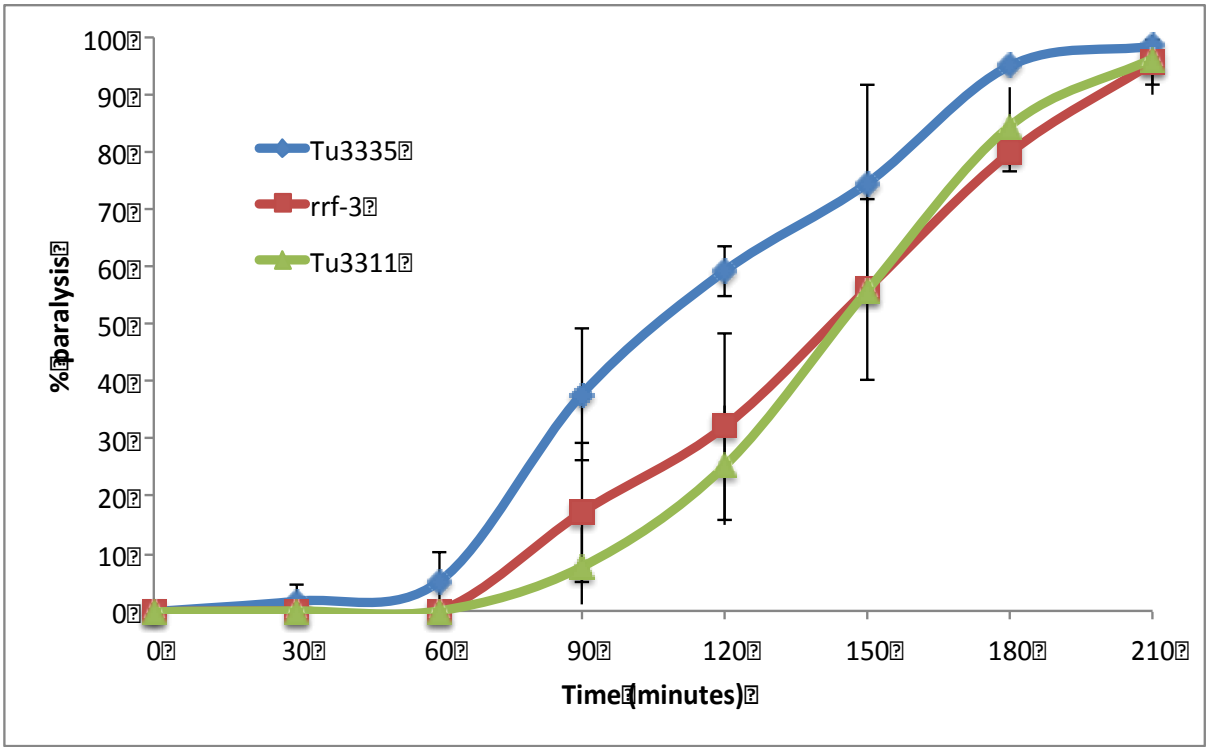

Figure 3.4 - **Tu3311 and rrf-3 show comparable rates of aldicarb-induced paralysis although the Tu3335 strain appears to be marginally more sensitive.** All assays were carried out in triplicate (N=3) as described in Figures 3.2 and 3.3. Error bars represent standard deviation.

As rab-3 is known to cause a characteristic RIC shift when knocked down or mutated in *C. elegans,* this genetic knockdown was used as a positive control for RNAi efficacy and to test whether additional RIC changes could be detected in Tu3311 worms. The rab-3 knockdown in *Tu3311* was tested, and the predicted RIC phenotype was observed (Figure 3.5), after optimizing assay conditions by increasing the IPTG concentration in feeding plates to 4mM, and performing paralysis assays on second-generation (F2) worms. Egl-30 is another gene that is known to cause a RIC phenotype. An example of *Tu3311* knockdown with egl-30 can be seen in Figure 3.6, and rab-3 knockdown in *rrf-3* in Figure 3.7. Although RIC phenotypes were seen in both Tu3311 and rrf-3 strains, the *Tu3311* gave a more consistent phenotype in our hands. This in combination with the neuronal restriction of RNAi sensitivity in the Tu3311 strain led to the selection of Tu3311 worms

as the preferred strain for subsequent large-scale assays. *Tu3335* was also tested as a potential host strain for systematic aldicarb sensitivity assays. Interestingly, the Tu3335 strain showed an even greater RIC shift following rab-3 knockdown (Figure 3.8). However, due to the issues of altered motility in this strain a decision was made to perform planned high throughput screens in the Tu3311 strain and reserve the Tu3335 strain, to retest borderline positive candidates observed in the Tu3311 strain.

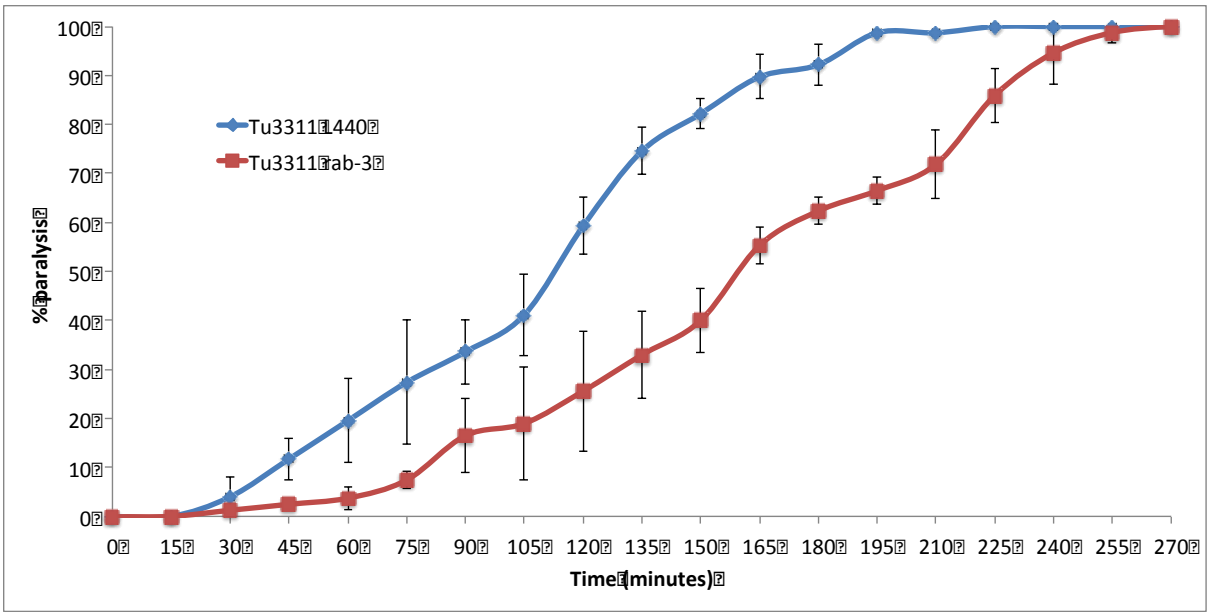

Figure 3.5 **- Rab-3 induced RIC phenotypes can still be detected in Tu3311 neuro-sensitive worms.** To assess whether additional RIC phenotypes could be detected in the Tu3311strain of worms, which have an inherent mild RIC phenotype. TU3311 worms were picked onto 4mM IPTG feeding plates seeded with bacteria containing either a rab-3 dsRNA vector (know RIC positive) or an empty L440 dsRNA vector control. Following gene knockdown as described in materials and methods, F2 generation worms were picked onto 1mM aldicarb plates and the relative rate of paralysis was periodically measured over a 270-minute period. In each case, assays were performed in triplicate (n=3) and error bars represent standard deviation

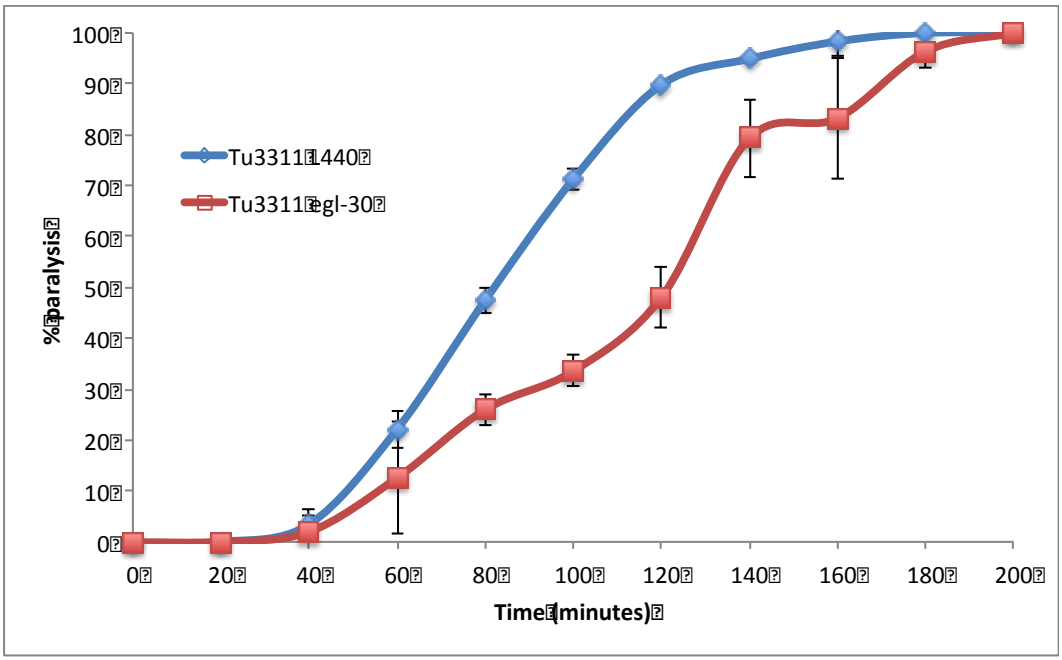

Figure 3.6 - **Egl-30 induced RIC phenotypes can still be detected in Tu3311 neuro-sensitive worms.** To assess whether additional RIC phenotypes could be detected in the Tu3311strain of worms, which have an inherent mild RIC phenotype. Egl-30 and control RNAi knockdown assays were performed prior to aldicarb sensitivity assays as described for Figure 3.5 The relative rate of paralysis was periodically measured over 200 minutes. In each case, assays were performed in triplicate (n=3) and error bars represent standard deviation.

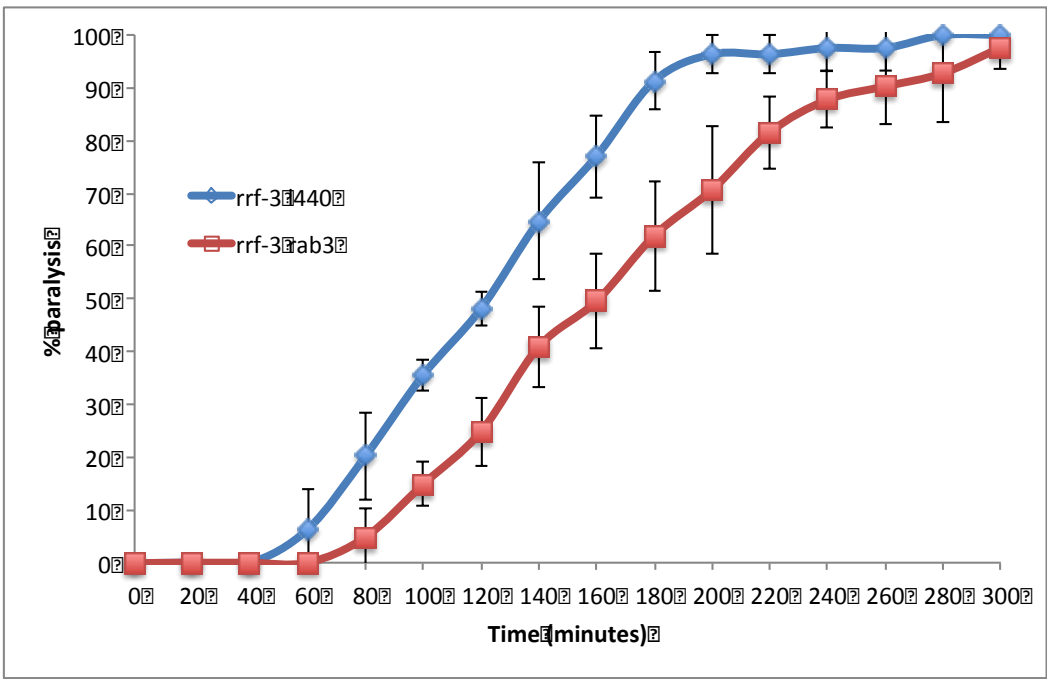

Figure 3.7 - **Effect of rab-3 knockdown in the globally RNAi sensitive rrf-3 worm strain.** As for experiments performed in the Tu3311 worm strain positive (rab-3) and negative (L440 vector) assays were performed in triplicate (N=3), with numbers of paralyzed worms being counted periodically over a 300 minute period. Error bars represent standard deviation.

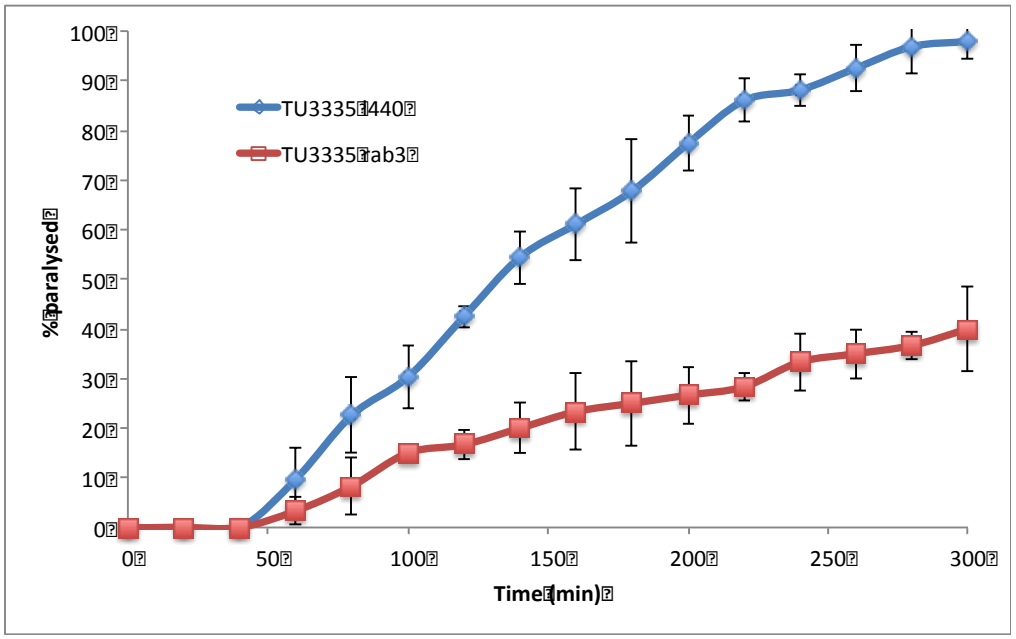

Figure 3.8 - **Knockdown of rab-3 induces a strong RIC effect in Tu3335 neurosensitive worms.** To assess the effects of inhibiting rab-3 expression in the alternate neurosensitive RNAi strain Tu3335. Assays were carried out in triplicate (n=3) with test (rab-3) or control (L440) RNAi knockdown and aldicarb sensitivity assays were performed as described in Figure 3.5. Error bars represent standard deviation.

To carry out the higher throughput assays, it was necessary to pick a time point that could be used to reliably capture alterations in aldicarb-induced paralysis. Due to aldicarb batch variability, prior to performing all high-throughput screens, the worm strain of interest was knocked down with the negative (L440) and positive (rab-3 or egl-30) controls, and picked onto aldicarb plates. The representative rate of paralysis was then measured, and a standard time point chosen for each batch, where a significant change in the percentage paralysis was observed. This was found to be within the range of 100-160 minutes, as indicated in figure legends.

3.3.3 *C. elegans* network generation

Wormnet version 3 (Cho et al., 2014) and the Worm Interactome Version 8 (Simonis et al., 2009) were used to chelate information about C. elegans PPIs known at the time of network generation. From Wormnet, genetic interactions were removed, as were co-expression, gene neighbourhoods, phylogenetic profiles, co-citation and protein tertiary structures. The remaining protein interactions were either high-throughput, small/medium scale for *C. elegans* as well as the interologs: *D. melanoganster* (fly), *H. sapiens*, *D. rerio* (zebrafish) and *S. Cerevisiae* (budding yeast). The worm interactome consists of eight Y2H PPI screens for C. elegans proteins, as well as curated PPIs and interologs. The modified Wormnet and worm interactome networks were merged, generating a network of 9668 nodes and 125674 edges (Supplementary Figure 3.1).

Wormbase was used to annotate genes according to their aldicarb-sensitivity phenotype, based on existing annotation of genes for 'Resistance to Aldicarb' and 'Hypersensitivity to Aldicarb'. In addition, data mining was carried out using PubMed, in order to find other genes, which caused an aldicarb-sensitivity phenotype when their expression was altered. A list of the genes found to cause resistance or hypersensitivity to aldicarb are provided in Supplementary Figure 3.1. Although 252 genes were annotated as causing a RIC (240) or HIC (12) phenotype, only 195 of these had any known interaction partners, hence only these proteins could be used to generate aldicarb-related protein interaction networks (Supplementary Figure 3.2 shows the aldicarb nodes not represented in the network).

One-step aldicarb related networks were created using known RIC/HIC proteins as the core/seed nodes. Proteins interacting with these core proteins in a one-step network are known as nearest neighbours. The network of proteins known to have an aldicarb phenotype together with all nearest neighbours contains 3162 nodes and 6195 edges (Figure 3.9), including 184 proteins (red nodes) that when knocked down/mutated or overexpressed confer a RIC phenotype and 11 proteins (blue node) with a known HIC phenotype. The 2967 grey nodes in this network represent non-phenotypically characterized proteins that are candidates for the connectivity analysis.

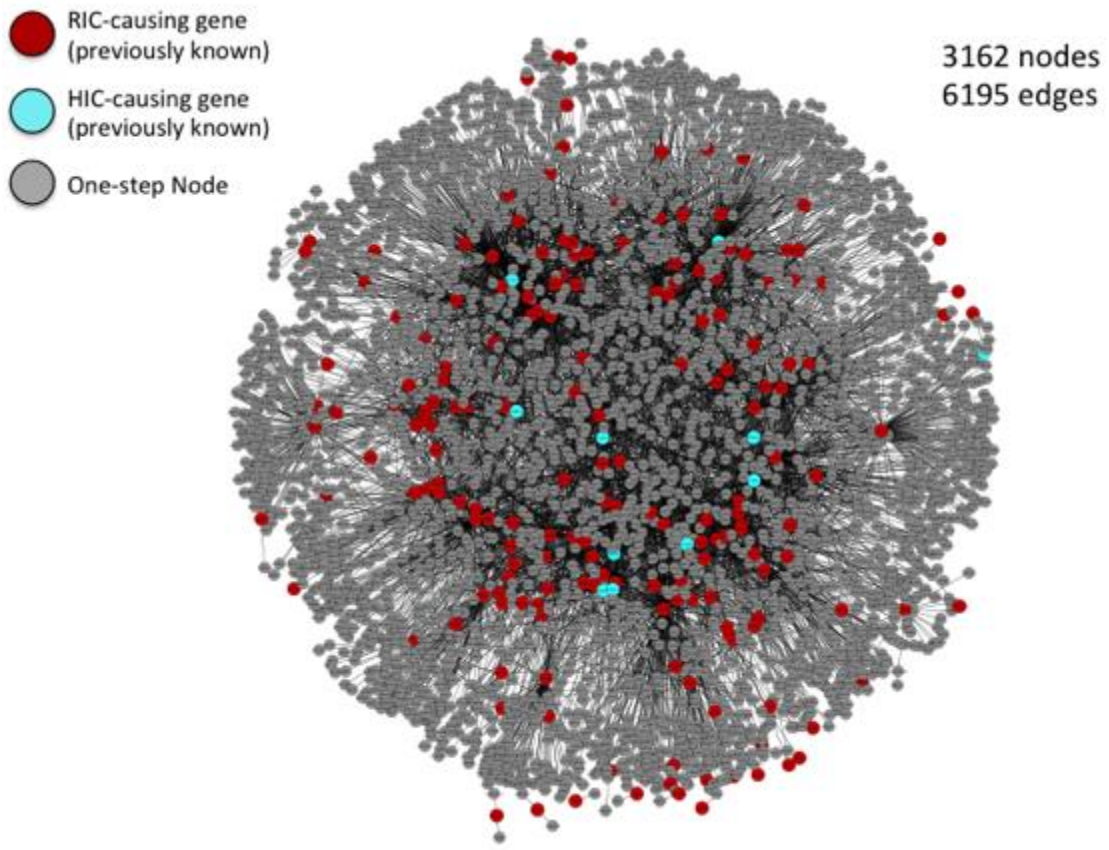

Figure 3.9 - **A one-step *C. elegans* aldicarb sensitivity network.** The core nodes (red and blue) are proteins known to cause a RIC or a HIC phenotype respectively, while grey nodes are one step connected proteins with no known aldicarb phenotype. Cytoscape v2.8 was used to generate this network.

3.3.4 Connectivity

A simple method to prioritize nodes for phenotypic screening is to rank uncharacterized nodes according to their connectivity with proteins that are already known to have some form of aldicarb phenotype.

For this analysis, interactions between nearest neighbours that do not involve a protein known to have an aldicarb-sensitivity phenotype were removed from the one-step network. The connecting nodes were then degree-sorted with respect to connectivity to RIC- or HIC- proteins. Table 3.1 contains a ranked list of the top 100 highly connected candidate proteins for phenotypic testing and the availability of appropriate dsRNA constructs in the Vidal RNAi library.

3.3.5 Aldicarb-screening of novel candidate proteins identified by network connectivity analysis

ID	Gene Symbol	Degree	Connectivity	Rnai
AC7.2	soc-2	26	1	Yes
B0001.4	B0001.4	19	2	No
B0024.9	trx-2	18	3	No
B0025.1	vps-34	18	4	No
B0034.3	casy-1	17	5	No
B0035.10	his-45	16	6	Yes
B0035.11	leo-1	15	7	Yes
B0035.13	B0035.13	13	8	Yes
B0035.4	pfd-4	13	9	No
B0035.7	his-47	13	10	No
B0035.8	his-48	13	11	No
B0035.9	his-46	13	12	Yes
B0041.4	rpl-4	13	13	Yes
B0205.3	rpn-10	12	14	Yes
B0205.6	B0205.6	12	15	Yes
B0205.7	kin-3	12	16	Yes
B0218.3	pmk-1	12	17	No
B0222.2	pitr-2	12	18	Yes
B0228.5	trx-1	11	19	No
B0228.7	B0228.7	11	20	Yes
B0250.1	rpl-2	11	21	Yes
B0250.5	B0250.5	11	22	No
B0252.4	cyn-10	10	23	No
B0261.2	let-363	10	24	Yes
B0272.1	tbb-4	10	25	No
B0272.3	B0272.3	10	26	Yes
B0280.1	glr-2	10	27	Yes
B0280.3	rpia-1	10	28	Yes
B0280.9	B0280.9	10	29	No
B0281.3	B0281.3	10	30	Yes
B0286.3	B0286.3	10	31	Yes
B0303.15	mrpl-11	10	32	No
B0303.3	B0303.3	9	33	No
B0336.10	rpl-23	9	34	Yes
B0336.2	arf-1.2	9	35	Yes
B0348.6	ife-3	9	36	Yes
B0365.1	acly-2	9	37	No
B0393.1	rps-0	9	38	No
B0395.3	B0395.3	9	39	Yes
B0403.4	pdi-6	9	40	Yes
B0412.4	rps-29	9	41	Yes
C01G10.8	C01G10.8	9	42	Yes
C34B2.6	C34B2.6	9	43	Yes
C47E8.5	daf-21	9	44	Yes
C53H9.1	rpl-27	9	45	No
D2045.6	cul-1	8	46	Yes
F15C11.2	ubql-1	8	47	No
F18G5.3	gpa-12	8	48	Yes
F20H11.3	mdh-2	8	49	Yes
F22D6.3	nars-1	8	50	No

ID	Gene Symbo	Degree	Connectivity	Rnai
F25H5.4	eef-2	8	51	Yes
F33H1.2	gpd-4	8	52	Yes
F45F2.12	his-8	8	53	Yes
F52D10.3	ftt-2	8	54	No
F55G1.11	his-60	8	55	Yes
F56C9.1	gsp-2	8	56	Yes
F56E10.2	daam-1	8	57	Yes
F56F3.5	rps-1	8	58	Yes
JC8.3	rpl-12	8	59	No
K01H12.2	ant-1.3	8	60	No
K03A1.6	his-38	8	61	Yes
K04G2.1	iftb-1	8	62	No
K06C4.2	his-28	8	63	Yes
K07D4.3	rpn-11	8	64	Yes
K10B3.7	gpd-3	8	65	Yes
K10B3.8	gpd-2	7	66	Yes
K12C11.2	smo-1	7	67	Yes
M03F4.2	act-4	7	68	No
M28.5	M28.5	7	69	Yes
R08C7.3	htz-1	7	70	No
T01C3.6	rps-16	7	71	Yes
T04C12.4	act-3	7	72	Yes
T04C12.5	act-2	7	73	Yes
T04C12.6	act-1	7	74	Yes
T04C9.1	T04C9.1	7	75	Yes
T08B2.10	rps-17	7	76	Yes
T09F3.3	gpd-1	7	77	Yes
T10C6.11	his-4	7	78	Yes
T20F5.2	pbs-4	7	79	Yes
T20G5.1	chc-1	7	80	Yes
T21H3.3	cmd-1	7	81	Yes
T22F3.4	rpl-11.1	7	82	No
W01B11.3	nol-5	7	83	Yes
W08E3.3	ola-1	7	84	Yes
W09B6.1	W09B6.1	7	85	Yes
Y22D7AL.5	hsp-60	7	86	Yes
Y24D9A.4	rpl-7A	7	87	Yes
Y43C5A.6	rad-51	7	88	No
Y46E12BL.2	Y46E12BL.2	7	89	No
Y48G8AL.8	rpl-17	7	90	Yes
Y48G9A.3	gcn-1	7	91	Yes
Y50D7A.6	klp-20	7	92	Yes
Y54F10BM.2	iffb-1	7	93	No
Y55F3AR.1	Y55F3AR.1	7	94	Yes
Y71H2AM.19	laf-1	7	95	Yes
Y71H2B.3	ppfr-4	7	96	Yes
ZC434.2	rps-7	7	97	Yes
ZK131.5	his-11	7	98	Yes
ZK131.9	his-15	7	99	Yes
ZK370.2	sma-2	6	100	Yes

Table 3.1 - **A list of the Top 100 proteins ranked according to the relative degree of connectivity to known RIC/HIC proteins within a RIC /HIC one step network**. Following network generation, interactions between the one-step nodes were removed. The one-step nodes were then degree-sorted and ranked. The availability of RNAi clones for the top 100 proteins is also indicated.

As seventy of the hundred most highly connected candidate proteins had corresponding dsRNA clones in the Vidal *C. elegans* RNAi library, knockdown of these genes were tested in the *Tu3311* strain to allow identification of additional proteins that contribute to or regulate synaptic function. In addition, the relative utility of the different network biology algorithms for capturing novel synaptic regulators could be compared.

Figure 3.10 and Table 3.2 show the percentage change in paralysis in comparison to a negative control, in which *Tu3311* worms were treated with the empty vector (L440). Comparison of the mean normalized difference in the rates of paralysis compared to the control, rather than absolute individual rates allowed data from different days to be plotted on the same graph, improving data interpretation. Unpaired t-tests were performed on comparative percentage paralysis data between control (L440) and candidate knockdown worms, in each case p values < 0.05 were considered as significant.

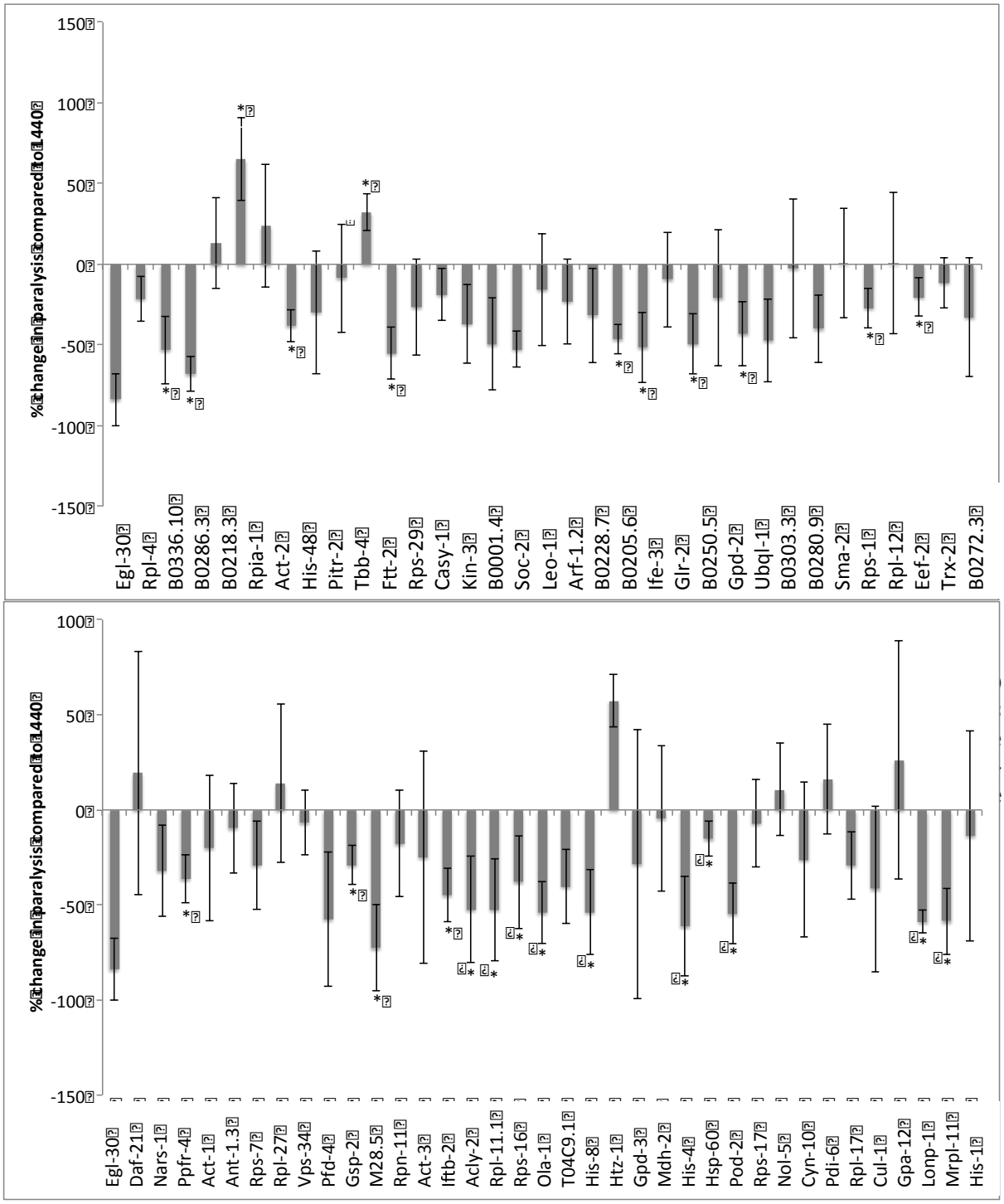
150
100
50
0
-50
-100
-150
Egl-30
Rpl-4
B0336.10
B0286.3
B0218.3
Rpia-1
Act-2
His-48
Pitr-2
Tbb-4
Ftt-2
Rps-29
Casy-1
Kin-3
B0001.4
Soc-2
Leo-1
Arf-1.2
B0228.7
B0205.6
Ife-3
Glr-2
B0250.5
Gpd-2
Ubql-1
B0303.3
B0280.9
Sma-2
Rps-1
Rpl-12
Eef-2
Trx-2
B0272.3
100
50
0
-50
-100
-150
Egl-30
Daf-21
Nars-1
Ppfr-4
Act-1
Ant-1.3
Rps-7
Rpl-27
Vps-34
Pfd-4
Gsp-2
M28.5
Rpn-11
Act-3
Iftb-2
Acly-2
Rpl-11.1
Rps-16
Ola-1
T04C9.1
His-8
Htz-1
Gpd-3
Mdh-2
His-4
Hsp-60
Pod-2
Rps-17
Nol-5
Cyn-10
Pdi-6
Rpl-17
Cul-1
Gpa-12
Lonp-1
Mrpl-11
His-1

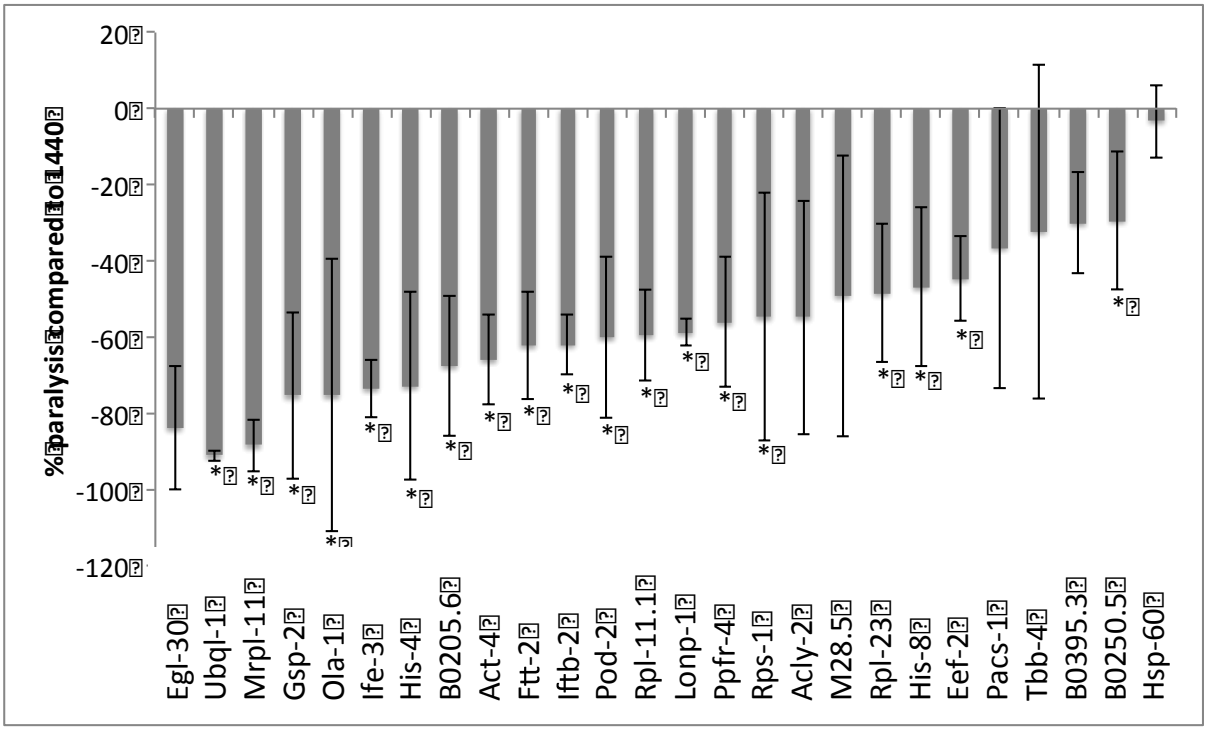

Figure 3.11 - **Independent secondary validation of aldicarb sensitivity phenotype.** A replicate series of targeted RNAi aldicarb sensitivity assays (n=3) was performed as shown in Figure 3.10, however in this case paralysis was measured after 160 minutes exposure to aldicarb. As before (*) represent significant changes in aldicarb induced paralysis. Data linked to this plot is shown in Table 3.3. Error bars represent standard deviation.

Aldicarb screens were performed twice measuring the rate of paralysis between 140 and 160 minutes. This resulted in the identification of 19 reproducibly significant hits. Figure 3.11 and table 3.3 show the second aldicarb-sensitivity assay carried out.

Gene Symbol	Wormbase Gene ID	Gene Name	% change compared to L440	Standard Deviation	P Value	Significant?
AC7.2	WBGene00004929	soc-2	-52.57	11.05	0.008	Yes
B0205.6	WBGene00015021	B0205.6	-46.34	9.09	0.009	Yes
B0250.5	WBGene00007122	B0250.5	-49.40	18.57	0.039	Yes
B0272.1	WBGene00006538	tbb-4	32.41	11.43	0.006	Yes
B0280.9	WBGene00015104	B0280.9	-40.05	20.75	0.049	Yes
B0286.3	WBGene00015116	pacs-1	-68.04	10.59	0.005	Yes
B0303.15	WBGene00015133	mrpl-11	-58.64	17.49	0.012	Yes
B0336.10	WBGene00004435	rpl-23	-53.04	21.01	0.015	Yes
B0348.6	WBGene00002061	ife-3	-51.46	21.77	0.025	Yes
B0365.1	WBGene00007150	acly-2	-52.39	27.99	0.048	Yes
B0395.3	WBGene00007175	B0395.3	65.23	25.84	0.011	Yes
C34B2.6	WBGene00016391	C34B2.6	-58.87	6.11	0.003	Yes
F15C11.2	WBGene00008852	ubql-1	-43.10	20.04	0.037	Yes
F25H5.4	WBGene00001167	eef-2	-20.35	11.66	0.049	Yes
F45F2.12	WBGene00001882	his-8	-53.77	22.53	0.027	Yes
F52D10.3	WBGene00001502	ftt-2	-55.16	15.87	0.006	Yes
F56C9.1	WBGene00001748	gsp-2	-29.04	10.27	0.020	Yes
F56F3.5	WBGene00004470	rps-1	-27.00	12.35	0.028	Yes
K04G2.1	WBGene00010560	iftb-1	-44.79	14.01	0.017	Yes
M03F4.2	WBGene00000066	act-4	-38.15	9.79	0.012	Yes
M28.5	WBGene00010896	M28.5	-72.63	22.69	0.011	Yes
T04C9.1	WBGene00020209	T04C9.1	-40.27	19.68	0.046	Yes
T10C6.11	WBGene00001878	his-4	-61.15	26.12	0.038	Yes
T22F3.4	WBGene00004422	rpl-11.1	-52.46	26.86	0.032	Yes
W08E3.3	WBGene00012344	ola-1	-53.97	16.24	0.016	Yes
W09B6.1	WBGene00004076	pod-2	-54.69	15.97	0.010	Yes
Y22D7AL.5	WBGene00002025	hsp-60	-15.37	9.15	0.049	Yes
Y71H2B.3	WBGene00022193	ppfr-4	-36.37	12.42	0.027	Yes

Gene Symbol	Wormbase Gene ID	Gene Name	% change compared to L440	Standard Deviation	P Value	Significant?
B0001.4	WBGene00007089	B0001.4	-49.53	28.46	0.073	No
B0024.9	WBGene00007099	trx-2	-11.34	15.64	0.322	No
B0025.1	WBGene00006932	vps-34	-6.79	17.11	0.552	No
B0034.3	WBGene00000403	casy-1	-18.76	15.97	0.159	No
B0035.11	WBGene00007110	leo-1	-15.67	34.64	0.504	No
B0035.4	WBGene00007107	pfd-4	-57.42	35.33	0.064	No
B0035.8	WBGene00001922	his-48	-29.69	38.11	0.271	No
B0041.4	WBGene00004415	rpl-4	-21.35	13.91	0.079	No
B0205.7	WBGene00002191	kin-3	-36.86	24.70	0.069	No
B0218.3	WBGene00004055	pmk-1	13.06	28.02	0.414	No
B0222.2	WBGene00015054	pitr-2	-8.53	33.62	0.695	No
B0228.7	WBGene00015064	B0228.7	-31.78	29.10	0.172	No
B0252.4	WBGene00000886	cyn-10	-26.12	40.93	0.363	No
B0272.3	WBGene00007129	B0272.3	-32.73	37.08	0.217	No
B0280.1	WBGene00015099	ggtb-1	-9.36	29.44	0.621	No
B0280.3	WBGene00015101	rpia-1	23.82	37.98	0.285	No
B0303.3	WBGene00015125	B0303.3	-2.61	43.16	0.922	No
B0336.2	WBGene00000182	arf-1.2	-22.95	26.38	0.228	No
B0403.4	WBGene00015168	pdi-6	16.20	28.84	0.384	No
B0412.4	WBGene00004498	rps-29	-26.46	29.95	0.224	No
C47E8.5	WBGene00000915	daf-21	19.52	64.10	0.599	No
C53H9.1	WBGene00004441	rpl-27	13.92	41.52	0.585	No
D2045.6	WBGene00000836	cul-1	-41.55	43.58	0.189	No
F18G5.3	WBGene00001674	gpa-12	26.15	62.65	0.461	No
F20H11.3	WBGene00003162	mdh-2	-4.52	38.38	0.849	No
F22D6.3	WBGene00003815	nars-1	-32.03	23.92	0.138	No
JC8.3	WBGene00004424	rpl-12	0.67	43.65	0.922	No
K01H12.2	WBGene00010485	ant-1.3	-9.71	23.47	0.515	No
K07D4.3	WBGene00004467	rpn-11	-17.84	28.04	0.340	No
K10B3.7	WBGene00001685	gpd-3	-28.54	70.68	0.527	No
K10B3.8	WBGene00001684	gpd-2	-20.92	42.24	0.448	No
K12C11.2	WBGene00004888	smo-1	-47.16	25.93	0.051	No
R08C7.3	WBGene00019947	htz-1	57.42	13.98	0.126	No
T01C3.6	WBGene00004485	rps-16	-37.89	24.49	0.057	No
T04C12.4	WBGene00000065	act-3	-25.02	55.63	0.486	No
T04C12.6	WBGene00000063	act-1	-20.09	38.38	0.427	No
T08B2.10	WBGene00004486	rps-17	-7.13	23.09	0.630	No
T10C6.14	WBGene00001875	his-1	-13.62	55.32	0.696	No
W01B11.3	WBGene00020915	nol-5	10.71	24.18	0.462	No
Y48G8AL.8	WBGene00004429	rpl-17	-29.24	17.98	0.072	No
ZC434.2	WBGene00004476	rps-7	-28.95	23.33	0.120	No
ZK370.2	WBGene00004856	sma-2	0.70	33.83	0.973	No

Table 3.2 – Background data associated with Figure 3.10

Gene Symbol	Wormbase Gene ID	Gene Name	% Change Compared To L440	Standard Deviation	P value	Significant?
Y71H2B.3	WBGene00022193	ppfr-4	-56.17	17.06	0.006	Yes
W09B6.1	WBGene00004076	pod-2	-60.08	21.16	0.008	Yes
W08E3.3	WBGene00012344	ola-1	-75.30	35.65	0.024	Yes
T22F3.4	WBGene00004422	rpl-11.1	-59.54	11.97	0.014	Yes
T10C6.11	WBGene00001878	his-4	-72.88	24.59	0.007	Yes
M03F4.2	WBGene00000066	act-4	-65.95	11.72	0.001	Yes
K04G2.1	WBGene00010560	iftb-1	-61.97	7.99	0.002	Yes
F56F3.5	WBGene00004470	rps-1	-54.84	32.53	0.044	Yes
F56C9.1	WBGene00001748	gsp-2	-75.42	21.75	0.007	Yes
F52D10.3	WBGene00001502	ftt-2	-62.16	14.14	0.018	Yes
F45F2.12	WBGene00001882	his-8	-46.88	20.83	0.039	Yes
F15C11.2	WBGene00008852	ubql-1	-91.08	1.41	0.000	Yes
C34B2.6	WBGene00016391	C34B2.6	-58.87	3.53	0.000	Yes
B0348.6	WBGene00002061	ife-3	-73.44	7.59	<0.0001	Yes
B0336.10	WBGene00004435	rpl-23	-48.43	18.18	0.018	Yes
B0303.15	WBGene00015133	mrpl-11	-88.41	6.88	0.001	Yes
B0250.5	WBGene00007122	B0250.5	-29.42	18.04	0.049	Yes
B0205.6	WBGene00015021	B0205.6	-67.52	18.38	0.007	Yes
F25H5.4	WBGene00001167	eef-2	-44.78	11.11	0.002	Yes
Y22D7AL.5	WBGene00002025	hsp-60	-3.33	9.62	0.752	No
M28.5	WBGene00010896	M28.5	-49.14	36.90	0.100	No
B0395.3	WBGene00007175	B0395.3	-30.13	13.21	0.106	No
B0365.1	WBGene00007150	acly-2	-54.80	30.74	0.158	No
B0286.3	WBGene00015116	pacs-1	-36.54	36.84	0.168	No
B0272.1	WBGene00006538	tbb-4	-32.26	43.87	0.290	No

Table 3.3 – Background data associated with Figure 3.11.

3.3.6 Data analysis of novel effectors of aldicarb sensitivity identified from network connectivity screens

Wormbase and Wormmine were used to investigate the potential function of the subset of newly identified proteins that conferred modified aldicarb phenotypes when knocked down (Table 3.4). This analysis revealed similarities that enabled some of the identified proteins to be grouped together. For example, rpl-11.1 and rpl-23 are both components of the large ribosomal subunit. Two histone genes (his-4 and his-8) were also identified and other proteins are known to be involved in either transcription or translation. For example eef-2 is a translation elongation factor, and ife-3 is an mRNA-cap binding protein. Analysis of the data using the DAVID process enrichment tool revealed the most enriched processes to be associated with embryonic and larval development (Table 3.5).

Gene Symbol	Wormbase Gene ID	Gene Name	Description
B0303.15	WBGene00015133	mrpl-11	Encodes an ortholog of human MRPL11 (mitochondrial ribosomal protein 11).
			Involved in embryonic and larval development, receptor-mediated endocytosis and reproduction.
F15C11.2	WBGene00008852	ubql-1	Encodes an ortholog of the human UBQLN1 (Ubiquilin) family. Involved in the determination of lifespan. Predicted to be able to bind damamged DNA.
M03F4.2	WBGene00000066	act-4	Encodes an actin isoform most similar to act-2; an act-4 reporter gene is expressed in body wall and vulval muscles and the spermatheca.
F56C9.1	WBGene00001748	gsp-2	Encodes an ortholog of human PPP1CA (protein phosphatase 1, catalytic subunit, alpha isozyme) and PPP1CC (protein phosphatase 1, catalytic subunit, gamma isozyme).
			Involved in embryonic development, locomotion, peptidyl-serine dephosphorylation, cytokinesis, meiotic chromosome segregation, mitotic nuclear division and the molting cycle.
F45F2.12	WBGene00001882	his-8	Encodes an H2B histone. His-8 is contained within the histone gene cluster HIS2.
W08E3.3	WBGene00012344	ola-1	Encodes an ortholog of OLA1 (ObG-like ATPase 1). Involved in embryonic development. Predicted to have GTP binding activity.
B0250.5	WBGene00007122	B0250.5	Encodes an ortholog of human HIBADH (3-hydroxyisobutyrate dehydrogenase). Predicted to have the ability to bind NAD,
			and dehydrogenate 3-hydroxyisobutyrate and phosphogluconate, based on protein domain information.
F56F3.5	WBGene00004470	rps-1	Encodes a small ribosomal subunit S3A protein.
K04G2.1	WBGene00010560	iftb-1	Encodes the C. elegans ortholog of translation initiation factor 2 beta (eIF2beta); by homology, IFTB-1 is predicted to function in translation initiation and start codon recognition.
			Loss of iftb-1 indicates it's activity is required for processes including growth, development, and body morphogenesis. Loss in adult animals extends lifespan.
F52D10.3	WBGene00001502	ftt-2	Encodes a 14-3-3 protein. Required the regulation of the localization of YAP-1 product, a Yes-associated protein (Yap) homolog, between the cytoplasm and the nucleus.
W09B6.1	WBGene00004076	pod-2	Encodes an acetyl-CoA carboxylase. By sequence similarity, POD-2 is predicted to catalyze the first step in de novo fatty acid biosynthesis. POD-2 is required for proper embryonic
			polarity and for osmotic protection of the eggshell; pod-2 activity is also required for molting.
B0205.6	WBGene00015021	B0205.6	Encodes an ortholog of NFS1 (NFS1 cysteine desulfurase). Involved in embryonic and larval development and reproduction. Predicted to have cysteine desulfurase and
			pyridoxal phosphate binding activity, based on protein domain information.
T22F3.4	WBGene00004422	rpl-11.1	Encodes a large ribosomal subunit L11 protein.
B0336.10	WBGene00004435	rpl-23	Encodes a large ribosomal subunit L23 protein.
T10C6.11	WBGene00001878	his-4	Encodes an H2B histone.
Y71H2B.3	WBGene00022193	ppfr-4	Encodes the C. elegans ortholog of TAP42, a protein phosphatase 2A (PP2A) regulatory subunit. PPFR-4(RNAi) in wild-type animals results in fertility defects in F1 hermaphrodites,
			who exhibit a 90-95% decrease in the total number of eggs laid.
F25H5.4	WBGene00001167	eef-2	Encodes a homolog of translation elongation factor 2 (EF-2), a GTP-binding protein essential for the elongation phase of protein synthesis. EEF-2 is required for embryogenesis and
			vulval morphogenesis, and is expressed during all stages of development, including the dauer larval stage.
C34B2.6	WBGene00016391	C34B2.6	Encodes a homolog of the Lon mitochondrial protease. Loss of C34B2.6 activity results in impaired proteolysis of the ATFS-1 bZip transcription factor that partitions between the
			mitochondria and the nucleus and functions as part of the mitochondrial unfolded protein response (UPRmt).
B0348.6	WBGene00002061	ife-3	Encodes one of five C. elegans homologs of the mRNA cap-binding protein eIF4E.

Table 3.4 - A brief description of hits from the connectivity screen. Information was derived from Wormbase.

Biological Process	Count	Genes
Embryonic development ending in birth or egg hatching	15	mrpl-11, act-4, gsp-2, his-8, cola-1, rps-1, scbp-2, pod-2, rpl-23, B0205.6, rpl-11.1, his-4, ppfr-4, eef-2, lonp-1, ife-3
Nematode larval development	11	mrpl-11, act-4, his-4, his-8, ppfr-4, eef-2, rps-1, scbp-2, F52D10.3, pod-2, rpl-23, B0205.6
Larval development	11	mrpl-11, act-4, his-4, his-8, ppfr-4, eef-2, rps-1, scbp-2, F52D10.3, pod-2, rpl-23, B0205.6
Post-embryonic development	11	mrpl-11, act-4, his-4, his-8, ppfr-4, eef-2, rps-1, scbp-2, F52D10.3, pod-2, rpl-23, B0205.6
Growth	10	mrpl-11, act-4, his-4, his-8, ppfr-4, eef-2, rps-1, scbp-2, F52D10.3, rpl-23, B0205.6
Translation	7	mrpl-11, eef-2, rps-1, scbp-2, ife-3, rpl-23, rpl-11.1
Hermaphrodite genitalia development	6	act-4, ppfr-4, eef-2, rps-1, scbp-2, rpl-11.1
Genitalia development	6	act-4, ppfr-4, eef-2, rps-1, scbp-2, rpl-11.1
Sex differentiation	6	act-4, ppfr-4, eef-2, rps-1, scbp-2, rpl-11.1
Reproductive developmental process	6	act-4, ppfr-4, eef-2, rps-1, scbp-2, rpl-11.1
Molting cycle, protein-based cuticle	4	gsp-2, rps-1, pod-2, rpl-23
Molting cycle, collagen and cuticulin-based cuticle	4	gsp-2, rps-1, pod-2, rpl-23
Molting cycle	4	gsp-2, rps-1, pod-2, rpl-23
Translational initiation	2	scbp-2, ife-3
Fatty acid biosynthetic process	2	pod-2, lonp-1
Fatty acid metabolic process	2	pod-2, lonp-1

Table 3.5 - Top ranked biological processes identified by DAVID Biological Process Enrichment tool. A list of gene symbols corresponding to novel proteins found to effect aldicarb sensitivity following network connectivity analysis were entered into the DAVID functional enrichment package using default settings.

Worm Gene Symbol	Wormbase Gene ID	Worm Gene Name	Human Gene Symbol	Human Entrez ID	DIOPT Score
B0205.6	WBGene00015021	B0205.6	NFS1	9054	8.816
B0250.5	WBGene00007122	B0250.5	HIBADH	11112	10.769
B0303.15	WBGene00015133	mrpl-11	MRPL11	65003	9.819
B0336.10	WBGene00004435	rpl-23	RPL23	9349	7.858
B0348.6	WBGene00002061	ife-3	EIF4E	1977	8.808
C34B2.6	WBGene00016391	C34B2.6	LONP1	9361	9.809
F15C11.2	WBGene00008852	ubql-1	UBQLN1	29979	7.809
F45F2.12	WBGene00001882	his-8	HIST1H2BA	255626	3.89
F52D10.3	WBGene00001502	ftt-2	YWHAZ	7534	7.898
F56C9.1	WBGene00001748	gsp-2	PPP1CA	5499	8.879
F56F3.5	WBGene00004470	rps-1	RPS3A	6189	8.859
K04G2.1	WBGene00010560	iftb-1	EIF2S2	8894	6.798
M03F4.2	WBGene00000066	act-4	ACTG1	71	5.868
T10C6.11	WBGene00001878	his-4	HIST1H2BA	255626	4.8
T22F3.4	WBGene00004422	rpl-11.1	RPL11	6135	8.859
W08E3.3	WBGene00012344	ola-1	OLA1	29789	8.816
W09B6.1	WBGene00004076	pod-2	ACACA	31	7.808
Y71H2B.3	WBGene00022193	ppfr-4	IGBP1	3476	10.769
F25H5.4	WBGene00001167	eef-2	EEF2	1938	7.858

Table 3.6 - A list of human orthologs of worm genes/proteins that were identified via network connectivity analysis and found to cause significant changes in aldicarb sensitivity following RNAi induced knockdown. Diopt FlyRNAI (Hu et al., 2011) was used to elucidate the closest human ortholog. The DIOPT score refers to how many databases predicted the ortholog match.

Human orthologs of proteins found to confer changes in aldicarb induced phenotypes were elucidated using DIOPT Fly RNAi (Hu et al., 2011). Table 3.6 shows the human orthologs, as well as their DIOPT score, which indicate how many ortholog databases predicted the worm-human ortholog match. SynaptomeDB was then used to establish if human orthologs had a pre- or post-synaptic distribution (Pirooznia et al., 2012). Interestingly, of the nineteen novel positive hits, eleven were found in the synaptome, and their localization was found to be predominantly post-synaptic (Table 3.7).

Gene Symbol	Gene Name	Human Gene Symbol	Synaptome Localization
C34B2.6	C34B2.6	LONP1	PostSynaptic
M03F4.2	act-4	ACTG1	PreSynaptic Active Zone
F52D10.3	ftt-2	YWHAZ	PreSynaptic Active Zone, PostSynaptic
W08E3.3	ola-1	OLA1	PostSynaptic
T22F3.4	rpl-11.1	RPL11	PostSynaptic
B0348.6	ife-3	EIF4E	PostSynaptic
B0336.10	rpl-23	RPL23	PostSynaptic
F56C9.1	gsp-2	PPP1CA	PostSynaptic
F56F3.5	rps-1	RPS3A	PostSynaptic
W09B6.1	pod-2	ACACA	PostSynaptic
F25H5.4	eef-2	EEF2	PreSynaptic, PostSynaptic

Table 3.7 - Synaptome localization of the human orthologs of the worm genes found in the connectivity screen to cause a significant aldicarb-sensitivity phenotype. Data was gathered using SynaptomeDB. Human orthologs were elucidated using Diopt flyRNAi.

Gene Name	Degree	Rank
rpl-23	16	6
act-4	12	14
ftt-2	11	19
B0205.6	9	35
ife-3	9	36
B0250.5	9	38
ubql-1	9	40
rps-1	8	48
eef-2	8	50
gsp-2	7	68
scbp-2	7	73
rpl-11.1	7	75
ola-1	7	78
his-8	7	81
his-4	7	85
pod-2	7	88
mrpl-11	7	99
ppfr-4	8	56
lonp-1	7	98

Table 3.8 - A degree ranked list of interaction partners for novel connectivity hits not previously known to cause an aldicarb-sensitivity phenotype. Data was derived from the one-step known aldicarb sensitivity network (Figure 3.9) and corresponds to Figure 3.12

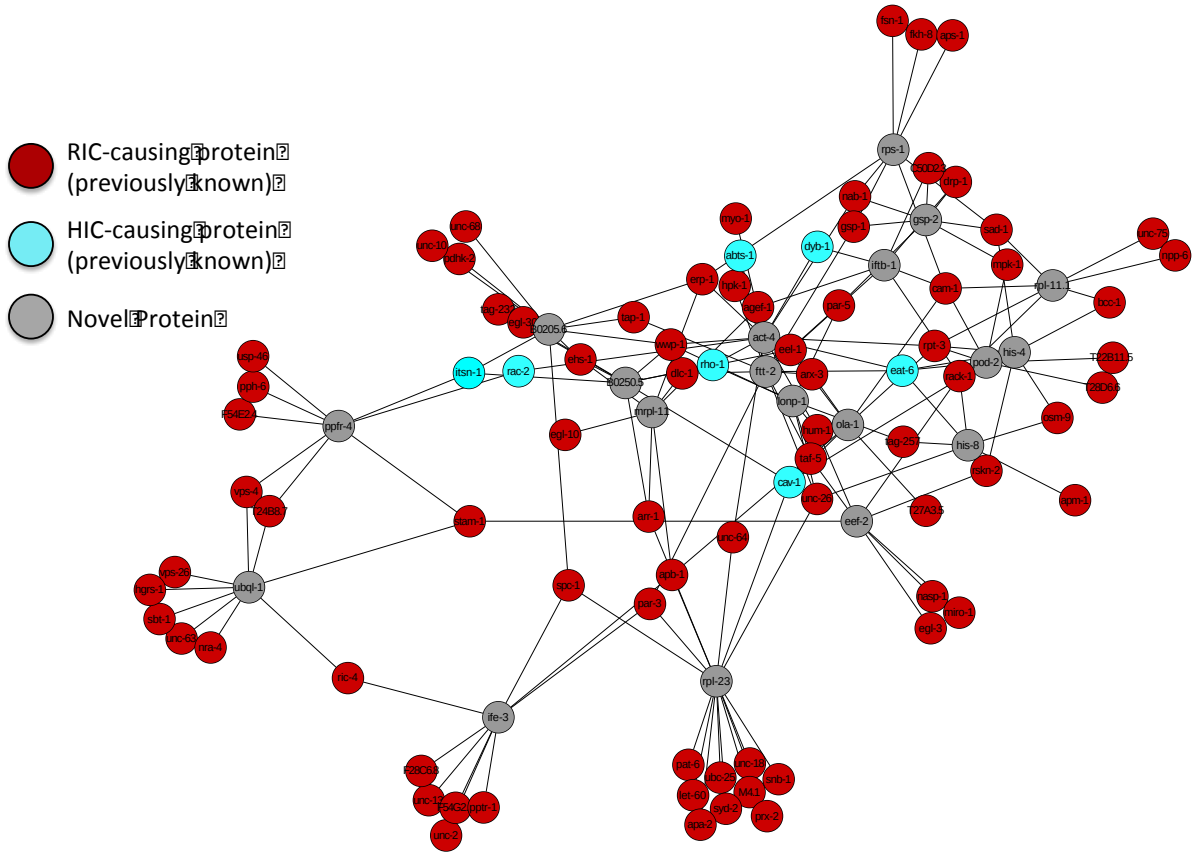

Figure 3.12 - **Network showing the novel aldicarb-sensitivity genes found in the connectivity screen, and their interacting partners, which were previously known to cause an aldicarb-sensitivity phenotype.** Grey nodes represent novel hits, red nodes indicate genes that cause a RIC phenotype when expression is altered, and blue nodes correspond to genes that cause a HIC phenotype when expression is altered. Cytoscape version 3 was used to generate this network, and interaction data was extracted from the one-step known aldicarb sensitivity network (Figure 3.9).

Many of the previously known aldicarb hits have interactions with multiple novel regulators. Figure 3.12 shows a network displaying the novel hits found in this connectivity informed screen, and interacting with previously known aldicarb-sensitivity genes. Table 3.8 summarizes the connectivity scores of novel the regulators identified in this screen, while previously known aldicarb nodes that interact with multiple novel modulators identified in this screen are shown in Table 3.9.

Gene Name	Connectivity to hits	Aldicarb Phenotype	Hits Connected To
eat-6	5	HIC	pod-2, his-8, his-4, act-4, ttt-2
rack-1	5	RIC	rpl-11.1, his-8, his-4, scbp-2, eef-2
rpt-3	5	RIC	pod-2, rpl-11.1, ola-1, his-4, act-4
cam-1	5	RIC	pod-2, rpl-11.1, ola-1, rps-1, scbp-2
cav-1	4	HIC	pod-2, B0250.5, ola-1, rpl-23
wwp-1	4	RIC	B0205.6, B0250.5, lonp-1, act-4
apb-1	4	RIC	ola-1, mrpl-11, rpl-23, ife-3
unc-26	4	RIC	his-8, lonp-1, rpl-23, ttt-2
sad-1	4	RIC	rpl-11.1, gsp-2, his-4, rps-1
erp-1	4	RIC	B0205.6, rps-1, mrpl-11, act-4
ehs-1	3	RIC	B0205.6, B0250.5, mrpl-11
par-3	3	RIC	rpl-23, ttt-2, ife-3
arx-3	3	RIC	ola-1, act-4, ttt-2
gsp-1	3	RIC	gsp-2, rps-1, ttt-2
rho-1	3	HIC	B0250.5, lonp-1, act-4
taf-5	3	RIC	lonp-1, ttt-2, eef-2
hum-1	3	RIC	lonp-1, act-4, eef-2
par-5	3	RIC	gsp-2, lonp-1, ttt-2
nab-1	3	RIC	gsp-2, rps-1, act-4
stam-1	3	RIC	ubql-1, eef-2, stam-1
eel-1	3	RIC	B0250.5, ola-1, scbp-2
itsn-1	3	HIC	B0205.6, B0250.5, ppfr-4
rskn-2	3	RIC	his-8, his-4, eef-2
arr-1	3	RIC	B0250.5, mrpl-11, rpl-23
spc-1	2	RIC	B0205.6, rpl-23
bcc-1	2	RIC	rpl-11.1, his-4
tag-257	2	RIC	his-8, lonp-1
unc-64	2	RIC	act-4, rpl-23
dyb-1	2	HIC	act-4, scbp-2
dlc-1	2	RIC	mrpl-11, ttt-2
osm-9	2	RIC	his-8, his-4
vps-4	2	RIC	ubql-1, ppfr-4
C50D2.3	2	RIC	gsp-2, scbp-2
agef-1	2	RIC	mrpl-11, scbp-2
mpk-1	2	RIC	pod-2, gsp-2
T24B8.7	2	RIC	ubql-1, ppfr-4
drp-1	2	RIC	gsp-2, scbp-2
tap-1	2	RIC	B0205.6, ttt-2
rac-2	2	HIC	act-4, ppfr-4
ric-4	2	RIC	ubql-1, ife-3

Table 3.9 – A list of genes that were previously known to cause an aldicarb-sensitivity phenotype and interact with multiple novel hits from the connectivity screen. Data was extracted from the one-step aldicarb network (Figure 3.9). Genes are listed if they interacted with more than one novel hit, and were known to cause a RIC or HIC phenotype when their expression was altered.

Gene symbols from the network shown in Figure 3.12 were imported into DAVID, to determine if any synaptic biological processes were enriched. 10 genes were found to be associated with synaptic transmission, seven of these specifically in cholinergic transmission (Table 3.10). Although these are genes previously shown to cause RIC or HIC phenotypes, by looking at their novel interaction partners, it may be possible to provide some insight into the mechanism by which they confer the observed changes in aldicarb sensitivity, and by extrapolation synaptic function. One interesting interaction partner is *ric-4*, which is the worm ortholog of SNAP-25. SNAP-25 is essential at the presynaptic terminal membrane for SNARE vesicle fusion. RIC-4 interacts with the novel hits ubql-1 and ife-3, providing a link to their potential synaptic function.

Gene Name	Biological Process	Aldicarb	Novel Protein Interaction Partners
dyb-1	Synaptic Transmission, Cholinergic	HIC	act-4, ftb-1
ric-4	Synaptic Transmission, Cholinergic	RIC	ubql-1, ife-3
unc-18	Synaptic Transmission, Cholinergic	RIC	rpl-23
unc-64	Synaptic Transmission, Cholinergic	RIC	act-4, rpl-23
unc-10	Synaptic Transmission, Cholinergic	RIC	B0205.6
unc-63	Synaptic Transmission, Cholinergic	RIC	ubql-1
unc-75	Synaptic Transmission, Cholinergic	RIC	rpl-11.1
ehs-1	Synaptic Transmission	RIC	B0205.6, B0250.5, mrpl-11
syd-2	Synaptic Transmission	RIC	rpl-23
unc-2	Synaptic Transmission	RIC	ife-3

Table 3.10 – Synaptic transmission is enriched when genes from the novel aldicarb-sensitivity genes from the connectivity screen and their interacting partners that cause an aldicarb-phenotype were inputted into DAVID. Functional clustering was carried out and biological enrichment assessed.

Furthermore when the novel genes are extracted from the main *C. elegans* networks, interactions can be seen between some of the novel regulators (Figure 3.13) suggesting they may also be in some way functionally related. However, these interactions are all derived from interolog data, observed between

orthologous human or yeast proteins. In Figure 3.13 red edges denote interactions found in either high or low throughput human protein interaction studies. Blue edges represent interactions found in both *S. cerevisiae* and humans, while black edges have only been seen in *S. cerevisiae*. In Table 3.11 novel effector proteins are degree sorted, showing that eef-2 is highly connected to 10 other novel protein effectors of aldicarb sensitivity. As eef-2 is a translation elongation factor it may be required for their protein synthesis or may have an additional as yet undefined role.

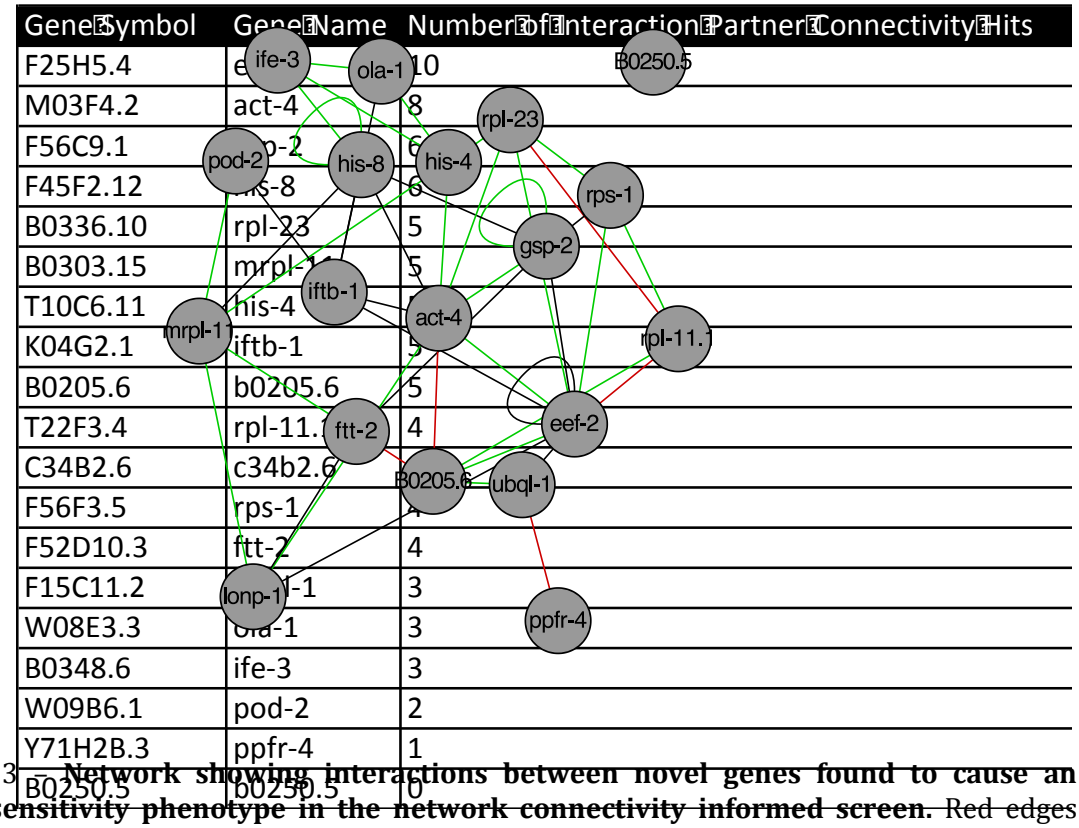

Gene Symbol	Gene Name	Number of Interaction Partner Connectivity Hits
F25H5.4	e	10
M03F4.2	act-4	8
F56C9.1	p-2	6
F45F2.12	is-8	6
B0336.10	rpl-23	5
B0303.15	mrpl-	5
T10C6.11	his-4	
K04G2.1	iftb-1	
B0205.6	b0205.6	5
T22F3.4	rpl-11.	4
C34B2.6	c34b2.6	
F56F3.5	rps-1	
F52D10.3	ftt-2	4
F15C11.2	l-1	3
W08E3.3	ola-1	3
B0348.6	ife-3	3
W09B6.1	pod-2	2
Y71H2B.3	ppfr-4	1
B0250.5	b0250.5	0

Table 3.11 – Degree ranked list of interactions between novel connectivity genes that caused a significant change in aldicarb sensitivity.

Figure 3.13 – **Network showing interactions between novel genes found to cause an aldicarb-sensitivity phenotype in the network connectivity informed screen.** Red edges denote interactions found using the human orthologs, black edges represent interactions found in *S. cerevisiae*, and green edges denote interactions found in both humans and *S. cerevisiae*. Cytoscape was used to generate the network, and a merge of Wormnet and the worm interactome were used to elucidate interactions between the hits.

The novel aldicarb-sensitivity genes were then added to the core list of RIC/HIC-causing genes, and a one-step network was re-generated, resulting in a new network containing 3925 proteins connected by 10357 interactions (Figure 3.14).

3.3.7 Shell Analysis in the aldicarb network

The first shell of the aldicarb one step network represents direct physical interaction partners of aldicarb-sensitivity proteins. Due to the complexity of synaptic transmission it is possible that indirect regulators may also cause a change in aldicarb sensitivity when knocked down, even though they do not directly bind aldicarb-sensitivity genes. It could also be hypothesized that interactions between a gene and a known aldicarb-sensitivity gene become more indirect, they are less likely to cause a phenotype, in line with the "guilt-by-association" principle. To test which of these hypotheses was correct, we assessed whether proteins currently thought to be less connected to known aldicarb-sensitivity proteins would be less likely to cause an aldicarb-sensitivity phenotype, than

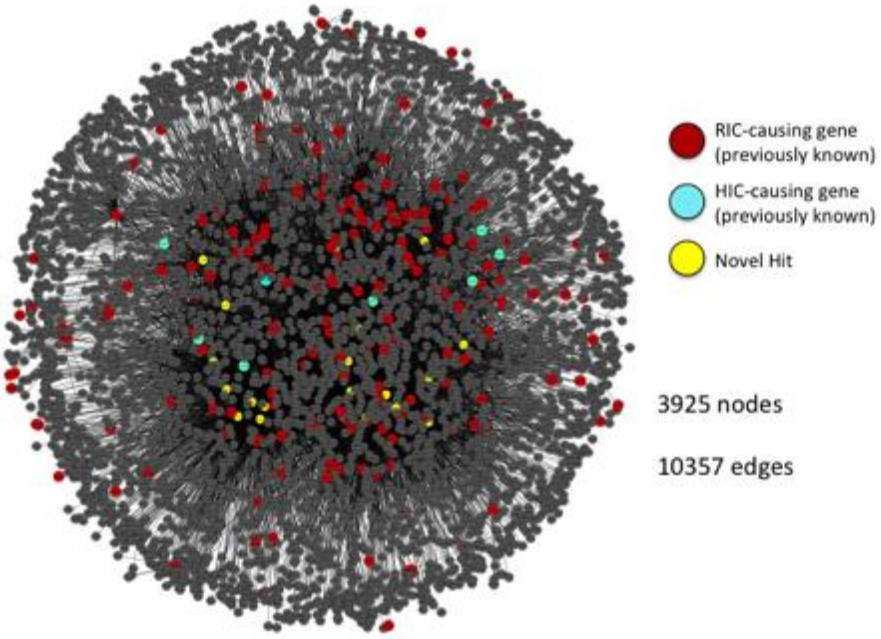

Figure 3.14 – **One-step aldicarb sensitivity network, using previously known RIC (red nodes), HIC (blue nodes) and novel regulator proteins (yellow nodes) as a core.** Cytoscape version 3 was used to generate the network. Wormbase and literature mining were used to investigate the previously known RIC and HIC related genes.

those that had high connectivity and were directly connected to multiple aldicarb-sensitivity proteins.

To identify candidate proteins with reduced connectivity to known regulators of the aldicarb phenotype a one-step aldicarb network was used as a core. Unique proteins connected to the one-step nodes were then selected to define the second two-step "shell". Additional interactions to proteins in this second shell were then selected (by looking at adjacent edges) to create a third "shell". Sequential creation of shells continued until no

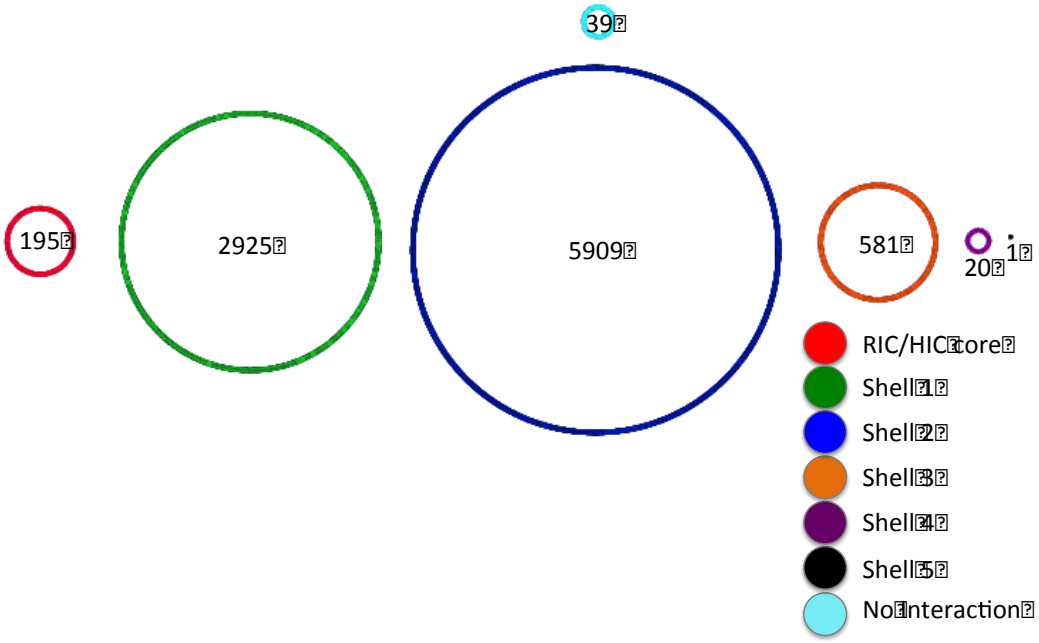

Figure 3.15 – **Shell analysis of the merged Wormnet v3 and Vidal CCSB Worm Interactome, using the previously known aldicarb-sensitivity genes as a core.** Red nodes represent the core, which consists of the genes previously known to cause a RIC or a HIC phenotype. Green nodes represent the proteins that interact with the core proteins i.e. shell 1. Royal blue nodes represent proteins that interact with shell 1, which are not in the core (shell 2). Orange nodes represent proteins that interact with shell 2 and are not found in shell 1 (shell 3). Purple nodes represent proteins that interact with shell 3 but are not found in shell 2 (shell 4). The black node represents the one protein that interacts with shell 4 and is not in shell 3.) Light blue nodes are those that are found in no shells. Edges have been hidden. Cytoscape v2.8 was used to generate this network.

more proteins could be connected, resulting in 5 sequential shells containing 2925, 5909, 581, 20 and 1 proteins, respectively (Figure 3.15). 39 nodes in the network had no connection to aldicarb-sensitivity genes.

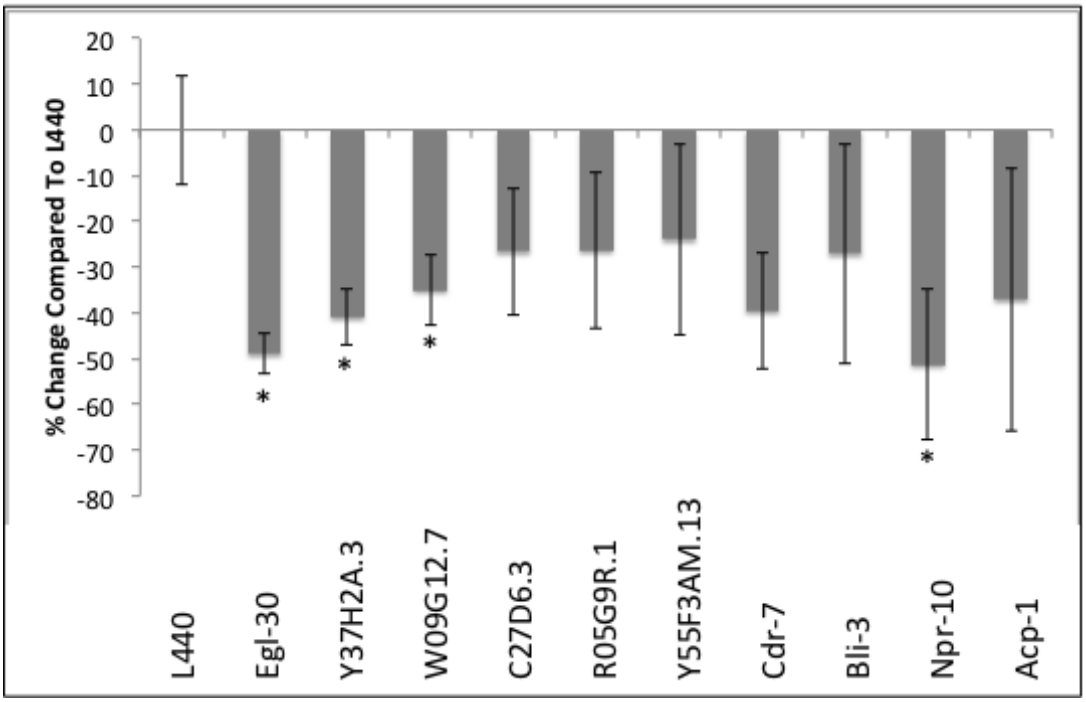

Figure 3.16 – **Testing of a selection of genes from the shell 4 using the aldicarb-sensitivity genes as a core.** RNAi knockdown and aldicarb sensitivity assays were performed as described in Figure 3.5., and the percentage of paralyzed worms was calculated at 140 minutes. The percentage change to L440 was then calculated and plotted. Egl-30 was the positive control. Hits are significant and marked with an asterix if calculated P values calculated (Section 2.5) are less than 0.05. N=3. Error bars represent standard deviation.

The single gene found in shell 5 (K08H10.2) did not have a dsRNA-expressing bacterial clone available. Nine genes from the fourth shell were knocked down in *Tu3311*. A significant RIC phenotype was observed when three of the nine genes are knocked down (Figure 3.16 and Table 3.12). These were *Y37H2A.3* (WBGene00012563), *W09G12.7* (WBGene00021121) and *npr-10* (WBGene00008278). *Cdr-7* (WBGene00010472) was also very close to being significant. Previously, 27% of the candidates tested in the first shell (those with the highest connectivity, and direct connectivity to aldicarb genes) led to a significant result. Here, although the test set is far lower, 33% of candidates led to a result. It is however important to note that due to time limitations, secondary validation of these outer shells were not carried out.

Gene Symbol	Wormbase Gene ID	Gene Name	% change compared to L440	Standard Deviation	P Value	Significant?
M01D7.7	WBGene00001196	egl-30	-48.94	11.93	0.0256	Yes
Y37H2A.3	WBGene00012563	Y37H2A.3	-40.92	4.31	0.0108	Yes
W09G12.7	WBGene00021121	W09G12.7	-35.03	6.04	0.0244	Yes
C27D6.3	WBGene00016161	C27D6.3	-26.61	7.6	0.1499	No
R05G9R.1	WBGene00019906	R05G9R.1	-26.36	13.82	0.2152	No
Y55F3AM.13	WBGene00021930	Y55F3AM.13	-23.97	16.99	0.3274	No
K01D12.13	WBGene00010472	cdr-7	-39.56	20.8	0.0504	No
F56C11.1	WBGene00000253	bli-3	-27.06	24.06	0.3353	No
C53C7.1	WBGene00008278	npr-10	-51.28	15.37	0.0461	Yes
ZK563.6	WBGene00022770	acp-1	-37.05	28.69	0.2764	No

Table 3.12 –Background data associated with Figure 3.16.

We also tested these outer shell candidates in the *Tu3335* strain (Figure 3.17 and Table 3.13). It is interesting to note that *W09G12.7* also shows a RIC phenotype in this strain,

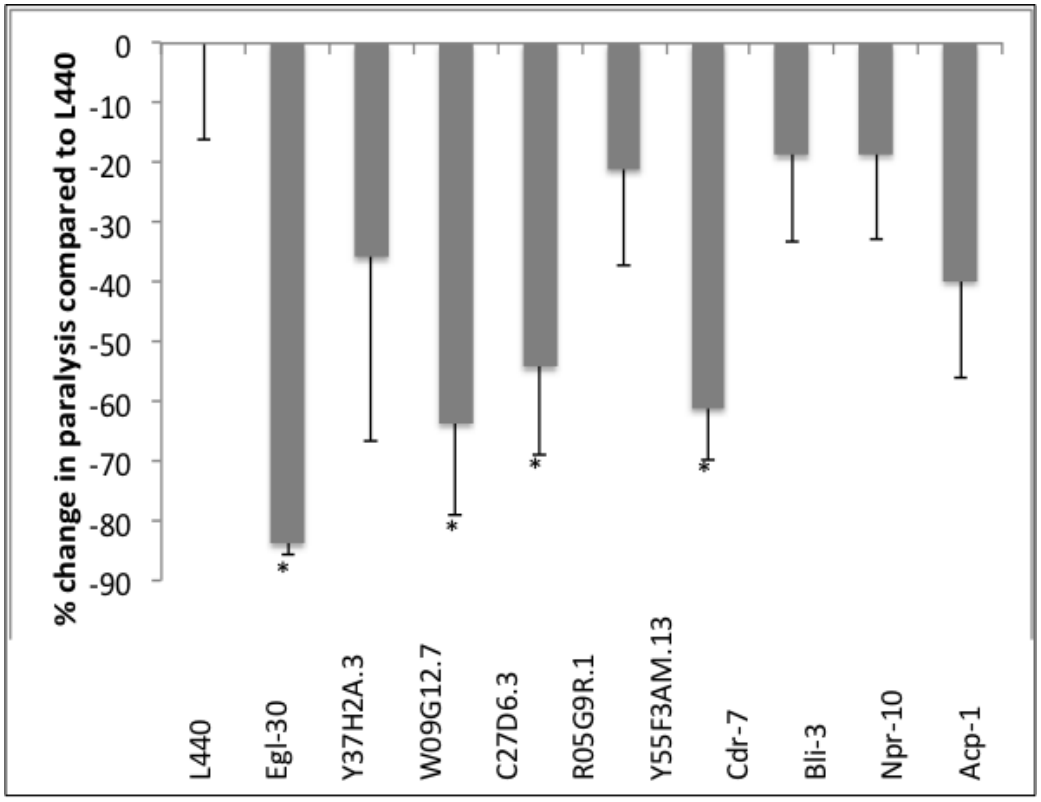

Figure 3.17 – **Testing of a selection of genes from the outer shells using the aldicarb-sensitivity genes as a core.** RNAi knockdown and aldicarb sensitivity assays were performed as described in Figure 3.5, and the percentage of paralyzed worms was calculated at 140 minutes. The percentage change to L440 was then calculated and plotted. Egl-30 was the positive control. Hits are significant and marked with an asterix if calculated P values calculated (Section 2.5) are less than 0.05. N=3. Error bars represent standard deviation.

but no other overlap between the two strains was seen. Two other knockdowns led to significant RIC phenotypes in *Tu3335* – these were *C27D6.3* (WBGene00016161) and

Y55F3AM.13 (WBGene00021930). Only eight candidates were tested meaning 32.5% of candidates gave a significant RIC phenotype in *Tu3335*.

Gene Symbol	Wormbase Gene ID	Gene Name	% Change compared to L440	Standard Deviation	P Value	Significant?
M01D7.7	WBGene00001196	egl-30	-83.75	16.16	0.005	Yes
C27D6.3	WBGene00016161	C27D6.3	-54.21	1.86	0.039	Yes
C53C7.1	WBGene00008278	npr-10	-18.51	13.7	0.309	No
K01D12.13	WBGene00010472	cdr-7	-18.74	14.46	0.305	No
R05G9R.1	WBGene00019906	R05G9R.1	-21.08	16.1	0.296	No
W09G12.7	WBGene00021121	W09G12.7	-63.59	15.39	0.027	Yes
Y55F3AM.13	WBGene00021930	Y55F3AM.13	-61.1	8.66	0.011	No
ZK563.6	WBGene00022770	acp-1	-39.76	16.24	0.100	No
Y37H2A.3	WBGene00012563	Y37H2A.3	-35.85	30.95	0.328	No

Table 3.13 – Background data associated with Figure 3.17.

Some potentially interesting novel candidate proteins were identified while testing proteins in the outer interaction shells. One of these proteins was W09G12.7 (human ortholog FAM133A), which consistently showed a significant RIC phenotype. This protein is as yet uncharacterized as is cdr-7. The only information known about C27D6.3 is that it is involved in locomotion. The final protein found to have a positive phenotype in this small data set was npr-10, which is predicted to have neuropeptide Y receptor activity due to its protein domain structure. Its human ortholog is Prolactin Releasing Hormone Receptor (PRLHR). All of these hits require further validation and characterization to establish their potential roles in synaptic physiology.

3.3.8 Using betweenness to identify novel effectors of aldicarb sensitivity

To prioritize genes based on relative betweenness scores, the same aldicarb-sensitivity genes used for the connectivity algorithm were again utilized as core nodes. However, due to the lack of predictive power of the connectivity algorithm, an additional subset of core nodes was added based on their Gene Ontology (GO) terms. Supplementary table 3.3

shows the GO terms and genes that were selected. The hypothesis was that addition of these *synaptic transmission* related nodes to the network could enable the betweenness algorithm to better predict novel functional regulators of synaptic function, which could be detected by aldicarb sensitivity assays.

The Network Analysis plugin on Cytoscape was used to rank the betweenness of nodes in the extended one-step known aldicarb/synaptic transmission network (Figure 3.18), which contained 3459 protein nodes and 75428 interactions. Table 3.14 lists the 100 proteins with highest betweenness values, and the availability of RNAi clones in the knockdown library. Aldicarb core nodes were not ranked in this table, but ranged from having high betweenness (as high or higher than the novel genes) to very low betweenness. There is a large degree of overlap between the highest connected nodes and nodes with highest betweenness values (Figure 3.19 and Table 3.15), with 37 proteins being found in both datasets. In total, 67 genes in the list had available RNAi clones, of which 37 had already been tested in the previous connectivity screen, leaving 30 additional proteins that were only found in the betweenness dataset.

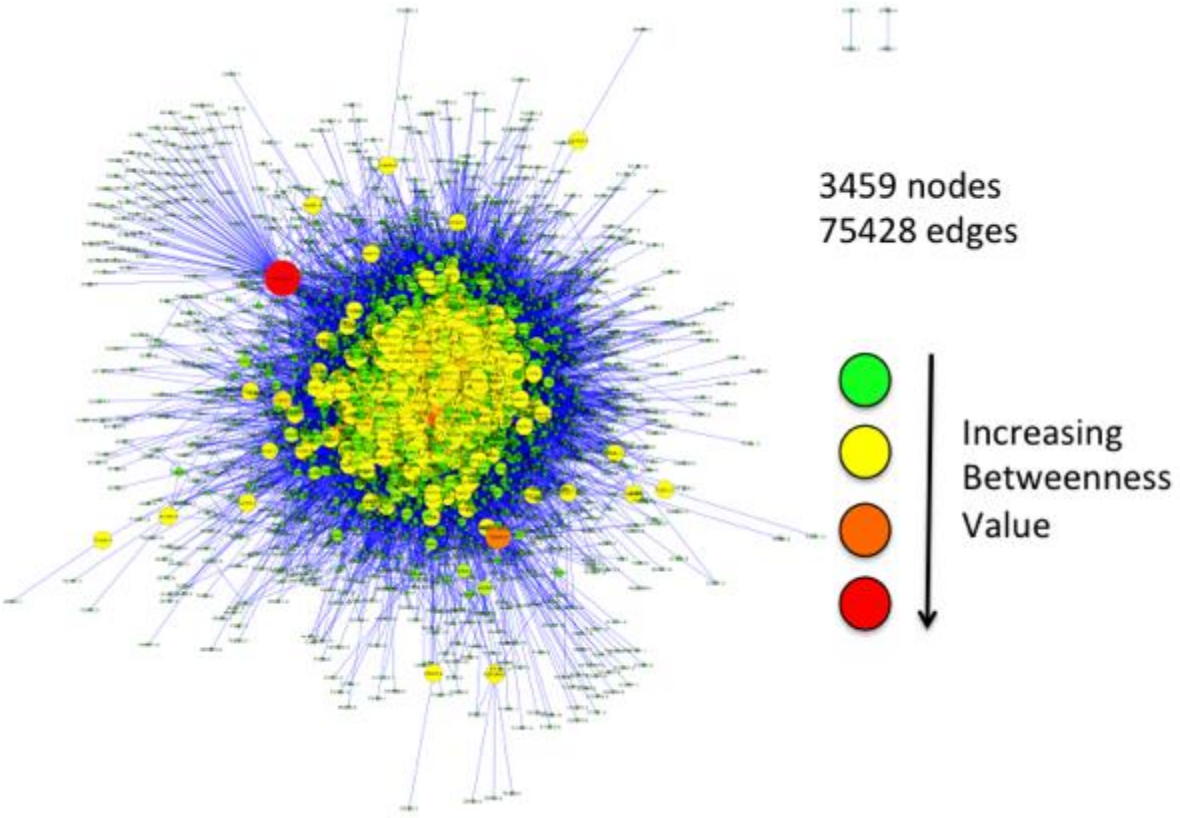

Figure 3.18 - **Network to show betweenness rankings of genes in a one-step aldicarb and synaptic transmission network.** A one-step network was created using the known aldicarb-sensitivity genes and known genes involved in synaptic function (from GO terms). Betweenness was then calculated using the NetworkAnalyzer Plugin on Cytoscape, and the top 100 betweenness ranked genes (not including known aldicarb-sensitive genes) were tested (provided they were in the RNAi library). Colours denote the level of betweenness, with green being the lowest and red being the highest-ranking betweenness nodes.

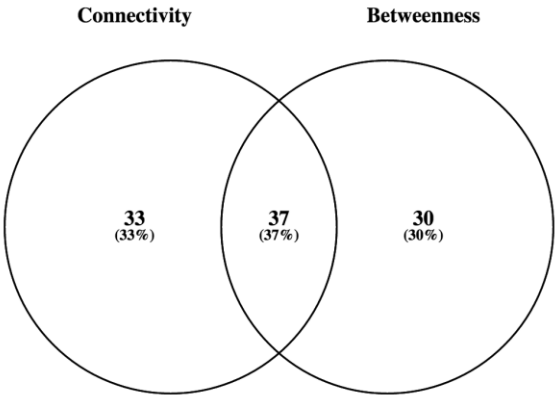

Figure 3.19 – Venn diagram showing the overlap between candidate effectors identified in both connectivity and betweenness network analysis.

Gene Name	Betweenness Centrality	Betweenness Ranking	Rnai
rpn-10	0.01446289	1	No
rpl-4	0.01327419	2	Yes
his-46	0.01147944	3	No
rps-0	0.00953103	4	Yes
pmk-1	0.00819131	5	Yes
F10F2.2	0.00795573	6	No
his-38	0.00781085	7	No
his-47	0.00753449	8	No
ftt-2	0.00747005	9	Yes
act-4	0.00727339	10	Yes
sma-2	0.00690071	11	Yes
rpl-27	0.00685742	12	Yes
his-45	0.0066567	13	No
C01G10.8	0.00664515	14	No
pacs-1	0.00648567	15	Yes
trx-1	0.00623208	16	No
daf-21	0.0061012	17	Yes
pitr-2	0.00588545	18	Yes
B0035.13	0.00581559	19	No
laf-1	0.00577273	20	No
rpl-23	0.00568412	21	Yes
tbb-4	0.00562789	22	Yes
rpl-2	0.00558434	23	No
htz-1	0.00528366	24	Yes
pbs-4	0.00509202	25	No
pod-2	0.00474082	26	Yes
ant-1.3	0.00454172	27	Yes
his-28	0.00450048	28	No
cmd-1	0.00446641	29	No
his-48	0.00445807	30	Yes
B0395.3	0.00437873	31	Yes
rpia-1	0.00432888	32	Yes
gcn-1	0.00420023	33	No
mdh-2	0.00404524	34	Yes
cul-1	0.0039867	35	Yes
rps-18	0.00396697	36	Yes
W02A2.9	0.00387459	37	No
glr-1	0.00360248	38	Yes
rps-29	0.0035667	39	Yes
soc-2	0.00354351	40	Yes
nars-1	0.00344108	41	Yes
B0280.9	0.00336552	42	Yes
gpd-2	0.00335692	43	Yes
Y46E12BL.2	0.00333671	44	No
emb-8	0.00333547	45	Yes
mrpl-11	0.00331015	46	Yes
cpsf-1	0.00328232	47	Yes
gpd-4	0.00322292	48	No
sti-1	0.00322012	49	No
leo-1	0.00319567	50	Yes
Y55F3AM.14	0.00317359	51	Yes
cyc-1	0.00316899	52	Yes
smo-1	0.00314698	53	Yes
B0228.7	0.00313343	54	Yes
lonp-1	0.0031087	55	Yes
his-11	0.00308458	56	No
tag-174	0.00306346	57	Yes
spr-2	0.00302763	58	Yes
vps-16	0.00298784	59	Yes
rad-51	0.00296991	60	Yes
rpl-38	0.00288523	61	Yes
ife-3	0.00287895	62	Yes
cgh-1	0.00286619	63	Yes
pgk-1	0.00285258	64	Yes
eef-2	0.0028429	65	Yes
pcn-1	0.0027868	66	No
kin-3	0.00277493	67	Yes
cfim-2	0.00277219	68	Yes
B0001.4	0.00276876	69	Yes
rpl-12	0.0026817	70	Yes
gsp-2	0.00267409	71	Yes
swsn-1	0.00266304	72	Yes
B0281.3	0.00265989	73	No
spe-5	0.00262109	74	Yes
fars-3	0.00260524	75	No
pfd-4	0.00255666	76	Yes
pkn-1	0.00253968	77	Yes
eif-3b	0.00253316	78	Yes
B0272.3	0.00251809	79	Yes
C33F10.12	0.00251744	80	Yes
glp-4	0.00251291	81	Yes
dhc-1	0.00250561	82	No
ubql-1	0.0024664	83	Yes
scbp-2	0.00245909	84	Yes
his-15	0.00245177	85	No
goa-1	0.00244342	86	No
sqd-1	0.00243936	87	No
Y66H1A.4	0.00238334	88	Yes
unc-16	0.00237395	89	Yes
cyp-25a5	0.00237308	90	Yes
his-4	0.00236978	91	Yes
daam-1	0.0023615	92	No
rpl-30	0.00233505	93	Yes
trx-2	0.00232712	94	Yes
B0250.5	0.00232511	95	Yes
tag-335	0.0022897	96	Yes
vdac-1	0.00226132	97	Yes
rpn-11	0.00225889	98	Yes
casy-1	0.00225303	99	Yes
rpl-7A	0.00221131	100	No

Table 3.14 – Highest ranking betweenness proteins/genes from the one-step aldicarb and synaptic related network (not including genes previously known to cause a RIC of HIC phenotype). Betweenness was measured using the Network analyzer plugin on Cytoscape.

Aldicarb screens were carried out on the betweenness candidates as described for preceding connectivity screens. Data presented in Figure 3.20 and Table 3.16 show that 10 of the 30 candidate proteins showed reproducibly pronounced changes in rate of aldicarb-induced paralysis. Significantly, all of these positive phenotypes were independently validated at a 160-minute time point (Figure 3.21 and Table 3.17), with the exception of rpy-1, which displayed no change in aldicarb sensitivity.

Gene Name	Screen	Gene Name	Screen	Gene Name	Screen
trx-2	Connectivity	eef-1A.1	Betweenness	arf-1.2	Connectivity and Betweenness
ubql-1	Connectivity	rps-6	Betweenness	rpl-27	Connectivity and Betweenness
rps-16	Connectivity	ZK1098.1	Betweenness	rps-29	Connectivity and Betweenness
ant-1.3	Connectivity	cyn-7	Betweenness	pacs-1	Connectivity and Betweenness
M28.5	Connectivity	B0361.6	Betweenness	B0250.5	Connectivity and Betweenness
htz-1	Connectivity	unc-37	Betweenness	rpl-17	Connectivity and Betweenness
rpl-12	Connectivity	T22D1.3	Betweenness	kin-3	Connectivity and Betweenness
his-8	Connectivity	his-67	Betweenness	smo-1	Connectivity and Betweenness
rpn-11	Connectivity	his-68	Betweenness	B0001.4	Connectivity and Betweenness
ola-1	Connectivity	vdac-1	Betweenness	sma-2	Connectivity and Betweenness
casy-1	Connectivity	rpl-13	Betweenness	pitr-2	Connectivity and Betweenness
vps-34	Connectivity	rpl-35	Betweenness	tbb-4	Connectivity and Betweenness
cul-1	Connectivity	eef-1A.2	Betweenness	his-48	Connectivity and Betweenness
rpl-11.1	Connectivity	inf-1	Betweenness	pmk-1	Connectivity and Betweenness
B0205.6	Connectivity	rps-20	Betweenness	B0272.3	Connectivity and Betweenness
gpa-12	Connectivity	ruvb-2	Betweenness	ife-3	Connectivity and Betweenness
B0228.7	Connectivity	glp-4	Betweenness	act-4	Connectivity and Betweenness
hsp-60	Connectivity	Y54E10A.10	Betweenness	act-1	Connectivity and Betweenness
soc-2	Connectivity	mrpl-47	Betweenness	gsp-2	Connectivity and Betweenness
ggtb-1	Connectivity	his-3	Betweenness	leo-1	Connectivity and Betweenness
gpd-3	Connectivity	rpl-30	Betweenness	rps-7	Connectivity and Betweenness
gpd-2	Connectivity	cdk-12	Betweenness	B0303.3	Connectivity and Betweenness
pfd-4	Connectivity	orc-1	Betweenness	act-3	Connectivity and Betweenness
mrpl-11	Connectivity	rpl-1	Betweenness	rps-1	Connectivity and Betweenness
nol-5	Connectivity	rpl-38	Betweenness	acly-2	Connectivity and Betweenness
nars-1	Connectivity	rps-18	Betweenness	B0280.9	Connectivity and Betweenness
eif-2beta	Connectivity	rpl-7	Betweenness	ftt-2	Connectivity and Betweenness
pod-2	Connectivity	air-2	Betweenness	rpia-1	Connectivity and Betweenness
pdi-6	Connectivity	rpy-1	Betweenness	cyn-10	Connectivity and Betweenness
his-4	Connectivity	eef-2	Connectivity and Betweenness	rpl-4	Connectivity and Betweenness
T04C9.1	Connectivity	rps-17	Connectivity and Betweenness	rpl-23	Connectivity and Betweenness
ppfr-4	Connectivity	B0395.3	Connectivity and Betweenness	his-1	Connectivity and Betweenness
lonp-1	Connectivity	daf-21	Connectivity and Betweenness	mdh-2	Connectivity and Betweenness
pab-1	Betweenness	T10C6.14	Connectivity and Betweenness		

Table 3.15 – Table to show the overlap between connectivity and betweenness screens. Genes found in both screens encode proteins that have both high connectivity to known RIC or HIC proteins or high betweenness scores in an extended RIC/HIC and synaptic transmission network.

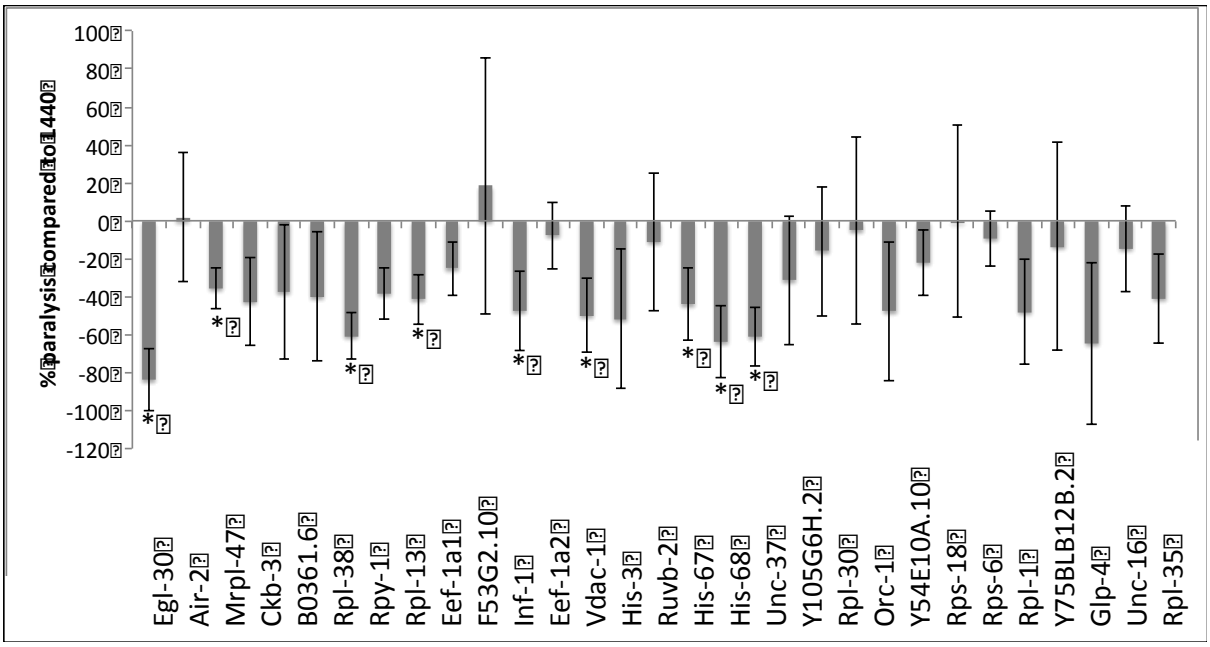

Figure 3.20 – **Aldicarb-sensitivity screening of genes with high betweenness values in the one-step aldicarb and synaptic-related network.** RNAi knockdown and aldicarb sensitivity assays were performed as described in Figure 3.5, with the percentage measured at 140 minutes. The percentage change to L440 was then calculated and plotted. Egl-30 was the positive control. Hits are significant and marked with an asterix if calculated P values calculated (Section 2.5) are less than 0.05. N=3. Error bars represent standard deviation.

Gene Symbol	Wormbase Gene ID	Gene Name	% Change Compared To L440	Standard Deviation	P Value	Significant?
C18H9.7	WBGene00004507	rpy-1	-60.68	12.54	0.008	Yes
W02D3.9	WBGene00006773	unc-37	-61.14	15.54	0.010	Yes
T23D8.6	WBGene00001942	his-68	-63.67	18.93	0.013	Yes
B0261.4	WBGene00015092	mrpl-47	-35.58	10.70	0.019	Yes
C32E8.2	WBGene00004425	rpl-13	-38.31	13.49	0.020	Yes
F31E3.5	WBGene00001168	eef-1A.1	-41.29	13.25	0.024	Yes
R03G5.1	WBGene00001169	eef-1A.2	-47.57	20.75	0.027	Yes
T10C6.12	WBGene00001877	his-3	-49.85	19.71	0.028	Yes
T23D8.5	WBGene00001941	his-67	-44.06	18.83	0.034	Yes
F53G12.10	WBGene00004418	rpl-7	-25.22	14.08	0.048	Yes
Y71F9AL.13	WBGene00004412	rpl-1	-47.95	27.80	0.053	No
B0285.1	WBGene00007135	cdk-12	-42.63	23.30	0.056	No
T22D1.10	WBGene00020687	ruvb-2	-51.87	36.63	0.084	No
Y54E10A.10	WBGene00021830	Y54E10A.10	-21.94	17.51	0.132	No
Y87G2A.5	WBGene00006936	glp-4	-64.44	42.80	0.136	No
ZK652.4	WBGene00004449	rpl-35	-40.81	23.63	0.139	No
Y39A1A.12	WBGene00012650	orc-1	-47.64	36.59	0.194	No
C06B8.8	WBGene00004452	rpl-38	-40.03	34.17	0.202	No
Y105E8A.16	WBGene00004489	rps-20	-31.44	33.79	0.202	No
ZK1098.1	WBGene00014218	ZK1098.1	-14.57	22.72	0.359	No
Y71A12B.1	WBGene00004475	rps-6	-9.39	14.65	0.366	No
Y106G6H.2	WBGene00003902	pab-1	-16.05	34.23	0.478	No
R05G6.7	WBGene00019900	vdac-1	-7.64	17.72	0.515	No
B0361.6	WBGene00015160	B0361.6	-37.42	35.59	0.628	No
T22D1.3	WBGene00020682	T22D1.3	-11.07	36.29	0.633	No
F57B9.6	WBGene00002083	inf-1	18.57	67.62	0.638	No
Y75B12B.2	WBGene00000883	cyn-7	-13.54	54.58	0.663	No
Y106G6H.3	WBGene00004444	rpl-30	-5.05	49.30	0.873	No
B0207.4	WBGene00000099	air-2	1.97	34.07	0.925	No
Y57G11C.16	WBGene00004487	rps-18	-0.18	50.53	0.996	No

Table 3.16 – Background data associated with Figure 3.20.

Gene Symbol	Wormbase Gene ID	Gene Name	% Change Compared To L440	Standard Deviation	P Value	Significant?
B0261.4	WBGene00015092	mrpl-47	-56.82	9.98	0.001	Yes
B0285.1	WBGene00007135	cdk-12	-77.36	3.81	0.001	Yes
C32E8.2	WBGene00004425	rpl-13	-78.17	3.20	0.001	Yes
T10C6.12	WBGene00001877	his-3	-78.37	11.00	0.001	Yes
W02D3.9	WBGene00006773	unc-37	-78.74	10.69	0.001	Yes
T23D8.5	WBGene00001941	his-67	-84.89	10.71	0.001	Yes
F31E3.5	WBGene00001168	eef-1A.1	-70.71	19.22	0.005	Yes
R03G5.1	WBGene00001169	eef-1A.2	-34.83	9.72	0.011	Yes
T23D8.6	WBGene00001942	his-68	-57.77	28.72	0.029	Yes
C18H9.7	WBGene00004507	rpy-1	-20.02	60.23	0.597	No

Table 3.17 – Background data associated with Figure 3.21.

3.9 Data mining of betweenness hits

Proteins showing a positive phenotype from the betweenness analysis were analyzed in Wormbase, to extract functional descriptors (Table 3.18). Again multiple histone proteins including, *his-67* (WBGene00001941) and *his-68* (WBGene00001942), ribosomal proteins and transcription factors were found in this screen. When the list of novel gene symbols were inputted into DAVID, similar trends as seen for data from connectivity screens were seen, including development and chromatin organization and assembly (Table 3.19).

Table 3.20 shows the betweenness ranking of the hits (including those that were also found in the connectivity screen). There did not seem to be a bias, as nodes with a higher betweenness rating were no more likely to show a phenotype than those with a lower betweenness ranking. This suggests that the algorithm is not the best for prioritizing nodes to elucidate novel effectors of synaptic function, but may still elucidate interesting effectors. However, no analysis was carried out on genes with a low betweenness score in this network, in order to test the validity of this prioritization method.

The human orthologs of the betweenness candidates were found using DIOPT fly RNAI (Table 3.21). Interestingly, only one of the human orthologs, *rpl-13* was found in the SynaptomeDB (Pirooznia et al., 2012). However, nine of the common hits shared between the connectivity and betweenness screens were also found in the synaptome database (Table 3.22).

Positive hits identified in the connectivity and betweenness screens were then investigated to assess the extent of physically association between two sets of proteins that were found to share common functional phenotypes (Figure 3.22 and Table 3.23). Interestingly, his-67 interacts with six of the other positive hits, forming a cluster of interconnected proteins. In contrast, unc-37 (WBGene00006773) does not interact with any of the other novel effectors of aldicarb sensitivity.

A network was then generated to show the interaction of positive effectors identified in betweenness screens with previously known aldicarb-sensitivity and synaptic-related nodes (Figure 3.23). There is a spread in the connectivity of the hits to aldicarb and/or synaptic related genes. Unc-37 only has one interaction partner, yet others like rpl-23 have 23 (Table 3.24). Many genes that were previously known to cause an aldicarb-phenotype, or have synaptic related GO terms also interacted with multiple novel protein effectors identified in this study (Table 3.25).

Gene Symbol	Wormbase Gene ID	Gene Name	Screen	Description
F31E3.5	WBGene00001168	eef-1A.1	Betweenness	Identical to EEF-1A.2. Encodes a translation elongation factor 1-alpha homolog essential for fertility, the viability of embryos and germline maintenance.
R03G5.1	WBGene00001169	eef-1A.2	Betweenness	Identical to EEF-1A.1.
W02D3.9	WBGene00006773	unc-37	Betweenness	Encodes the ortholog of Groucho, a *D. Melanogaster* protein, and is known to be essential in the specification of neuronal cell fate. It is also known to interact genetically with transcriptional mediator components.
B0285.1	WBGene00007135	cdk-12	Betweenness	Predicted to bind ATP and have protein kinase activity. Involved in embryonic and larval development, locomotion and receptor-mediated endocytosis.
T23D8.5	WBGene00001941	his-67	Betweenness	Encodes an H4 histone required for embryonic viability and growth.
T23D8.6	WBGene00001942	his-68	Betweenness	Encodes an H2A histone.
C32E8.2	WBGene00004425	rpl-13	Betweenness	Encodes a large ribosomal subunit L13 protein.
B0261.4	WBGene00015092	mrpl-47	Betweenness	Thought to be a structural component of the ribosome, and is involved in the determination of adult lifespan, embryonic and larval development, and oogenesis.
T10C6.12	WBGene00001877	his-3	Betweenness	Encodes an H2A histone, and is predicted to function as a component of the nucleosome.
F56C9.1	WBGene00001748	gsp-2	Betweenness and Connectivity	Encodes an ortholog of human PPP1CA (protein phosphatase 1, catalytic subunit, alpha isozyme) and PPP1CC (protein phosphatase 1, catalytic subunit, gamma isozyme).
M03F4.2	WBGene00000066	act-4	Betweenness and Connectivity	Encodes an actin isoform most similar to act-2; an act-4 reporter gene is expressed in body wall and vulval muscles and the spermatheca.
B0250.5	WBGene00007122	B0250.5	Betweenness and Connectivity	Encodes an ortholog of human HIBADH (3-hydroxyisobutyrate dehydrogenase). Predicted to have the ability to bind NAD,
F56F3.5	WBGene00004470	rps-1	Betweenness and Connectivity	Encodes a small ribosomal subunit S3A protein.
F52D10.3	WBGene00001502	ftt-2	Betweenness and Connectivity	Encodes a 14-3-3 protein. Required the regulation of the localization of YAP-1 product, a Yes-associated protein (Yap) homolog, between the cytoplasm and the nucleus.
B0336.10	WBGene00004435	rpl-23	Betweenness and Connectivity	Encodes a large ribosomal subunit L23 protein.
F25H5.4	WBGene00001167	eef-2	Betweenness and Connectivity	Encodes a homolog of translation elongation factor 2 (EEF-2), a GTP-binding protein essential for the elongation phase of protein synthesis. EEF-2 is required for embryogenesis and vulval morphogenesis, and is expressed during all stages of development, including the dauer larval stage.
B0348.6	WBGene00002061	ife-3	Betweenness and Connectivity	Encodes one of five *C. elegans* homologs of the mRNA cap-binding protein eIF4E.

Table 3.18 – Description of genes with high betweenness that caused a significant change in aldicarb sensitivity. Genes found to be in the top 100 connectivity and betweenness tables, which caused a significant change in aldicarb sensitivity are shown. Data was mined from Wormbase.

Biological Process	Count	Gene Name(s)
Embryonic development ending in birth or egg hatching	15	act-4, gsp-2, eef-1a2, rps-1, rpl-23, eef-1a1, his-3, mrpl-47, unc-37, eef-2, his-67, cdk-12, his-68, ife-3, rpl-13
Nematode larval development	14	act-4, eef-1a2, rps-1, ftt-2, rpl-23, eef-1a1, his-3, mrpl-47, unc-37, eef-2, his-67, cdk-12, his-68, rpl-13
Larval development	14	act-4, eef-1a2, rps-1, ftt-2, rpl-23, eef-1a1, his-3, mrpl-47, unc-37, eef-2, his-67, cdk-12, his-68, rpl-13
Post-embryonic development	14	act-4, eef-1a2, rps-1, ftt-2, rpl-23, eef-1a1, his-3, mrpl-47, unc-37, eef-2, his-67, cdk-12, his-68, rpl-13
Growth	13	act-4, eef-1a2, rps-1, ftt-2, rpl-23, eef-1a1, mrpl-47, his-3, eef-2, his-67, cdk-12, his-68, rpl-13
Translation	8	eef-1a1, mrpl-47, eef-1a2, eef-2, rps-1, ife-3, rpl-23, rpl-13
Hermaphrodite genitalia development	8	act-4, his-3, unc-37, eef-2, rps-1, cdk-12, his-67, his-68
Genitalia development	8	act-4, his-3, unc-37, eef-2, rps-1, cdk-12, his-67, his-68
Sex differentiation	8	act-4, his-3, unc-37, eef-2, rps-1, cdk-12, his-67, his-68
Reproductive developmental process	8	act-4, his-3, unc-37, eef-2, rps-1, cdk-12, his-67, his-68
Reproductive process in a multicellular organism	7	eef-1a1, his-3, gsp-2, eef-1a2, unc-37, his-68, ftt-2
Multicellular organism reproduction	7	eef-1a1, his-3, gsp-2, eef-1a2, unc-37, his-68, ftt-2
Chromatin organization	4	his-3, gsp-2, his-67, his-68
Chromosome organization	4	his-3, gsp-2, his-67, his-68
Oviposition	4	his-3, gsp-2, his-68, ftt-2
Reproductive behavior in a multicellular organism	4	his-3, gsp-2, his-68, ftt-2
Reproductive behavior	4	his-3, gsp-2, his-68, ftt-2
Molting cycle, collagen and cuticulin-based cuticle	3	gsp-2, rps-1, rpl-23
Molting cycle, protein-based cuticle	3	gsp-2, rps-1, rpl-23
Molting cycle	3	gsp-2, rps-1, rpl-23
Chromatin assembly	3	his-3, his-67, his-68
Nucleosome organization	3	his-3, his-67, his-68
Nucleosome assembly	3	his-3, his-67, his-68
Protein-DNA complex assembly	3	his-3, his-67, his-68
DNA packaging	3	his-3, his-67, his-68
Chromatin assembly or disassembly	3	his-3, his-67, his-68

Table 3.19 – Biological process enrichment of hits from the betweenness screens. Hits from the betweenness screen (including those found in both the connectivity and betweenness data sets) were inputted into DAVID, and functional clustering was carried out. The count signifies how many genes were enriched in particular biological processes.

Gene Name	Betweenness Centrality	Betweenness Ranking
rpl-23	0.0097127	7
ftt-2	0.00933241	8
R03G5.1	0.00625393	15
gsp-2	0.00600663	16
act-4	0.00567444	18
T23D8.5	0.00559809	19
W02D3.9	0.00557579	20
ife-3	0.00483473	26
C32E8.2	0.00476624	27
B0250.5	0.0046099	28
B0285.1	0.00416142	36
B0261.4	0.00371284	44
eef-2	0.00363815	46
F31E3.5	0.0033845	54
T10C6.12	0.00321661	59
T23D8.6	0.00321597	60
F56F3.5	0.00304557	66

Table 3.20 – Betweenness ranking of hits from the betweenness screen. Betweenness was measured in the one-step aldicarb and synaptic transmission-related one-step network. Betweenness centrality was measured using the network-analyzer plugin on Cytoscape.

Worm Gene Symbol	Wormbase Gene ID	Worm Gene Name	Human Entrez ID	Human Gene Symbol	DIOPT Score
B0261.4	WBGene00015092	mrpl-47	57129	MRPL47	7.809
B0285.1	WBGene00007135	cdk-12	8621	CDK13	7.809
B0285.1	WBGene00007135	cdk-12	51755	CDK12|CDK13	7.809
C32E8.2	WBGene00004425	rpl-13	6137	RPL13	8.859
T10C6.12	WBGene00001877	his-3	8338	HIST2H2AC	2.901
W02D3.9	WBGene00006773	unc-37	7090	TLE3	5.848
F31E3.5	WBGene00001168	eef-1A.1	1915	EEF1A1	2.93
R03G5.1	WBGene00001169	eef-1A.2	1917	EEF1A2	7.808
T23D8.6	WBGene00001942	his-68	8338	HIST2H2AC	2.901

Table 3.21 – Human orthologs of the hits found solely in the betweenness screen. Diopt FlyRNAI (Hu et al., 2011) was used to elucidate the closest human ortholog. The DIOPT score refers to how many databases predicted the ortholog match.

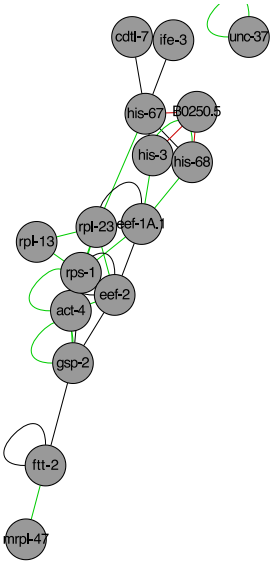

Figure 3.22 – **Interconnectivity of betweenness hits.** Cytoscape version 3 was used to merge the Wormbase and worm interactome networks, in order to visualize interaction partners between the hits elucidated in the betweenness screen. Interactions between human orthologs are shown in red, *S. cerevisiae* in black, and both human and *S. cerevisiae* in green.

Gene Name	Screen	Number of Betweenness Hit Interactors
his-67	Betweenness	6
eef-2	Betweenness|Connectivity	5
rpl-23	Betweenness|Connectivity	5
rps-1	Betweenness|Connectivity	5
gsp-2	Betweenness|Connectivity	4
his-3	Betweenness	4
eef-1a1	Betweenness	4
his-68	Betweenness	4
act-4	Betweenness|Connectivity	3
B0250.5	Betweenness|Connectivity	3
rpl-13	Betweenness	2
ftt-2	Betweenness|Connectivity	2
cdk-12	Betweenness	1
unc-37	Betweenness	1
ife-3	Betweenness|Connectivity	1
mrpl-47	Betweenness	1

Table 3.23 – The number of other novel hits each hit from the betweenness screen interacts with. This data was generated from the network shown in Figure 3.22, which shows interactions between the novel betweenness genes that caused a significant change in aldicarb sensitivity.

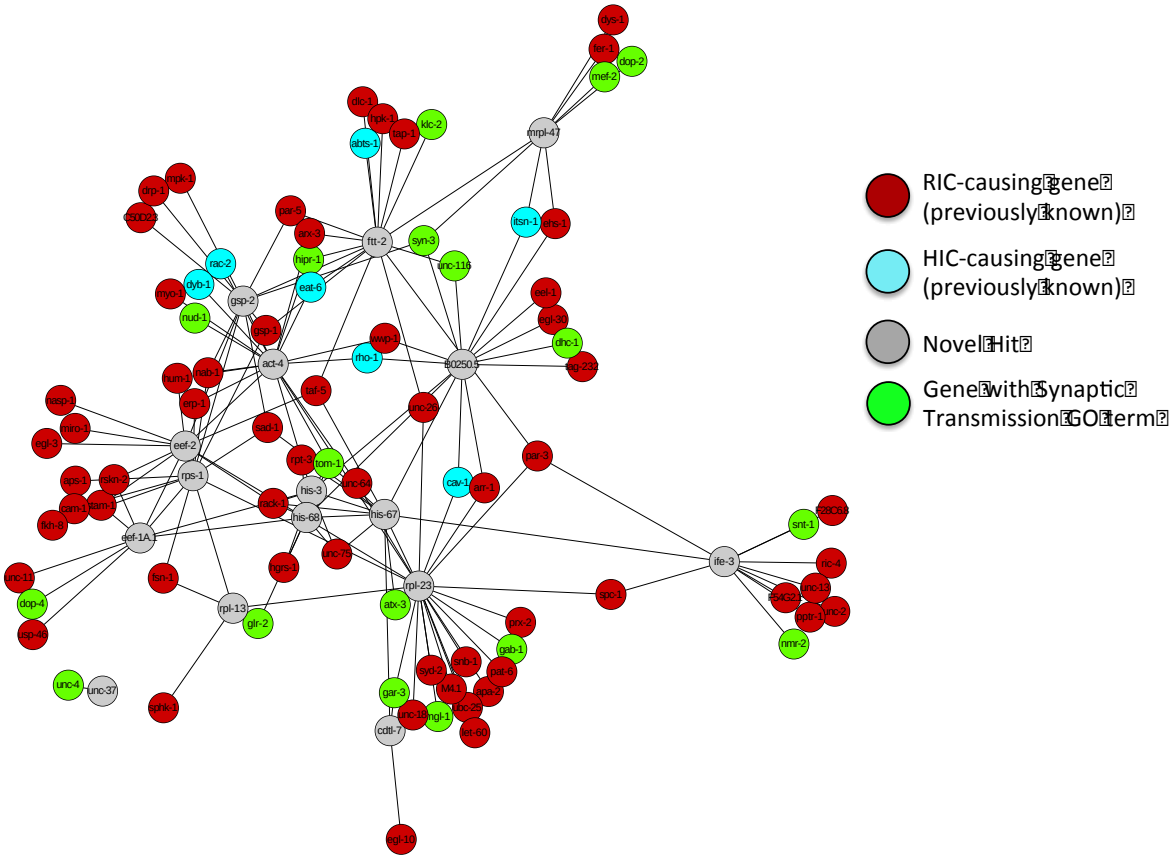

Figure 3.23 – **Network showing the hits elucidated from the betweenness screen, and the interactors previously known to cause an aldicarb-sensitivity phenotype. Grey** nodes represent the novel hits, red indicate genes previously shown to cause a RIC phenotype, and blue are genes previously shown to cause a HIC phenotype. Green nodes represent genes that are not known to cause an aldicarb-sensitivity phenotype, but do have synaptic related GO terms. The aldicarb and synaptic-transmission related network (Figure 3.18) was used to elucidate these interactions, and Cytoscape was used for visualization.

Proteins contained in the betweenness and aldicarb one-step network were analyzed using the DAVID biological enrichment tool. Again synaptic transmission and cholinergic neurotransmission appear as enriched processes, with 9 genes having GO terms of synaptic transmission, of which 3 are specific to cholinergic neurons (Table 3.26). All of these 9 genes were previously known to cause aldicarb phenotypes. When looking at their interacting proteins, it is interesting to note that *unc-75* interacts with three of the novel effectors with high betweenness ranking and low connectivity values (his-68, *his-67* and *his-3*). These are all histone proteins, and *unc-75* is required for neuron-specific splicing of unc-32.

Gene Symbol	Wormbase Gene ID	Gene Name	Number of aldicarb/synaptic related interactors
W02D3.9	WBGene00006773	unc-37	1
C32E8.2	WBGene00004425	rpl-13	4
B0285.1	WBGene00007135	cdk-12	5
B0261.4	WBGene00015092	mrpl-47	8
F31E3.5	WBGene00001168	eef-1A.1	9
T10C6.12	WBGene00001877	his-3	9
T23D8.6	WBGene00001942	his-68	10
B0348.6	WBGene00002061	ife-3	11
F56C9.1	WBGene00001748	gsp-2	12
F25H5.4	WBGene00001167	eef-2	13
F56F3.5	WBGene00004470	rps-1	13
T23D8.5	WBGene00001941	his-67	13
B0250.5	WBGene00007122	B0250.5	15
F52D10.3	WBGene00001502	ftt-2	16
M03F4.2	WBGene00000066	act-4	18
B0336.10	WBGene00004435	rpl-23	23

Table 3.24 – Table showing the number of known aldicarb-sensitivity genes each hit from the betweenness screen interacts with. This corresponds with the network shown in figure 3.23. The aldicarb and synaptic-transmission related network (figure 3.18) was used to elucidate interaction partners of the genes in the betweenness screen, which caused a significant change in aldicarb sensitivity.

The core list of aldicarb-sensitivity genes was updated to include novel protein effectors identified in betweenness informed screens, generating a network (Figure 3.24) with 4565 nodes and 14372 edges.

Gene Name	Biological Process	Aldicarb	Hit Interactor(s)
dys-1	Synaptic Transmission, Cholinergic	RIC	mrpl-47
dyb-1	Synaptic Transmission, Cholinergic	HIC	act-4
ric-4	Synaptic Transmission, Cholinergic	RIC	ife-3
unc-18	Synaptic Transmission, Cholinergic	RIC	cdk-12, rpl-23
unc-64	Synaptic Transmission, Cholinergic	RIC	act-4, rpl-23
unc-75	Synaptic Transmission, Cholinergic	RIC	his-68, his-67, his-3
ehs-1	Synaptic Transmission	RIC	mrpl-47, B0250.5
syd-2	Synaptic Transmission	RIC	rpl-23
unc-2	Synaptic Transmission	RIC	ife-3

Table 3.26 – Synaptic transmission is enriched when genes from the novel aldicarb-sensitivity genes from the betweenness screen and their interacting partners that cause an aldicarb-phenotype are inputted into DAVID. Functional clustering was carried out and biological process enrichment assessed (using standard DAVID parameters).

Gene Symbol	Aldicarb/Synaptic Related	Number of Interacting Hits	Interacting Gene Symbol(s)
tom-1	Synaptic Related	4	his-3, his-67, act-4, his-68
rack-1	RIC	4	his-3, his-67, eef-2, his-68
rpt-3	RIC	4	his-3, his-67, act-4, his-68
nab-1	RIC	3	rps-1, act-4, gsp-2
syx-5	Synaptic Related	3	B0250.5, mrpl-47, gsp-2
sad-1	Synaptic Related|RIC	3	rps-1, his-67, gsp-2
taf-5	RIC	3	his-67, ftt-2, eef-2
gsp-1	RIC	3	rps-1, ftt-2, gsp-2
unc-75	Synaptic Related|RIC	3	his-3, his-67, his-68
unc-64	Synaptic Related|RIC	2	act-4, rpl-23
hipr-1	Synaptic Related	2	ftt-2, act-4
ehs-1	Synaptic Related|RIC	2	B0250.5, mrpl-47
gar-3	Synaptic Related	2	cdk-12, rpl-23
mgl-1	Synaptic Related	2	cdk-12, rpl-23
unc-18	Synaptic Related|RIC	2	cdk-12, rpl-23
eat-6	HIC	2	ftt-2, act-4
spc-1	RIC	2	ife-3, rpl-23
unc-116	Synaptic Related	2	ftt-2, B0250.5
hum-1	RIC	2	act-4, eef-2
unc-26	Synaptic Related|RIC	2	ftt-2, rpl-23
rom-4	HIC	2	B0250.5, mrpl-47
rskn-2	RIC	2	eef-1a1, eef-2
rho-1	HIC	2	act-4, B0250.5

Table 3.25 – Genes that were previously known to cause an aldicarb-sensitivity phenotype or had a related synaptic transmission GO term, which interacted with multiple novel hits from the connectivity screen. Data was extracted from the one-step aldicarb network (Figure 3.9). Genes are listed if they interacted with more than one novel hit, and were known to cause a RIC or HIC phenotype when their expression was altered.

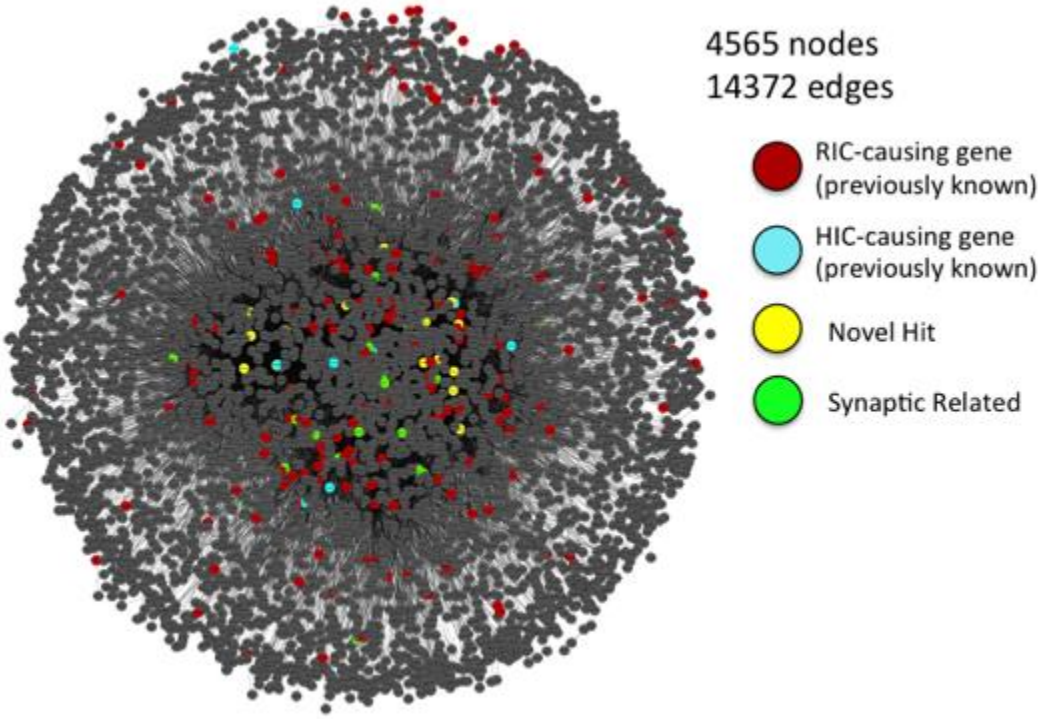

Figure 3.24 – **One-step network using a core of the aldicarb-sensitivity genes and novel betweenness hits.** Yellow nodes indicate betweenness hits, green indicate nodes found in both connectivity and betweenness screens, red are previously known to cause RIC phenotypes, and blue are previously known to cause a HIC phenotype. Cytoscape version 3 was used to generate this network.

3.3.10 Analysis of proteins found to have positive effects on synaptic function in both connectivity and betweenness screens

As there is a large degree of overlap between the connectivity and betweenness datasets, the crossover between the hits was analyzed. As can be seen from data presented in Table 3.27 and Figure 3.25, 8 of the novel protein effectors had both high connectivity and betweenness values. However, it is interesting to note that two of the candidates (C18H9.7 and W02D3.9) had no known interaction with aldicarb-sensitivity genes/proteins. Also, although C18H9.7 (rpy-1) interacts with proteins that have synaptic related GO terms and W02D3.9 (unc-37) is associated with synaptic transmission, neither was previously known to have an aldicarb modifying phenotype. In the independent validation stage, C18H9.7 did not cause an aldicarb-phenotype. However unc-37 showed a 78.7% reduction in paralysis compared to the negative control ($p = 0.0007$). For this reason a full time course experiment after knocking down the unc-37 (in *Tu3311*) was carried out. This confirmed the result (Figure 3.26), showing that network mediated expansion of GO terms is a useful approach to reveal potential novel effectors of synaptic function.

The data generated from both of these screens was added to the current aldicarb and synaptic-related one-step network as core attributes. This expanded the network to contain 4590 nodes and 14753 edges (Figure 3.27).

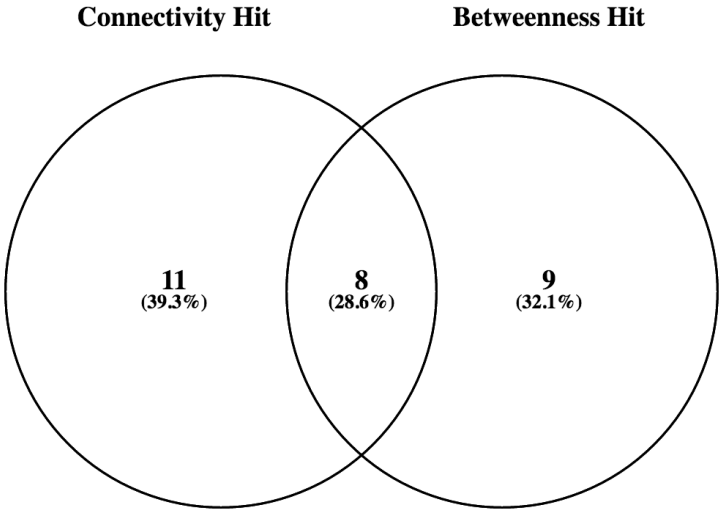

Figure 3.25 – **A Venn Diagram to show the overlap in genes found to cause a change in aldicarb sensitivity, which had both high betweenness and connectivity.** Gene lists of the hits were inputted into a Venn diagram program (Venny), which generated the diagram, and shows that 8 genes are shared between the data sets.

Gene Name	Screen
ppfr-4	Connectivity
pod-2	Connectivity
ola-1	Connectivity
rpl-11.1	Connectivity
his-4	Connectivity
scbp-2	Connectivity
his-8	Connectivity
ubql-1	Connectivity
lonp-1	Connectivity
mrpl-11	Connectivity
B0205.6	Connectivity
rpl-13	Betweenness
cdk-12	Betweenness
mrpl-47	Betweenness
his-68	Betweenness
his-3	Betweenness
eef-1a1	Betweenness
his-67	Betweenness
gsp-2	Betweenness & Connectivity
eef-2	Betweenness & Connectivity
rps-1	Betweenness & Connectivity
B0250.5	Betweenness & Connectivity
ife-3	Betweenness & Connectivity
ftt-2	Betweenness & Connectivity
act-4	Betweenness & Connectivity
rpl-23	Betweenness & Connectivity

Table 3.27 – Table to show the hits found in the connectivity and betweenness screens, and which were found in both screens.

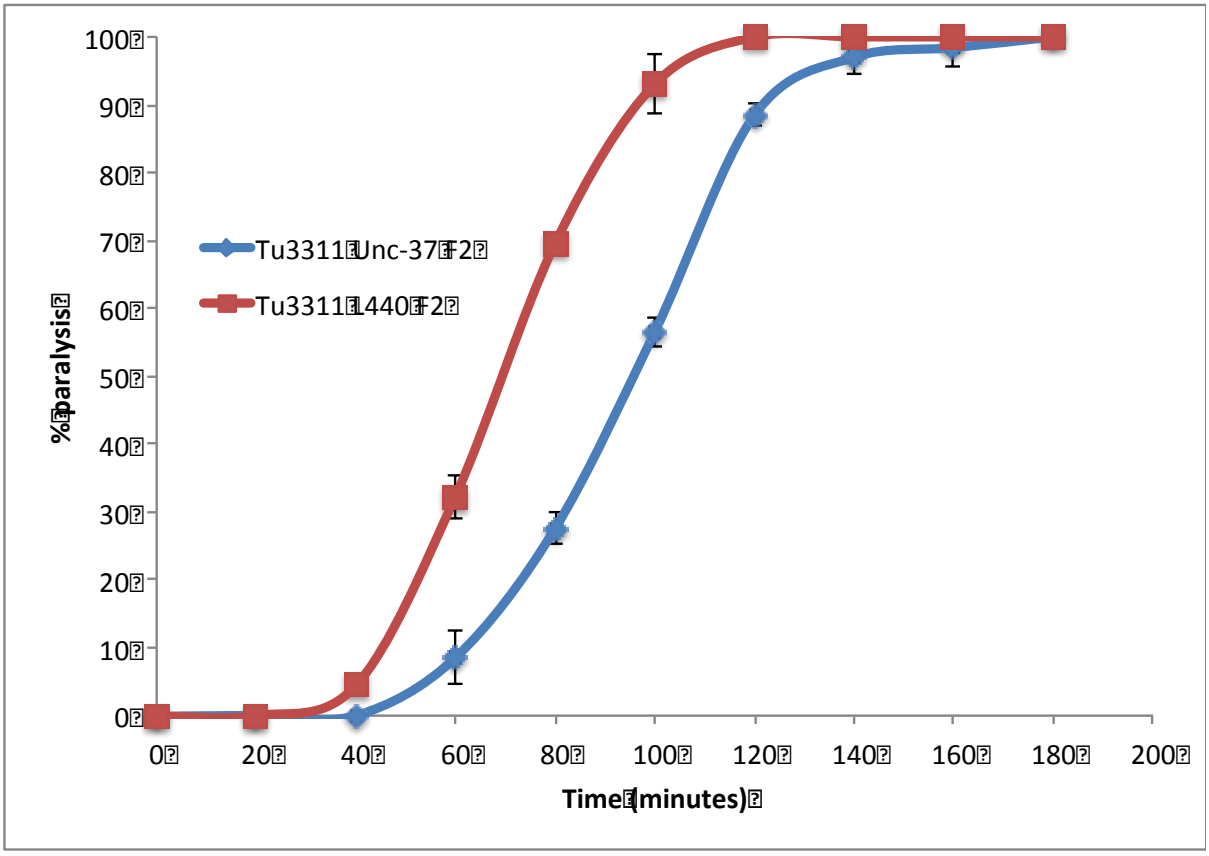

Figure 3.26 – **Full time course aldicarb-sensitivity assay when unc-37 was knocked down in Tu3311.** 4mM IPTG feeding plates were seeded with unc-37 or empty L440 vector dsRNA expressing bacteria. After the plates were dry, adult worms were picked onto plates. Four days later, plates were bleached to another set of unc-37/L440 seeded 4mM IPTG feeding plates. Three days after this the worms (F2 generation) were picked onto 1mM aldicarb plates. Worms were prodded with a metal wire every 20 minutes, and paralysis was assessed. The percentage of paralysis at each time point was calculated and plotted. Unc-37 knockdown leads to a RIC phenotype. N=3. Error bars represent standard deviation.

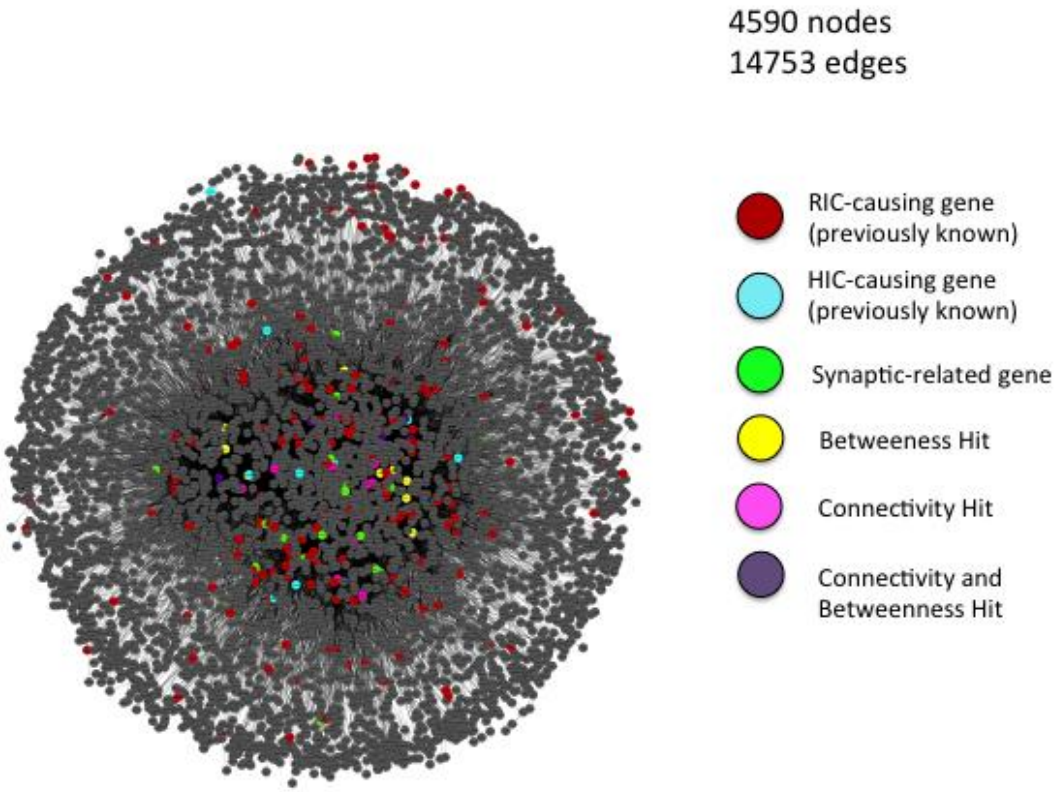

Figure 3.27 – **One-step network using a core of the aldicarb-sensitivity genes and novel betweenness and connectivity hits.** Yellow nodes indicate genes that were found to cause a significant change in aldicarb sensitivity, which were in the top 100 betweenness screen (from the one-step aldicarb and synaptic transmission network). Dark blue nodes indicate the hits genes that were only found as to be in the top 100 connected genes (from the one-step aldicarb network), which caused a significant change in aldicarb sensitivity when knocked down. Green nodes indicate hit genes found in both connectivity and betweenness screens. Red nodes indicate genes that were previously known to cause RIC phenotypes, and light blue nodes indicate genes that were previously known to cause a HIC phenotype. Cytoscape version 2 was used to generate this network, using a spring embedded network.

3.4 Discussion

3.4.1 Connectivity and Betweenness as Graph Theory Methods

Multiple different conclusions can be gathered from the *C. elegans* experiments carried out in this chapter. These results firstly highlight some of the difficulties faced when analyzing networks. The betweenness and connectivity screens showed a large degree of overlap, and many hits were found that had both high

betweenness and connectivity values. There is the possibility that genes with higher connectivity may exhibit high levels of non-specific binding of proteins or sociological bias. However, as a proportion of genes that had a high number of physical associations with known aldicarb genes, also showed an aldicarb phenotype, this limits the theory that high connectivity may be non-specific, and therefore not functionally relevant. The principle of sociological bias was shown in other RNAi screens carried out in *C. elegans*, where genes affected in Aβ and polyQ over-expressing mutants, led to 27 common genes of which 20 had a high connectivity in a global network (Khabirova et al., 2014). Genes that have been discovered to be disease-relevant are inevitably more studied, leading to disproportionate information relating to related proteins in public databases. Nevertheless, it is logical to conclude that high connectivity to known aldicarb sensitivity nodes may by the principle of "Guilt by association" (Oliver, 2000) and phenology prediction methods, indicate a novel functional association. For example, if a translation factor such as eef-2 is knocked down, it is logical that the level of many proteins would be affected, leading to changes in aldicarb-sensitivity, as multiple biological processes would be affected. Therefore, connectivity is a simple yet relevant algorithm to use to attempt to elucidate novel effectors of synaptic function.

As connectivity only looks at the nearest edges of a given node, it is a non-ideal graph theory analytic method if we want to look at features more in line with the global architecture of the network. However, when focused on the one-step network, it does reveal some interesting trends. Firstly, a large number of histone-related proteins were found. This is possibly intuitive as decreasing the levels of

histone proteins would affect the transcription of many genes. There are many different ways that an aldicarb-sensitivity change could occur. Not only could there be a change in exocytosis of acetylcholine or GABA, but also knockdowns that change the efficiency/number of postsynaptic receptors would also cause an effect. The genes being knocked down could be causing an indirect effect much further downstream, which leads to paralysis. This could be the case where transcription/translation factors or histone proteins were knocked down. However, it is interesting to note that other histone proteins were included in the screens (his-48, his-1 and htz-1), but knockdown did not lead to a significant change in aldicarb-sensitivity.

It has previously been suggested that proteins with a high betweenness but low connectivity may be important linking proteins between modules of a network (Joy et al., 2005). As mentioned in 3.3.11 unc-37 fulfilled this role. The 'synaptic transmission' GO term is associated with unc-37, but it has not been reported to interact with any known aldicarb-sensitivity genes and did not have a reported aldicarb modulating phenotype. Its only interaction partner, which shares the same GO term is F26C11.2 (unc-4). Unc-37 is a co-repressor of unc-4, which is an essential homeodomain protein required for synaptic choice (Pflugrad, Meir, Barnes, & Miller 3rd, 1997; Schneider et al., 2012). Specifically, it has been shown to prevent the expression of Ventral B motor neuron (VB) genes in ventral A motor neurons (VA) (via repression of Wnt signaling in VA neurons). Backwards locomotion requires AVA interneurons connecting to VA motor neurons. Unc-4 mutants have the VA motor neurons connecting instead to AVB interneurons, leading to defective backward locomotion (Schneider et al., 2012). Although,

knockdown of unc-4 has not been tested in the aldicarb-sensitivity assay, it's RNAi clone is available in the Vidal RNAi library. It would therefore be interesting to test whether this gene also causes a RIC phenotype when knocked down in Tu3311. Both the VA and VB neurons are cholinergic, so we predict that the genetic knockdown may lead to a change in cholinergic signaling. This would require further testing.

3.4.2 Hits connected to known aldicarb-sensitivity genes

By looking at the interaction partners of the connectivity hits, ric-4 emerged as an aldicarb-sensitivity protein, which connects to the novel genes ife-3 and ubql-1. As mentioned previously ric-4 is the worm ortholog of SNAP-25. The human orthologs of ife-3 and ubql-1 are EIF4E and UBQLN1, respectively. Both of these interactions were found in the Wormnet interaction data (Cho et al., 2014). The interaction between EIF4E and SNAP-25 was found in humans, and the interaction between UBQLN1 and SNAP-25 was identified in human high throughput protein-protein interaction studies.

UBQLN1 plays a regulatory role in autophagy and the Endoplasmic Reticulum Associated Degradation (ERAD) pathway via the ubiquitin-proteasome system. Loss of UBQLN1 has been observed in the brains of patients with Alzheimer's disease (Natunen et al., 2016), UBQLN1 is also found in neurofibrillary tangles and Lewy bodies (Mah, Perry, Smith, & Monteiro, 2000). Analysis of data from BIOGRID revealed interactions between UBQLN1 and two pre-senilins (PSEN1 and PSEN2), which form the catalytic subunit of γ-secretase, which in turn is

responsible for cleaving both Notch and APP. Novel data from this study shows that decreasing the expression of ubql-1 induced a RIC phenotype. Further analysis is required to investigate the mechanistic role of the proteasome system in the aldicarb-sensitivity phenotype.

EIF4e is a translation initiation factor, which is known to play a key role in learning and memory. Single nucleotide polymorphisms in EIF4E have been found in families with autism (Waltes et al., 2014), but the potential effects of mutation or functional perturbation on synaptic function were not described before this study. Therefore, further investigation of ife-3 mutants is needed to better elucidate its role at the synapse.

3.4.3 Overlapping hits from previous screens

Some preliminary RNAi screens had previously been carried out in the lab (unpublished data). Although these studies were not directly complementary one potentially common hit was shared between these screens. This was ftt-2 (WBGene00001502). Ftt-2 is required for controlling localization of Yap-1 between the nucleus and cytoplasm. Yap-1 knockout mutants have been shown to have an extended lifespan (Iwasa et al., 2013). Ftt-2 has also been reported to control the localization of daf-16, the Forkhead Box O (FOXO) ortholog, which acts downstream of the insulin/IIS pathway. This pathway is also crucial in the determination of lifespan. Other genes found to cause lifespan extension, unc-64 and unc-31, also cause RIC phenotypes when mutated, through defects in neurotransmitter secretion. This suggests that a similar effect could be occurring

in the ftt-2 knockdown. To assess this in the future, it would be necessary to measure the levels of acetylcholine being released in the knockdown, possibly through the use of fluorescent reporters. Whether ftt-2 knockdown itself leads to lifespan extension has also not been tested.

3.4.4 Transcription and Translation Factors

One interesting cluster of genes that came from both the connectivity and betweenness screens were translation elongation factors. In the betweenness screen, eef-1A.1 and eef-1A.2 both caused significant RIC phenotypes. Their human orthologs are EEF1A1/EEF1A2. In the connectivity screen, three elongation factors (eef-2, iftb-1 and ife-3) all induced a RIC phenotype. Elongation factor 1A (EEF1A) functions in a GTP-dependent manner, bringing the aminoacylated-tRNA to the ribosome. It has 2 isoforms, EEF1A1 and EEF1A2, which are 92% identical and have 98% amino acid similarity (Soares & Abbott, 2013). Despite their similarity they have a highly differential pattern of expression with EEF1A1 being expressed in the majority of tissues, with the exception of adult neurons and muscle cells, which instead express EEF1A2. A paper published in 2014 highlighted the role of EEf1A1 in the heat shock response (HSR), showing that EEF1A1 (but not EEF1A2) was required for HSP70 induction during heat shock (Vera et al., 2014). EEF1A1 was found to bind to heat shock factor 1 (HSF1), enhancing it's binding to the HSP70 promoter of heat shock proteins. Interestingly motor neurons do not express EEF1A1, and instead express it's isoform EEF1A2. Deregulation of the heat shock response has been reported in numerous neurodegenerative diseases (for example Parkinson's disease, Amyotrophic

lateral sclerosis and Alzheimer's disease). This paper suggests that this may explain why there is a lack of heat shock response in these neurons, as well as suggesting that the expression of EEF1A1 in the motor neurons may be a potential therapy for such diseases. The fact that a RIC phenotype has been confirmed in this study suggests it plays an important role in *C. elegans* neurons. It would therefore be interesting to test whether there has been an effect on the transcription of known *C. elegans* heat shock proteins following knock-down, in order to see if the delayed paralysis is due to a changed transcription of these genes.

EEF2 has been shown to play a direct role in a form of Spinocerebellar Ataxia 26 (SCA26) (Hekman et al., 2012). This disease is characterized with cerebellar atrophy and Purkinje cell degeneration. Patients display a progressive gait incoordination, and often show poor coordination of hands, speech and eye movement. Interestingly, this paper also showed that the P596H mutation in the yeast ortholog of EEF2 was linked to an increased rate of shifting to the -1 reading frame, leading to changes in proteostasis. In this study we found that EEF2 caused a RIC phenotype, and as well as having high connectivity and betweenness values in the one-step aldicarb network. EEF-2 was also highly interconnected between the hits. This suggests that it may be playing a role in multiple biological processes, which need further delineation.

3.4.5 Lonp-1/LONP1

Lonp-1 is another interesting hit from the connectivity screen. The human ortholog of C34B2.6 is Lon peptidase 1 (LONP1), which is a mitochondrial matrix protein that belongs to the lon family of ATP-dependent proteases. It is a key protein in degrading oxidatively damaged proteins in the mitochondria. LONP1 has been shown to be up-regulated during periods of transient stress, but down regulated as ageing progresses (Ngo, Pomatto, & Davies, 2013). Defects in mitochondrial protein quality control have been associated with numerous neurodegenerative diseases. Neuronal tissues are highly dependent on mitochondria as they have limited glycolysis capabilities (due to a lack of 6-phophofructo-2-kinase/fructose-2,6 bisphosphate, isoform 3 (PFKFB3) (Herrero-Mendez et al., 2009). A patient with hereditary spastic paraplegia (SPG13) was shown to have decreased expression of LONP1, which was hypothesized to act as a compensatory mechanism following mutation of the HSPD1 gene, which encodes the mitochondrial chaperonin HSP60 mutation (Hansen et al., 2008). How dysregulated mitochondrial function (possibly via the unfolded protein response) alters cholinergic or GABA signaling would be of interest for further study.

3.4.6 Data from outer shells of RIC network

From these connectivity and betweenness screens, it is not obvious as to whether they help prioritize genes that will cause a RIC or a HIC phenotype. However, a handful of genes were elucidated by this method. To attempt to understand how appropriate the "guilt-by-association" principle was, and whether indirect interaction partners could cause an aldicarb-sensitivity phenotype, we found the least connected proteins to proteins known to cause aldicarb-sensitivity

phenotypes. In both *Tu3311* and *Tu3335*, knockdown of some of the genes in the outer shells lead to a significant change in aldicarb sensitivity.

From this data it is possible to make three pragmatic conclusions: While known physical association with a given protein may be a powerful indication that the two partners are functionally and phenotypically linked, this concept of guilt by association or phenology prediction (Oliver, 2000) may be most relevant to investigating common components of a particular molecular machine, or simplistic process with a well defined measurable endpoint. In this case the functional boundary of the network should be quickly exceeded and proteins in more distant shells may be expected to have less influence on the phenotype under investigation. In terms of a process as complex as synaptic transmission these rational assumptions appear to be too simplistic.

The apparent abundance of synaptic effectors in shells unconnected with known RIC/HIC proteins may be due to two factors. First, interaction networks may be incomplete, so phenotypically related proteins may still appear unconnected. Secondly, disruption of proteins involved in superficially unrelated processes may have indirect but measurable effects on the efficiency of synaptic processes. For this reason it may not be logical to expect proximity within a protein interaction network to be a reliable indicator of a proteins potential to influence synaptic activity. Understanding the potential impact of non-intuitive regulators of synaptic function and the relative impact of disruption to more generic cellular functions may prove valuable in understanding or evaluating the phenotypic consequences of age related neuronal somatic mutations. In this context our data

would predict the existence of many more proteins whose function is not required for viability but is required for optimal synaptic function and plasticity.

The background of the worms may also cause the difference in genes coming through as hits in the screen – *Tu3335* has been reported to be more sensitive than *Tu3311*, so the use of *Tu3335* is possible for future experiments where borderline results are seen in *Tu3311*.

3.4.7 Conclusions

Some interesting genes were found to cause a novel RIC phenotype in the neurosensitive *Tu3311* strain when connectivity and betweenness values were ranked functionally relevant worm protein interaction networks, with some having reported neuropathological roles in humans. However, for the next stage of experimentation we decided to try a different method of prioritizing candidates to test for novel effectors of aldicarb sensitivity.

Chapter 4 – Sodium Valproate (VPA)

4.1 Abstract

Sodium valproate is a drug that is commonly used to treat bipolar disorder and epilepsy. Surprisingly, the Falciani group observed that VPA induced paralysis in sma-6 mutant worms (Munasinghe, 2015). To further investigate the effects of VPA dosage in worms the Falciani group performed a detailed analysis of global gene expression profiles in wild type worms treated with increasing concentrations of VPA (Munasinghe, 2015) . Gene expression changes were ranked according to degree of correlation with VPA dose and values were assigned to nodes within a one-step known RIC/HIC protein interaction network (as described in chapter 3). A bespoke clustering algorithm was then used to identify network modules that contained clusters of interconnected proteins that exhibit VPA induced changes in gene expression. Nodes within modules that had not previously been tested for aldicarb-sensitivity were then systematically knocked down to assess their potential influence on synaptic transport, as measured by induced changes in the rate of aldicarb induced paralysis. Significantly, knockdown of 16 genes lead to a reproducible RIC phenotype, while depletion of dylt-1 induced a positive HIC phenotype. In addition to these functional studies the raw microarray data was re-analyzed, and both DAVID and Ingenuity packages were used to perform pathway/process enrichment analyses. This analysis highlighted enriched changes in neuron development, highlighting the involvement of genes involved in neurological diseases, such as epilepsy, Alzheimer's and Huntington's disease.

4.2 Introduction

4.2.1 Sodium Valproate

Sodium valproate, also known as valproic acid (VPA), is widely used in the treatment of epilepsy, bipolar disorder and in cases of schizophrenia. Although in medical use since 1962, the precise mechanism of action of VPA remains unclear, VPA has been implicated in GABA neurotransmission, is a known teratogen, and is also known to be a histone deacetylase inhibitor. As such, it appears that VPA has a complex mode of action, which may in part be mediated by global effects on gene transcription. Previous studies have shown that VPA may have both anti-cancer and neuromodulatory/neuroprotective properties. In *C. elegans,* VPA has also been shown to extend lifespan and play a role in both inositol and diacylglycerol signaling (Tokuoka, Saiardi, & Nurrish, 2008).

A previous study by the Falciani group (University of Birmingham and University of Liverpool) led to the surprising observation that VPA induces paralysis in sma-6 mutant worms (Munasinghe, 2015) . To further investigate the effects of VPA dosage in worms, they performed a detailed microarray analysis of VPA dose (3-24mM) on global gene expression in wild type N2 worms. In collaboration, a gene set enrichment analysis (GSEA) was then performed to identify sets of genes that exhibited similar dose dependent changes in gene expression. To complement this data a one-step known RIC/HIC protein interaction network (as described in chapter 3) was generated from a simplified version of Wormnet version 1 and the CCSB worm interactome (Simonis et al., 2009), which contained only known *C. elegans* interactions.

These two datasets were then brought together to generate a known RIC/HIC one-step interaction network in which RIC nodes were assigned phenotypic confidence scores. A bespoke clustering algorithm was used, which correlates this information with dose response correlation scores for each node in order to generate drug response phenotypic network modules. Predicted modules contained both known RIC/HIC and non-RIC/HIC nodes. Therefore, on the basis that connected nodes within these modules may share common functions or phenotypes all nodes within modules that had not previously been tested for aldicarb-sensitivity were systematically knocked down to assess their potential influence on synaptic transport, as measured by induced changes in the rate of aldicarb induced paralysis.

4.2.2. Aims

The aims of this chapter were to:

- Perform high-throughput aldicarb-sensitivity assays after knocking down genes relating to previously untested proteins within predicted network modules
- Carry out bioinformatics analyses to identify regulators/effectors of synaptic function that have known orthologs in the human synaptome and to define the known functions of all elucidated proteins
- Re-analyze the *C. elegans* VPA microarray data to identify the full complement of genes that are significantly up- and down-regulated following exposure to VPA.

- Compare this data with that from other published studies on VPA induced changes in gene expression, in order to identify conserved effects or functional signatures.

4.3 Results

4.3.1 Data mining of genes in RIC/VPA related modules

Data mining of candidates in the identified sub-networks was firstly carried out as shown in Figure 4.1. Genes relating to proteins contained in each of the four identified modules are shown in Tables 4.1 – 4.4, together with an indication of their known aldicarb phenotype. To gain insight into possible pathways that VPA could be affecting, a list of all genes found in the modules was generated, and DAVID was used to elucidate enriched pathways following VPA treatment in *C. elegans,* using the online Kyoto Encyclopedia of Genes and Genomes (KEGG) database. Pathways enriched are shown in Table 4.5. From this it can be seen that endocytosis, Wnt signaling, TGF-β signaling and MAPK signaling are all enriched, showing the diverse responses that VPA may be conferring on the organism.

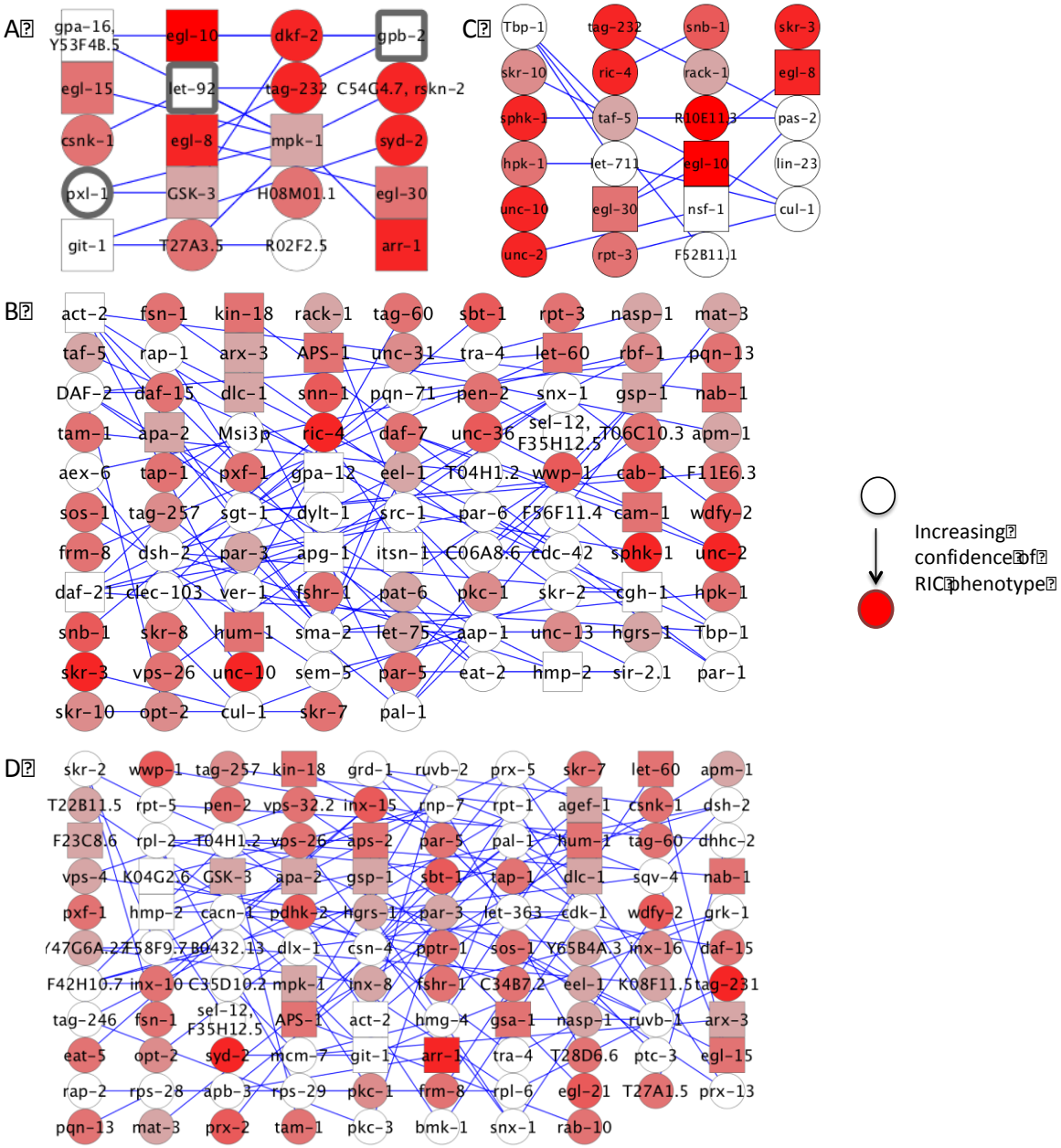

Figure 4.1 **- Subnetworks identified following gene set enrichment analysis of microarray data for N2 worms treated with VPA.** A and B show two separate interaction modules identified from the Vidal CCSB worm interactome, and C and D show two modules identified from the simplified Wormnet version 1. Red nodes indicate genes known to cause a RIC phenotype when their expression is altered, with the strength of the red colour indicating the confidence of the score. Square nodes indicate genes whose human orthologs were found in the synaptomeDB. White nodes represent genes not known to cause a RIC phenotype, and white nodes with bold outlines represent novel genes that had dsRNA available in the RNAi library. Networks were generated using Cytoscape, and module analysis was carried out by the Falciani group.

Wormbase ID	Gene Symbol	Gene Name	RIC
WBGene00000195	F53H8.2	arr-1	Y
WBGene00008317	C54G4.7	C54G4.7	Y
WBGene00013709	Y106G6E.6	csnk-1	Y
WBGene00012019	T25E12.4	dkf-2	Y
WBGene00001179	F28C1.2	egl-10	Y
WBGene00001184	F58A3.2	egl-15	Y
WBGene00001196	M01D7.7	egl-30	Y
WBGene00001177	B0348.4	egl-8	Y
WBGene00001746	Y18D10A.5	GSK-3	Y
WBGene00010373	H08M01.1	H08M01.1	Y
WBGene00003401	F43C1.2	mpk-1	Y
WBGene00006364	F59F5.6	syd-2	Y
WBGene00044077	T18H9.7	tag-232	Y
WBGene00008805	F14F3.2	git-1	N
WBGene00001678	Y95B8A.5	gpa-16	N
WBGene00001680	F52A8.2	gpb-2	N
WBGene00002363	F38H4.9	let-92	N
WBGene00016197	C28H8.6	pxl-1	N
WBGene00019834	R02F2.5	R02F2.5	N
WBGene00020841	T27A3.5	T27A3.5	N

Table 4.1 – Genes found in the CCSB Vidal subnetwork 1, showing Wormbase ID, gene symbols and gene names, together with previously known RIC phenotype. All data was extracted from Wormbase.

Wormbase ID	Gene Symbol	Gene Name	RIC
WBGene00000001	Y110A7A.10	aap-1	N
WBGene00000064	T04C12.5	act-2	N
WBGene00000089	Y87G2A.4	aex-6	N
WBGene00000161	T20B5.1	apa-2	Y
WBGene00000158	Y105E8A.9	apg-1	N
WBGene00000150	F55A12.7	apm-1	Y
WBGene00000159	F29G9.3	APS-1	Y
WBGene00000201	Y79H2A.6	arx-3	Y
WBGene00015516	C06A8.6	C06A8.6	N
WBGene00000277	C23H4.1	cab-1	Y
WBGene00000289	C01G6.8	cam-1	Y
WBGene00000390	R07G3.1	cdc-42	N
WBGene00000479	C07H6.5	cgh-1	N
WBGene00012036	T26E3.1	clec-103	N
WBGene00000836	D2045.6	cul-1	N
WBGene00000911	C10C5.6	daf-15	Y
WBGene00000898	Y55D5A.5	DAF-2	N
WBGene00000915	C47E8.5	daf-21	N
WBGene00000903	B0412.2	daf-7	Y
WBGene00001005	T26A5.9	dlc-1	Y
WBGene00001102	C27A2.6	dsh-2	N
WBGene00008764	F13G3.4	dylt-1	N
WBGene00001133	Y48B6A.4	eat-2	N
WBGene00022069	Y67D8C.5	eel-1	Y
WBGene00008707	F11E6.3	F11E6.3	Y
WBGene00018991	F56F11.4	F56F11.4	N
WBGene00001494	H09G03.2	frm-8	Y
WBGene00008239	C50H2.1	fshr-1	Y
WBGene00001499	C26E6.5	fsn-1	Y
WBGene00001674	F18G5.3	gpa-12	N
WBGene00001747	F29F11.6	gsp-1	Y
WBGene00004101	C07G1.5	hgrs-1	Y
WBGene00001979	K05C4.6	hmp-2	N
WBGene00001994	F20B6.8	hpk-1	Y
WBGene00006386	F30F8.8	taf-5	Y
WBGene00018516	F46G11.3	tag-257	Y
WBGene00006523	F26G5.9	tam-1	Y
WBGene00006524	C44H4.5	tap-1	Y
WBGene00006542	T20B12.2	Tbp-1	N
WBGene00018740	F53B3.1	tra-4	N
WBGene00006750	T10A3.1	unc-10	Y
WBGene00006752	ZK524.2	unc-13	Y
WBGene00006742	T02C5.5	unc-2	Y
WBGene00006767	ZK897.1	unc-31	Y
WBGene00006772	C50C3.9	unc-36	Y
WBGene00006894	T17A3.1	ver-1	N
WBGene00006931	T20D3.7	vps-26	Y
WBGene00008402	D2013.2	wdfy-2	Y

WBGene00016250	C30C11.4	hsp-110	Y
WBGene00002035	F29D10.4	hum-1	N
WBGene00006405	Y116A8C.36	itsn-1	Y
WBGene00002201	T17E9.1	kin-18	Y
WBGene00002335	ZK792.6	let-60	Y
WBGene00202503	-	let-75	Y
WBGene00003134	F10C5.1	mat-3	N
WBGene00003516	C43E11.6	nab-1	Y
WBGene00007500	C09H10.6	nasp-1	Y
WBGene00006438	C01F6.6	nrfl-1	Y
WBGene00003912	C38D4.6	pal-1	N
WBGene00003916	H39E23.1	par-1	N
WBGene00003918	F54E7.3	par-3	Y
WBGene00003920	M117.2	par-5	Y
WBGene00003921	T26E3.3	par-6	N
WBGene00003932	T21D12.4	pat-6	Y
WBGene00003975	T28D6.9	pen-2	Y
WBGene00003877	K04E7.2	pept-2	Y
WBGene00004032	F57F5.5	pkc-1	Y
WBGene00004104	C14C11.8	pqn-13	N
WBGene00004153	T23F1.6	pqn-71	Y
WBGene00004254	T14G10.2	pxf-1	Y
WBGene00010556	K04D7.1	rack-1	N
WBGene00004307	C27B7.8	rap-1	Y
WBGene00004316	F37A4.7	rbf-1	Y
WBGene00004364	Y22F5A.3	ric-4	Y
WBGene00004503	F23F12.6	rpt-3	Y
WBGene00011392	T03D8.3	sbt-1	N
WBGene00004769	F35H12.3	sel-12	N
WBGene00004774	C14F5.5	sem-5	N
WBGene00019893	R05F9.10	sgt-1	N
WBGene00004800	R11A8.4	sir-2.1	Y
WBGene00004816	Y105C5B.13	skr-10	N
WBGene00004808	F46A9.4	skr-2	Y
WBGene00004809	F44G3.6	skr-3	Y
WBGene00004813	Y47D7A.1	skr-7	Y
WBGene00004814	C52D10.9	skr-8	N
WBGene00004856	ZK370.2	sma-2	Y
WBGene00004897	T10H9.4	snb-1	Y
WBGene00004913	Y38C1BA.2	snn-1	N
WBGene00004927	C05D9.1	snx-1	Y
WBGene00004947	T28F12.3	sos-1	Y
WBGene00007918	C34C6.5	sphk-1	N
WBGene00005077	Y92H12A.1	src-1	N
WBGene00011449	T04H1.2	t04h1.2	Y
WBGene00020289	T06C10.3	T06C10.3	Y
WBGene00007009	Y65B4BR.4	wwp-1	Y

Table 4.2 – Genes found in the Vidal CCSB subnetwork 2.

Wormbase ID	Gene Symbol	Gene Name	RIC
WBGene00000836	D2045.6	cul-1	N
WBGene00001179	F28C1.2	egl-10	Y
WBGene00001196	M01D7.7	egl-30	Y
WBGene00001177	B0348.4	egl-8	Y
WBGene00009924	F52B11.1	F52B11.1	N
WBGene00001994	F20B6.8	hpk-1	Y
WBGene00002845	F57B9.2	let-711	N
WBGene00003009	K10B2.1	lin-23	N
WBGene00003818	H15N14.2	nsf-1	N
WBGene00003923	D1054.2	pas-2	N
WBGene00011216	R10E11.3	R10E11.3	Y
WBGene00010556	K04D7.1	rack-1	Y
WBGene00004364	Y22F5A.3	ric-4	Y
WBGene00004503	F23F12.6	rpt-3	Y
WBGene00004816	Y105C5B.13	skr-10	Y
WBGene00004809	F44G3.6	skr-3	Y
WBGene00004897	T10H9.4	snb-1	Y
WBGene00007918	C34C6.5	sphk-1	Y
WBGene00006386	F30F8.8	taf-5	Y
WBGene00044077	T18H9.7	tag-232	Y
WBGene00006542	T20B12.2	Tbp-1	N
WBGene00006750	T10A3.1	unc-10	Y
WBGene00006742	T02C5.5	unc-2	Y

Table 4.3 – Genes found in Wormnet V2 subnetwork 1

Wormbase ID	Gene Symbol	Gene Name	RIC
WBGene00000064	T04C12.5	act-2	N
WBGene00012386	Y6B3A.1	agef-1	Y
WBGene00000161	T20B5.1	apa-2	Y
WBGene00000163	R11A5.1	apb-3	N
WBGene00000150	F55A12.7	apm-1	Y
WBGene00000159	F29G9.3	APS-1	Y
WBGene00000157	F02E8.3	aps-2	Y
WBGene00000195	F53H8.2	arr-1	Y
WBGene00000201	Y79H2A.6	arx-3	Y
WBGene00015194	B0432.13	B0432.13	N
WBGene00000257	F23B12.8	bmk-1	N
WBGene00007912	C34B7.2	C34B7.2	Y
WBGene00016440	C35D10.2	C35D10.2	N
WBGene00012230	W03H9.4	cacn-1	N
WBGene00000405	T05G5.3	cdk-1	N
WBGene00000816	Y55F3AM.15	csn-4	N
WBGene00013709	Y106G6E.6	csnk-1	Y
WBGene00000911	C10C5.6	daf-15	Y
WBGene00012948	Y47H9C.2	dhhc-2	N
WBGene00001005	T26A5.9	dlc-1	Y
WBGene00013583	Y80D3A.3	dlx-1	N
WBGene00001102	C27A2.6	dsh-2	N
WBGene00001136	F13G3.8	eat-5	Y
WBGene00022069	Y67D8C.5	eel-1	Y
WBGene00001184	F58A3.2	egl-15	Y
WBGene00001189	F01D4.4	egl-21	Y
WBGene00017735	F23C8.6	F23C8.6	Y
WBGene00018371	F42H10.7	F42H10.7	N
WBGene00019060	F58F9.7	F58F9.7	N
WBGene00001494	H09G03.2	frm-8	Y
WBGene00008239	C50H2.1	fshr-1	Y
WBGene00001499	C26E6.5	fsn-1	Y
WBGene00008805	F14F3.2	git-1	N
WBGene00001690	R08B4.1	grd-1	N
WBGene00001708	F19C6.1	grk-1	N
WBGene00001745	R06A10.2	gsa-1	Y
WBGene00001746	Y18D10A.5	GSK-3	Y
WBGene00001747	F29F11.6	gsp-1	Y
WBGene00044072	ZK1128.5	ham-3	Y
WBGene00004101	C07G1.5	hgrs-1	N
WBGene00001974	T20B12.8	hmg-4	N
WBGene00001979	K05C4.6	hmp-2	Y
WBGene00002035	F29D10.4	hum-1	Y
WBGene00002132	T18H9.5	inx-10	Y
WBGene00002137	R12E2.9	inx-15	Y
WBGene00002138	R12E2.5	inx-16	Y
WBGene00002130	ZK792.2	inx-8	N
WBGene00010565	K04G2.6	K04G2.6	Y
WBGene00019544	K08F11.5	K08F11.5	Y
WBGene00002201	T17E9.1	kin-18	N
WBGene00002583	B0261.2	let-363	Y
WBGene00002335	ZK792.6	let-60	Y
WBGene00003134	F10C5.1	mat-3	N
WBGene00003912	C38D4.6	pal-1	Y
WBGene00003918	F54E7.3	par-3	Y
WBGene00003920	M117.2	par-5	Y
WBGene00022719	ZK370.5	pdhk-2	Y
WBGene00003975	T28D6.9	pen-2	N
WBGene00004032	F57F5.5	pkc-1	Y
WBGene00004034	F09E5.1	pkc-3	Y
WBGene00012348	W08G11.4	pptr-1	N
WBGene00004104	C14C11.8	pqn-13	Y
WBGene00004198	F32A5.6	prx-13	N
WBGene00004192	ZK809.7	prx-2	N
WBGene00004194	C34C6.6	prx-5	Y
WBGene00004210	Y110A2AL.8	ptc-3	Y
WBGene00004254	T14G10.2	pxf-1	N
WBGene00004273	T23H2.5	rab-10	N
WBGene00004308	C25D7.7	rap-2	N
WBGene00004390	K04G7.10	rnp-7	N
WBGene00004413	B0250.1	rpl-2	N
WBGene00004417	R151.3	rpl-6	N
WBGene00004497	Y41D4B.5	rps-28	N
WBGene00004498	B0412.4	rps-29	N
WBGene00004501	C52E4.4	rpt-1	N
WBGene00004505	F56H1.4	rpt-5	N
WBGene00007784	C27H6.2	ruvb-1	Y
WBGene00020687	T22D1.10	ruvb-2	N
WBGene00011392	T03D8.3	sbt-1	N
WBGene00004769	F35H12.3	sel-12	Y
WBGene00004808	F46A9.4	skr-2	N
WBGene00004813	Y47D7A.1	skr-7	Y
WBGene00004927	C05D9.1	snx-1	N
WBGene00004947	T28F12.3	sos-1	Y
WBGene00005022	F29F11.1	sqv-4	N
WBGene00006364	F59F5.6	syd-2	Y
WBGene00011449	T04H1.2	t04h1.2	Y
WBGene00020679	T22B11.5	T22B11.5	Y
WBGene00020837	T27A1.5	T27A1.5	Y
WBGene00012126	T28D6.6	T28D6.6	N
WBGene00044063	ZK430.2	tag-231	Y
WBGene00018516	F46G11.3	tag-257	Y
WBGene00006523	F26G5.9	tam-1	Y
WBGene00006524	C44H4.5	tap-1	Y
WBGene00018740	F53B3.1	tra-4	N
WBGene00006931	T20D3.7	vps-26	Y
WBGene00016497	C37C3.3	vps-32.2	Y
WBGene00021334	Y34D9A.10	vps-4	Y
WBGene00008402	D2013.2	wdfy-2	Y
WBGene00007009	Y65B4BR.4	wwp-1	Y
WBGene00021651	Y47G6A.27	Y47G6A.27	Y
WBGene00022027	Y65B4A.3	Y65B4A.3	Y
WBGene00003159	F32D1.10	mcm-7	Y
WBGene00003401	F43C1.2	mpk-1	Y
WBGene00003516	C43E11.6	nab-1	Y
WBGene00007500	C09H10.6	nasp-1	Y
WBGene00006438	C01F6.6	nrfl-1	N
WBGene00003877	K04E7.2	opt-2	Y

Table 4.4 – Genes found in the Wormnet V2 subnetwork 2.

KEGG Pathway	Number of Genes	Gene Name(s)
Endocytosis	15	aps-2, arr-1, ver-1, cdc-42, par-3, hgrs-1, vps-32.2, did-2, vps-20, par-6, vps-4, wwp-1, grk-1, pkc-3, apa-2
Wnt signaling pathway	13	let-92, skr-7, ruvb-1, skr-8, gsk-3, egl-8, skr-3, skr-2, hmp-2, pptr-1, lin-23, cul-1, skr-10
TGF-beta signaling pathway	8	let-92, skr-7, skr-8, skr-3 skr-2, cul-1, skr-10, mpk-1
MAPK signaling pathway	10	unc-2, gpa-12, let-60, arr-1, sos-1, cdc-42, unc-36. sem-5, mpk-1, kin-18
ErbB signaling pathway	7	aap-1, let-60, gsk-3, sos-1, let-363, sem-5, mpk-1
Progesterone-mediated oocyte maturation	7	aap-1, cdk-1, let-60, gpa-16, mat-3, daf-21, mpk-1
Natural killer cell mediated cytotoxicity	5	aap-1, let-60, sos-1, sem-5, mpk-1
Dorso-ventral axis formation	4	let-60, sos-1, sem-5, mpk-1
Ubiquitin mediated proteolysis	10	eel-1, skr-7, skr-8, skr-3, skr-2, lin-23, mat-3, cul-1, wwp-1, skr-10

Table 4.5 – Top ranked KEGG pathways identified by DAVID functional enrichment analysis, using standard parameters with genes from all identified modules analysed.

Wormbase Gene ID	Gene Symbol	Gene Name	Aldicarb Phenotype	Biological Process
WBGene00006750	T10A3.1	unc-10	RIC	Synaptic vesicle priming, exocytosis and transport, Synaptic transmission
WBGene00004364	Y22F5A.3	ric-4	RIC	Synaptic vesicle priming and exocytosis, Synaptic transmission
WBGene00001177	B0348.4	egl-8	RIC	Acetylcholine secretion, Dopamine receptor signaling pathway, Synaptic transmission
WBGene00006767	ZK897.1	unc-31	RIC	Neurotransmitter secretion, Synaptic vesicle transport, Synaptic transmission
WBGene00006752	ZK524.2	unc-13	RIC	Neurotransmitter secretion, Synaptic vesicle transport, Synaptic transmission
WBGene00004913	Y38C1BA.2	snn-1	RIC	Neurotransmitter secretion, Synaptic transmission
WBGene00001189	F01D4.4	egl-21	RIC	Acetylcholine Secretion, Synaptic transmission
WBGene00002138	R12E2.5	inx-16	RIC	Synaptic transmission
WBGene00006364	F59F5.6	syd-2	RIC	Synaptic vesicle transport, Synaptic transmission
WBGene00001745	R06A10.2	gsa-1	RIC	Dopamine receptor signaling pathway
WBGene00001179	F28C1.2	egl-10	RIC	Dopamine receptor signaling pathway
WBGene00001680	F52A8.2	gpb-2	Unknown	Dopamine receptor signaling pathway

Table 4.6 – Neurological pathways found to be enriched when merged lists of genes from all subnetworks were analysed in DAVID.

When analyzing biological enrichment, some of the affected genes were found to be associated with neurological 'biological processes' (Table 4.6). Four genes were found in the dopamine receptor-signaling pathway, including egl-10 (F28C1.2), gsa-1 (R06A10.2), egl-8 (B0348.4) and gpb-2 (F52A8.2). Of these only gpb-2 was not previously known to cause a RIC phenotype. Nine further genes were generally involved in synaptic transmission. These were unc-10 (T10A3.1), ric-4 (Y22F5A.3), egl-8 (B0348.4), unc-31 (ZK897.1), unc-13 (ZK524.2), snn-1 (Y38C1BA.2), egl-21 (F01D4.4), inx-16 (R12E2.5) and syd-2 (F59F5.6). Some of these genes also had more specific neurological process association. This analysis provides further support to the fact that the predicted modules may well contain potentially novel regulators, or effectors of synaptic function, as hypothesized by the principle of "guilt-by-association".

Gene Symbol	Wormbase ID	Gene Name	RNAi
WBGene00001102	C27A2.6	dsh-2	Yes
WBGene00004498	B0412.4	rps-29	Yes
WBGene00016250	C30C11.4	hsp-110	Yes
WBGene00001708	F19C6.1	grk-1	Yes
WBGene00000001	Y110A7A.10	aap-1	Yes
WBGene00000479	C07H6.5	cgh-1	Yes
WBGene00019834	R02F2.5		Yes
WBGene00004034	F09E5.1	pkc-3	Yes
WBGene00001680	F52A8.2	gpb-2	Yes
WBGene00004927	C05D9.1	snx-1	Yes
WBGene00004505	F56H1.4	rpt-5	Yes
WBGene00004308	C25D7.7	rap-2	Yes
WBGene00004198	F32A5.6	prx-13	Yes
WBGene00004856	ZK370.2	sma-2	Yes
WBGene00019893	R05F9.10	sgt-1	Yes
WBGene00004808	F46A9.4	skr-2	Yes
WBGene00006405	Y116A8C.36	itsn-1	Yes
WBGene00003921	T26E3.3	par-6	Yes
WBGene00018991	F56F11.4		Yes
WBGene00020687	T22D1.10	ruvb-2	Yes
WBGene00000089	Y87G2A.4	aex-6	Yes
WBGene00008805	F14F3.2	git-1	Yes
WBGene00003923	D1054.2	pas-2	Yes
WBGene00013583	Y80D3A.3	ceh-51	Yes
WBGene00044072	ZK1128.5	ham-3	Yes
WBGene00004774	C14F5.5	sem-5	Yes
WBGene00005022	F29F11.1	sqv-4	Yes
WBGene00004153	T23F1.6	pqn-71	Yes
WBGene00002363	F38H4.9	let-92	Yes
WBGene00004307	C27B7.8	rap-1	Yes
WBGene00000405	T05G5.3	cdk-1	Yes
WBGene00004390	K04G7.10	rnp-7	Yes
WBGene00003916	H39E23.1	par-1	Yes
WBGene00000390	R07G3.1	cdc-42	Yes
WBGene00015516	C06A8.6		Yes
WBGene00003159	F32D1.10	mcm-7	Yes
WBGene00000836	D2045.6	cul-1	Yes
WBGene00012230	W03H9.4	cacn-1	Yes
WBGene00016197	C28H8.6	pxl-1	Yes
WBGene00019060	F58F9.7		Yes
WBGene00004194	C34C6.6	prx-5	Yes
WBGene00001674	F18G5.3	gpa-12	Yes
WBGene00008764	F13G3.4	dylt-1	Yes
WBGene00004417	R151.3	rpl-6	Yes
WBGene00004769	F35H12.3	sel-12	Yes
WBGene00018371	F42H10.7	ess-2	Yes
WBGene00000257	F23B12.8	bmk-1	Yes
WBGene00012948	Y47H9C.2	dhhc-2	Yes
WBGene00018740	F53B3.1	tra-4	Yes
WBGene00006542	T20B12.2	tbp-1	Yes
WBGene00008317	C54G4.7		Yes
WBGene00000816	Y55F3AM.15	csn-4	Yes
WBGene00007784	C27H6.2	ruvb-1	Yes
WBGene00004501	C52E4.4	rpt-1	Yes
WBGene00000163	R11A5.1	apb-3	Yes
WBGene00006894	T17A3.1	ver-1	Yes
WBGene00011449	T04H1.2		Yes
WBGene00016440	C35D10.2	gipc-1	Yes
WBGene00001974	T20B12.8	hmg-4	Yes
WBGene00000915	C47E8.5	daf-21	Yes

Table 4.7 – List of module genes to be tested in aldicarb-sensitivity screens. Gene information was collated from Wormbase, showing availability of corresponding RNAi clones in the Vidal dsRNA feeding library.

To functionally test the predicted set of novel synaptic effectors, the higher throughput aldicarb-sensitivity assay was used to test proteins in each module that did not have a known aldicarb-sensitivity phenotype. Table 4.7 shows a list of the candidate genes for which dsRNA clones were available, and thus were used to knock down of target genes in the *Tu3311* strain. In total, 60 genes were identified, that did not have known RIC phenotypes, but did have available dsRNA clones.

4.3.2 Screening of module analysis hits

In order to assess aldicarb sensitivity, adult worm paralysis was assessed as described in Materials and Methods. Results from module informed aldicarb sensitivity screens are shown in Figure 4.2 and percentage changes in paralysis and corresponding *p*-values are provided in Table 4.8. Sixteen of the tested candidates showed a significant ($p<0.05$) RIC or HIC paralysis phenotype compared to the negative control. Gpb-2 was previously associated with the dopamine receptor signaling pathway and displayed a significant ($p<0.01$, n = 3) RIC phenotype when knocked down with a -59.4±16.4% (mean±SD) reduction paralysis compared to the negative control.

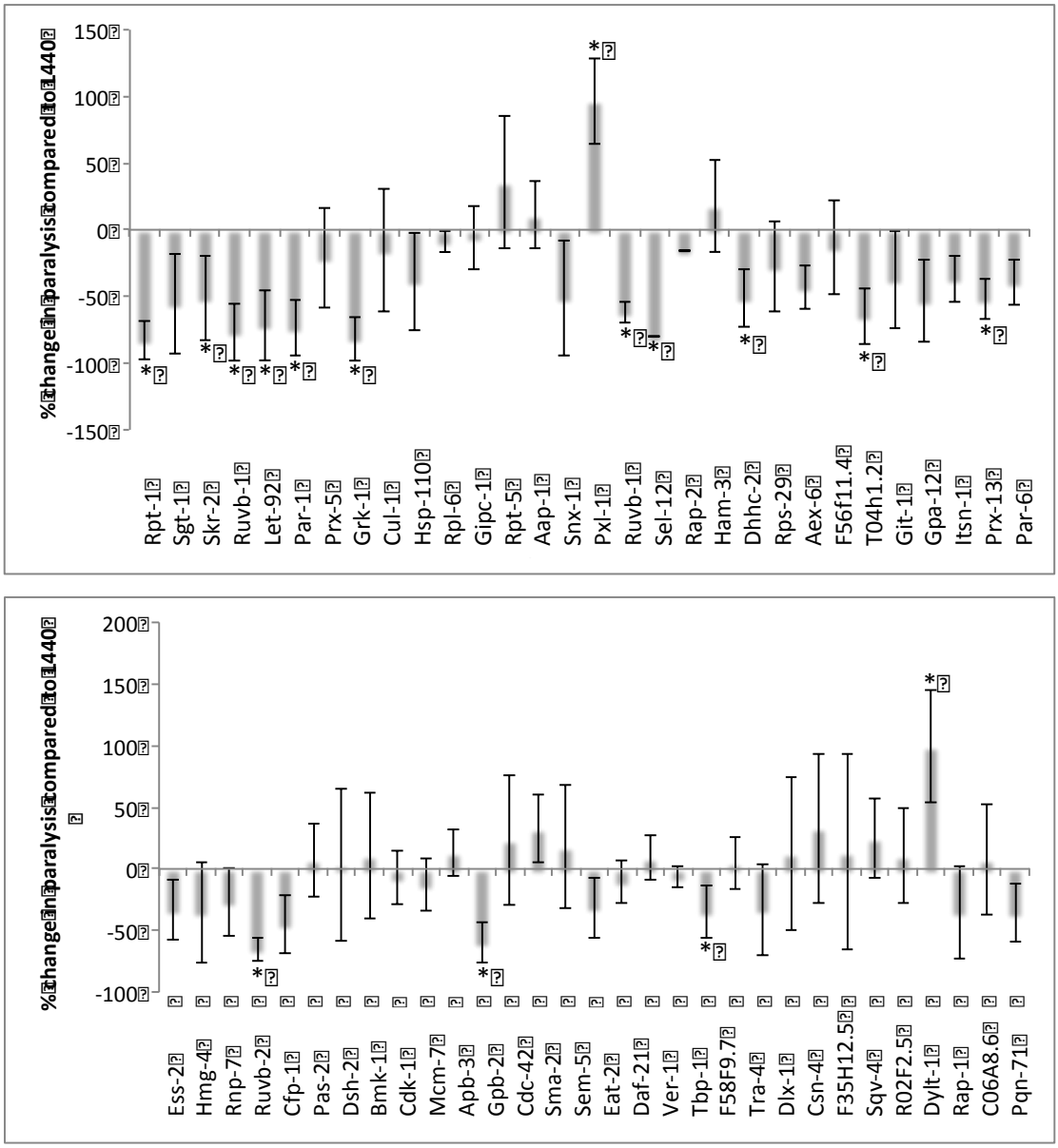

Figure 4.2 **– Results from aldicarb sensitivity screening following RNAi mediated knockdown of module genes in *Tu3311* neurosensitive worms**. Adult worm paralysis was assessed as described in Materials and Methods. The percentage change in paralysis for each gene is shown in comparison to a L440 empty vector negative control. * denotes $p<0.05$. N=3. Error bars represent standard deviation.

Gene Symbol	Gene Name	Wormbase Gene ID	% Change Compared to L440	Standard Deviation	P Value	Significant?
C07H6.5	cgh-1	WBGene00000479	-76.82838585	21.30124181	0.0037	Yes
C27H6.2	ruvb-1	WBGene00007784	-62.09313296	7.492181256	0.0013	Yes
C28H8.6	pxl-1	WBGene00016197	96.55589509	32.11783875	0.0011	Yes
C52E4.4	rpt-1	WBGene00004501	-82.86327143	14.88159377	0.0008	Yes
F13G3.4	dylt-1	WBGene00008764	99.23844808	45.90871086	0.0152	Yes
F19C6.1	grk-1	WBGene00001708	-81.55870156	16.55655272	0.0012	Yes
F32A5.6	prx-13	WBGene00004198	-52.1762157	14.72709623	0.0322	Yes
F35H12.3	sel-12	WBGene00004769	-80.58504875	18.1313949	0.003	Yes
F38H4.9	let-92	WBGene00002363	-71.71743172	26.2659172	0.0097	Yes
F46A9.4	skr-2	WBGene00004808	-51.34840963	31.5754137	0.0495	Yes
F52A8.2	gpb-2	WBGene00001680	*-59.40762321*	16.43420336	0.0087	Yes
F58F9.7	f58f9.7	WBGene00019060	-34.98756563	21.4650472	0.0487	Yes
H39E23.1	par-1	WBGene00003916	-73.8984699	20.60631898	0.0038	Yes
T04H1.2	t04h1.2	WBGene00011449	-64.79288222	21.49648609	0.0271	Yes
T22D1.10	ruvb-2	WBGene00020687	-64.88204141	9.664656666	0.0145	Yes
Y47H9C.2	dhhc-2	WBGene00012948	-51.49943237	21.58105518	0.0485	Yes
B0412.4	rps-29	WBGene00004498	-27.68788725	33.62070055	0.2792	No
C05D9.1	snx-1	WBGene00004927	-51.25989431	43.61084793	0.1189	No
C06A8.6	c06a8.6	WBGene00015516	7.575116539	45.23460869	0.7853	No
C14F5.5	sem-5	WBGene00004774	17.88625268	49.64437347	0.5596	No
C25D7.7	rap-2	WBGene00004308	-15.76058606	25.22280893	0.3537	No
C27A2.6	dsh-2	WBGene00001102	3.414757129	61.73821005	0.9282	No
C27B7.8	rap-1	WBGene00004307	-35.04265965	37.60819153	0.1895	No
C30C11.4	hsp-110	WBGene00016250	-38.47456479	36.85940032	0.147	No
C34C6.6	prx-5	WBGene00004194	-21.14854258	37.71704796	0.3882	No
C35D10.2	gipc-1	WBGene00016440	-5.988182379	23.63564031	0.6909	No
C47E8.5	daf-21	WBGene00000915	-10.18810728	17.47946636	0.3715	No
D1054.2	pas-2	WBGene00003923	7.444820925	29.88498153	0.6835	No
D2045.6	cul-1	WBGene00000836	-15.38450015	46.31498902	0.5967	No
F14F3.2	git-1	WBGene00008805	-37.4745888	36.33959935	0.1962	No
F18G5.3	gpa-12	WBGene00001674	-53.30731189	30.65471603	0.0754	No
F23B12.8	bmk-1	WBGene00000257	10.81587591	51.23120394	0.7307	No
F29F11.1	sqv-4	WBGene00005022	24.99437793	32.32523605	0.2394	No
F32D1.10	mcm-7	WBGene00003159	-13.00734953	21.34065003	0.3748	No
F35H12.5	f35h12.5	WBGene00018077	32.7878975	60.57506843	0.3964	No
F42H10.7	ess-2	WBGene00018371	-33.43209511	23.90613011	0.1384	No
F52B11.1	cfp-1	WBGene00009924	-44.58160809	23.76081867	0.0781	No
F53B3.1	tra-4	WBGene00018740	4.576890886	20.79287431	0.7223	No
F56F11.4	f56f11.4	WBGene00018991	-13.008422	35.70541702	0.5856	No
F56H1.4	rpt-5	WBGene00004505	35.56149733	49.74307477	0.2672	No
K04G7.10	rnp-7	WBGene00004390	-26.79826673	28.21375797	0.2408	No
R02F2.5	r02f2.5	WBGene00019834	10.57148059	38.37121559	0.6551	No
R05F9.10	sgt-1	WBGene00019893	-55.44122754	37.5878478	0.0644	No
R07G3.1	cdc-42	WBGene00000390	23.55634169	52.72059453	0.4734	No
R11A5.1	apb-3	WBGene00000163	13.197378	19.04167007	0.2571	No
R151.3	rpl-6	WBGene00004417	-8.709337281	8.247828919	0.1516	No
T05G5.3	cdk-1	WBGene00000405	-6.99967881	21.55535016	0.615	No
T17A3.1	ver-1	WBGene00006894	8.717401454	18.05974785	0.4492	No
T20B12.2	tbp-1	WBGene00006542	-6.567992599	8.285119891	0.2451	No
T20B12.8	hmg-4	WBGene00001974	-35.16546301	40.80127926	0.2539	No
T23F1.6	pqn-71	WBGene00004153	-35.86646848	23.58717037	0.063	No
T26E3.3	par-6	WBGene00003921	-39.52816562	16.72639659	0.0665	No
W03H9.4	cacn-1	WBGene00012230	13.42890241	79.41563912	0.7836	No
Y110A7A.10	aap-1	WBGene00000001	10.71231799	25.21273348	0.4855	No
Y116A8C.36	itsn-1	WBGene00006405	-36.79987161	17.56030829	0.0807	No
Y48B6A.4	eat-2	WBGene00001133	-31.22982676	24.67303678	0.0946	No
Y55F3AM.15	csn-4	WBGene00000816	12.67345051	62.28587316	0.7424	No
Y80D3A.3	dlx-1	WBGene00013583	-32.88753799	37.30082716	0.2025	No
Y87G2A.4	aex-6	WBGene00000089	-43.19109546	16.0955386	0.0515	No
ZK1128.5	ham-3	WBGene00044072	17.9452376	34.54485796	0.3622	No
ZK370.2	sma-2	WBGene00004856	32.15586307	27.4714632	0.0825	No

Table 4.8 – Background data for phenotypic trends shown in Figure 4.2.

Due to the limited predictive power to elucidate novel effectors as discussed in chapter 3, more vigorous methods for determining whether a genetic knockdown may lead to a significant RIC or HIC phenotype were adopted. To do this, as well as independently validating the genes found to cause a significant RIC or HIC phenotype, borderline candidates were also analysed. This was both through the use of an independent screen and also through the use of the alternative *Tu3335* strain, which is reported to be more sensitive to neuronal RNAi than *Tu3311* (but has an additional mutation in *mec-6*).

In order to gain confidence in the assay and worm strains chosen for the analyses, some of the positive hits from the initial screen in *Tu3311* (Chapter 3) were re-tested. When choosing borderline candidates to re-test, genes were picked that showed a greater than 20% absolute change in paralysis compared to the negative control. However, variability between plates in this sub set of assays was high, resulting in insignificant *p*-values. Therefore, secondary independent testing was carried out on positive hits, as well as candidates that originally showed high variability, but had high average percentage changes compared to a negative control. For example, these included gpa-12 (-53±30.7%, mean±SD), rap-1 (-35±37.6%), and itsn-1 (-37±7.6%) (Table 4.8). Finally, genes that showed less than 20% change in aldicarb-sensitivity but high variability between replicates (*cacn-1* and *csn-4*) were also included in these secondary screens. In each case genes were again knocked down in the *Tu3311* strain. However, in this case a two time-point aldicarb-sensitivity assay was used to assess the relative percentage of paralyzed worms. The additional time points chosen for this assay were 140 and 160 minutes. To compensate for worm batch variability in rates of paralysis, we

considered a positive phenotype to be reproducible if two out of three selected time points (100, 140 and 160 minutes) showed significant changes in paralysis relative to the batch control. Unfortunately, *skr-2* and *F58F9.7* knockdown were unable to be re-screened due to technical issues.

Figure 4.3 and Tables 4.9 and 4.10 show the relative paralysis phenotypes following knockdown of each target gene, at both 140 and 160 minutes. In total, 14 genes showed a significant change in paralysis in at least two of the three time points tested (Table 4.11). All displayed a significant RIC phenotype, with the exception of *dylt-1*, whose knockdown caused a significant HIC phenotype.

4.3.3 Re-screening candidates in the Tu3335 strain

After the second screening of module genes in *Tu3311*, large changes in standard deviation and large percentage changes in paralysis (>20%) for some genes were still being observed. For this reason the alternate *Tu3335* strain was used to assess phenotypes following gene knockdown, as it is claimed to be more sensitive to neuronal RNAi than *Tu3311*.

As an initial test, four of the genes (sel-12, ruvb-1, ruvb-2 and itsn-1) that previously showed a strong change in aldicarb sensitivity when knocked down in the *Tu3311* strain were re-screened in *Tu3335*, as well as egl-30, which was included as a positive control. Knockdown of all of these genes also lead to significant changes in aldicarb sensitivity in the *Tu3335* worm strain (Figure 4.4 and Table 4.12).

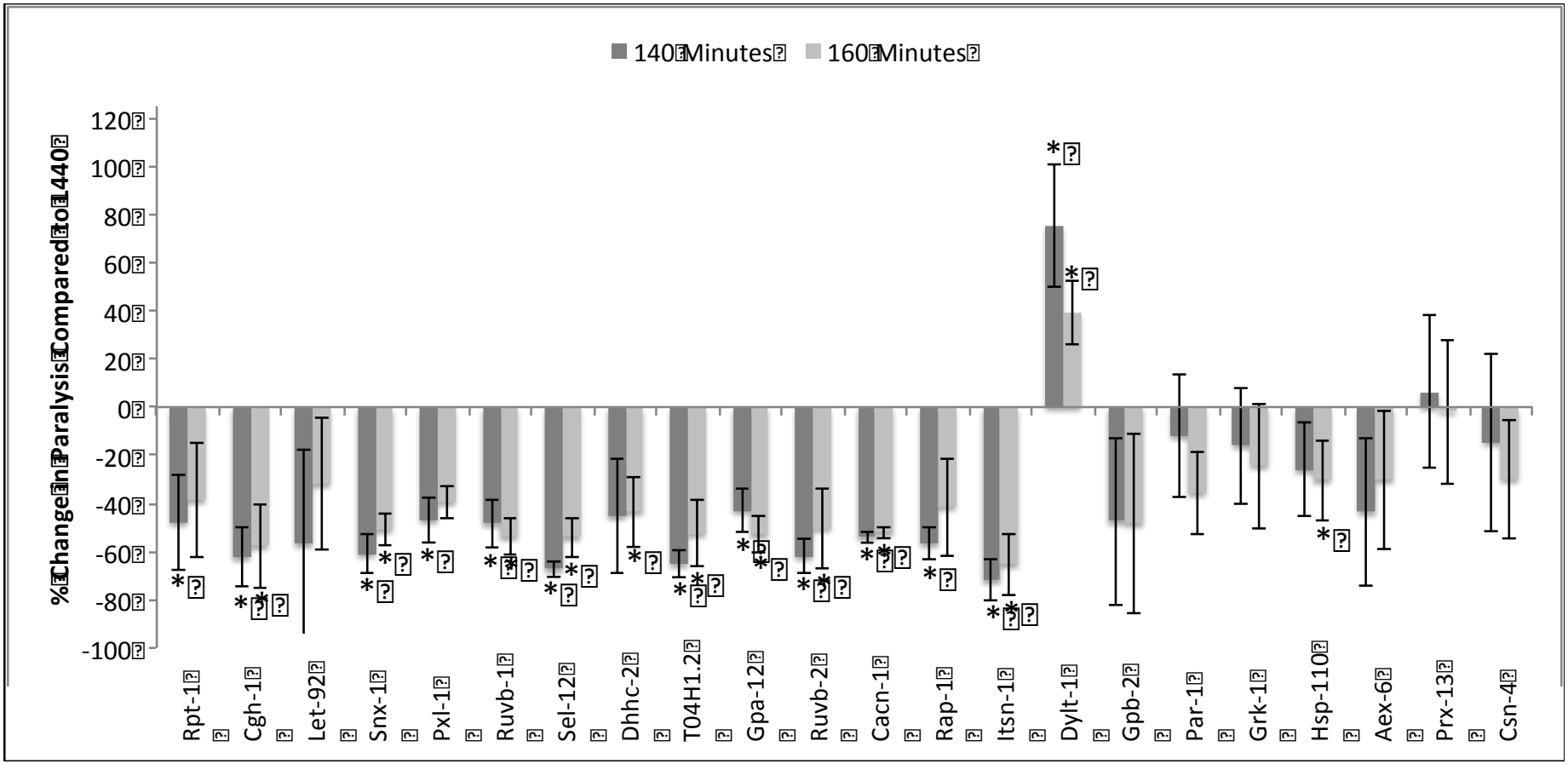

Figure 4.3 - **Genes showing a significant change in paralysis at 140 minutes following RNAi mediated knockdown in *Tu3311* .** Paralysis of adult worms was assessed as described in Materials and Methods. The percentage change in paralysis for each gene is shown in comparison to a L440 empty vector negative control. * denotes $p<0.05$. N=3. Error bars represent standard deviation.

Gene Symbol	Gene Name	% Change in Paralysis at 140 Minutes	Standard Deviation 140 Minutes	P Value 140 Minutes	Significant at 140 Minutes?
C52E4.4	rpt-1	-47.84382284	19.71845279	0.0377	Yes
C07H6.5	cgh-1	-62.35246235	12.03083555	0.01	Yes
F38H4.9	let-92	-56.78155754	39.22318268	0.0103	Yes
C05D9.1	snx-1	-60.93669363	8.211252701	0.0392	Yes
C28H8.6	pxl-1	-46.88403881	9.345544622	0.0088	Yes
C27H6.2	ruvb-1	-48.3047007	9.983682395	0.0017	Yes
F35H12.3	sel-12	-67.31526898	3.190623489	0.0128	Yes
Y47H9C.2	dhhc-2	-45.27472527	23.80872318	0.0661	No
T04H1.2	t04h1.2	-65.10220549	5.512786697	0.0102	Yes
F18G5.3	gpa-12	-42.89044289	9.287932933	0.0438	Yes
T22D1.10	ruvb-2	-61.99245802	7.30078279	0.0001	Yes
W03H9.4a	cacn-1	-53.88266249	2.426084822	0.0002	Yes
C27B7.8	rap-1	-56.6784704	6.89420201	0.0293	Yes
Y116A8C.36	itsn-1	-71.86728792	8.689874688	0.0053	Yes
F13G3.4	dylt-1	75.29069767	25.2670397	0.0138	Yes
F52A8.2	gpb-2	-47.38920802	34.86845931	0.0824	No
H39E23.1	par-1	-11.89992361	25.37967305	0.4467	No
F19C6.1	grk-1	-15.92538804	24.18595659	0.2773	No
C30C11.4	hsp-110	-26.18492618	19.42914968	0.1359	No
Y87G2A.4	aex-6	-43.57565511	30.52554186	0.1074	No
F32A5.6	prx-13	6.424825175	31.59512781	0.7325	No
Y55F3AM.15	csn-4	-14.64038643	36.90029831	0.4447	No

Table 4.9 – Data associated with phenotypic trends observed at the 140 minute time points shown in Figure 4.3.

Gene Symbol	Gene Name	% Change in Paralysis at 160 Minutes	Standard Deviation 160 Minutes	P Value 160 Minutes	Significant at 160 Minutes?
C52E4.4	rpt-1	-38.66068088	23.76690912	0.0563	No
C07H6.5	cgh-1	-57.67195767	17.37406322	0.0097	Yes
F38H4.9	let-92	-31.93765248	27.16597683	0.0815	No
C05D9.1	snx-1	-50.89585054	6.44556188	0.0285	Yes
C28H8.6	pxl-1	-39.44369097	7.009042523	0.0575	No
C27H6.2	ruvb-1	-53.83886145	7.340000985	0.005	Yes
F35H12.3	sel-12	-54.05022632	8.282775151	0.0389	Yes
Y47H9C.2	dhhc-2	-43.49745331	14.52485366	0.0213	Yes
T04H1.2	t04h1.2	-52.62801714	13.78357755	0.0344	Yes
F18G5.3	gpa-12	-52.9419835	7.653214686	0.012	Yes
T22D1.10	ruvb-2	-50.39407298	16.95433373	0.0007	Yes
W03H9.4a	cacn-1	-52.20884063	2.25108648	0.0004	Yes
C27B7.8	rap-1	-41.46095102	20.30765579	0.0571	No
Y116A8C.36	itsn-1	-65.34401365	12.68974417	0.0038	Yes
F13G3.4	dylt-1	39.23267327	13.11617603	0.0162	Yes
F52A8.2	gpb-2	-48.37759983	37.16672446	0.1053	No
H39E23.1	par-1	-35.6761027	17.16806615	0.0681	No
F19C6.1	grk-1	-24.35410154	26.01005208	0.2169	No
C30C11.4	hsp-110	-30.41526375	17.01973103	0.0398	Yes
Y87G2A.4	aex-6	-30.34695921	28.54973196	0.1593	No
F32A5.6	prx-13	-1.862427329	29.92083321	0.9103	No
Y55F3AM.15	csn-4	-29.9568275	24.55914914	0.1457	No

Table 4.10 - Data associated with phenotypic trends observed at the 160 minute time points shown in Figure 4.3.

Gene Symbol	Gene Name	100 Minute	140 Minute	160 Minute	Overall
C52E4.4	rpt-1	Yes	Yes	No	Yes
C07H6.5	cgh-1	Yes	Yes	Yes	Yes
F38H4.9	let-92	Yes	Yes	No	Yes
C05D9.1	snx-1	No	Yes	Yes	Yes
C28H8.6	pxl-1	Yes	Yes	No	Yes
C27H6.2	ruvb-1	Yes	Yes	Yes	Yes
F35H12.3	sel-12	Yes	Yes	Yes	Yes
Y47H9C.2	dhhc-2	Yes	No	Yes	Yes
T04H1.2	t04h1.2	Yes	Yes	Yes	Yes
F18G5.3	gpa-12	No	Yes	Yes	Yes
T22D1.10	ruvb-2	Yes	Yes	Yes	Yes
W03H9.4a	cacn-1	No	Yes	Yes	Yes
Y116A8C.36	itsn-1	No	Yes	Yes	Yes
F13G3.4	dylt-1	Yes	Yes	Yes	Yes
F52A8.2	gpb-2	Yes	No	No	No
H39E23.1	par-1	Yes	No	No	No
F19C6.1	grk-1	Yes	No	No	No
C30C11.4	hsp-110	No	No	Yes	No
Y87G2A.4	aex-6	No	No	No	No
F32A5.6	prx-13	Yes	No	No	No
Y55F3AM.15	csn-4	No	No	No	No
C27B7.8	rap-1	No	Yes	No	No

Table 4.11 – Summary of aldicarb screens carried out on candidates from the module analysis screen. The 100 minute time point was assessed in a primary assay, while the 140 and 160 minute time points were analysed in an independent secondary assay. Yes and NO indicate if the calculated p value was less or greater than 0.05 respectively. If genetic knockdown of a target led to a significant result in two of the three time points, it is indicated a positive overall hit.

		100 minutes			140 minutes		
Gene Symbol	Gene Name	% change	Stdev	P Value	% change	Stdev	P Value
L440	L440	0	1.51391012	-	0	1.7719606	
egl-30	M01D7.7	-100	0	<0.0001	-97.400249	2.59990028	<0.0001
sel-12	F35H12.3	-47.174452	7.84753486	0.0039	-41.839849	5.9743545	0.0024
ruvb-1	C27H6.2	-72.586412	15.8299626	0.0102	-69.582909	16.3816698	0.0133
ruvb-2	T22D1.10	-61.992458	4.21510891	0.0001	-50.394073	9.78858914	0.007
itsn-1	Y116A8C.36	-41.016473	13.7067805	0.0404	-40.65785	7.86515104	0.007

Table 4.12 – Data relating to phenotypic trends shown in figure 4.4.

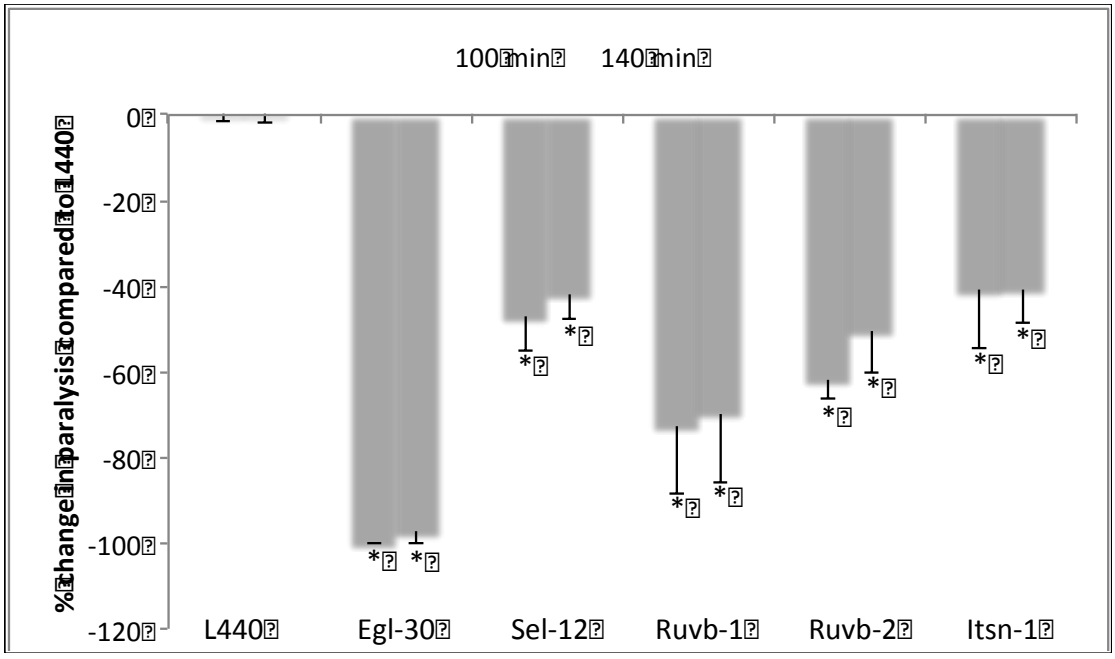

Figure 4.4 – **Phenotypic trends in aldicarb-sensitivity following knockdown of a selection positive controls in Tu3335**. Adult worm paralysis was assessed at 100 and 140 minutes as described in Materials and Methods. In each case, percentage change in paralysis is shown compared to a L440 empty vector negative control. * denotes $p<0.05$. N=3. Error bars represent standard deviation.

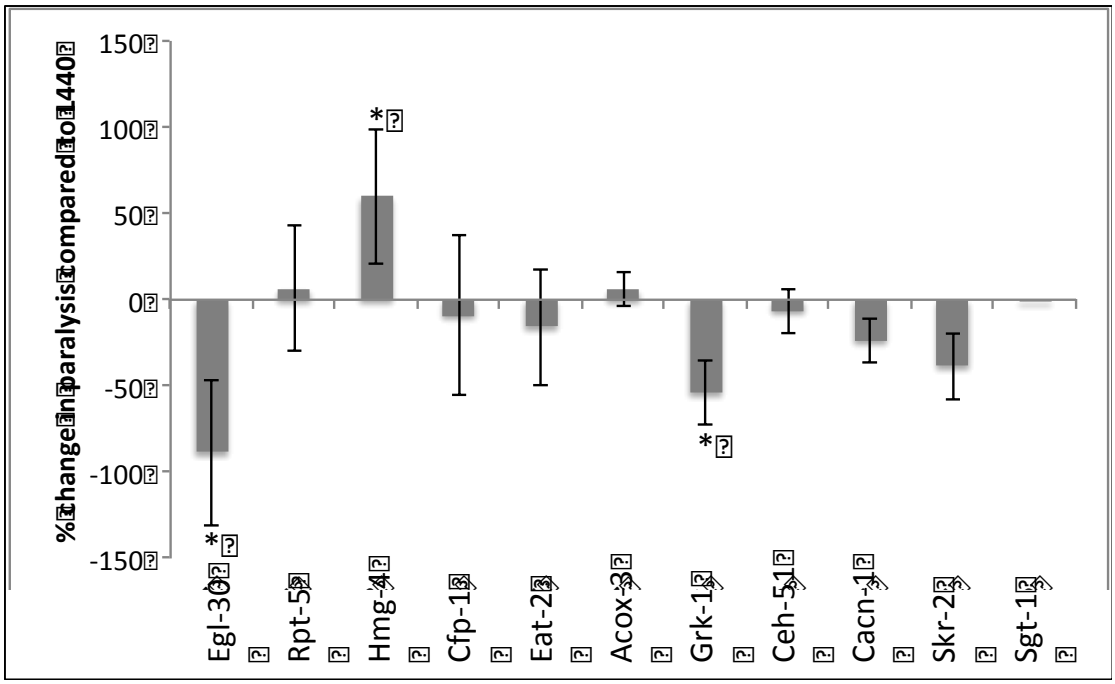

Figure 4.5 - **Aldicarb-sensitivity screening of borderline candidates in Tu3335, which were either nearly significant, or had large change in paralysis in two of the three plates but large standard deviations.** Paralysis of adult worms was assessed at 140 minutes as described in Materials and Methods. Percentage change in paralysis for each gene is compared to a L440 empty vector negative control. * denotes $p<0.05$. n=3. The percentage change to L440 was then calculated and plotted. M01D7.7 (egl-30) is included as a positive control. * denotes $p<0.05$. N = 3. Error bars represent standard deviation.

Gene Symbol	Gene Name	% Change	Standard Deviation	P value
egl-30	M01D7.7	-88.569533	4.133951837	0.0139
rpt-5	F56H1.4	6.45576533	42.25505538	0.8133
hmg-4	T20B12.8	59.9911583	36.34373235	0.0194
cfp-1	F52B11.1	-9.1217549	39.12498281	0.6981
eat-2	Y48B6A.4	-15.708812	46.05780195	0.6018
F58F9.7	F58F9.7	5.8994152	33.85705879	0.5288
grk-1	F19C6.1	-54.052583	9.49864401	0.0424
dlx-1	Y80D3A.3	-6.325952	18.6980827	0.7624
cacn-1	W03H9.4	-23.720108	13.08339314	0.2325
skr-2	F46A9.4	-38.37181	12.66186478	0.1016
sgt-1	R05F9.10	-0.0478141	19.47208174	0.9975

Table 4.13 – Data relating to phenotypic trends shown in Figure 4.5. Hmg-4 and grk-1 lead to significant HIC and RIC phenotypes, respectively.

Having confirmed the potential utility of *Tu3335*, a selection of candidate genes were selected for retesting if they were close to showing a significant RIC or HIC phenotype, or if two of the three plates of worms showed greater than 20% change in paralysis. Figure 4.5 and Table 4.13 show the results from these screens, which show that knockdown of grk-1 (F19C6.1) led to a significant RIC phenotype, while hmg-4 (T20B12.8) knockdown caused a HIC phenotype.

Brief descriptions of genes showing a positive phenotype are shown in Table 4.14, while Table 4.15 lists their closest human orthologs, which were identified using DIOPT fly RNAi (Hu et al., 2011). Overall, sixteen of the novel candidate genes caused a significant change in aldicarb-sensitivity when knocked down in *Tu3311* and/or *Tu3335 worms*.

Gene Symbol	Gene Name	Brief Description (From Wormbase)
C05D9.1	snx-1	Encodes the ortholog of VPS5/SNX1 subunit of the core retromer complex. Regulates retrograde endosome-to-golgi trafficking
C07H6.5	cgh-1	Encodes a putative RNA helicase, which is expected to enable decapping-dependent mRNA degradation
C27H6.2	ruvb-1	Encodes a AAA+ ATPase and functions as a component of the TOR signaling pathway, which enables robust protein synthesis.
C28H8.6	pxl-1	Required for organized myofilament structure in the pharynx and pharyngeal muscle
C52E4.4	rpt-1	Encodes a predicted ATPase subunit of the 19s complex of the proteasome
F13G3.4	dylt-1	May negatively regulate dynein, and encodes a putative light chain subunit of dynein
F18G5.3	gpa-12	Encodes a member of the G Protein alpha subunit family. Functions upstream of PLC-3 and EGL-8, as well as TPA-1 in pathways regulating feeding and growth.
F19C6.1	grk-1	Encodes a Serine/Threonine Protein kinase, closely resembling G Protein Coupled Receptor (GPCR) kinases.
F35H12.3	F35H12.3	Encodes a transmembrane protein orthologous to presenilins. During development, may positively regulate the lin-12 and glp-1 notch signaling pathways.
F38H4.9	let-92	Encodes the catalytic subunit of protein phosphatase 2a. Required for embryogenesis, larval development, axonal guidance in the DD and VD neurons
T04H1.2	t04h1.2	Encodes the ortholog of human GTPBP2.
T20B12.8	hmg-4	Predicted to be a member of the FACT (Facilitates Chromatin Transcription) complex, and acts as a transcription elongation factor.
T22D1.10	ruvb-2	Involved in RNAi, locomotion, development and receptor-mediated endocytosis. Predicted to have ATP binding and DNA helicase activity.
W03H9.4	cacn-1	Encodes the ortholog of Drosophila CACTIN. Required for distal tip migration and normal growth.
Y116A8C.36	itsn-1	An endocytic adaptor protein. Required for synaptic vesicle recycling.
Y47H9C.2	dhhc-2	Palmitoyl-acyl transferase involved in the determination of adult lifespan.

Tu3335 worms. Data was mined from Wormbase.

Worm Gene Symbol	Worm Gene Name	Wormbase Gene ID	Human Gene Symbol	Human Gene ID
C05D9.1	snx-1	WBGene00004927	SNX2	6643
C07H6.5	cgh-1	WBGene00000479	DDX6	1656
C27H6.2	ruvb-1	WBGene00007784	RUVBL1	8607
C28H8.6	pxl-1	WBGene00016197	PXN	5829
C52E4.4	rpt-1	WBGene00004501	PSMC2	5701
F13G3.4	dylt-1	WBGene00008764	DYNLT3	6990
F18G5.3	gpa-12	WBGene00001674	GNA12	2768
F19C6.1	grk-1	WBGene00001708	GRK5	2869
F35H12.3	sel-12	WBGene00004769	PSEN2	5664
F38H4.9	let-92	WBGene00002363	PPP2CA	5515
T04H1.2	t04h1.2	WBGene00011449	GTPBP2	54676
T20B12.8	hmg-4	WBGene00001974	SSRP1	6749
T22D1.10	ruvb-2	WBGene00020687	RUVBL2	10856
W03H9.4	cacn-1	WBGene00012230	CACTIN	58509
Y116A8C.36	itsn-1	WBGene00006405	ITSN1	6453
Y47H9C.2	dhhc-2	WBGene00012948	zdhhc9	79683

Table 4.15 – Human orthologs of genes from the module analysis screen that caused a significant change in aldicarb-sensitivity. Orthologs were elucidated using DIOPT FlyRNAi.

4.3.4 Data mining of module hits

SynaptomeDB was used to query whether any of the human orthologs of worm proteins found to be novel effectors of synaptic function were known to be localised pre- or post-synaptically. As shown in Table 4.16, five of the novel effector genes (cgh-1 (C07H6.5), let-92 (F38H4.9), snx-1 (C05D9.1), ruvb-1 (C27B7.8) and itsn-1 (Y116A8C.36)) were localized postsynaptically, while one gene (gpa-12 (F18G5.3)) was localised pre-synaptically.

Gene Name	Human Gene Symbol	Synapse Localization
cgh-1	DDX6	PostSynaptic
let-92	PPP2CA	PostSynaptic
snx-1	SNX2	PostSynaptic
gpa-12	GNA12	PostSynaptic
itsn-1	PostSynaptic	PostSynaptic

Table 4.16 – Human orthologs of the genes from the module analysis screen that caused a significant change in aldicarb-sensitivity, which were found in the SynatomeDB.

The network used with the microarray data set was a simplified version of Wormnet version 2 and the CCSB interactome, created previously in the Sanderson group. As the network is a one-step RIC network, this led us to query whether any of the nodes tested were previously known to cause a HIC phenotype. Interestingly, itsn-1 (Y116A8C.36) has been shown to have this phenotype. However, in this study, a clear RIC phenotype was observed with a 71 and 65% decrease paralysis at 140 and 160 minutes (Table 4.9 and 4.10). This highlights possible strain-differences in observed phenotypes.

The list of module derived genes that caused RIC or HIC phenotypes were entered into DAVID for functional enrichment analysis. Three genes were found to have links to pathways previously found in the modules – Wnt, TGF-β and MAPK signaling. GPA12 is linked to MAPK signaling, let-92 is linked to both Wnt and TGF-β, and RUVB1 is linked to Wnt signaling. Also, three of the 16 orthologs have known disease association. There are many sequence variants of GNA-12 that lead to diversity of human height. Notably, PSEN2 encodes presenilin-2, and is linked with type 4 Alzheimer's disease, as well as cardiomyopathy. ZDHHC9 encodes a palmitoyl-acyl transferase required for N- and H-Ras palmitoylation, and mutations in this gene are associated with X-linked mental retardation.

4.3.5 Updating the *C. elegans* aldicarb network

The novel effectors of aldicarb-sensitivity were annotated on the merged Wormnet and Vidal interactome (Chapter 3, section 3,3.4), and a one-step aldicarb network was created. This network contained 4536 nodes and 14200 edges (Figure 4.6). A one-step network was also created from the module derived positive hits, in order to reveal patterns of connectivity to known RIC and HIC proteins. Four of the interacting partners (other than itsn-1) were known to be HIC, and 31 have RIC phenotypes (Table 4.17). This generated a network of 1203 nodes and 1478 edges (Figure 4.7). Although there were no overlapping hits between the previous screens and this study, some of the hits were found to be interacting partners of the positive effectors from our module analysis, and 21 of the connectivity and betweenness hits were also found to interact with hits from the functional module screens (Table 4.18).

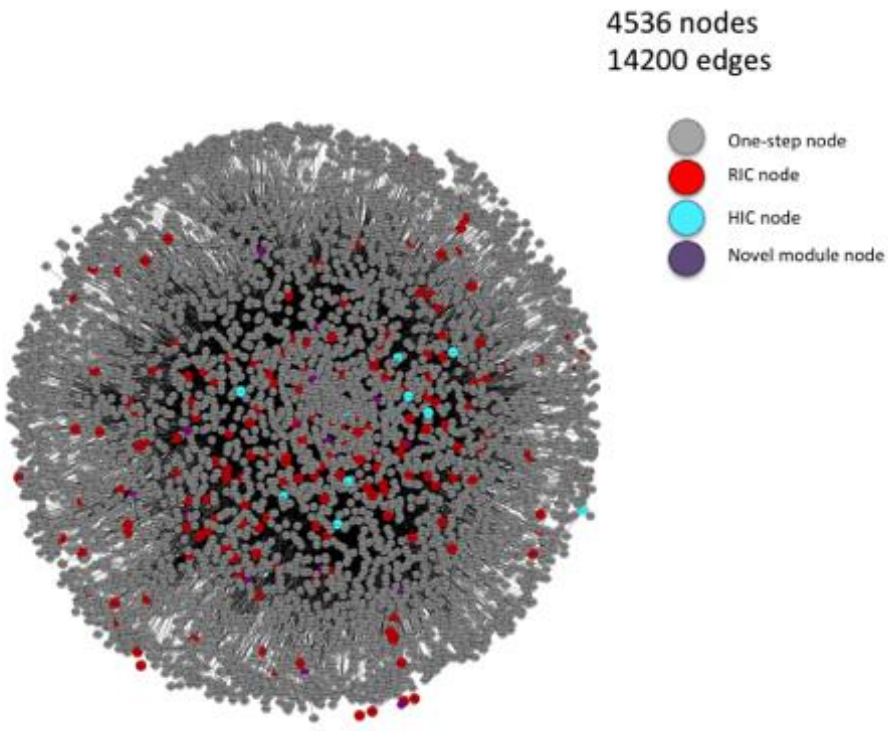

Figure 4.6 **– Updated one-step aldicarb sensitivity network.** Red nodes indicate RIC genes, Blue nodes represent HIC genes and Purple nodes are the novel hits from the module screen. The previously known RIC and HIC genes were collated from Wormbase. A spring-embedded layout was used to generate this network in Cytoscape.

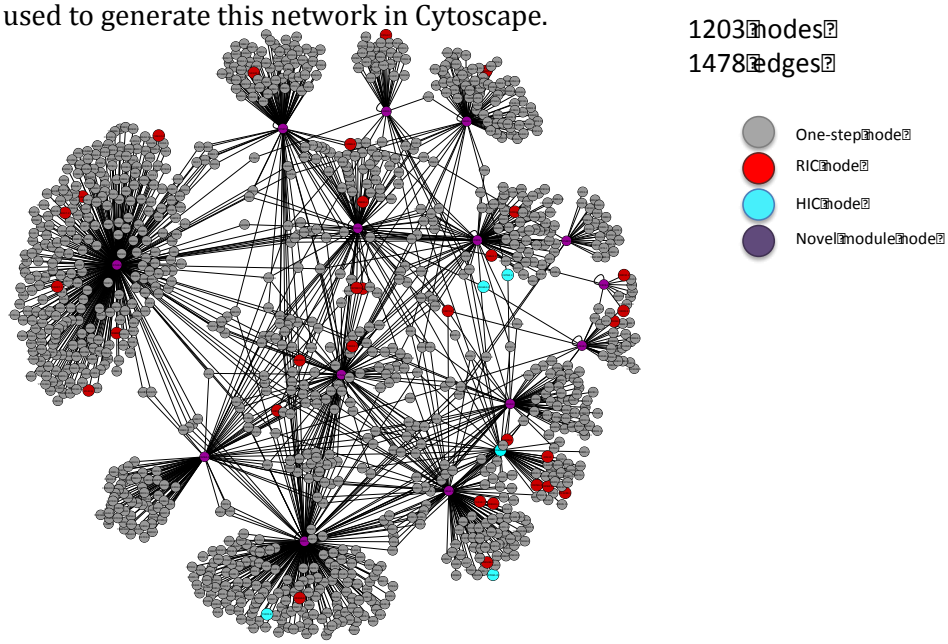

Figure 4.7 **– One-step network of module hits.** Purple nodes represent module genes that induced a significant change in aldicarb sensitivity following RNAi knockdown. Red nodes represent genes that were known to cause a RIC phenotype, and Blue nodes are genes known to cause a HIC phenotype. Grey nodes represent interaction partners of module proteins. A merge of Wormnet version 3 and the worm interactome were used to identify one-step interaction partners for module proteins.

Gene Symbol	Gene Name	Aldicarb Phenotype	Connected Gene Name(s) found in Module
C01G6.8	cam-1	RIC	ruvb-2
C10C5.6	daf-16	RIC	cgh-1
C32E8.10	unc-11	RIC	itsn-1
C50H2.1	fshr-1	RIC	grk-1, gpa-12
D2013.2	wdfy-2	RIC	snx-1
F20B6.8	hpk-1	RIC	gpa-12
F23F12.6	rpt-3	RIC	ruvb-1
F26G5.9	tam-1	RIC	t04h1.2
F29D10.4	hum-1	RIC	grk-1
F30F8.8	taf-5	RIC	grk-1
F37A4.7	rbf-1	RIC	dylt-1
F43C1.2	mpk-1	RIC	pxl-1, let-92
JC8.10	dyb-1	RIC	itsn-1
K04D7.1	unc-26	RIC	cgh-1
M117.2	rack-1	RIC	cgh-1
M142.6	par-5	RIC	cgh-1
R06A10.2	rle-1	RIC	ruvb-1
T12E12.4	gsa-1	RIC	cgh-1
T14G10.2	drp-1	RIC	ruvb-1
T18H9.7	cav-1	RIC	let-92
T20D3.7	pxf-1	RIC	rpt-1, snx-1
T28D6.9	tag-232	RIC	sel-12, let-92
W08G11.4	vps-26	RIC	let-92
Y106G6E.6	pen-2	RIC	let-92
Y18D10A.5	pptr-1	RIC	pxl-1
Y22F5A.3	csnk-1	RIC	itsn-1
Y65B4BR.4	gsk-3	RIC	cgh-1
Y67D8C.5	ric-4	RIC	gpa-12, ruvb-1
Y6B3A.1	unc-25	RIC	gpa-12
Y71H2B.10	rho-1	RIC	gpa-12, ruvb-1
ZK1248.3	wwp-1	RIC	rpt-1
T13F2.8	eel-1	HIC	ruvb-2
Y37D8A.23	agef-1	HIC	let-92
F47G6.1	apb-1	HIC	sel-12, t04h1.2
Y51H4A.3	ehs-1	HIC	pxl-1, gpa-12

Table 4.17 – Table showing known RIC and HIC proteins that interact with novel module derived effectors of aldicarb sensitivity. This data correlates with the network shown in Figure 4.7.

4.3.6 Analysis of Microarray Data

The previous analysis, which led to the GSEA and module generation, examined changes in gene expression, i.e. whether genes were increased or decreased to a similar level in response to different concentrations of VPA. In this study, the microarray data was re-analysed to determine which genes were significantly up

or down regulated compared to the zero VPA control, using a two-fold change significance threshold at each concentration (the log2 fold change cut off is set at 1.). This analysis was performed in *R* using the *limma* package, which allows users to analyse gene expression data from both microarrays and RNA-seq experiments. The microarray data used in this study was generated using the *C. elegans* (V2) Gene Expression Microarray. In brief, data is first read, corrected for background, and then normalised before a linear model is fitted to expression data for each gene, to determine significant changes in gene expression between conditions. For this modeling approach, two matrices are required. The first of these is the design matrix, wherein each row corresponds to an array in the experiment. The second is the contrast matrix, where the comparisons to be made are written, for example the 3mM VPA treatment against the control. After linear model fitting, *Limma* uses the Bayes method to determine standard errors. Here, the concentrations of VPA used were 0, 3, 6, 9, 12, 15, 18 and 24mM, and comparisons were made between each concentration and zero.

4.3.7 Visualization of microarray data

The *pHeatmap* package in R was used to generate heatmaps of genes showing VPA-induced changes in gene expression. Examples of genes that demonstrate increasing levels of expression with VPA concentration are shown in Figure 4.8 A, and examples demonstrating downregulation are shown in Figure 4.8 B.

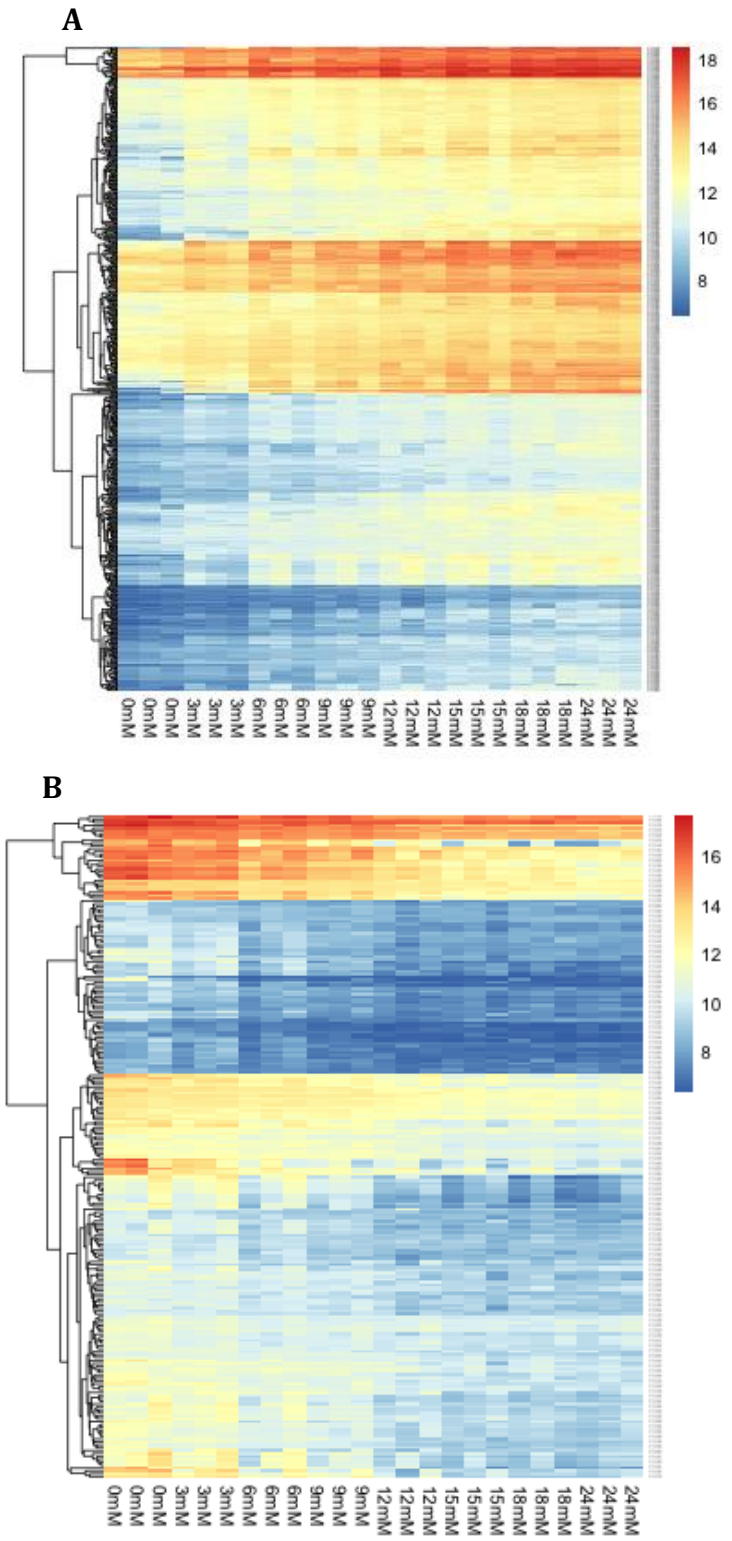

Figure 4.8 **– Heatmap of example genes showing A. upregulation and B. downregulation for N2 worms treated with increasing concentrations of sodium VPA.** Microarray data was visualized using the *pHeatmap* package in R. Colours indicate the level of expression of each gene (arbitrary units) at each concentration, increasing from blue to red.

4.3.8 Data mining of microarray lists

Gene lists were merged using an R script that aggregates rows if the designated column is identical (e.g. Wormbase Gene ID). This led to a non-redundant list of 944 genes that were up regulated, and 306 genes were down regulated following exposure to any concentration of VPA (Table 4.19). The probe IDs were converted to Wormbase IDs using Biomart. It is important to note that when converting from Agilent to Wormbase IDs, multiple probes may be associated with one gene.

VPA Concentration (mM)	Down-regulated Genes	Up-regulated Genes
3	1	30
6	23	157
9	51	242
12	178	456
15	224	570
18	302	1057
24	338	1230
Merged	306	921

Table 4.19 – Number of genes that were up or down regulated following microarray analysis of N2 worms treated with varying concentrations of VPA. Analysis was carried out using R using the *limma* package. Comparisons were made between the gene expression levels at each concentration of VPA against the negative control, when zero VPA was used. As there were overlaps in the significantly up and down regulated genes, a merged list of genes was created where duplicates were removed.

The number of different concentrations at which each gene was found to be differentially expressed was then analysed. In all, 22 genes were up regulated at every concentration measured, while only one gene (*R05H10.7*) displayed down regulation at all concentrations (Table 4.20). Changes observed for all other genes are shown in Supplementary Tables 4.1-4.6.

Gene Name	Change	Confidence	Concentrations Observed
Cyp-13a7	UpRegulation	7	18mM|3mM|6mM|9mM|12mM|15mM|24mM
Ech-9	UpRegulation	7	18mM|3mM|6mM|9mM|12mM|15mM|24mM
Lbp-8	UpRegulation	7	18mM|3mM|6mM|9mM|12mM|15mM|24mM
Pgp-1	UpRegulation	7	18mM|3mM|6mM|9mM|12mM|15mM|24mM
C40H1.8	UpRegulation	7	18mM|3mM|6mM|9mM|12mM|15mM|24mM
Clec-167	UpRegulation	7	18mM|3mM|6mM|9mM|12mM|15mM|24mM
F58B4.5	UpRegulation	7	18mM|3mM|6mM|9mM|12mM|15mM|24mM
K08D8.6	UpRegulation	7	18mM|3mM|6mM|9mM|12mM|15mM|24mM
Cyp-13a4	UpRegulation	7	18mM|3mM|6mM|9mM|12mM|15mM|24mM
Cyp-13a5	UpRegulation	7	18mM|3mM|6mM|9mM|12mM|15mM|24mM
T16G1.6	UpRegulation	7	18mM|3mM|6mM|9mM|12mM|15mM|24mM
Clec-9	UpRegulation	7	18mM|3mM|6mM|9mM|12mM|15mM|24mM
ZK896.5	UpRegulation	7	18mM|3mM|6mM|9mM|12mM|15mM|24mM
C37C3.10	UpRegulation	7	18mM|3mM|6mM|9mM|12mM|15mM|24mM
Asp-12	UpRegulation	7	18mM|3mM|6mM|9mM|12mM|15mM|24mM
F39E9.1	UpRegulation	7	18mM|3mM|6mM|9mM|12mM|15mM|24mM
F49F1.7	UpRegulation	7	18mM|3mM|6mM|9mM|12mM|15mM|24mM
K11H12.4	UpRegulation	7	18mM|3mM|6mM|9mM|12mM|15mM|24mM
Pho-14	UpRegulation	7	18mM|3mM|6mM|9mM|12mM|15mM|24mM
Y45G12C.4	UpRegulation	7	18mM|3mM|6mM|9mM|12mM|15mM|24mM
Clec-210	UpRegulation	7	18mM|3mM|6mM|9mM|12mM|15mM|24mM
F33H12.7	UpRegulation	7	18mM|3mM|6mM|9mM|12mM|15mM|24mM
F39E9.1	UpRegulation	7	3mM|6mM|9mM|12mM|15mM|18mM|24mM
R05H10.7	DownRegulation	7	3mM|6mM|9mM|12mM|15mM|18mM|24mM

Table 4.20 – *C. elegans* genes found to be regulated for every VPA concentration tested. Following microarray analysis of N2 worms treated with varying concentrations of VPA, the concentrations at which a given gene was up or down regulated were analysed. Those that were significantly changed at each concentration of VPA, in comparison to the negative control (when no VPA was used), are listed.

Lists of significantly upregulated or downregulated genes were analysed in DAVID to establish enrichment of biological processes, molecular functions and perform KEGG or PANTHER pathway analysis.

4.3.9 DAVID analysis of downregulated genes

When analysing biological processes enriched in the downregulated gene list, GO mappings annotated directly by the source database were used, i.e. parent GO terms were not included. Analysis of downregulated genes identified five genes

with roles in nervous system development (Table 4.21). These were syd-1 (WBGENE00006363), *dex-1* (WBGENE00017028), *cwn-2* (WBGENE00000858), *unc-86* (WBGENE00006818) and *syg-2* (WBGENE00007750). *Syd-1* was negatively regulated at 18mM, *dex-1* at 12, 15, 18 and 24mM, *syg-2* at 24mM, and *cwn-2* and *unc-86* were down regulated at 12mM VPA. This analysis suggests that there are selective changes in gene expression dependent on the concentration of VPA used. Significantly, at this range of concentrations, VPA appears to be imposing changes in neuronal functions.

Another biological process enrichment tool available in DAVID (BP_FAT) was also used, which takes into account parental GO terms, as this may reveal other genes involved in neuronal processes. These parental GO terms associated with neuronal function are shown in Table 4.22. From this it can be seen that 20 genes are associated (via parental GO terms) to nervous system development. Although many are not directly annotated with this GO term, these genes are still valid for further analysis.

GO Term	Biological Process	Count	Worm Name(s)
GO:0050830	Defense response to gram-positive bacterium	7	spp-2, spp-1, clec-7, clec-172, clec-82, clec-52, math-38
GO:0006629	Lipid metabolic process	11	C40H1.7, Y49E10.17, asm-3, lipl-2, lipl-1, C39B5.14, K03H6.2, lipl-3, fat-5, fat-6, T10B5.7
GO:0033564	Anterior/posterior axon guidance	3	cwn-2, lad-2, fmi-1
GO:0005975	Carbohydrate metabolic process	8	Y105E8B.9, chil-23, glct-2, H18N23.2, hex-1, F11A5.5, glct-4, T19H5.6
GO:0045087	Innate immune response	11	R07C12.1, spp-1, thn-1, ZC262.9, clec-170, clec-172, K08D10.14, clec-86, clec-82, fat-6, R07C12.3
GO:0016358	Dendrite development	4	unc-52, unc-86, W03D8.8, dma-1
GO:0007399	Nervous system development	5	syd-1, dex-1, cwn-2, unc-86, syg-2
GO:0007413	Axonal fasciculation	5	ten-1, plx-2, syd-9, Y105E8B.9, W03D8.8
GO:0042759	Long-chain fatty acid biosynthetic process	2	fat-5, fat-6
GO:0009612	Response to mechanical stimulus	3	jnk-1, unc-86, glr-1
GO:0007275	Multicellular organism development	11	syd-1, cfz-2, ceh-32, ten-1, ceh-22, plx-2, hbl-1, cwn-2, fat-5, daao-1, fat-6
GO:0016042	Lipid catabolic process	3	lipl-2, lipl-1, lipl-3
GO:0050650	Chondroitin sulfate proteoglycan biosynthetic process	2	glct-2, glct-4
GO:0030204	Chondroitin sulfate metabolic process	2	glct-2, glct-4
GO:0006952	Defense response	5	thn-2, spp-1, glf-1, lys-3, fmo-2
GO:1904937	Sensory neuron migration	2	cfz-2, cwn-2
GO:0043252	Sodium-independent organic anion transport	2	F47E1.2, F47E1.4

Neurological Process	Count	Worm Name(s)
Neuron projection development, neuron development, neuron differentiation, neurogenesis	18	cfz-2, dex-1, egl-46, plx-2, cwn-2, unc-52, unc-86, syd-9, nab-1, ron-12, jnk-1, ten-1, Y105E8B.9, lad-2, W03D8.8, syg-2, fmi-1, dma-1
Nervous system development	20	syd-1, cfz-2, egl-46, dex-1, plx-2, cwn-2, unc-52, unc-86, syd-9, nab-1, ron-12, jnk-1, ten-1, Y105E8B.9, nsy-4, lad-2, W03D8.8, syg-2, fmi-1, dma-1
Axon development	15	cfz-2, egl-46, plx-2, unc-86, cwn-2, syd-9, ron-12, ten-1, jnk-1, Y105E8B.9, lad-2, W03D8.8, syg-2, fmi-1, dma-1
Axonogen		
Axon guid		

GO Term	Molecular Function	Count	Worm Name(s)
GO:0030246	carbohydrate binding	21	clec-36, clec-51, clec-60, clec-49, clec-7, clec-48, clec-172, clec-86, clec-28, clec-52, clec-61, clec-170, clec-82, clec-160, clec-43
GO:0005198	structural molecule activity	5	ifc-1, fp-1, unc-52, fa-3, fd-1
GO:0008378	galactosyltransferase activity	3	T09E11.10, E03H4.11, C47F8.6
GO:0017154	semaphorin receptor activity	2	plx-2, kvs-1
GO:0016790	thiolester hydrolase activity	2	W03D8.8, T05E7.1
GO:0016717	oxidoreductase activity	2	fat-5, fat-6
GO:0048495	roundabout binding	2	syd-1, dma-1
GO:0004553	hydrolase activity, hydrolyzing O-glycosyl compounds	4	Y105E8B.9, chil-23, hex-1, T19H5.6
GO:0004768	stearoyl-CoA 9-desaturase activity	2	fat-5, fat-6
GO:0005215	transporter activity	5	F47E1.2, EEED8.2, T07H12.5, F, F47E1.4
GO:0051015	actin filament binding	3	cor-1, nab-1, hcam-1

The enrichment of molecular functions for downregulated genes was then examined (Table 4.23). The most highly enriched molecular function was carbohydrate binding, with 21 genes being directly associated with this GO term. Two genes were predicted to encode proteins with thiolester hydrolase activity. These two genes were *T05E7.1* (WBGene00020258), - downregulated at 15, 18 and 24mM VPA –and *W03D8.8* (WBGene00020989) – downregulated at 24mM VPA treatment. The human orthologs of these genes are members of the acyl-coA thioesterases (ACOT) and bile acid CoA: amino acid N-acyltransferase (BAAT) families. Both of these families in humans show palmitoyl-CoA hydrolase activity. When considering knockdown of *dhhc-2*, a palmitoyl acyl transferase, caused a RIC phenotype previously, this provides a few more links between the role of palmitoylation activity and VPA.

Pathway enrichment was also performed using PANTHER. Although no pathways had multiple genes associated with them, many of the genes were found to be linked to potentially interesting pathways, or were themselves interesting genes (Table 4.24). Genes of particular neurological interest included: *Jnk-1* (WBGene00002178), which is involved in the amyloid-secretase pathway as well as Ras and TGF-β signaling. *Cwn-2* (WBGene00000858) is involved in the presenilin pathway and wnt signaling, and *Ace-3* (WBGene00000037) is an abnormal acetylcholinesterase. As well as *cwn-2, cfz-2* is also associated with Wnt signaling, as it is the *C. elegans* frizzled homolog. *Cfz-2* is also down regulated following exposure to VPA, further suggesting a role of Wnt signaling as a mediator of VPA induced changes.

Wormbase Gene ID	Gene Symbol	Gene Name	Valproate Concentration (mM)	Panther Pathway
WBGene00000037	Y48B6A.8	ace-3	12|15|18|24	P00042:Muscarinic acetylcholine receptor signaling
WBGene00000478	F27E11.3	cfz-2	18|24	P00012:Cadherin signaling pathway, P00057:Wnt signaling pathway
WBGene00000708	M199.5	col-135	9|12|15|18|24	P00031:Inflammation mediated by chemokine and cytokine signaling pathway
WBGene00000858	W01B6.1	cwn-2	12	P00004:Alzheimer disease-presenilin pathway, P00005:Angiogenesis,P00012:Cadherin signaling, pathway,P00057:Wnt signaling pathway
WBGene00001477	K08C7.5	fmo-2	12|15|18|24	P05914:Nicotine degradation
WBGene00001612	C06E1.4	glr-1	18	P00037:Ionotropic glutamate receptor pathway, P00039:Metabotropic glutamate receptor group III pathway
WBGene00002178	B0478.1	jnk-1	15|18	P00003:Alzheimer disease-amyloid secretase pathway, P00005:Angiogenesis,P00006:Apoptosis signaling pathway,
WBGene00002178	B0478.1	jnk-1	15|18	P00010:B cell activation, P00018:EGF receptor signaling pathway, P00020:FAS signaling pathway
WBGene00002178	B0478.1	jnk-1	15|18	P00029:Huntington disease,P00049:Parkinson Disease, P00034:Integrin signaling pathway, P00035:Interferon-gamma,P00046:Oxidative Stress Response
WBGene00002178	B0478.1	jnk-1	15|18	P00052:TGF-beta signaling, T Cell activation, P00054:Toll receptor signaling, P04393:Ras signaling pathway
WBGene00002975	C35C5.5	lev-8	18	P00044:Nicotinic acetylcholine receptor signaling pathway
WBGene00003514	T18D3.4	myo-2	12	P00016:Cytoskeletal regulation by RHO GTPase, P00031:Inflammation, P00044:Nicotinic acetylcholine receptor signaling pathway, P00057:Wnt Signaling
WBGene00004281	Y11D7A.4	rab-28	12|15|18|24	P00047:PDGF signaling pathway, P00052:TGF-beta signaling pathway
WBGene00006759	ZK617.1	unc-22	15|18|24	P00016:Cytoskeletal regulation by RHO GTPase, P00031:Inflammation
WBGene00006777	C27H6.1	unc-41	15|18|24	P00023:General transcription regulation,P00055:Transcription regulation by bZIP transcription factor
WBGene00007401	C07A9.5		12	P00034:Integrin signaling
WBGene00007969	C36A4.9	acs-19	15 and 24	P02722:Acetate utilization,P02754:Methylcitrate cycle
WBGene00009773	F46B6.8	lipl-2	12|15|18|24	P02727:Androgen/estrogene/progesterone biosynthesis,
WBGene00009896	F49E11.11	scl-3	15|18|24	P00048:PI3 kinase pathway
WBGene00010062	F54F3.3	lipl-1	15|18|24	P02727:Androgen/estrogene/progesterone biosynthesis,
WBGene00011283	R90.1		12|18|24	P00049:Parkinson disease,P00057:Wnt signaling
WBGene00017677	F21F8.2	asp-11	6|9|12|15|18|24	P00004:Alzheimer disease-presenilin pathway
WBGene00018304	F41G3.12	agr-1	24	P00034:Integrin signaling pathway
WBGene00020016	R11G11.14	lipl-3	12|15|18|24	P02727:Androgen/estrogene/progesterone biosynthesis,
WBGene00020393	T10B5.7		24	P02727:Androgen/estrogene/progesterone biosynthesis,
WBGene00021703	Y48G9A.10	cpt-3	6|9|12|15|18|24	P00043:Muscarinic acetylcholine receptor

Table 4.24 – Panther analysis of down regulated genes. Following microarray analysis of N2 worms treated with varying concentrations of VPA, the downregulated genes were analysed by inputting into DAVID for gene ontology and pathway annotation. Panther was used to elucidate pathways the genes were associated with. There was no clustering of genes in specific pathways, but individual genes had neurologically relevant pathways associated with them, listed in this table.

4.3.10 DAVID analysis of upregulated genes

Genes that were significantly upregulated in response to VPA were entered into DAVID. Biological processes showing significant enrichment of genes include the innate immune response (104 assigned genes), oxidation-reduction (44 assigned genes) and transmembrane transport (30 assigned genes), A list of all of the enriched biological processes in the up-regulated data set, which are potentially affected by VPA treatment are shown in Table 4.25.

Of most interest are those that could potentially affect neuropeptide signaling, including nlp-28 (WBGene00003766), nlp-29 (WBGene00003767), nlp-30 (WBGene00003768), nlp-31 (WBGene00003769), nlp-33 (WBGene00003771), and nlp-34 (WBGene00015046). These are all neuropeptide-like proteins, although little other information is currently available for these proteins. Nlp-29 and nlp-33 play a role in innate immunity, and nlp-30 and nlp-31 are part of the YGGW amide neuropeptide family, which are expressed in the hypodermis.

Molecular functions with the highest number of assigned genes were transferase activity (63 assigned genes), structural constituent of cuticle (62 assigned genes), and hydrolase activity (52 assigned genes). These are shown in Table 4.26.

GO Term	Biological Process	Count
GO:0045087	innate immune response	104
GO:0052696	flavonoid glucuronidation	28
GO:0009813	flavonoid biosynthetic process	28
GO:0050829	defense response to Gram-negative bacterium	26
GO:0008152	metabolic process	96
GO:0055114	oxidation-reduction process	44
GO:1990170	stress response to cadmium ion	6
GO:0030968	endoplasmic reticulum unfolded protein response	13
GO:0010332	response to gamma radiation	5
GO:0006508	proteolysis	31
GO:0040002	collagen and cuticulin-based cuticle development	13
GO:0055085	transmembrane transport	30
GO:0031640	killing of cells of other organism	3
GO:0051603	proteolysis involved in cellular protein catabolic process	8
GO:0006952	defense response	12
GO:0006629	lipid metabolic process	17
GO:0050832	defense response to fungus	5
GO:0043171	peptide catabolic process	5
GO:1990169	stress response to copper ion	3
GO:0034219	carbohydrate transmembrane transport	3
GO:0008652	cellular amino acid biosynthetic process	4
GO:0006665	sphingolipid metabolic process	5
GO:0006820	anion transport	7
GO:0008643	carbohydrate transport	4
GO:0035434	copper ion transmembrane transport	3
GO:0016311	dephosphorylation	6
GO:0042908	xenobiotic transport	2
GO:0007218	neuropeptide signaling pathway	6

Table 4.25 - Biological process enrichment of genes that were up regulated in response to N2 worms being treated with VPA. Following microarray analysis of N2 worms treated with varying concentrations of VPA, the significantly upregulated genes from each concentration comparison were analysed by inputting into DAVID for gene ontology and pathway annotation. Biological processes enriched in the up regulated gene set are listed (using BP_DIRECT), as well as the number of genes clustered in each process.

GO Term	Molecular Function	Count
GO:0042302	structural constituent of cuticle	62
GO:0016758	transferase activity, transferring hexosyl groups	28
GO:0015020	glucuronosyltransferase activity	23
GO:0004185	serine-type carboxypeptidase activity	11
GO:0016491	oxidoreductase activity	43
GO:0042329	structural constituent of collagen and cuticulin-based cuticle	7
GO:0004497	monooxygenase activity	18
GO:0016705	oxidoreductase activity, acting on paired donors, with incorporation or reduction of molecular oxygen	17
GO:0016740	transferase activity	63
GO:0005506	iron ion binding	17
GO:0030246	carbohydrate binding	29
GO:0004180	carboxypeptidase activity	7
GO:0008194	UDP-glycosyltransferase activity	7
GO:0020037	heme binding	18
GO:0042626	ATPase activity, coupled to transmembrane movement of substances	10
GO:0022857	transmembrane transporter activity	14
GO:0008239	dipeptidyl-peptidase activity	5
GO:0015562	efflux transmembrane transporter activity	4
GO:0008233	peptidase activity	21
GO:0016787	hydrolase activity	52
GO:0004364	glutathione transferase activity	6
GO:0051119	sugar transmembrane transporter activity	3
GO:0016887	ATPase activity	10
GO:0016757	transferase activity, transferring glycosyl groups	12
GO:0016747	transferase activity, transferring acyl groups other than amino-acyl groups	8
GO:0003993	acid phosphatase activity	5
GO:0003959	NADPH dehydrogenase activity	3
GO:0008236	serine-type peptidase activity	5
GO:0004222	metalloendopeptidase activity	10
GO:0008237	metallopeptidase activity	11
GO:0051213	dioxygenase activity	4
GO:0052689	carboxylic ester hydrolase activity	4
GO:0005375	copper ion transmembrane transporter activity	3
GO:0008395	steroid hydroxylase activity	5
GO:0008559	xenobiotic-transporting ATPase activity	2

Table 4.26 – Molecular function enrichment of genes that were up regulated in response to N2 worms being treated with VPA. Following microarray analysis of N2 worms treated with varying concentrations of VPA, the significantly up regulated genes from each concentration were merged and analysed by inputting into DAVID for gene ontology and pathway annotation. Molecular functions enriched in the up regulated gene set are listed (using MF_DIRECT), as well as the number of genes associated with the molecular functions.

The PANTHER tool was then used to identify other neurologically relevant genes. Like in the downregulated gene set, no enrichment of pathways with multiple genetic associations was elucidated. However, some individual genes were found to have relevance to human disease (Table 4.27). Arf-1.1 (WBGene00000190) is involved in integrin signaling, and has been linked to Huntington's disease. Rab-

11.2 (WBGene00004275) is also linked to Huntington's disease by the PDGF pathway. Genes linked to Alzheimer's disease include Lrx-1 (WBGene00003075), zmp-2 (WBGene00019212) and asp-12 (WBGene00017678), which all form part of the presenilin pathway. Another gene found to be up regulated was Snb-2 (WBGene00004898), which is the *C. elegans* ortholog of human VAMP3 and VAMP1. It is involved in SNARE interactions in vesicular transport and was up regulated at 12, 15, 18 and 24mM VPA. These data provide some insight into possible molecular processes that may mediate therapeutic affects of VPA in neurodegenerative or cognitive disorders.

Although this method of analyzing the microarray data was different to that carried out previously (Munasinghe, 2015) , as the two methods of analyzing the same raw data were very different, common trends can be seen. For example in both methods, Wnt signaling and TGF-β signaling were clustered. The neuropeptide like genes were also found in both analyses (Munasinghe, 2015), although many other genes did not overlap.

The down-regulated and up-regulated gene lists were inputted together into DAVID, to see whether other genes with neurological biological process associations would be found (Table 4.28). Interestingly three upregulated genes were found to be associated with axonogenesis (adding to the 12 down-regulated genes previously elucidated in Table 3.23). These were vem-1 (WBGene00006890), which was up-regulated at 18mM VPA, vhp-1 (WBGene00006923), up-regulated at 24mM VPA, and dpy-18 (WBGene00001077), up-regulated at both 18 and 24mM VPA.

Wormbase Gene ID	Gene Symbol	Gene Name	Valproate Concentration (mM)	Panther Pathway
WBGene00021487	Y40B10A.2	comt-3	12|15|18|24	P00001:Adrenaline and noradrenaline biosynthesis, P05912:Dopamine receptor mediated signaling pathway
WBGene00012518	Y32B12A.3	comt-2	12|24	P00001:Adrenaline and noradrenaline biosynthesis, P05912:Dopamine receptor mediated signaling pathway
WBGene00019212	H19M22.3	zmp-2	18|24	P00004:Alzheimer disease-presenilin pathway
WBGene00017678	F21F8.4	asp-12	3|6|9|12|15|18|24	P00004:Alzheimer disease-presenilin pathway
WBGene00003075	T04H1.6	lrx-1	6|9	P00004:Alzheimer disease-presenilin pathway
WBGene00009692	F44E5.5		24	P00006:Apoptosis signaling pathway, P00049:Parkinson disease
WBGene00006539	T04H1.9	tbb-6	18|24	P00016:Cytoskeletal regulation by Rho GTPase, P00025:Hedgehog signaling pathway, P00029:Huntington disease
WBGene00004382	F59A6.6	rnh-1.0	12|18|24	P00017:DNA replication
WBGene00000190	F45E4.1	arf-1.1	24	P00029:Huntington Disease, P00034:Integrin signaling pathway
WBGene00004275	W04G5.2	rab-11.2	15|18|24	P00029:Huntington disease, P00047:PDGF signaling pathway
WBGene00000755	R09A8.4	col-182	24	P00031:Inflammation mediated by chemokine and cytokine signaling pathway, P00034:Integrin signaling pathway
WBGene00019644	K11D12.4	cpt-4	9|12|15|18|24	P00043:Muscarinic acetylcholine receptor 2 and 4 signaling pathway
WBGene00006923	F08B1.1	vhp-1	24	P00046:Oxidative stress response
WBGene00015087	B0252.1		6|9|12|15|18|24	P00048:PI3 kinase pathway
WBGene00001433	Y18D10A.25	fkb-8	18|24	P00052:TGF-beta signaling pathway
WBGene00015660	C09H5.2	catp-3	9|12|15|18|24	P00060:Ubiquitin proteasome pathway
WBGene00001149	K02A4.1	bcat-1	18|24	P02724:Alanine biosynthesis, P02748:Isoleucine biosynthesis, P02749:Leucine biosynthesis, P02785:Valine biosynthesis
WBGene00003982	R11H6.1	pes-9	12|15|18|24	P02728:Arginine biosynthesis
WBGene00022752	ZK484.6		18|24	P02735:Cobalamin biosynthesis
WBGene00010759	K10H10.2	cysl-2	15|18|24	P02737:Cysteine biosynthesis
WBGene00018174	F38B6.4		15|18|24	P02738:De novo purine biosynthesis
WBGene00016957	C55F2.1	atic-1	24	P02738:De novo purine biosynthesis
WBGene00003844	K11C4.4	odc-1	18|24	P02758:Ornithine degradation
WBGene00014206	ZK1058.6	nit-1	18|24	P02771:Pyrimidine metabolism
WBGene00016265	C30F12.6	nmur-4	18|24	P04394:Thyrotropin-releasing hormone receptor signaling pathway
WBGene00015048	B0218.2	faah-2	12|15|18|24	P05728:Anandamide_degradation,
WBGene00019515	K08B4.3	ugt-19	12|15|18|24	P05914:Nicotine degradation
WBGene00019379	K04A8.10		24	P05914:Nicotine degradation
WBGene00018543	F47C10.6	ugt-32	24	P05914:Nicotine degradation
WBGene00017336	F10D2.11	ugt-41	6|9|12|15|18|24	P05914:Nicotine degradation
WBGene00017331	F10D2.5	ugt-40	12|15|18|24	P05914:Nicotine degradation
WBGene00017329	F10D2.2	ugt-39	6|9|12|15|18|24	P05914:Nicotine degradation
WBGene00017315	F09G2.6	ugt-36	18	P05914:Nicotine degradation
WBGene00015692	C10H11.3	ugt-25	18|24	P05914:Nicotine degradation
WBGene00015449	C04F5.7	ugt-63	12|18	P05914:Nicotine degradation
WBGene00013901	ZC443.6	ugt-16	18|24	P05914:Nicotine degradation
WBGene00009255	F29F11.2	ugt-34	24	P05914:Nicotine degradation
WBGene00008486	F01D4.2	ugt-44	6|9|12|15|18|24	P05914:Nicotine degradation
WBGene00007946	C35A5.2	ugt-33	18	P05914:Nicotine degradation
WBGene00007885	C33A12.6	ugt-21	6|9|12|15|18|24	P05914:Nicotine degradation
WBGene00007455	C08F11.8	ugt-22	12|15|18|24	P05914:Nicotine degradation
WBGene00007422	C08B6.1	ugt-17	9|12|15|18|24	P05914:Nicotine degradation
WBGene00001479	F53F4.5	fmo-4	18|24	P05914:Nicotine degradation

Table 4.27– Panther pathway enrichment of genes up regulated in response to VPA. Following microarray analysis of N2 worms treated with varying concentrations of VPA, the down regulated genes were analysed by inputting into DAVID for gene ontology and pathway annotation. Panther was used to elucidate pathways the genes were associated with. There was no clustering of genes in specific pathways, but individual genes had pathways associated with them, listed in this table.

GO Term	Biological Process	Count
GO:0045087	innate immune response	115
GO:0009813	flavonoid biosynthetic process	28
GO:0052696	flavonoid glucuronidation	28
GO:0050829	defense response to Gram-negative bacterium	29
GO:0008152	metabolic process	115
GO:0055114	oxidation-reduction process	55
GO:0050830	defense response to Gram-positive bacterium	11
GO:0006629	lipid metabolic process	28
GO:1990170	stress response to cadmium ion	6
GO:0006508	proteolysis	38
GO:0030968	endoplasmic reticulum unfolded protein response	13
GO:0010332	response to gamma radiation	5
GO:0006952	defense response	17
GO:0051603	proteolysis involved in cellular protein catabolic process	11
GO:0055085	transmembrane transport	38
GO:0040002	collagen and cuticulin-based cuticle development	15
GO:0031640	killing of cells of other organism	3
GO:0006637	acyl-CoA metabolic process	4
GO:0006665	sphingolipid metabolic process	6
GO:0033564	anterior/posterior axon guidance	3
GO:0016042	lipid catabolic process	6
GO:1990169	stress response to copper ion	3
GO:0050832	defense response to fungus	5
GO:0034219	carbohydrate transmembrane transport	3
GO:0043171	peptide catabolic process	5
GO:0005975	carbohydrate metabolic process	15
GO:0046513	ceramide biosynthetic process	3
GO:0016311	dephosphorylation	7
GO:0008652	cellular amino acid biosynthetic process	4
GO:0007409	axonogenesis	15

Table 4.28 – Biological process enrichment of genes that showed differential regulation (both downregulated and upregulated gene sets) in response to N2 worms being treated with VPA. Following microarray analysis of N2 worms treated with varying concentrations of VPA, the significantly upregulated genes from each concentration comparison were analysed by inputting into DAVID for gene ontology and pathway annotation. Biological processes directly associated to the gene lists are shown.

4.3.11 Using WebGestalt to find disease pathways

To enable further investigation into the possible spectrum of pathways being affected by VPA, both the up and downregulated *C. elegans* genes were converted

into their human orthologs (Supplementary Tables 4.7 and 4.8). Some *C. elegans* have multiple possible human orthologs, which must be considered when converting gene IDs. To decide this, the human ortholog with the highest percentage identity, similarity and lowest percentage gaps were used. WebGestalt (B. Zhang, Kirov, & Snoddy, 2005) was then used to carry out gene set enrichment analysis, and assess potential disease association. Following this analysis, human IDs with neurological disease associations were converted back into worm orthologs for further analysis.

Fifteen of the *C.* elegans genes that were down regulated following exposure to VPA were found to have human orthologs associated with mental disorders. These include HIP1, whose *C. elegans* ortholog is Y18D10A.22 (WBGene00014864). HIP1 is huntingtin-interacting protein, and has a clear link with the neurodegenerative Huntington's disease. Nine of these genes including Y18D10A.22 were also linked to other disorders of the nervous system. Seven of the genes that were up regulated in response to VPA were found to be associated with spinal dysraphism, which refers to spinal cord malformations (Table 4.29). A list of all of the disease groups associated with up or down regulated genes is provided in Table 4.30.

Wormbase Gene ID	Worm Gene name	Worm Gene symbol	Human Gene symbol	Disorder	Valproate Regulation
WBGene00007691	C23H4.2	C23H4.2	CBS	Spinal dysraphism	Up Regulated
WBGene00018138	folt-2	F37B4.7	SLC19A1	Spinal dysraphism	Up Regulated
WBGene00019322	ahcy-1	K02F2.2	AHCY	Spinal dysraphism	Up Regulated
WBGene00018174	F38B6.4	F38B6.4	GART	Spinal dysraphism	Up Regulated
WBGene00021215	Y18H1A.11	Y18H1A.11	PCYT1A	Spinal dysraphism	Up Regulated
WBGene00022856	cth-2	ZK1127.10	CTH	Spinal dysraphism	Up Regulated
WBGene00000512	ckb-2	B0285.9	CHKA	Spinal dysraphism	Up Regulated
WBGene00022076	daao-1	Y69A2AR.5	DAO	Mental disorders	Down Regulated
WBGene00017594	F19C7.4	F19C7.4	PRSS16	Mental disorders	Down Regulated
WBGene0001759	F19C7.2	F19C7.2	PRSS16	Mental disorders	Down Regulated
WBGene00017184	ncam-1	F02G3.1	NCAM1	Mental disorders	Down Regulated
WBGene00016841	magu-3	C50F2.8	CASK	Mental disorders and Nervous System	Down Regulated
WBGene00016523	C39B5.5	C39B5.5	CST3	Mental disorders and Nervous System	Down Regulated
WBGene00015077	B0238.13	B0238.13	ACHE	Mental disorders and Nervous System	Down Regulated
WBGene00014864	Y18D10A.22	Y18D10A.22	HIP1	Mental disorders and Nervous System	Down Regulated
WBGene00004346	rgs-3	C29H12.3	RGS4|RGS2	Mental disorders	Down Regulated
WBGene00002975	lev-8	C35C5.5	CHRNA1|CHRNA2|CHRNE	Mental disorders and Nervous System	Down Regulated
WBGene00002243	lad-2	Y54G2A.25	NRCAM	Mental disorders	Down Regulated
WBGene00002057	ifd-1	R04E5.10	NES	Mental disorders and Nervous System	Down Regulated
WBGene00002055	ifc-1	F37B4.2	NES	Mental disorders and Nervous System	Down Regulated
WBGene00001612	glr-1	C06E1.4	GRIA3	Mental disorders and Nervous System	Down Regulated
WBGene00000037	ace-3	Y48B6A.8	BCHE	Mental disorders and Nervous System	Down Regulated

Table 4.29 – Table to show worm genes that had significant changes in expression in response to valproate treatment, which have human orthologues with known roles in mental disorders and/or nervous system disorders. WebGestalt was used for this analysis. Following microarray analysis of N2 worms treated with varying concentrations of VPA, the down or up regulated genes were analysed by converting the genes to their human orthologs (using DIOPT flyRNAi). These lists were then inputted into WebGestalt, where disease pathway analysis was carried out.

A

Disease Association	Count
Drug resistance	18
Metabolic diseases	25
Translocation, genetic	21
Cardiovascular diseases	20
Hyperbilirubinemia	7
Metabolism, Inborn errors	17
Drug Interaction with drug	17
Mental Disorders	21
Cholestasis	8
Fatty liver	11

B

Disease Association	Count
Metabolic diseases	22
Protein deficiency disease	14
Fatty liver	12
Tangier disease	6
Alpha 1-antitrypsin deficiency	6
Drug resistance	13
Translocation, genetic	15
Ototoxicity	7
Spinal dysraphism	7
Diabetes mellitus	13

Table 4.30 – A count of the number of downregulated (A) and upregulated (B) genes with disease associations. Following microarray analysis of N2 worms treated with varying concentrations of VPA, the down or up regulated genes were analysed by converting the genes to their human orthologs (using DIOPT flyRNAi). These lists were then inputted into WebGestalt, where disease pathway analysis was carried out. The count refers to how many genes from the list were found to be associated with each disease process.

4.3.12 Ingenuity analysis of downregulated genes

As different pathway analysis tools use different algorithms and provide variable coverage and definitions of biological processes, there is added value in using multiple tools to analysing data from differential gene expression studies. *Ingenuity* is another bioinformatics tool that can be used to analyse and interpret the potential functional implications of differential gene expression profiles. However, it is important to note that Ingenuity is not fully compatible with *C. elegans* data. Firstly, a significant number of differentially expressed *C. elegans* genes could not be mapped in the *Ingenuity* software. This may be because they are hypothetical proteins or proteins with no known human orthologs. With respect to those genes that are mapped, 109 were significantly up regulated, while 39 genes were significantly down regulated (Supplementary Tables 4.9 and 4.10).

Sets of differentially regulated genes were then analysed to investigate disease association. This means that several worm genes may be assigned to a single human ortholog. In some instances this can result in the some human genes being represented in both the up- and down-regulated subsets, as observed for MFSD8, which is associated with neuronal ceroid lipofuscinosis 8. *Three C.* elegans genes in the gene lists were orthologous to MFSD8 orthologs are F14D7.6 (down regulated) and C25E10.4 (up regulated) and F52F10.2 (up regulated). This gene therefore is discounted from the analysis.

Neurological disease pathways and functions associated with the down-regulated gene set are presented in Table 4.31. From the GSEA in Webgestalt, some of these genes had already been associated with mental disorders. However, this analysis gave no further information regarding, for example the category of mental disorder. Five genes, AGRN (WBGene00018304), GRIA3 (WBGene00001612), CYP3A4 (WBGene00007963), HSPG2 (WBGene00006787) and MAPK8 (WBGene00002178) were associated with Alzheimer's disease. Also, Gria3 is known to be linked to synaptic transmission and X-linked mental retardation.

Wormbase Gene ID	Human Gene Symbol	Disease/Function
WBGene00001612	GRIA3	X-linked mental retardation type 94, alzheimer's disease, major depression coordination, synaptic transmission
WBGene00001475	CELSR1	Neural tube defect
WBGene00006787	HSPG2	Neural tube defect, Alzheimer's disease
WBGene00004830	KCNMA1	generalized epilepsy with paroxysmal dyskinesia, ataxia coordination, nervous system differentiation, synaptic transmission
WBGene00018304	AGRN	Alzheimer's disease, nervous system differentiation, movement disorder, congenital myasthenic syndrome type 8, survival
WBGene00007963	CYP3A4	Alzheimer's disease, major depression
WBGene00020016	LIPA	Alzheimer's disease, apoptosis
WBGene00002178	MAPK8	Alzheimer's disease, nervous system proliferation, apoptosis, neural tube defect
WBGene00017184	NCAM1	prepulse inhibition, nervous system development, proliferation, major depression, movement disorder, ataxia, apoptosis
WBGene00020509	HEXB	coordination, movement disorder, adult and juvenile Sandhoff disorder, ataxia
WBGene00002055	LMNB2	nervous system development, differentiation, major depression
WBGene00002243	NRCAM	prepulse inhibition, nervous system development, proliferation,synaptic transmission, ataxia, neuromuscular disease
WBGene00006498	TENM2	nervous system development
WBGene00000858	WNT5B	nervous system development and function
WBGene00022076	DDO	prepulse inhibition, learning
WBGene00000478	FZD8	nervous system proliferation
WBGene00000966	HSD17B6	major depression
WBGene00000188	ARL3	movement disorder
WBGene00003514	MYH7B	movement disorder, neuromuscular disease
WBGene00001398	SCD2	neuromuscular disease
WBGene00001523	TMLHE	epsilon-trimethyllysine hydroxylase deficiency
WBGene00004281	RAB28	apoptosis
WBGene00008793	MFSD8	Neuronal ceroid lipofuscinosis 7

Table 4.31 – Ingenuity disease analysis of genes down regulated in response to N2 worm treatment with VPA, where neuronal related diseases/disorders were selected. Following microarray analysis of N2 worms treated with varying concentrations of VPA, significantly down regulated genes were inputted into Ingenuity Pathway Analysis (IPA), and disease associations were found.

Wormbase Gene ID	Human Gene Symbol	Disease/Function
WBGene00003408	ABCC1	epilepsy, cytotoxicity, neuroblastoma
WBGene00003409	ABCC3	cytotoxicity, analgesia, neuroblastoma
WBGene00006418	SGPL1	apoptosis of cerebellar macroneurons
WBGene00003996	Abcb1b	analgesia
WBGene00015048	FAAH	analgesia, excitation of dopaminergic neurons
WBGene00003914	NPEPPS	analgesia
WBGene00003573	SLC8B1	proliferation of cortical astrocytes
WBGene00019979	SLC2A3	epilepsy, excitation of rhodose ganglion neurons
WBGene00009801	PLA2G6	abnormal morphology of gray matter, dystonia, parkinsonism, infantile neuroaxonal dystrophy, Hallervorden-Spatz disease Karak syndrome, Parkinson disease, disorder of basal ganglia
WBGene00016957	ATIC	primary central nervous system lymphoma
WBGene00018174	GART	primary central nervous system lymphoma
WBGene00015359	IDE	neuroblastoma, olfactory esthesioneuroblastoma
WBGene00006530	TUBA1C	neuroblastoma, disorder of basal ganglia
WBGene00003995	ABCB1	epilepsy, dystonia, akathsia, disorder of basal ganglia, movement disorder
WBGene00015010	PTS	dystonia
WBGene00016340|WBGene00016335	GBA	epilepsy, parkinsonism, Gaucher disease, progressive myoclonic epilepsy type 4 with renal failure, disorder of basal ganglia, movement disorder
WBGene00010762|WBGene00000972	WWOX	epilepsy, autosomal recessive spinocerebellar ataxia type 12, early infantile epileptic encephalopathy type 28
WBGene00008741	CTSA	galactosialidosis type I & II, juvenile/adult type galactosialidosis, movement disorder
WBGene00018398	SPTLC2	hereditary sensory neuropathy type IC
WBGene00017312	SLC20A2	idiopathic basal ganglia calcification type 1, disorder of basal ganglia
WBGene00008793	MFSD8	neuronal ceroid lipofuscinosis 7
WBGene00012295	NMNAT3	Wallerian degeneration
WBGene00001778|WBGene00001770|WBGene00001755|WBGene00001761|	HPGDS	demyelination of cerebellum, astrocytosis demyelination of cerebellum, astrocytosis demyelination of cerebellum, astrocytosis demyelination of cerebellum, astrocytosis
WBGene00019322	AHCY	disorder of basal ganglia, movement disorder
WBGene00001577	CPNE5	disorder of basal ganglia, movement disorder
WBGene00001077	P4HA1	disorder of basal ganglia, movemment disorder
WBGene00006890	PGRMC1	disorder of basal ganglia, movement disorder

Table 4.32 – Ingenuity disease analysis of genes up regulated in response to VPA, where neuronal related diseases/disorders were selected. Following microarray analysis of N2 worms treated with varying concentrations of VPA, significantly down regulated genes were inputted into Ingenuity Pathway Analysis (IPA), and disease associations were found.

VPA is used to treat epilepsy, and the worm ortholog of KCNMA1, slo-1 (WBGene00004830) is significantly down regulated upon VPA treatment. KCNMA1 is linked to generalized epilepsy. Other potentially interesting links to neuronal effects were also revealed through the Ingenuity analysis – multiple genes were linked to neuronal development and differentiation, some of which were also identified using DAVID. However, some other genes were uniquely identified by Ingenuity analysis. These include NCAM1 (*C. elegans* ortholog: WBGene00017184), TENM2 (*C. elegans* ortholog: WBGene00006498), WNT5B (*C. elegans* ortholog: WBGene00000858), AGRN (*C. elegans* ortholog: WBGENE00018304). CELSR1 (*C. elegans* ortholog: WBGene00001475), HSPG2 (WBGene00006787), LMNB2 (*C. elegans* ortholog: WBGENE00002055), MAPK8 (*C. elegans* ortholog: WBGENE00002178), and KCNMA1 (*C. elegans* ortholog: WBGene00004830). These results clearly link VPA to neuronal development and differentiation, and may also provide clues as to processes involved in VPA action.

4.3.13 Ingenuity analysis of upregulated genes

Disease associations of the up regulated genes are shown in Table 4.32. Analysis of the up regulated gene set in Ingenuity identified five genes associated with epilepsy (Table 4.31), which may relevant to VPA's therapeutic role or mode of action. These are ABCC1 (*C. elegans* ortholog: WBGene00003408), SLC2A3 (*C. elegans* ortholog: WBGene00019979), ABCB1 (*C. elegans* ortholog: WBGene00003995), GBA (*C. elegans* orthologs: WBGene00016340 and

WBGene00016335) and WWOX (*C. elegans* orthologs: WBGene00010762 and WBGene00000972).

Two up regulated genes were found to be associated with Parkinson's disease – PLA2G6 (*C. elegans* ortholog: WBGene00009801) and GBA (*C. elegans* ortholog: WBGene00016340 and WBGene00016335), again suggesting that VPA may affect functions that contribute to neurodegenerative disease. However, from this analysis it is not possible to say whether the effect of these changes may be beneficial or detrimental.

4.3.14 Comparison of microarray data with results from other VPA studies

To identify conserved effects of VPA treatment, other microarrays studies exploring VPA treatment were found. Using the EBI ArrayExpress database, six VPA-treated microarray experiments were identified that could be readily analysed using R. Two neuronal-related microarrays were derived from the developing hippocampus and cortex of foetal mice brain samples (E14.5, Accession Number: E-GEOD-42904), and mouse neural differentiated embryonic stem cells (nESCs, Accession Number: E-GEOD-50217). Both of these samples are developmentally relevant. Table 4.33 shows a list of the microarrays used in this chapter.

Valproate Microarray	Model	Analysed or Extracted?
C. elegans	Adult	Analysed
Mouse Brain	Development	Analysed
Mouse Neural ESC	Development	Analysed
Rat Brain	Adult	Extracted from literature
Rat Cortical Neurons	Adult	Extracted from literature
Mouse NT2 neurospheres	Development	Extracted from literature

Table 4.33 – Summary of the microarray data compared in this analysis. Analysed refers to having and processing the raw data using the limma package in R. If raw data was not available, the processed and published data was downloaded and used.

DAVID was used to convert Affymetrix ID's into official gene symbols. Following this, all of the up and down regulated genes were converted into their respective *C. elegans* orthologs using Biomart, before comparing lists of significantly up and down regulated genes. For all of the analyses a cut-off value of a 2-fold change was used to determine significance.

When comparing DAVID profiles, all three analyses (mouse foetal brain, nESC and *C. elegans*) had an enrichment of genes in neuron development and biological processes associated with differentiation. When focusing on the nESC data, many neurological processes were enriched. As well as a variety of neuronal development related processes, such as axonogenesis (6 genes), synaptic transmission was also clearly enriched, with seven associated genes being up regulated. TGF-β and Wnt signaling are also enriched in the nESC microarray. Ten genes were found to be involved in Wnt receptor signaling, and three in TGF-β signaling. These pathways were also found in the original analysis of data from the *C. elegans* VPA dose response microarray data. GAD-1 and GAD-2 were both up regulated in response to VPA and are known to be important enzymes in GABA biosynthesis. Table 4.34 shows biological pathways that were enriched in this

analysis, while Table 4.35 shows the results of pathway enrichment analysis performed on this data.

Seven genes were shared between the nESC and worm datasets (Table 4.36). Ace-3 (WBGene00000037) was present in both datasets, which infers a possible conserved effect of VPA on cholinergic signaling. The mouse ortholog of Ace-3 is BCHE. Significantly, Ace-3 and BCHE are down regulated in *C. elegans* and mice nESC, respectively. Glr-1 (WBGene00001612) is a glutamate receptor – required for memory formation and response to light nose touch. However, this gene was down regulated in worms, but the mouse ortholog was up regulated in mouse. The human ortholog is GRIA3, which as mentioned previously has links to Alzheimer's disease and x-linked mental retardation. Fpn-1.2 (WBGene00019977) is again down regulated in both *C. elegans* and nESCs. The mouse ortholog of Fpn-1.2 is SLC40A1, and the human ortholog is Ferroportin (SLC40A1), which plays an important role in forebrain patterning, and the closure of neural tubules (Mao et al., 2010).

In the mouse E14.5 brain microarray data, 16 genes were linked to neuronal differentiation, and 11 in neuronal development (Table 4.37). Other enriched processes included the regulation of apoptosis, with 20 genes being significantly up or down regulated in response to VPA. VPA has been repeatedly reported to affect cellular proliferation and apoptosis, and has recently been used in cancer clinical trials.

Biological Processes	Mouse Gene Symbol(s)
Axonogenesis	foxd1 (-),hoxa2 (-),Ngfr (-),SEMA5A (-),LOC672215 (-),SLIT3 (-)
Forebrain Development	FEZF2 (+),lhx1 (+),Tal2 (+),EOMES (+),OTX1 (+),Otx2 (+),PGAP1 (+),Zic5 (+),
Midbrain Development	Tal2 (+),En2 (+),OTX1 (+),Otx2 (+),
Negative Regulation of Neuron Apoptosis	Agtr2 (-),dlx1 (-),TGFB3 (-),Erbb3 (-)
Neuron Differentiation	BARHL2 (+),dscam (+),FEZF2 (+),HELT (+),lhx1 (+),En2 (+),EOMES (+),OLIG1 (+),Otx2 (+),PAX7 (+),LOC100048863
Neuron Fate Commitment	OLIG1 (+),Otx2 (+),PAX7 (+),
Neuron Projection	foxd1 (-),hoxa2 (-),Lamb1-1 (-),Ngfr (-),SEMA5A (-),LOC672215 (-),SLIT3 (-)
Neurotransmitter biosynthetic process	Gad1 (+),GAD2 (+),
Regulation of nervous system development	dlx1 (-),hoxa2 (-),hoxd3 (-),Igf1 (-),nefm (-),Serpinf1 (-),LOC672215 (-),six1 (-),THY1 (-)
Regulation of neuron differentiation	hoxa2 (-),hoxd3 (-),nefm (-),LOC672215 (-),six1 (-),THY1 (-)
Regulation of synpatic transmission	Grm5 (+),GRM8 (+),Gm3888 (+),Dgi1 (+),
Synaptic transmission	CHRM3 (+),Gabrg2 (+),Gjd2 (+),GRM8 (+),Gad1 (+),GAD2 (+),SLC17A6 (+),
Transmission of nerve impulse	CHRM3 (+),Gabrg2 (+),Gjd2 (+),GRM8 (+),Gad1 (+),GAD2 (+),SLC17A6 (+),
Wnt Signaling	rspo2 (+),Rspo3 (+),LOC100048863 (+),wnt8b (+),DKK2 (-),DKK3 (-),FZD4 (-),FRZB (-),ROR2 (-),sfrp2 (-)

Table 4.34 – Biological process enrichment of genes following VPA treatment of mouse neural differentiated embryonic stem cells. Following microarray analysis of the raw data, significantly up and down regulated genes were inputted into DAVID for gene ontology and pathway analysis. Biological processes enriched in the data sets are listed, which are related to neurological function. (-) indicates that the gene was down regulated

Pathway	Mouse Gene Symbol(s)
Metabotropic glutamate receptor group III pathway	LOC100044431 (+),Grm5 (+),GRM8 (+),SLC17A6 (+),
Heterotrimeric G-protein signaling pathway-Gq alpha and Go alpha mediated pathway	RASGRP1 (+),CHRM3 (+),Grm5 (+),GRM8 (+),RGS2 (+),
Gamma-aminobutyric acid synthesis	Gad1 (+),GAD2 (+),
P00037:Ionotropic glutamate receptor pathway	CACNG3 (+),LOC100044431 (+),SLC17A6 (+),
TGF-Beta Signaling Pathway	BMP5 (-),DCN (-),Ltbp1 (-),TGFB3 (-)
Wnt Signaling Pathway	Cdh19 (-),cdh5 (-),FZD4 (-),FRZB (-),HOXA5 (-),HOXB4 (-),hoxb5 (-),HOXB7 (-),HOXC4 (-),HOXC5 (-),Hoxc6 (-),Myh3 (-),sfrp2 (-)

Table 4.35 – Pathway enrichment of genes following VPA treatment of mouse neural differentiated embryonic stem cells. Following microarray analysis of the raw data, significantly up and down regulated genes were inputted into DAVID for gene ontology and pathway analysis. Panther was used to analyse pathway enrichment. Pathways with more than one gene association are listed. (-) indicates that the gene was down regulated following VPA treatment. (+) indicates that the gene was up regulated following VPA treatment.

Wormbase Gene ID	Mouse Gene Symbol	Worm Regulation	Mouse Regulation
WBGene00003514	Myh-3	-	-
WBGene00000037	Bche	-	-
WBGene00001612	Gria3	-	+
WBGene00002975	Chrna5	-	-
WBGene00019977	SLC40A1	-	-
WBGene00011803	Trhde	+	+
WBGene00002260	Crabp2	+	-

Table 4.36 – Table showing the overlapping genes between the mouse neural differentiated embryonic stem cells and *C. elegans* microarray data sets. (+) indicates the gene was up regulated, and (-) indicates the gene was down regulated in response to VPA treatment.

Biological Processes	Mouse Gene Symbol(s)
Neuron Differentiation	EFHD1 (+),FARP2 (+),FEZF2 (-),RASGRF1 (+),LOC100047726 (-),SOX5 (-),TBR1 (-),CCKAR (-),DFNA5 (-),NEUROD4 (-),NEUROG1 (-),NRTN (+),
	ONECUT2 (+),OTX2 (+),RET (+),STAT3 (+)
Neuron Development	EFHD1 (+),FARP2 (+),FEZF2 (-),RASGRF1 (+),FOXG1 (-),TBR1 (-),CCKAR (-),NEUROD4 (-),NRTN (+),ONECUT2 (+),RET (+),
Neural Crest cell migration	NRTN (+),RET (+),ZEB2 (-),
Regulation of apoptosis	MTHFS (-),BBC3 (+),BMF (+),BAG3 (+),BIK,BID (+),GCH1 (+),IKBIP (+),AGTR1A (+),AVEN (-),CDKN1A (+),HSPA1B (+),MITF (+),MALT1 (+),NMNAT1 (-),
	NAIF1 (-),PMAIP1 (+),GM7084 (+),PRKCD (+),TCF7 (+)
Positive Regulation of Cell Death	BBC3 (+),BIK,BID (+),GCH1 (+),IKBIP (+),CDKN1A (+),NAIF1 (-),PMAIP1 (+),PLEKHF1 (+),PRKCD (+),
Regulation of MAPK activity	FGD4 (-),CAV1 (-),PXN (+),TRIB3 (+),ZEB2 (-),

Table 4.37 – Neuronal Biological Process Enrichment of genes from the mouse E14.5 hippocampus following VPA treatment. Following microarray analysis of the raw data, significantly up and down regulated genes were inputted into DAVID for gene ontology and pathway analysis. Biological processes enriched in the data sets are listed, which are related to neurological function. (-) indicates that the gene was down regulated following VPA treatment. (+) indicates that the gene was up regulated following VPA treatment.

When converted to worm orthologs, 32 genes were shared between the mouse brain and worm datasets (Table 4.38). Many worm orthologs map to only one mouse gene, and this is especially the case for GSTA4. 11 mouse genes were conserved between the two data sets, including fzd-5, whose *C. elegans* ortholog is cfz-2 (WBGene00000478). However, these display opposite changes in gene expression following VPA treatment. Nevertheless this highlights a possible VPA role in Wnt signaling.

There are eleven overlapping genes between the nESC and developing mouse brain (Table 4.39). Although the majority has opposite changes in expression in response to VPA, SALL1 and DEPDC1A were downregulated in both microarrays. OXT2 is also down regulated in both arrays and is linked to neuronal differentiation. FEZF2 is involved in neuron development and differentiation, and is up regulated in the nESC but downregulated in E14.5 arrays.

Two genes were found in each of the mouse brain, embryonic stem cell and worm data sets (Table 4.40). These were Chrna5 (Worm ortholog: WBGene00002975, lev-8) and Crabp2 (Worm ortholog: WBGene00002260, lbp-8). The lev-8 gene, which encodes an acetylcholine receptor subunit, is down regulated in *C. elegans* and nESCs, but is upregulated in the mouse embryonic brain. This could highlight differences in expression levels dependent on the stage of development. Lbp-8 was up regulated in *C. elegans* and downregulated in both mice microarrays, and is a fatty acid binding protein.

Wormbase Gene ID	Mouse Gene Symbol	Worm Regulation	Mouse E14.5 Regulation
WBGene00000478	Fzd5	-	+
WBGene00001753	Gsta4	+	+
WBGene00001754	Gsta4	+	+
WBGene00001755	Gsta4	+	+
WBGene00001756	Gsta4	+	+
WBGene00001757	Gsta4	+	+
WBGene00001760	Gsta4	+	+
WBGene00001761	Gsta4	+	+
WBGene00001762	Gsta4	+	+
WBGene00001768	Gsta4	+	+
WBGene00001770	Gsta4	+	+
WBGene00001772	Gsta4	+	+
WBGene00001778	Gsta4	+	+
WBGene00001786	Gsta4	+	+
WBGene00001787	Gsta4	+	+
WBGene00002051	Lmna	-	+
WBGene00002055	Lmna	-	+
WBGene00002260	Crabp2	+	+
WBGene00002975	Chrna5	-	+
WBGene00003957	Prss16	+	+
WBGene00003959	Prss16	+	+
WBGene00006431	Fgd6	-	+
WBGene00011076	Scarb1	+	+
WBGene00016134	Prss16	+	+
WBGene00017592	Prss16	-	+
WBGene00017594	Prss16	-	+
WBGene00019979	Slc2a3	+	+
WBGene00002057	Lmna	-	+
WBGene00008273	Mfsd9	+	+
WBGene00018984	Prss16	+	+
WBGene00019211	Ppp1r3b	-	+
WBGene00019682	Prss16	+	+

Table 4.38 – Table showing the overlap of genes between the mouse e14.5 hippocampus, and *C. elegans* VPA studies. Microarrays were analysed using R and the limma package, using identical algorithms and fold cut off values. + indicates up regulation, and – indicates down regulation of the gene following VPA treatment.

Mouse Gene Symbol	nESC Regulation	E14.5 Regulation
sall1	-	-
chrna5	-	+
crabp2	-	+
tmem26	-	+
LRIG3	-	+
depdc1a	-	-
KDELR3	-	+
Tcfl5	-	+
FEZF2	+	-
Otx2	+	+
ST6GAL2	+	-

Table 4.39 – Overlap of differentially expressed genes between the mouse nESC and e14.5 hippocampal VPA microarrays. Microarrays were analysed using R and the limma package, using identical algorithms and fold cut off values. + indicates up regulation, and – indicates down regulation following VPA treatment.

Wormbase ID	Mouse Gene Symbol	Worm Regulation	Mouse Neural ESC Regulation	Mouse e14.5 brain Regulation
WBGene00002260	Crabp2	+	-	+
WBGene00002975	Chrna5	-	-	+

Table 4.40 – Overlap of differentially expressed genes between the mouse nESC, mouse E14.5 hippocampal, and *C. elegans* VPA microarrays. Microarrays were analysed using R and the limma package, using identical algorithms and fold cut off values. + indicates up regulation, and – indicates down regulation of the gene following VPA treat

Wormbase Gene ID	Human Gene Symbol	Human Regulation	Worm Regulation
WBGene00008621	Plb1	+	+
WBGene00000067	ACTRT2	-	+

Table 4.41 – Overlap of differentially expressed genes between the *C. elegans* and human NT2 neurospheres VPA microarrays. The processed microarray data from the human NT2 neurospheres was extracted from the literature and analysed. The *C. elegans* VPA microarray data was analysed using R and the limma package. + indicates up regulation, and – indicates down regulation, following VPA treatment.

Biological Process	Human Gene Symbol(s)
GO:0042981~regulation of apoptosis	B4GALT1 (+), PTPN6 (+), IFIH1 (+), BCL2L14 (+), MMP9 (+), RAG1 (+), CDH1 (+), DDIT3 (+), PLEKHF1 (+), BNIPL (+), NOTCH1 (-), ATG5 (+),
	NUPR1 (+), AGT (+), HMOX1 (+), FOXC1 (+), PRNP (+), IGFBP3 (+), SPP1 (+)
GO:0043065~positive regulation of apoptosis	PLEKHF1 (+), B4GALT1 (+), PTPN6 (+), BNIPL (+), NOTCH1 (-), NUPR1 (+), MMP9 (+), HMOX1 (+), IGFBP3 (+), DDIT3 (+)
GO:0043405~regulation of MAP kinase activity	PTPN6 (+), SPAG9 (-), CEACAM2 (+), AVPI1 (+), PXN (-), CEACAM1 (+), PTPN11 (+)
GO:0033209~tumor necrosis factor-mediated signaling pathway	KRT18 (+), KRT8 (+)
GO:0043066~negative regulation of apoptosis	NOTCH1 (-), ATG5 (+), AGT (+), RAG1 (+), FOXC1 (+), PRNP (+), SPP1 (+)
GO:0048568~embryonic organ development	GSC (+), HAND1 (+), ADM (+), KRT8 (+), GM5604, PBX1 (-), DDIT3 (+), PITX2 (+)
GO:0001701~in utero embryonic development	MAN2A1 (+), NOTCH1 (-), HAND1 (+), ADM (+), POU5F1 (+), KRT8 (+), APBA2 (-), FOXC1 (+), CDH1 (+), PITX2 (+)

Table 4.42 – Biological Process enrichment of differentially expressed genes from human NT2 neurospheres following VPA treatment. Lists of significantly up and down regulated genes were extracted from literature, and inputted into DAVID for gene ontology and pathway analysis. Biological processes that were enriched in this data set are listed. (+) indicates up regulation, and (–) indicates down regulation, following VPA treatment.

4.3.15 Comparison of *C. elegans* microarray with published data

Mining the literature for published VPA microarray studies, one study was found that also was developmentally relevant utilizing human NT2 neurospheres (Hill et al., 2013), a model of neuron development. It is important to note that different methods of analysis were used to extract datasets. For the neurosphere dataset, the same two-fold cut off was used as in our analysis. However, a significance level of 0.01 was used.

When comparing VPA microarrays of human NT2 neurospheres to *C. elegans,* only two common overlapping genes (Table 4.41), PLB1 (*C. elegans* ortholog: WBGene00008621) and ACTRT2 (*C. elegans* ortholog: WBGene00000067) were observed. NT2 neurospheres provide a model of neuronal differentiation. Interestingly when this gene list is entered into DAVID, there is no biological enrichment in genes controlling neuron development and differentiation, yet apoptosis remains a key biological process, along with other embryonic development processes. No neuronal-specific KEGG pathways are highlighted from this analysis. Many genes are altered that affect the response to wounding and apoptosis. Table 4.42 shows the biological processes enriched in this data set.

There are no other published VPA studies in *C. elegans*, and the only neural-related datasets were in developmental neuronal models/samples. As VPA most likely has multiple effects that are different between development and adulthood, we then looked at published microarray data, where the raw data was not available. These were from rat brain (Bosetti, Bell, & Manickam, 2005) and rat cortical neurons

(Fukuchi et al., 2009). In the rat brain study, a fold change cut-off of 1.4 was used, and the significance level was 0.05. In the rat cortical neuron study the same p value was used, but the fold change cut off was 2 as in our analyses.

The first microarray data extracted were from rat brain samples following chronic exposure to VPA. The analysed gene lists were imported in DAVID, and again neuron development and differentiation were enriched. As well as this, five genes were linked to synaptic transmission. When analysing disease relations, genes are clustered in three neurodegenerative diseases; Amyotrophic lateral sclerosis (ALS), Huntington's disease, and Alzheimer's disease. Table 4.43 shows the enriched biological processes and Table 4.44 shows the KEGG pathways of interest for the rat brain study.

There are three overlapping genes between the adult rat brain and *C. elegans* (Table 4.45) – these are ckb-2 (WBGene00000512), fat-5 (WBGene00001397) and fat-6 (WBGene00001398). Fat-5 and Fat-6's rat orthologs are both scd, and ckb-2 is Chka. Both of these are regulated in the same way from C. elegans to rats, with chka/ckb-2 being up regulated, and fat-5/fat-6/scd being down regulated in response to VPA. It must be noted, however, that the gene list published for this analysis only contained 81 genes. Scd is an acyl-CoA desaturase, which plays an important role in the synthesis of lipids. Chka is a choline kinase, which is required for the synthesis of phospholipids. This adds evidence to there being a link between VPA treatment and lipid metabolism.

Biological Process	Rat Gene Symbol(s)
GO:0050804~regulation of synaptic transmission	ARC (+), GRM3 (-), LOC689121 (-), GNAI2 (+), MAP1B (-), DLG4 (-), HTR2C (-)
GO:0051969~regulation of transmission of nerve impulse	ARC (+), GRM3 (-), LOC689121 (-), GNAI2 (+), MAP1B (-), DLG4 (-), HTR2C (-)
GO:0031644~regulation of neurological system process	ARC (+), GRM3 (-), LOC689121 (-), GNAI2 (+), MAP1B (-), DLG4 (-), HTR2C (-)
GO:0007611~learning or memory	CASP3 (+), PDE1B (-), LOC363956 (-), TMOD2 (-), APBB1 (-), RGD1566161 (-), VDAC1 (-)
GO:0006915~apoptosis	CASP3 (+), LOC363956 (-), PPP3R1 (-), BCL2L11 (-), PAWR (+), LOC684140 (-), APBB1 (-), LOC293190 (-), ACVR1C (-), RGD1566161 (-), VDAC1 (-)
GO:0012501~programmed cell death	CASP3 (+), LOC363956 (-), PPP3R1 (-), BCL2L11 (-), PAWR (+), LOC684140 (-), APBB1 (-), LOC293190 (-), ACVR1C (-), RGD1566161 (-), VDAC1 (-)
GO:0019226~transmission of nerve impulse	GAD2 (-), LOC363956 (-), SCD (-), SYT2 (-), TMOD2 (-), DLG2 (-), RGD1566161 (-), VDAC1 (-)
GO:0045161~neuronal ion channel clustering	DLG4 (-), DLG2 (-)
GO:0008219~cell death	CASP3 (+), LOC363956 (-), PPP3R1 (-), BCL2L11 (-), PAWR (+), LOC684140 (-), APBB1 (-), LOC293190 (-), ACVR1C (-), RGD1566161 (-), VDAC1 (-)
GO:0007268~synaptic transmission	GAD2 (-), LOC363956 (-), SYT2 (-), TMOD2 (-), DLG2 (-), RGD1566161 (-), VDAC1 (-)
GO:0042981~regulation of apoptosis	CASP3 (+), CREB1 (-), PPP3R1 (-), NR4A1 (+), HSPA1A (+), BCL2L11 (-), HSPA1B (+), LOC684140 (-), APBB1 (-), LOC293190 (-), ACVR1C (-), AKT2 (-)
GO:0030182~neuron differentiation	CASP3 (+), NRP1 (-), CREB1 (-), MAP1B (-), DLG4 (-), APBB1 (-), DLG2 (-)
GO:0048666~neuron development	NRP1 (-), CREB1 (-), MAP1B (-), DLG4 (-), APBB1 (-), DLG2 (-)
GO:0007612~learning	PDE1B (-), LOC363956 (-), APBB1 (-), RGD1566161 (-), VDAC1 (-)
GO:0048167~regulation of synaptic plasticity	ARC (+), MAP1B (-), DLG4 (-)

Table 4.43 – Biological pathways enriched in differentially expressed genes from rat brain samples following VPA treatment. Lists of significantly upregulated and downregulated genes were extracted from literature, and inputted into DAVID for gene ontology and pathway analysis. Biological processes that were

KEGG Pathway	Rat Gene Symbol(s)
rno04210:Apoptosis	CASP3 (+), PPP3R1 (-), BCL2L11 (-), PRKACB (-), LOC684140 (-), LOC293190 (-), AKT2 (-)
rno04010:MAPK signaling pathway	CASP3 (+), MAPK14 (+), PPP3R1 (-), NR4A1 (+), HSPA1A (+), PRKACB (-), HSPA1B (+), ACVR1C (-), AKT2 (-)
rno05014:Amyotrophic lateral sclerosis (ALS)	CASP3 (+), MAPK14 (+), PPP3R1 (-), BCL2L11 (-), LOC684140 (-), LOC293190 (-)
rno05016:Huntington's disease	CASP3 (+), LOC363956 (-), CREB1 (-), DLG4 (-), ITPR1 (-), RGD1566161 (-), VDAC1 (-)
rno05010:Alzheimer's disease	CASP3 (+), PPP3R1 (-), CALM3 (-), APBB1 (-), CALM2 (-), CALM-PS2 (-), ITPR1 (-), CALM1 (-)
rno04722:Neurotrophin signaling pathway	MAPK14 (+), CALM3 (-), CAMK2B (-), CALM2 (-), CALM-PS2 (-), CALM1 (-), AKT2 (-)

Table 4.44 – Pathways enriched in differentially expressed gene lists from rat brain samples following VPA treatment. Lists of significantly upregulated and downregulated genes were extracted from literature, and inputted into DAVID for gene ontology and pathway analysis. KEGG was used for pathway analysis, and pathways are listed if they had more than one gene associated with them. (+) indicates upregulation and (-) indicates downregulation following treatment.

Wormbase Gene ID	Rat Gene Symbol	Worm Regulation	Rat Regulation
WBGene00000512	Chka	+	+
WBGene00001397	Scd	-	-
WBGene00001398	Scd	-	-

Table 4.45 – Overlapping differentially expressed genes between the *C. elegans* and rat brain VPA microarrays. Data was extracted from literature for the rat brain VPA microarray data, as the raw form was not available. The *C. elegans* VPA microarray data was analysed using R and the *limma* package. + indicates upregulation and – indicates downregulation following treatment.

From the rat cortical neurons, interesting trends in biological process enrichment were observed (Table 4.46). Like in the other data sets, there is enrichment in genes associated with neuron development and differentiation, with 23 and 20 down regulated genes, respectively. Other examples of neuronal-specific processes clustered were neuropeptide signaling, axon guidance and synaptic vesicle transport. In the up regulated genes, there were also other neuron-specific biological processes enriched. Seventeen upregulated genes appear to be involved in neuron projection development. For example, there were six genes involved in the regulation of action potentials in neurons, and ten in the development of neuron projection. Throughout the data sets, there is conserved apoptosis enrichment. When looking at pathway enrichment, both Wnt and MAPK signaling are up regulated, and neurotrophin signaling is down regulated. Neurotrophins are essential for neuron development. Table 4.47 shows a list of relevant pathways identified by KEGG analysis.

Interestingly, 13 genes are conserved between the rat brain and rat cortical neuron samples. These include KCNC2, which is downregulated in both data sets, and is a voltage-gated potassium channel responsible for potassium transport in the brain. Csksr2 is an adapter protein involved in Ras signaling at synaptic

junctions and is also downregulated in response to VPA treatment in both data sets. Notably, Gabbr1 is down regulated in both, and is a component of the G-protein coupled receptor for GABA. This may provide a link between VPA and GABA neurotransmission. All shared genes are shown in Table 4.48. However, no genes are shared between all three of the rat brain, rat cortical neuron and *C. elegans* data sets.

When converted to worm orthologs, fourteen downregulated rat genes (seventeen worm genes) and eleven upregulated rat (32 worm genes) are shared between the rat cortical neurons and *C. elegans* (Table 4.49). Of interest were NRCAM, which is downregulated in both data sets, and is associated with nervous system development and synaptic transmission. HEXB is found in both data sets. However, this gene is upregulated in rat cortical neurons, and downregulated (hex-1, WBGene00020509) in the worm datasets. For many of these genes, there were also several worm orthologs found in our worm microarray data. Of note, similarly to the mouse brain, Gsta4 is conserved between species.

These results suggest a conservation of the effects of VPA on neuron development and differentiation, in both the developing and adult brain. Other pathways, such as WNT, TGF-β, MAPK, and apoptosis are also affected. VPA may also be affecting both cholinergic and GABA signaling.

Biological Process	Gene Symbol(s)
GO:0006916~anti-apoptosis	BDNF (+), CDC2 (+), PRKCI (+), DAD1 (+), ADAM17 (+), FOXO1 (+), HSPA1A (+), FAIM (+), GLO1 (+), HSPA1B (+), HBXIP (+), API5 (+)
GO:0006917~induction of apoptosis	LOC681486 (+), APH1B (+), STK17B (+), SMAD3 (+), STAT1 (+), PTEN (+), GCH1 (+), STAT4 (+), CDKN1B (+), DDX19A (+), CDKN2C (+), PSEN2 (+), DIABLO (+), APAF1 (+), CABC1 (+)
GO:0007218~neuropeptide signaling pathway	LPHN2 (-), PNOC (-), NPY (-), SSTR1 (-), GPR56 (-), ADCYAP1 (-)
GO:0007268~synaptic transmission	CPLX1 (-), NTF3 (-), SYT4 (-), PNOC (-), NPY (-), SPTBN2 (-), TMOD2 (-), ADNP (-), GRIK5 (-), APBA2 (-), CD24 (-), CACNA1C (-), GAD1 (-)
GO:0007409~axonogenesis	NRCAM (-), CDK5R1 (-), PTPRM (-), NRP1 (-), NTF3 (-), ANK3 (-), CXCR4 (-), RTN4R (-), ROBO2 (-), VCAN (-), DCLK1 (-)
GO:0007411~axon guidance	NRCAM (-), CDK5R1 (-), PTPRM (-), NRP1 (-), NTF3 (-), ANK3 (-), CXCR4 (-), ROBO2 (-)
GO:0007412~axon target recognition	BDNF (+), STXBP1 (+)
GO:0008038~neuron recognition	CDK5R1 (-), NRP1 (-), CXCR4 (-)
GO:0008366~axon ensheathment	TPO1 (+), CD9 (+), PPARD (+), EGR2 (+), HEXB (+), PLLP (+)
GO:0007272~ensheathment of neurons	TPO1 (+), CD9 (+), PPARD (+), EGR2 (+), HEXB (+), PLLP (+)
GO:0019228~regulation of action potential in neuron	TPO1 (+), CD9 (+), PPARD (+), EGR2 (+), HEXB (+), PLLP (+)
GO:0030182~neuron differentiation	CDK5R1 (-), PTPRM (-), NRP1 (-), GNAO1 (-), NTF3 (-), RTN4R (-), DPYSL4 (-), BRSK1 (-), KCNIP2 (-), GAS7 (-), ITGB1 (-), KCHIP2 (-), NRCAM (-), LINGO1 (-), ANK3 (-), CXCR4 (-), VEGFA (-), ROBO2 (-), VCAN (-), CD24 (-), DCLK1 (-), DSCAM (-)
GO:0031175~neuron projection development	ALS2 (+), FGFR1 (+), NRTN (+), EGR2 (+), MAP2K1 (+), FGFR1L (+), PAX6 (+), STXBP1 (+), LOC692021 (+), CTNNA1 (+), PTEN (+), ALCAM (+), SEMA5A (+), BDNF (+), NUMB (+), LOC290415 (+), PHGDH (+), CNTN4 (+)
GO:0031175~neuron projection development	CDK5R1 (-), PTPRM (-), NRP1 (-), GNAO1 (-), NTF3 (-), RTN4R (-), GAS7 (-), ITGB1 (-), NRCAM (-), LINGO1 (-), CXCR4 (-), ANK3 (-), ROBO2 (-), VCAN (-), CD24 (-), DCLK1 (-), DSCAM (-)
GO:0042981~regulation of apoptosis	IRAK1 (-), CDK5R1 (-), NTF3 (-), NELL1 (-), ARNT2 (-), ADNP (-), NFKBIA (-), NHA (-), PEA15A (-), LOC684638 (-), SRC (-), MAGED1 (-), AKT1 (-), ATF5 (-), PCGF2 (-), AKT1S1 (-), ANK3 (-), BOK (-), LCK (-), VEGFA (-), NEUROD1 (-), CD24 (-), NSMAF (-), MYC (-), IP6K2 (-)
GO:0043524~negative regulation of neuron apoptosis	BDNF (+), HDAC1 (+), WFS1 (+), MSH2 (+), LOC364295 (+), HDAC1L (+), LIG4 (+), GCLM (+), LOC360472 (+)
GO:0045664~regulation of neuron differentiation	NRP1 (-), RGS6 (-), RTN4R (-), ADNP (-), NEUROD1 (-), ROBO2 (-), CDH2 (-), CD24 (-), MT3 (-)
GO:0048489~synaptic vesicle transport	CPLX1 (-), SPTBN2 (-), APBA2 (-), CD24 (-)
GO:0048666~neuron development	CDK5R1 (-), PTPRM (-), NRP1 (-), GNAO1 (-), NTF3 (-), RTN4R (-), DPYSL4 (-), KCNIP2 (-), GAS7 (-), ITGB1 (-), KCHIP2 (-), NRCAM (-), LINGO1 (-), ANK3 (-), CXCR4 (-), VEGFA (-), ROBO2 (-), VCAN (-), CD24 (-), DCLK1 (-), DSCAM (-)
GO:0048812~neuron projection morphogenesis	CDK5R1 (-), NRP1 (-), PTPRM (-), NTF3 (-), RTN4R (-), GAS7 (-), ITGB1 (-), NRCAM (-), CXCR4 (-), ANK3 (-), ROBO2 (-), VCAN (-), DCLK1 (-), DSCAM (-)
GO:0050767~regulation of neurogenesis	ATF5 (-), LINGO1 (-), NRP1 (-), NTF3 (-), RGS6 (-), RTN4R (-), ADNP (-), NEUROD1 (-), ROBO2 (-), CDH2 (-), CD24 (-), MT3 (-)
GO:0050768~negative regulation of neurogenesis	ATF5 (-), LINGO1 (-), NRP1 (-), RTN4R (-), CD24 (-), MT3 (-)
GO:0051960~regulation of nervous system development	ATF5 (-), LINGO1 (-), NRP1 (-), NTF3 (-), RGS6 (-), RTN4R (-), ADNP (-), NEUROD1 (-), ROBO2 (-), CDH2 (-), CD24 (-), MT3 (-)

Table 4.46 - Biological pathways enriched in differentially expressed genes from rat cortical neuron samples following VPA treatment. Lists of significantly upregulated and downregulated genes were extracted from literature, and inputted into DAVID for gene ontology and pathway analysis. Neurologically relevant biological processes with more than one gene association are listed. (+) indicates upregulation, and (-) indicates downregulation following VPA treatment.

KEGG Pathways		
rno04010:MAPK signaling pathway	rno04310:Wnt signaling pathway	rno04722:Neurotrophin signaling pathway
FGFR1 (+)	SENP2 (+)	AKT1(-)
MAP2K1 (+)	LOC295194 (+)	MAGED1(-)
LOC499736 (+)	PPARD (+)	IRAK1(-)
FGFR1L (+)	PPP2R5A (+)	NTF3(-)
HSPA1A (+)	CCND2 (+)	PIK3CD(-)
PPM1B (+)	JUN (+)	NFKBIA(-)
HSPA1B (+)	CAMK2D (+)	CAMK2B(-)
DDIT3 (+)	SMAD3 (+)	ARHGDIB(-)
STK3 (+)	RGD1565588 (+)	
RGD1564956 (+)	FZD2 (+)	
LOC681749 (+)	CHP (+)	
MAPK1 (+)	AXIN2 (+)	
RPS6KA6 (+)	RGD1564956 (+)	
BDNF (+)		
ARRB2 (+)		
RPS6KA1 (+)		
DUSP14 (+)		
JUN (+)		
RGD1565588 (+)		
LOC365977 (+)		
CHP (+)		
GADD45B (+)		
MAP2K6 (+)		

Table 4.47 – Pathways enriched in differentially expressed gene lists from rat cortical neuron samples following VPA treatment. Lists of significantly upregulated and downregulated genes were extracted from literature, and inputted into DAVID for gene ontology and pathway analysis. KEGG was used for pathway analysis, and pathways are listed if they had more than one gene associated with them. (+) Indicates upregulation and (-) indicates down regulation following

Gene Symbol	Cortical Regulation	Brain Regulation
Kcnc2	-	-
Bbx	+	+
Mcm6	+	+
Cnksr2	-	-
Camk2b	-	-
Dpp6	-	-
Grm3	-	-
Zeb1	+	-
Tmod2	-	-
Gabbr1	-	-
Srd5a1	+	+
Hspa1a	+	+
Lta4h	+	+

Table 4.48 – Overlapping differentially expressed genes between the rat cortical neuron and brain samples following VPA treatment. Data was extracted from literature for the rat brain and rat cortical neuron VPA microarray data, as the raw form was not available. + indicates upregulation, and – indicates downregulation following treatment.

Wormbase Gene ID	Rat Symbol	Rat Regulation	Worm Regulation
WBGene00000768	Coro1a	-	-
WBGene00002260	Fabp7	-	+
WBGene00002243	Nrcam	-	-
WBGene00019322	Ahcy	-	+
WBGene00017471	Cfp	-	+
WBGene00011880	Cfp	-	-
WBGene00021487	Comtd1	-	+
WBGene00012518	Comtd1	-	+
WBGene00015479	Abcg4	-	+
WBGene00001149	Bcat1	-	+
WBGene00008479	B3gat1	-	-
WBGene00008160	B3gat1	-	-
WBGene00004275	Rab11b	-	+
WBGene00001577	Cpne5	-	+
WBGene00000067	Acta1	-	+
WBGene00008681	Plscr3	-	+
WBGene00017312	Slc20a1	-	+
WBGene00008479	B3gat2	+	-
WBGene00008160	B3gat2	+	-
WBGene00016507	Abhd4	+	+
WBGene00016506	Abhd4	+	+
WBGene00001077	P4ha1	+	+
WBGene00005649	Serpini1	+	+
WBGene00001824	Rest	+	-
WBGene00021503	Ctsa	+	+
WBGene00008741	Ctsa	+	+
WBGene00019605	Ctsa	+	+
WBGene00019617	Ctsa	+	+
WBGene00017969	Ctsa	+	+
WBGene00020509	Hexb	+	-
WBGene00016435	Nxn	+	+
WBGene00021796	Nxn	+	+
WBGene00008273	Mfsd9	+	+
WBGene00012467	Txnip	+	+
WBGene00012464	Txnip	+	+
WBGene00001757	Gsta4	+	+
WBGene00001772	Gsta4	+	+
WBGene00001761	Gsta4	+	+
WBGene00001754	Gsta4	+	+
WBGene00001753	Gsta4	+	+
WBGene00001762	Gsta4	+	+
WBGene00001778	Gsta4	+	+
WBGene00001770	Gsta4	+	+
WBGene00001756	Gsta4	+	+
WBGene00001787	Gsta4	+	+
WBGene00001786	Gsta4	+	+
WBGene00001768	Gsta4	+	+
WBGene00001755	Gsta4	+	+
WBGene00001760	Gsta4	+	+

Table 4.49 – Overlapping differentially expressed genes between the *C. elegans* and rat cortical neuron VPA microarrays. Data was extracted from literature for the rat cortical neuron VPA microarray data, as the raw form was not available. The *C. elegans* VPA microarray data was analysed using R and the *limma* package. + indicates upregulation and – indicates downregulation following treatment.

4.4 Discussion

4.4.1 Using *C. elegans* as a model system to screen for novel regulators of synaptic function

In this chapter, data from a previous global microarray gene expression study (Munasinghe, 2015) was reanalyzed, in which differential gene expression profiles were analysed following exposure of *C. elegans* N2 worms to increasing doses (3mM-24mM) of VPA. Unlike the initial analysis, where trends in gene expression profiles were correlated with increasing VPA dose, the full profile of all genes whose expression was significantly altered by exposure to VPA was investigated in this chapter. However, it may be significant to note that Wnt, MAPK and TGF-β pathways were enriched in both rounds of analysis.

From these screens sixteen candidates were found to cause a significant RIC or HIC phenotype. One of these, itsn-1, had previously been observed to cause a HIC phenotype (Rose et al., 2007), although this study was not tested in the *Tu3311* or *Tu3335* strains. They also reported a HIC phenotype in itsn-1 deletion mutants. Itsn-1 encodes intersectin, which has been shown to interact with proteins in both endo- and exocytic pathways, and has been reported to have an inhibitory effect of neurotransmission (Rose et al., 2007). In our studies this theory may still be valid, as inhibition of cholinergic signaling would confer a RIC phenotype. However, further investigation would be required to determine why wild-type worm knockdown or mutation of itsn-1 leads to hypersensitivity, whereas knocking down of the same gene in a neurosensitive strain leads to the opposite

phenotype. This result could possibly be due to a greater proportion of dsRNA reaching the neurons, and less entering the muscle.

Sel-12 is another interesting hit from the screens performed in this study. The human ortholog of Sel-12 is presenilin 2 (PSEN2). Both proteins are multi-pass trans-membrane proteins, however the role of presenilins in neurotransmission is not yet characterized. There is some evidence to suggest that PSEN2 may be a catalytic subunit of the γ-secretase complex, which cleaves proteins such as Notch receptors and APP (Lee et al., 2002). Mutations in PSEN2 have been shown to increase the cleavage of APP into the toxic Aβ42 molecule (in comparison to Aβ40, (Can Zhang, Browne, Kim, & Tanzi, 2010)), which form part of Alzheimer's disease related plaques. Presenilins have also been found to be essential for the regulation of neurotransmitter release (C Zhang et al., 2009). In our study, knockdown of sel-12 in a neurosensitive worm strain conferred a RIC phenotype, suggesting that knocking down presenilin could be effecting either excitatory (cholinergic) or inhibitory (GABA) signaling. If conserved in human neurons this phenotype could clearly have pathological consequences.

Dhhc-2 is a member of the palmitoyl-acyl transferase family of proteins. The human ortholog of *dhhc-2* is zDHHC9, which encodes the DHHC9 enzyme. DHHC9 is known to palmitoylate N-Ras and H-Ras (Swarthout et al., 2005b), and four mutations (one frame-shift, two missense, and one splice-site mutation) have been found in this gene to cause X-linked mental retardation (Mitchell et al., 2014). Palmitoylation of Ras is essential for its trafficking between the Golgi apparatus and the plasma membrane, and so clearly regulation of this process may well have

implications for cancer biology. However, protein palmitoylation has also been heavily implicated in neuronal plasticity and development (Fukata & Fukata, 2010). Given that data from each of the microarray studies showed a conserved role of VPA in neuronal development and differentiation, this makes dhhc-2 and the regulation of protein palmitoylation a very interesting area of further study into novel regulators of synaptic function or modulation.

4.4.2 VPA induced changes in neuronal genes

From the comparison of microarray datasets, some clear effects of VPA exposure can be established. VPA is known to be a teratogen as the chance of a foetus having neural tube defects is increased upon taking VPA during pregnancy (Alsdorf & Wyszynski, 2005). The data analysed in this study suggest that observed changes in expression of HSPG2, CELSR1 and MAPK8 might contribute to neural tube defects. Each of these genes was down regulated in response to VPA treatment. HSPG2 encodes the heparin sulphate proteoglycan perlecan, which has previously been associated with neural tube defects in mice (Allache, De Marco, Merello, Capra, & Kibar, 2012). Perlecan (also known as HSPG2) is essential for both cartilage and cephalic development. CELSR1 is a key member of the planar cell polarity (PCP) pathway, and mutations in CELSR1 have been shown to cause neural tube defects (Boutin, Goffinet, & Tissir, 2012). MAPK8 also known as JNK1, is a key component of the MAP kinase-signaling pathway, which is a conserved pathway, affected by VPA treatment. In mice, when JNK1 and JNK2 are both knocked out, neural tube defects are observed due to dysregulation of apoptosis in the brain (Kuan et al., 1999; Sabapathy et al., 1999).

Neuronal development and differentiation pathways were enriched in all studies , with the exception of the neurosphere study. Children born to mothers taking VPA during pregnancy have been reported to have an increase incidence of developing autism spectrum disorders. (Christensen et al., 2013). Interestingly, trends identified in this analysis may provide clues as to why this may occur. The human ortholog of the C. *elegans* gene lad-2 (WBGene00002243) is NRCAM, which plays a role in the outgrowth of neurites and the formation of nodes of Ranvier on myelinated neurons (Hortsch et al., 1996). NRCAM is a strong candidate for autism, from both association studies and studies in NRCAM-null mice (Marui et al., 2009; Moy, Nonneman, Young, Demyanenko, & Maness, 2009). Lad-2/NRCAM was down regulated in *C. elegans* and rat cortical neurons following exposure to VPA.

As well as being used to treat epilepsy, VPA has also been used in Alzheimer's disease trials (X. Z. Zhang, Li, & Zhang, 2010). In this study, multiple genes exhibiting VPA-induced changes in gene expression had human orthologs that have been linked to Alzheimer's disease. These include *C. elegans* orthologs of human HSPG2, AGRN, CYP3A4, LIPA and MAPK8 genes, all of which were down regulated following exposure to VPA. HSPG2 is found on chromosome 1p36, a region implicated in late-onset Alzheimer's disease. It, and other proteoglycans are linked to Alzheimer's due to their contribution to the increasing build-up of amyloid and tau plaques (Van Horssen, Wesseling, Van Den Heuvel, De Waal, & Verbeek, 2003). The role of HSPG2 is however controversial, with some studies showing no association to Alzheimer's disease. One study performed on a Finnish

population found associations in people who carried the apolipoprotein epsilon 4 (APOe4) allele, which is itself associated with a higher risk of Alzheimer's disease (Iivonen et al., 2003). For these reasons, the mechanisms of action of HSPG2 in this context remain unclear.

AGRN encodes Agrin, which is another heparin sulphate proteoglycan, and is an important constituent of the blood brain barrier. In mouse models of Alzheimer's disease, AGRN deletion in endothelial cells led to increased A_{β} levels in the brain, although deletion from neurons did not have this effect (Rauch et al., 2011). These results suggest that VPA may decrease heparin sulphate expression, which may have pathophysiological effects. LIPA is also located on human chromosome 10, with known associations to late onset Alzheimer's disease. LIPA protein is also known to be involved in cholesterol metabolism (von Trotha et al., 2006). More study is needed to understand whether down regulation of these genes is found in humans, and whether it is beneficial or detrimental to AD patients.

Four of the genes that were up regulated in response to VPA were previously linked to epilepsy. Of these, WWOX shows the clearest link, with a study showing that whole exon deletion of WWOX leads to both epilepsy and intellectual disability (Ben-Salem, Al-Shamsi, John, Ali, & Al-Gazali, 2015).

The *C. elegans* ortholog of the human KCNMA1 gene (slo-1) was down regulated in response to VPA. KCNMA1 is a calcium activated potassium channel subunit, and gain of function mutations in KCNMA1 have been linked to generalized

epilepsy and paroxysmal dyskinesia (Du et al., 2005). Therefore, this gene may be a target of VPA that is beneficial to epileptic patients.

PRSS16 is a schizophrenia-associated gene conserved between worms and the dataset from the developing mouse brain (at developmental stage e14.5). PRSS16 is up regulated in the e14.5 brain. Five *C. elegans* genes were significantly up regulated, whose closest human ortholog was PRSS16. These were pcp-2 (WBGene00003957), pcp-4 (WBGene00003959), C26B9.5 (WBGene00016134), F56F10.1 (WBGene00018984) and K12H4.7 (WBGene00019682). In a GWAS study in 2012, they found a ZNF804a single nucleotide polymorphism associated with schizophrenia and bipolar disorder, and showed that expression of this protein increased levels of PRSS16 (Girgenti, LoTurco, & Maher, 2012). VPA has been used in combination with antipsychotic medications, and studies have found that this combination of drugs resulted in an overall improvement in psychopathology, compared to using only the antipsychotic drug (Tseng et al., 2016). How increased PRSS16 leads to schizophrenia has not yet been explained, however, changes in the expression of the PRSS16 gene may explain some of the therapeutic benefits of VPA.

4.4.3 Conservation of signaling pathways following VPA treatment

Firstly, changes in the expression of genes involved in cholinergic signaling, such as ace-3/BCHE and lev-8/chrna5 were conserved between *C. elegans* and mice nESC, indicating that VPA causes changes to cholinergic signaling. Lev-8/chrna5 was shared between the mouse nESC, e14.5 brain and worm data sets, which is

the alpha subunit of an N-acetylcholine receptor. When the *C. elegans* microarray studies were initially carried out, the Falciani lab found that another ACh receptor subunit (acr-17) was also down regulated (Munasinghe, 2015). As ace-3/BCHE is down regulated in response to VPA, this suggests that decreased amounts of acetylcholine would be degraded at the synapse. However, whether this leads to increased excitatory neurotransmission remains to be elucidated. In the mouse nESC microarray data, genes involved in GABA synthesis and GABA receptor pathways were up regulated in response to VPA. However, this change was not observed in *C. elegans*.

Another conserved pathway altered in response to VPA treatment was Wnt signaling. Significantly, the Wnt signaling pathway was enriched in mouse nESC, rat cortical neurons and *C. elegans* microarrays. VPA treatment in rats has been suggested to promote Wnt signaling. Due to demethylation of wnt1 and wnt2 promoter regions, expression levels of wnt1 and wnt2 were reported to increase (Wang et al., 2010). Cwn-2 is a *C. elegans* Wnt ligand, and cfz-2 is a frizzled receptor, both of which were down regulated in response to VPA. Also, as VPA is a histone deacetylase inhibitor, it would be interesting to see if this deacetylase activity is conserved in worms, and whether it is of pathological relevance in humans.

VPA may also be affecting the MAP kinase signaling and TGF-β pathways as these pathways were found to be enriched for differentially expressed genes/proteins in several microarray dataset. There could even be cross talk between the MAP kinase, TGF-β and Wnt signaling pathways. In human hepatocytes, VPA has been

shown to promote the ERK signaling cascade, which again may be due to its HDAC activity. It would therefore be interesting to carry out a similar microarray analysis using a derivative of VPA, valpromide, which is identical to VPA but has no HDAC inhibitory activity (Fujiki, Sato, Fujitani, & Yamashita, 2013).

Apoptosis was enriched in all arrays analysed in this study and in data extracted from literature. Multiple studies have reported pro – and anti-apoptotic effects of VPA. For example, in human neuroblastoma cell lines, VPA treatment has been shown to enhance staurosporine-induced cell death by down-regulating surviving (Shah et al., 2013). However, there is conflicting data as to the role of KCNMA1 in apoptosis, as valpromide was also found to have caused this effect (Shah et al., 2013). However, in another paper, VPA was shown to be pro-apoptotic against neural progenitor cells (but not the embryonic stem cell derived glutamatergic neurons), which was found to be dependent on its HDAC activity (Fujiki et al., 2013). From these results it is clear that genes in the apoptotic pathway are altered in response to VPA treatment, but a consensus as to how this occurs, and whether it is different in development and adulthood is unclear.

4.4.4 Conclusion

From the re-analysis of available microarray data, many interesting pathways appear to be affected by exposure to VPA, especially in neuronal development and differentiation. Also, there appears to be some degree of evolutionary conservation of VPA-induced changes between species. This makes VPA an interesting effector in neurons, although further studies are needed to understand

the ability of VPA to influence synaptic function. Aldicarb screening of potential synaptic regulators identified in this study revealed some interesting candidates, including the novel regulator dhhc-2, which then became the focus of further functional studies.

Chapter 5 - Investigating the ability of Palmitoyl acyltransferases to affect synaptic function

5.1 Abstract

Results presented in Chapter 4 demonstrate that knockdown of the *C. elegans dhhc-2* gene in *Tu3311* worms caused a significant RIC phenotype. As *dhhc-2* is one of a family of 15 palmitoyl acyltransferase (PATs) encoded in the *C. elegans* genome, the next aim was to further investigate the *dhhc-2* knockdown phenotype and test the possibility that other members of the PAT family may also influence synaptic function. To address this point, aldicarb-sensitivity assays were performed on other PAT family members, following gene-targeted neuron-specific RNAi knockdown. In a complementary study, corresponding genetic knockouts of PAT family members were also analysed to assess relative aldicarb sensitivity. Interestingly, data from this study indicated that knockdown of dhhc-12 also led to reduced aldicarb sensitivity. Although genetic mutation of dhhc-2 did not cause a significant change in aldicarb sensitivity, mutation of dhhc-14 and dhhc-13 conferred significant RIC and HIC phenotypes, respectively.

Previous work performed in the Falciani group (Munasinghe, 2015) showed that VPA induced paralysis in sma-6 mutant worms. In addition, preliminary results suggested that combined treatment of VPA and aldicarb greatly increased the rate of paralysis in wild type worms. To further investigate this phenotype, these effects were reassessed in the N2, sma-6 and unc-38 worm strains, which were also used in the previous study (Munasinghe, 2015). The extent of VPA-induced paralysis was also examined in PAT mutant worms, and following targeted knockdown of PAT family members in the *Tu3311* strain.

To elucidate conserved effectors of synaptic function, mouse and human orthologs of *C. elegans* PAT family members were cloned. Cytoplasmic N-terminal fragments of mouse *zDHHC17, zDHHC13*, and a C-terminal fragment of human *zDHHC5* were cloned for use in the Matchmaker Y2H library screens, in order to identify novel interaction partners. Following stringently controlled screening of a normalized human foetal brain Y2H library, 35 novel interacting partners were identified, of which 7 had previously been shown to be palmitoylated. Unfortunately, although the N- and C-terminal fragments of *zDHHC9* (the human ortholog of *C. elegans dhhc-2*) were also tested in Y2H library screens, no interaction partners were identified. However, 17 novel interaction partners were found when full-length *zDHHC9* used analysed using the MYTH membrane Y2H system. Data from these interaction studies was assembled into a new PAT network, which provides a resource to inform future studies into the potential mechanism of action of human PAT family members.

5.2 Introduction

5.2.1 Understanding the *C. elegans* PAT family

The results from aldicarb-sensitivity screens (Chapter 4, section 4.3.2) demonstrated that targeted knockdown of the *C. elegans* PAT family member *dhhc-2* resulted in a significant and reproducible RIC phenotype. Palmitoylation is an essential reversible reaction; in which PATs facilitate the addition of palmitoyl-acyl groups onto substrate proteins. Families of PATs are found throughout evolution from yeast to *Drosophila,* zebrafish and humans. At the level of the

synapse, palmitoylation is known to play a crucial role in SNAP-25 folding during SNARE complex formation and neurotransmitter release (Washbourne P et al,. 2001). Defects in palmitoylation have also been linked to neurological diseases, including adult neuronal ceroid lipofuscinosis (ANCL), where mutations in the cysteine-string-domain of CSPα confer global changes in neuronal palmitoylation, affecting multiple synaptic proteins (Henderson et al., 2016).

To date, there have been few comparative studies performed on the PAT family members in *C. elegans,* with only one study (Edmonds & Morgan, 2014) performing systematic functional comparisons of family members. Bioinformatics analysis identified 15 PAT family members in *C. elegans* (*dhhc-1-14, and spe-10*), each of which contains the characteristic DHHC-CRD motif (Edmonds & Morgan, 2014). Although numerous phenotypic assays were previously performed (Tables 5.1 and 5.2), aldicarb-sensitivity assays were not carried out on the mutant strains nor following RNAi mediated knockdown of PAT family members. Also neuron-specific RNAi worm strains such as *Tu3311* were not used in previous studies, although the *rrf-3* RNAi hypersensitive strain was used. For this reason, other members of the *C. elegans* PAT family may also show aldicarb-sensitive phenotypes if tested in a different genetic background.

Strain	Gene	Allele	Mutation	Phenotypes previously observed
RB1044	dhhc-2	ok990	deletion	Reduced width
VC2067	dhhc-9	gk985	deletion	Reduced mean and median lifespan
VC2039	dhhc-12	gk1013	insertion/deletion	Reduced width, reduced thrashing in liquid, increased time to 90% mortality
VC108	dhhc-13	gk36	deletion	Increased median lifespan and increased time to 90% mortality
VC918	dhhc-14	ok1032	insertion/deletion	Reduced width, increased thrashing in liquid, decreased mean life span and decreased time to 90% mortality

Table 5.1 – Summary of previously reported phenotypes in genetic PAT mutant worms (Edmonds & Morgan, 2014)

RNAi	Phenotypes previously observed
dhhc-1	decreased time to 90% mortality
dhhc-6	decreased thrashing in liquid
dhhc-9 + dhhc-12	decreased time to 90% mortality
dhhc-10 + dhhc-1	increased thrashing in liquid, decreased time to 90% mortality
dhhc-13 + dhhc-14	increased median lifespan, decreased time to 90% mortality
spe-10 + dhhc-4	increased mean and median lifespan

Table 5.2 – Summary of previously reported phenotypes when *C. elegans* PAT family members were knocked down using RNAi (Edmonds & Morgan, 2014).

5.2.2 Using pharmacological agents to elucidate novel *C. elegans* phenotypes

Data presented in Chapter 4 was derived from microarray studies performed on wild-type worms exposed to increasing concentrations of VPA. In addition, VPA-induced paralysis had been observed in the *sma-6* mutant worm strain. VPA is an interesting drug due to its broad medical use to treat epilepsy and bipolar disorder. However, much remains to be understood about the underlying mechanism of VPA action. As *dhhc-2* was selected for further investigation based on network informed predictions from these previous studies, we were particularly interested to see whether genetic mutation or RNAi mediated neuron-specific knockdown of PAT family members would lead to VPA-induced paralysis. In addition, we wished to re-test if aldicarb and VPA had additive effects on the rate of paralysis of wild type worms, and test if comparable phenotypes were observed in PAT mutant strains and corresponding RNAi mediated knockdown studies. If altered expression of any of the PATs induced changes in aldicarb sensitivity profiles, this could be indicative of a role at either cholinergic or GABA terminals.

5.2.3 Use of multiple Y2H systems to identify novel interaction partners of human PATs

The principle of "Guilt by association" suggests that insight into the function or mode of action of a protein can be obtained by defining its interaction partners, as proteins that form part of the same complex may function in the same biological process (Oliver, 2000). Therefore, given the current paucity of data for human PAT family members we aimed to use two forms of Y2H assays to identify novel interaction partners. These may provide new insight into the mode of action or regulation of human PAT family members. Y2H library screens provide an unbiased method of screening for novel direct (or 'binary') interaction partners. Although PAT family members are found throughout evolution, few of these proteins have well defined partner profiles in any organism.

Also, little of the existing interaction data is derived from techniques such as Y2H, which defines only direct partner interactions. One exception to this was a study carried out on DHHC17 (also known as HIP14), where the enzyme was fragmented into three domains that still contained trans-membrane domains. Bait clones encoding these three domains were then pooled and used to screen a classical yeast-two-hybrid library (Butland et al., 2014). Although the classical Y2H system normally does not function well with trans-membrane proteins, in this study they found many novel interaction partners that appear to be physiologically relevant, due to a known relation with HTT.

As the aim of this work was to use *C. elegans* as a model system to provide new

insight into the diversity of synaptic regulation and the potential implications of genetic changes in human neurons, Y2H library screens were performed using human orthologs of C. *elegans* PAT family members.

5.2.4 Aims

The aims of this chapter were to:

- Perform aldicarb-sensitivity assays to assess the relative effects of PAT family member knockdown on synaptic function.
- Establish if knockdown of PAT family members influences VPA-induced paralysis.
- Elucidate the combined effects of aldicarb and VPA on PAT mutants or PAT RNAi treated neurosensitive worms.
- Identify conserved orthologs of PAT family members and create a multi species PAT family "interolog" protein-interaction network, containing all known and predicted PAT family member binding partners.
- Carry out MYTH library screens on full length PATs, in addition to classical Y2H screens on cytoplasmic fragments of a selection of PAT family members, in order to identify novel interaction partners and enhance local interactome coverage.
- Combine all known and novel PAT family protein interaction data to generate an improved one-step PAT interactome.

5.3 Results

5.3.1 Effect of aldicarb on PAT mutants and PAT RNAi knockdowns

Following RNAi knockdown of *C. elegans* PAT family members, aldicarb-sensitivity assays were performed, as described in Chapter 2, section 2.4. A paired T-test was performed on the percentage paralysis values for the negative control (L440) and *Tu3311* worms knocked down with each PAT family member. In each case, a significance threshold of p-value < 0.05 was imposed (Figures 5.1- 5.3 and Table 3.3). Data from this analysis show that in addition to *dhhc-2*, RIC phenotypes were also observed following RNAi mediated knockdown of *dhhc-3*, *dhhc-12* and *spe-10*. In addition, significant HIC phenotypes were observed following knockdown of *dhhc-1* and *dhhc-5* family members.

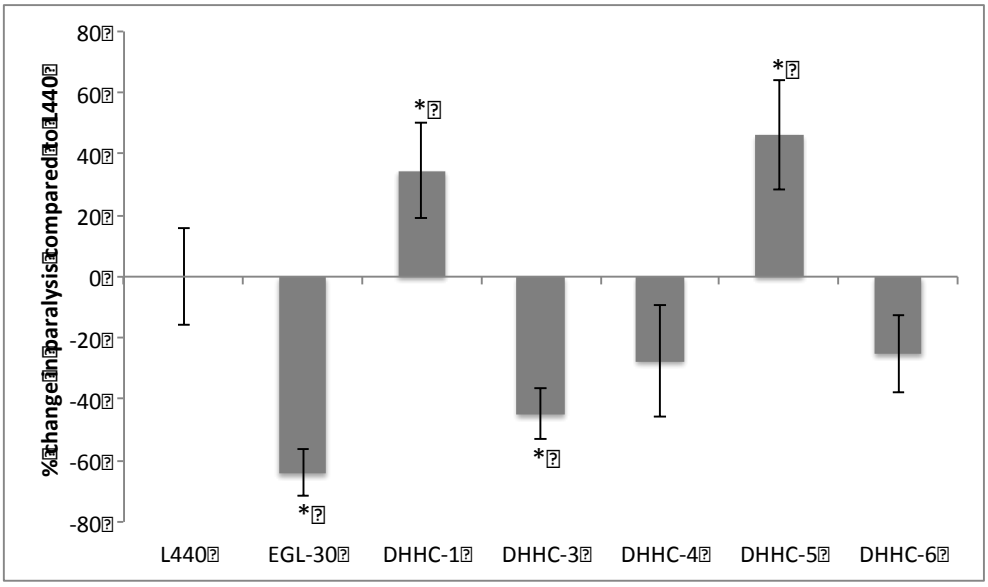

Figure 5.1 **– Induced changes in aldicarb sensitivity following RNAi mediated knockdown of *dhhc-1, -2, -3, -4, -5* and -6**. In each case aldicarb sensitivity assays were performed in triplicate on adult worms following RNAi mediated knockdown as described in materials and methods. Percentage paralysis was measured after 140 minutes. * denotes significance p< 0.05. n=3. Error bars represent standard deviation.

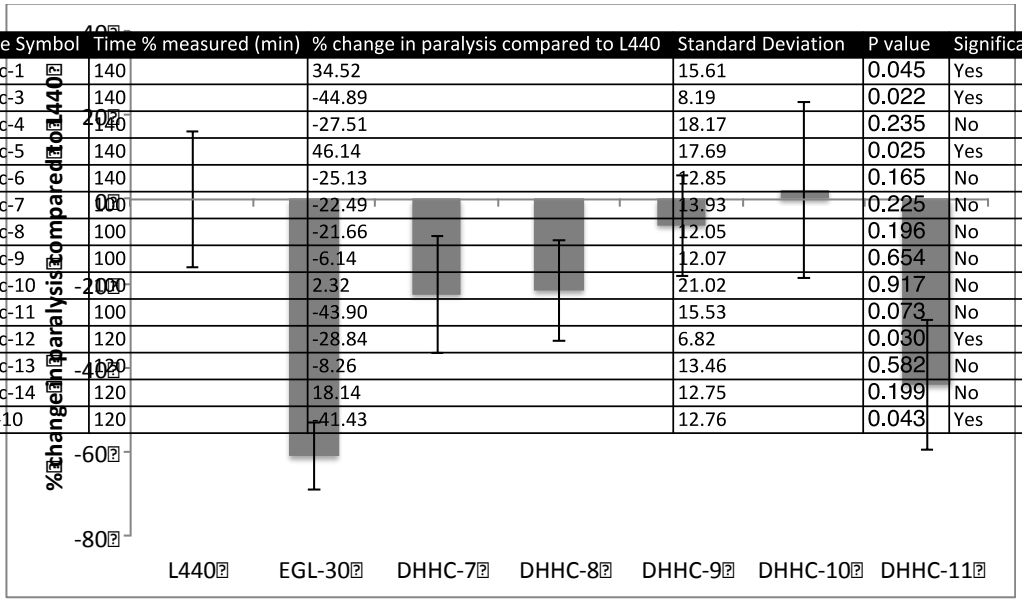

Gene Symbol	Time % measured (min)	% change in paralysis compared to L440	Standard Deviation	P value	Significant?
dhhc-1	140	34.52	15.61	0.045	Yes
dhhc-3	140	-44.89	8.19	0.022	Yes
dhhc-4	140	-27.51	18.17	0.235	No
dhhc-5	140	46.14	17.69	0.025	Yes
dhhc-6	140	-25.13	12.85	0.165	No
dhhc-7	100	-22.49	13.93	0.225	No
dhhc-8	100	-21.66	12.05	0.196	No
dhhc-9	100	-6.14	12.07	0.654	No
dhhc-10	100	2.32	21.02	0.917	No
dhhc-11	100	-43.90	15.53	0.073	No
dhhc-12	120	-28.84	6.82	0.030	Yes
dhhc-13	120	-8.26	13.46	0.582	No
dhhc-14	120	18.14	12.75	0.199	No
spe-10	120	-41.43	12.76	0.043	Yes

Figure 5.2 – **Induced changes in aldicarb sensitivity following RNAi mediated knockdown of *dhhc-7, -8, -9, -10, and -11***. In each case aldicarb sensitivity assays were performed in triplicate on adult worms following RNAi mediated knockdown as described in materials and methods. Percentage paralysis was measured after 140 minutes. * denotes significance p< 0.05. n=3. Error bars represent standard deviation.

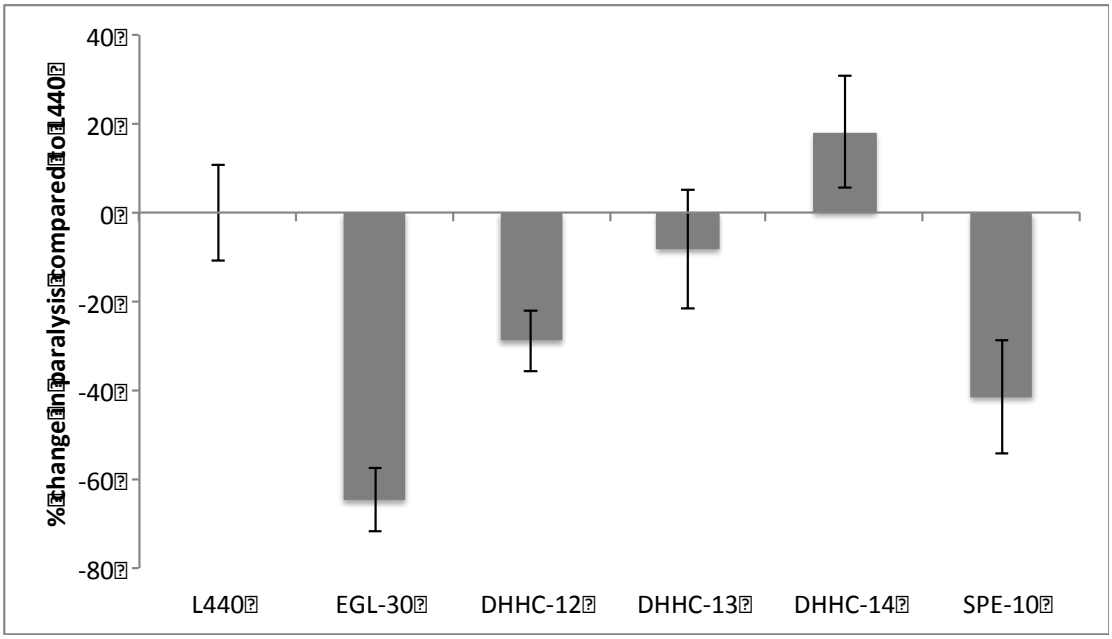

Figure 5.3 – **– Induced changes in aldicarb sensitivity following RNAi mediated knockdown of *dhhc-12, -13, -14, and spe-10***. In each case aldicarb sensitivity assays were performed in triplicate on adult worms following RNAi mediated knockdown as described in materials and methods. Percentage paralysis was measured after 140 minutes. * denotes significance p< 0.05. n=3. Error bars represent standard deviation.

To further explore these phenotypes, relative changes in aldicarb sensitivity were also assessed in genetic mutant strains of PAT family members (Figures 5.4 – 5.7). Mutants obtained from the CGC included: RB1044 (dhhc-2), VC2067 (dhhc-9), VC2039 (dhhc-12), VC108 (dhhc-13) and VC918 (dhhc-14). This analysis revealed some variation in phenotypes observed between RNAi knockdown and related genetic mutants, however, it should be noted that the parental worm strains are different in each case. Although neither *dhhc-13* nor *dhhc-14* exhibited significant changes in aldicarb sensitivity following RNAi knockdown in *Tu3311* worms, genetic mutants of *dhhc-13* (VC108) and *dhhc-14* (VC918) showed reproducible HIC and RIC phenotypes respectively. Detection of changes in aldicarb-sensitivity in RNAi assays but not in genetic mutants may indicate that the effect is occurring in the pre-synaptic neuron at neuromuscular junctions, as theoretically in the *Tu3311* strain knockdown should not be occurring in post-synaptic muscle cells. It is also possible that there could be varying degrees of functional compensation when the target gene is globally deleted throughout the whole worm. However, it is important to note that because assays were performed in a high-throughput format, the relative efficacy of RNAi knockdown or mutant perturbation of gene expression was not assessed. As such, only reproducible positive phenotypes can be interpreted with confidence. Results showing no effect following RNAi treatment (dhhc-13 and dhhc-14) may be due to inefficient depletion of the corresponding proteins.

Due to time restrictions RNAi-mediated knockdowns of PAT family members were not performed in the *Tu3335* strain.

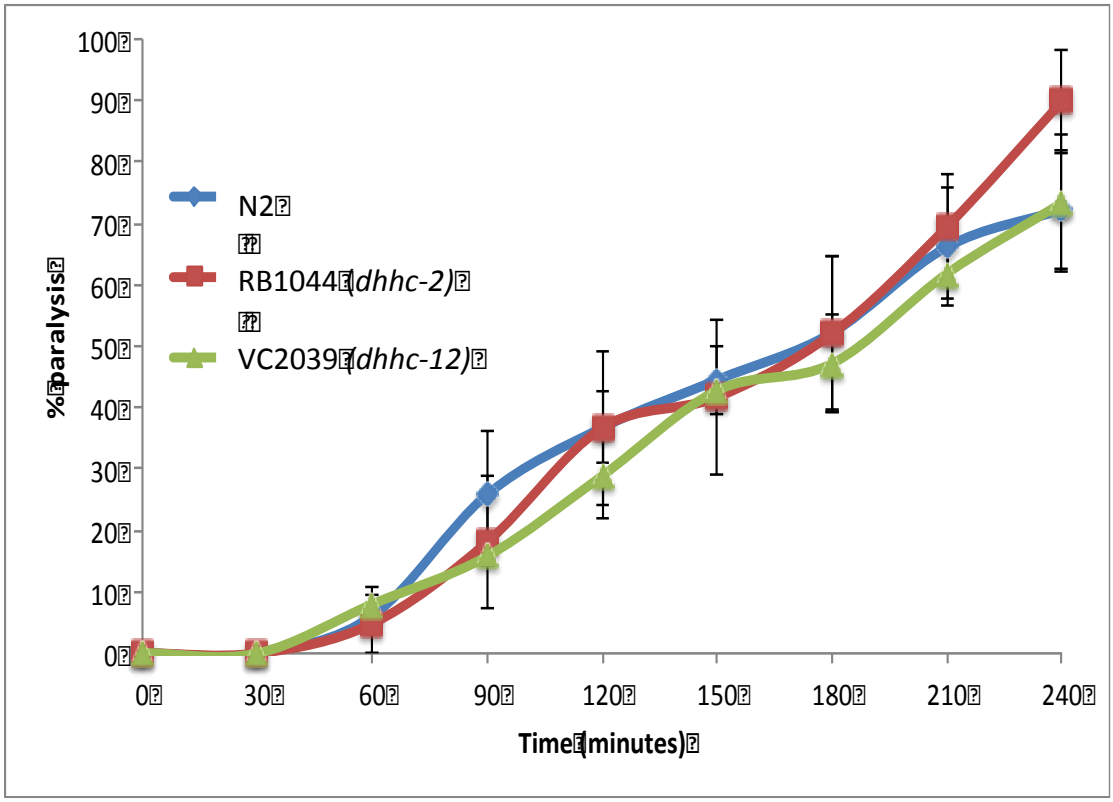

Figure 5.4 – **Full time-course aldicarb sensitivity assays performed on N2, *dhhc-2* (RB1044) and *dhhc-12* (VC2039) worm strains**. In each case 20 gravid mutant worms were picked onto 1mM aldicarb plates, and paralysis was assessed as described in materials and methods. n=3. Error bars represent standard deviation.

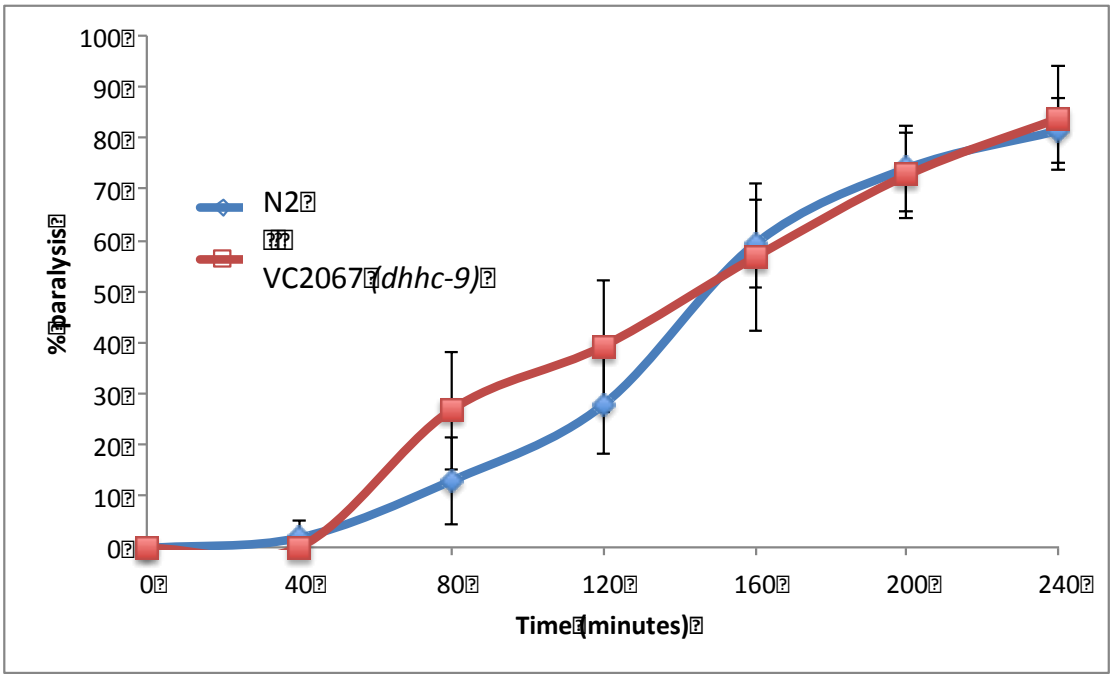

Figure 5.5 – **Full time-course 1mM aldicarb assay of N2 and *dhhc-9* (VC2067)**. 20 gravid mutant worms were picked onto 1mM aldicarb plates, and paralysis was assessed as described in materials and methods. n=3. Error bars represent standard deviation.

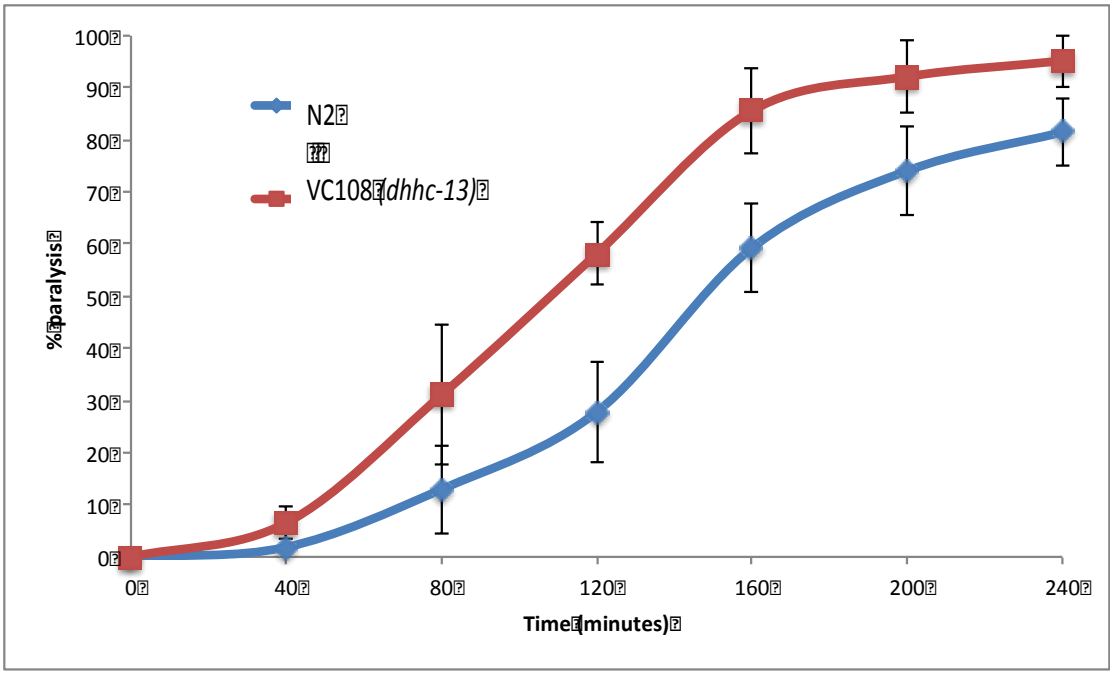

Figure 5.6– **Full time-course 1mM aldicarb assay of N2 and *dhhc-13* (VC108)**. 20 gravid mutant worms were picked onto 1mM aldicarb plates, and paralysis was assessed as described in materials and methods. n=3 . Error bars represent standard deviation.

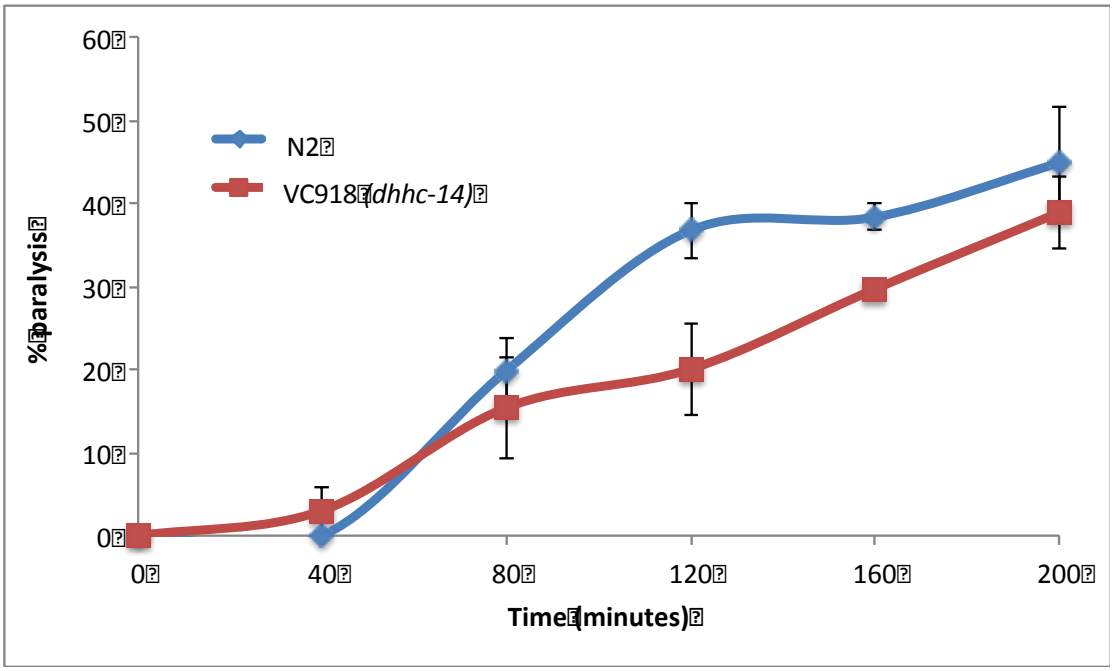

Figure 5.7 – **Full time-course 1mM aldicarb assay of N2 and *dhhc-14* (VC918)**. 20 gravid mutant worms were picked onto 1mM aldicarb plates, and paralysis was assessed as described in materials and methods. n=3. Error bars represent standard deviation.

5.3.2 Investigating the involvement of PAT family members in postsynaptic function.

Although results from the aldicarb-sensitivity assays indicate that PAT family members can influence the function of neuromuscular synapses, it was not possible to establish if the observed effects were specifically due to pre- or post - synaptic events. To test if the observed mutant phenotypes were a consequence of changes at the postsynaptic terminal, mutant and N2 worms were exposed to 0.1 mM levamisole, a well-characterized cholinergic receptor antagonist (Locke et al., 2008). Under these conditions a change in paralysis rate would indicate that the knockdown of a specific protein affected some required post-synaptic

function. Conversely, if the effect is specific to neurons, no phenotypic change would be observed in the presence of 0.1mM levamisole, although a change would be seen following aldicarb-sensitivity assays.

Levamisole sensitivity assays were carried out on all of the available PAT mutants and the sma-6 mutant (LT186). As LT186 mutation had previously been shown to cause a strong HIC phenotype in response to levamisole treatment this strain was also used as a positive control in this study (Figure 5.8 and Table 5.4) (Munasinghe, 2015). From this it can be seen that *dhhc-2* (RB1044), and *dhhc-13* (VC108) show a RIC phenotype in comparison to N2 worms at both of the selected time points.

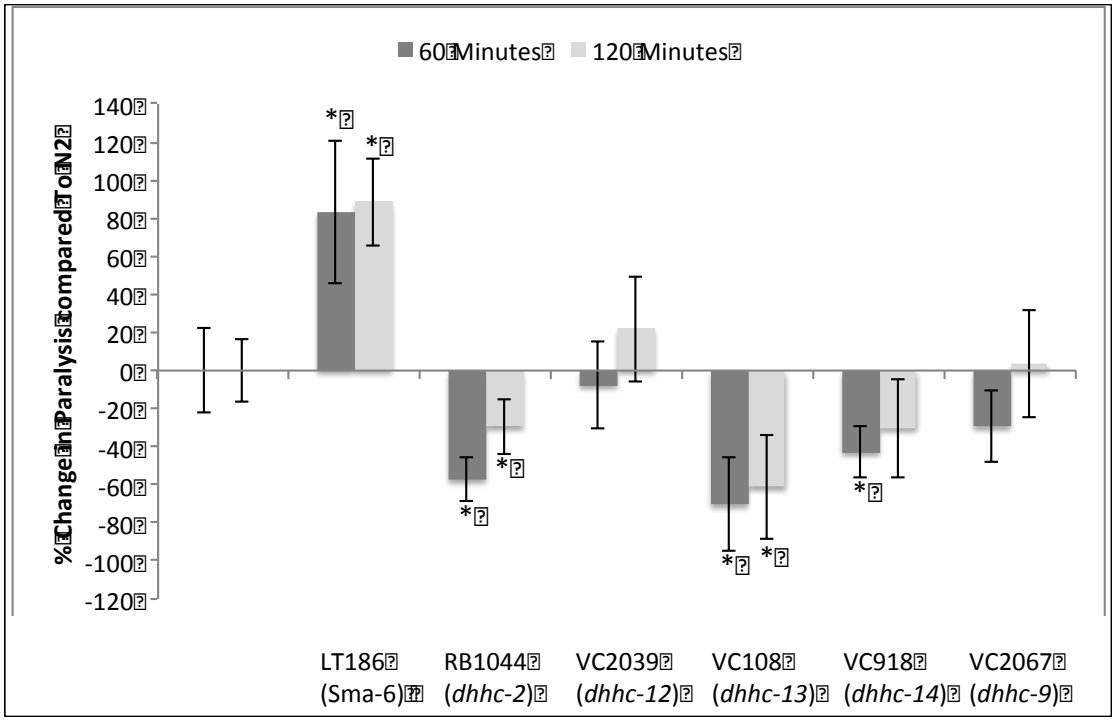

Figure 5.8 –Levamisole sensitivity assays performed on a selection of PAT family and sma-6 (LT186) mutant worm strains. In each case paralysis assays were performed as described in materials and methods and the percentage of paralysed worms compared to the N2 worms was determined after 60 and 120 minutes. * denotes significance ($p < 0.05$). n=3. Error bars represent standard deviation.

As the *Tu3311* worm strain was originally generated to allow preferential uptake of dsRNA into neurons, the effect of levamisole following dsRNA knockdown of PAT family members in the *Tu3311* strain was not tested.

Strain	% Change in Paralysis at 60 Minutes	Standard Deviation 60 Minutes	P Value	Significant?
N2	0.00	21.97	-	-
LT186	83.27	37.41	0.008	Yes
RB1044	-57.26	11.26	0.005	Yes
VC2039	-7.76	23.08	0.641	No
VC108	-70.33	24.28	0.013	Yes
VC918	-42.94	13.43	0.016	Yes
VC2067	-29.49	18.72	0.078	No

Strain	% Change in Paralysis at 120 Minutes	Standard Deviation 120 Minutes	P Value	Significant?
N2	0.00	16.38	-	-
LT186	88.64	23.01	<0.001	Yes
RB1044	-29.60	14.26	0.036	Yes
VC2039	21.81	27.83	0.249	No
VC108	-61.28	27.07	0.022	Yes
VC918	-30.50	26.11	0.126	No
VC2067	3.80	28.39	0.827	No

Table 5.4 – Data relating to phenotypes presented in Figure 5.8.

5.3.3 Comparison of aldicarb sensitivity scoring methods

Primary microarray data used in this study was initially generated and analyzed in the Falciani lab (Munasinghe, 2015), however, in that study neuronal phenotypes were assessed using a different scoring system to that classically used to assess changes in aldicarb sensitivity. In particular, movement of worms was visually monitored following pipetting onto aldicarb plates, rather than the conventional approach of assessing changes in response to touch. Using this approach the Falciani lab found evidence for a cooperative phenotype resulting from the combinatorial effects of VPA and aldicarb exposure.

To reassess this phenotype using conventional touch based methods of assessing paralysis aldicarb sensitivity assays were performed on N2, sma-6 mutant (LT186) and unc-38 (CB904) mutant worms. Data from assays performed in the Falciani lab show hypersensitivity to aldicarb (HIC phenotype) in LT186 mutant worms and resistance to aldicarb (RIC phenotype) in CB904 worms (Munasinghe, 2015). Re-analysis using conventional scoring methods showed that a HIC phenotype was reconfirmed in LT186 worms (Figure 5.9). However, in our assays CB904 did not display a significant RIC phenotype

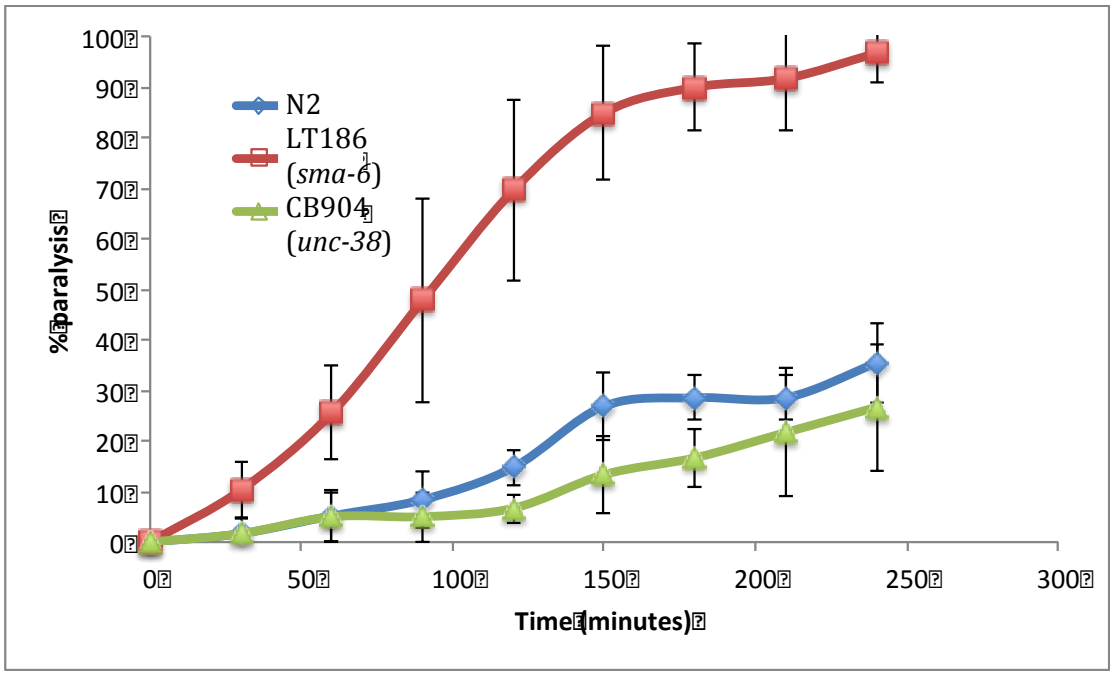

Figure 5.9 - **Results from conventional touch based aldicarb sensitivity assays performed on N2, sma-6 (LT186) and unc-38 (CB904) mutant worms**. In each case paralysis assays were performed in triplicate as described in materials and methods. Error bars indicate standard deviation. n=3.

Interestingly, whilst carrying out our initial high throughput screens (chapter 2), we also tested the effect of specifically knocking down sma-6 in neurons (in the *Tu3311* worm strain). However, we did not detect any HIC phenotype, suggesting that the aldicarb effect may be due to post-synaptic changes, which would agree

with preliminary data and conclusions from initial studies performed in the Falciani lab ((Munasinghe, 2015) (Figure 5.10).

5.3.4 Investigating the relative effects of VPA on genetically ablated PAT mutants

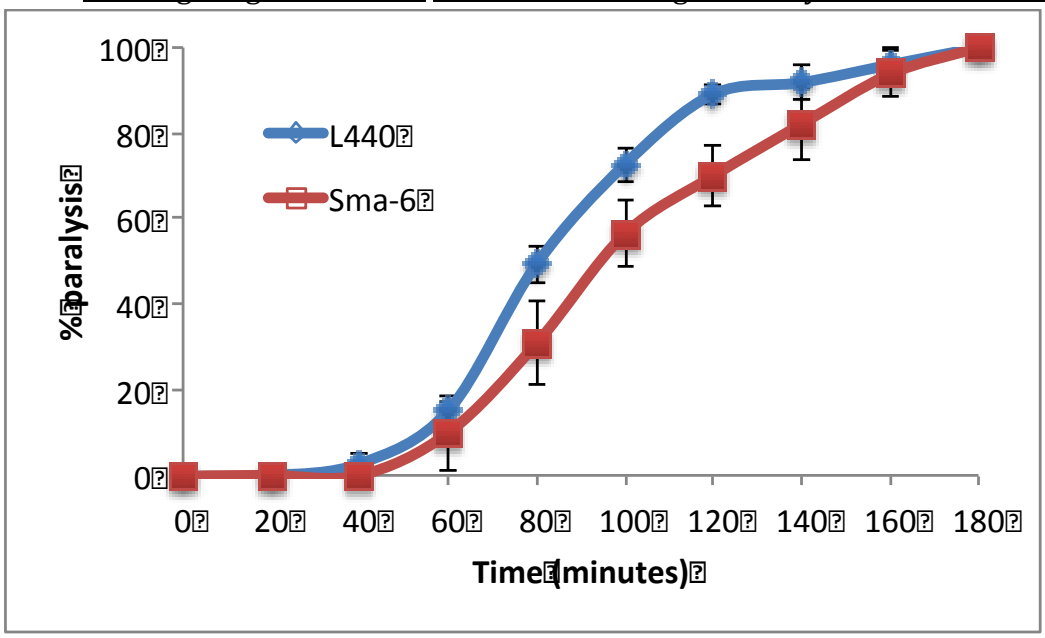

Figure 5.10 – **Change in aldicarb sensitivity following *sma-6* knockdown in *Tu3311* worms.** Paralysis assays were performed in triplicate as described in materials and methods. Error bars indicate standard deviation. n=3

and corresponding RNAi knockdowns

Prior to performing a global microarray analysis of the effects of VPA exposure, the Falciani group found that a sma-6 mutant strain of worms exhibited VPA-induced paralysis (Munasinghe, 2015). They then hypothesized that this phenotype may be the result of changes in some postsynaptic function.

Data from this study confirms that treating sma-6 mutant (LT186) worms with 15 mM VPA reproducibly causes significant paralysis (Figure 5.11). It is also interesting to note that low levels (<10 %) of paralysis were reproducibly seen in N2 worms (Figures 5.12 and 5.13) following exposure to 15 mM VPA, indicating that VPA may affect the normal function of neuromuscular synapses.

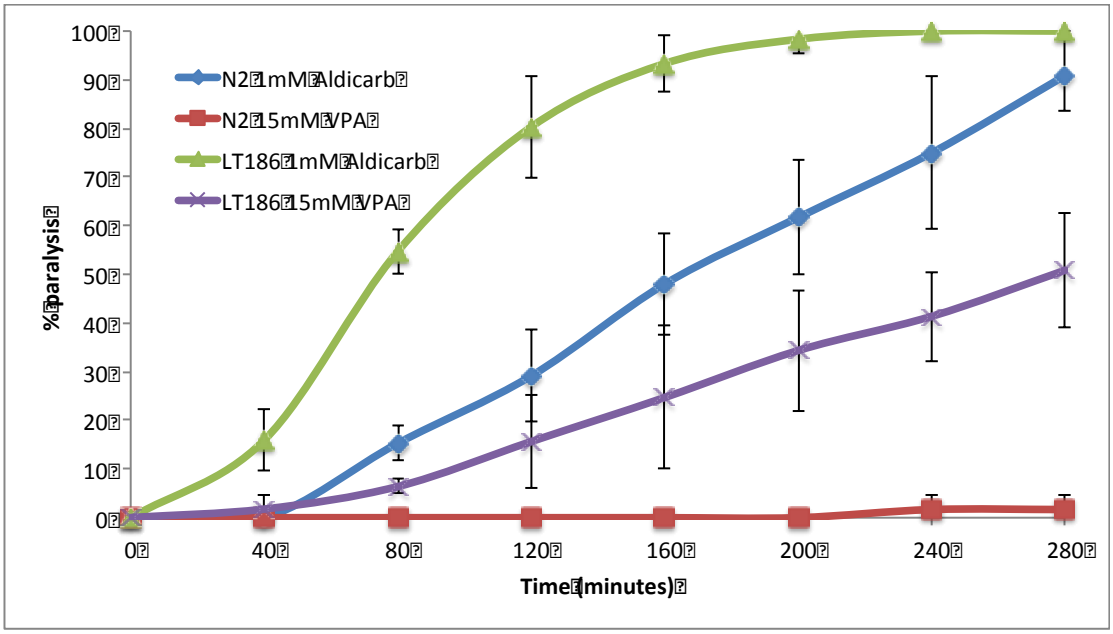

Figure 5.11 – **Independent and cumulative effects of 1 mM aldicarb and 15 mM VPA on the rate of paralysis of N2 and *sma-6* mutants (LT186) worms**. In each case paralysis was assessed in triplicate as described in materials and methods. Error bars indicate standard deviation.. n=3.

As the *C. elegans* dhhc-2 protein was initially identified as a potential regulator of synaptic function using a module prediction algorithm, applied to a combined RIC VPA response network (Chapter 4), we were interested to know if any other PAT family mutants would also confer increased paralysis when exposed to VPA. Initially, all members of available *C. elegans* PAT family member mutants were assessed using a full-time course assay (Figures 5.12 and 5.13). Although, *sma-6* (LT186) mutant worms showed the strongest paralysis phenotype some PAT mutants also showed signs of VPA-induced paralysis compared to N2 worms

(Table 5.5). In particular, both *dhhc-2* and *dhhc-14* showed a small but significant increase in paralysis in the presence of 15mM VPA.

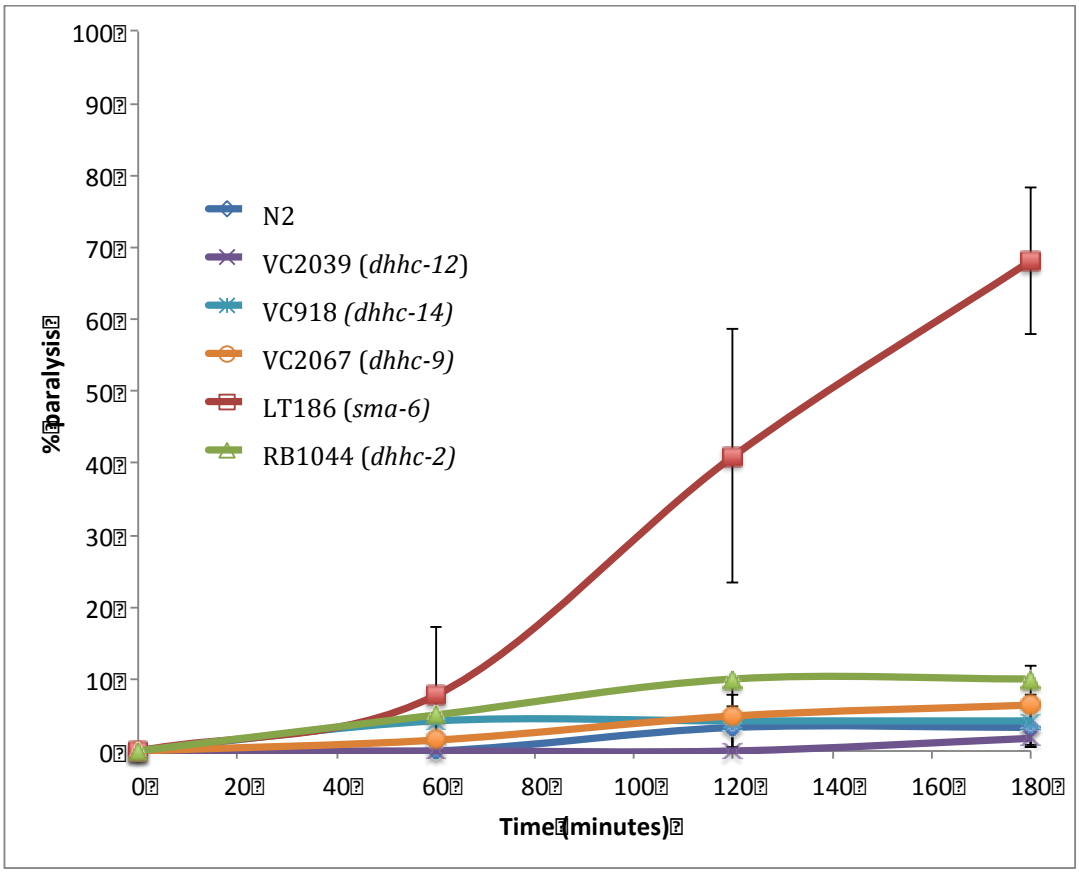

Figure 5.12 – **Comparative rates of VPA induced paralysis in PAT mutant worms**. LT186 is included as a positive control, previously known to cause paralysis. in each case paralysis assays were performed in triplicate as described in materials and methods. Error bars represent standard deviation. n=3.

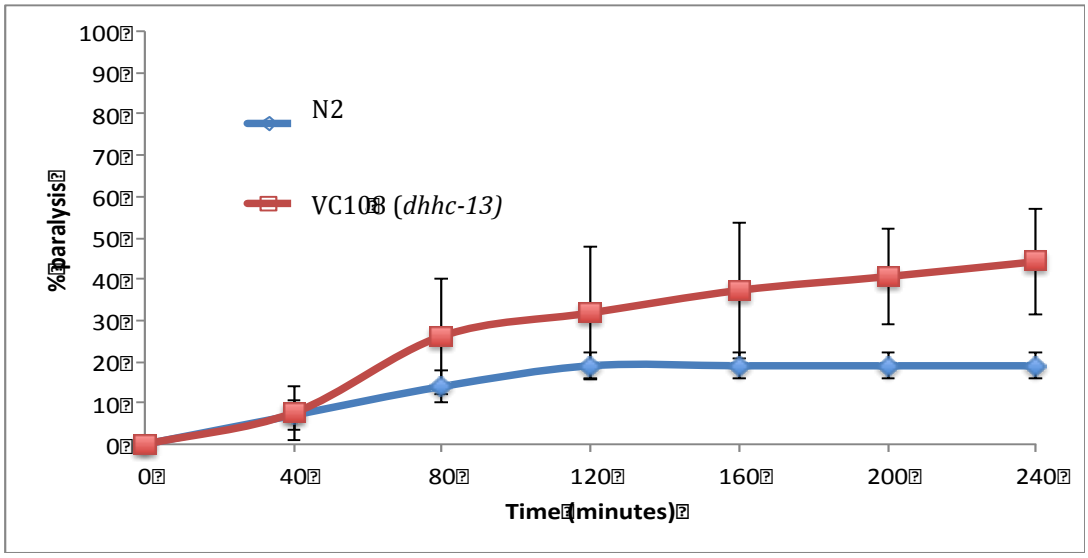

Figure 5.13 –**Analysis of VPA induced paralysis in dhhc-13 (VC108) mutant worms**. Paralysis assays were performed in triplicate as described in materials and methods. Error bars represent standard deviation . n=3.

Mutant	% change in paralysis (to N2)	Standard Deviation	P Value	Significant?
LT186	1994.01	1063.43	<0.001	Yes
RB1044	207.32	153.80	0.014	Yes
VC2039	-46.08	60.29	0.565	No
VC918	28.05	90.58	0.747	No
VC2067	95.57	138.58	0.435	No
VC108	132.59	44.95	0.030	Yes

Table 5.5 – Data relating to phenotypic trends shown in Figures 5.12 and 5.13

To investigate this phenotype further, the same assay was performed following RNAi mediated knockdown of each of the PAT family members in the neuro-sensitive *Tu3311* worm strain (Figure 5.14 and Table 5.6). The relative degree of paralysis was measured 140 minutes after exposure to 15mM VPA. *Dhhc-2* (18.5 % paralysis, p=0.015), dhhc-13 (12.4 % paralysis p = 0.0178) and dhhc-9 (23.2 % paralysis, p = 0.0488) all demonstrated significant paralysis.

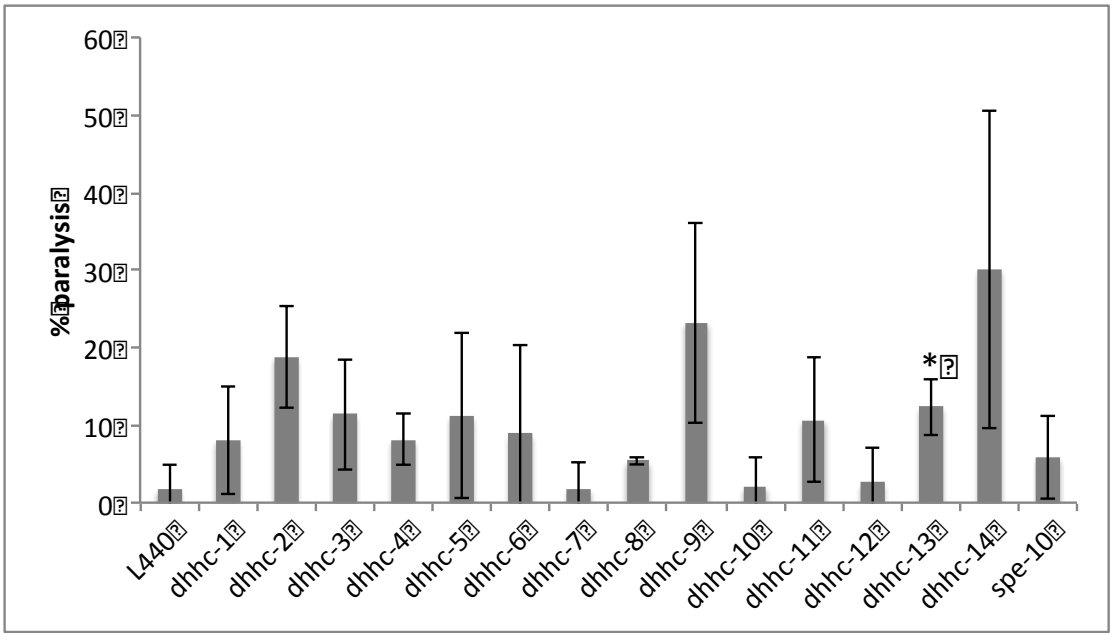

Figure 5.14 – **Comparison of VPA induced paralysis following RNAi mediated knockdown of PAT family members**. Paralysis assays were performed in triplicate as described in materials and methods. Error bars represent standard deviation. * denotes significance between the PAT and L440, where the $p < 0.05$. n=3.

Gene Symbol	% Paralysis at 140 Minutes	Standard Deviation	P Value	Significant?
L440	1.75	3.04	-	-
dhhc-1	8.09	7.01	0.224	No
dhhc-2	18.77	6.53	0.015	Yes
dhhc-3	11.35	7.12	0.098	No
dhhc-4	8.12	3.32	0.071	No
dhhc-5	11.18	10.59	0.212	No
dhhc-6	8.91	11.39	0.352	No
dhhc-7	1.85	3.21	0.970	No
dhhc-8	5.38	0.45	0.110	No
dhhc-9	23.23	12.93	0.049	Yes
dhhc-10	2.08	3.61	0.909	No
dhhc-11	10.71	8.11	0.148	No
dhhc-12	2.56	4.44	0.806	No
dhhc-13	12.35	3.63	0.018	Yes
dhhc-14	30.04	20.54	0.078	No
spe-10	5.89	5.37	0.310	No

Table 5.6 – Data relating to phenotypes shown in Figure 5.14.

5.3.5 Comparative effects of combined VPA and aldicarb treatment on the induction of paralysis in PAT family mutants and RNAi knockdowns

Previous unpublished data (Munasinghe, 2015) indicated that aldicarb and VPA act synergistically to increase aldicarb-sensitivity in wild-type worms. In particular, data from these preliminary studies showed an additive effect with regards to the observed rate of paralysis, suggesting that aldicarb and VPA are acting via different mechanisms to impose a change in synaptic function. To further investigate this phenotype it was necessary to establish if the same combinatorial phenotype could be reproduced using our scoring methodology in worms with a different genetic background. Significantly, our data confirmed that the combination of 1mM aldicarb and 15mM VPA confers a significant increase in the rate of paralysis of N2 worms when compared to 1 mM aldicarb alone (Figure 5.15).

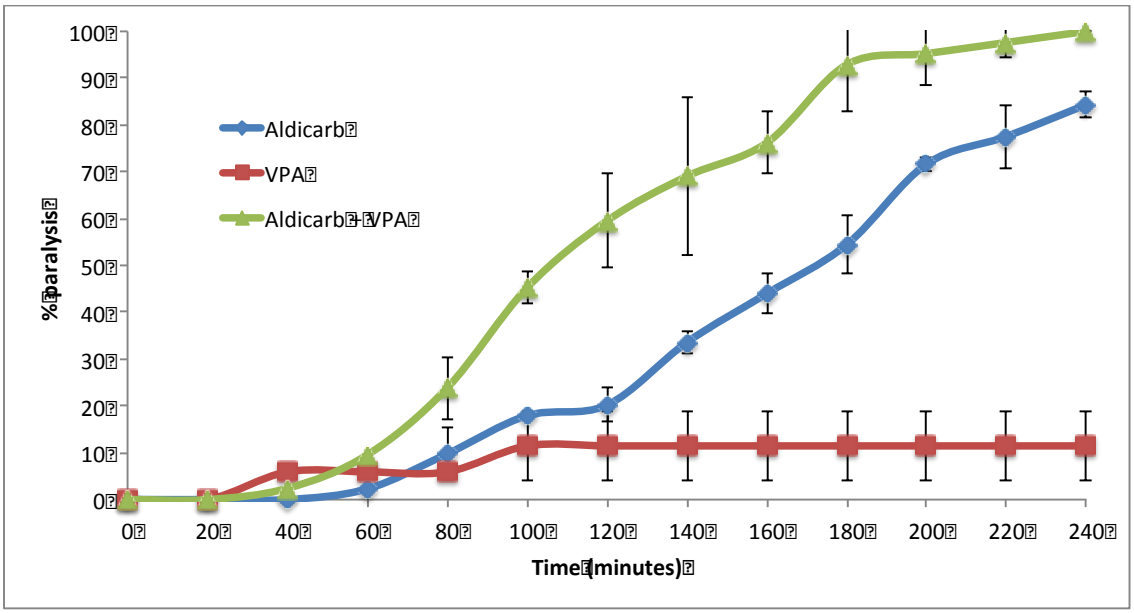

Figure 5.15 – **Additive effects of VPA and aldicarb on the rate of paralysis of N2 worms.** In each case assays were performed in triplicate as described in materials and methods. Error bars represent standard deviation. n=3.

Having established that the synergistic effects of VPA and aldicarb could be detected by conventional methods of assessing paralysis, we then tested this phenotype in the neurosensitive *Tu3311* strain. This secondary analysis was essential, as differences in aldicarb sensitivity between N2 and Tu3311 worms

had been observed previously (Chapter 3, Figure 3.2). In these assays, LT186 worms were used as a positive control as they are known to be hypersensitive to aldicarb and VPA in comparison to N2 worms (Munasinghe, 2015). Results from this comparative analysis show that the *Tu3311* strain reproducibly shows a higher rate of paralysis than N2 worms, although the *Tu3311* strain was not as hypersensitive as LT186 worms (Figure 5.16).

The combined effects of 1mM aldicarb and 15mM VPA were analyzed in worm strains in available PAT family member mutants, as well as in *Tu3311* knocked down with dsRNA specific to each family member. In all cases responses to

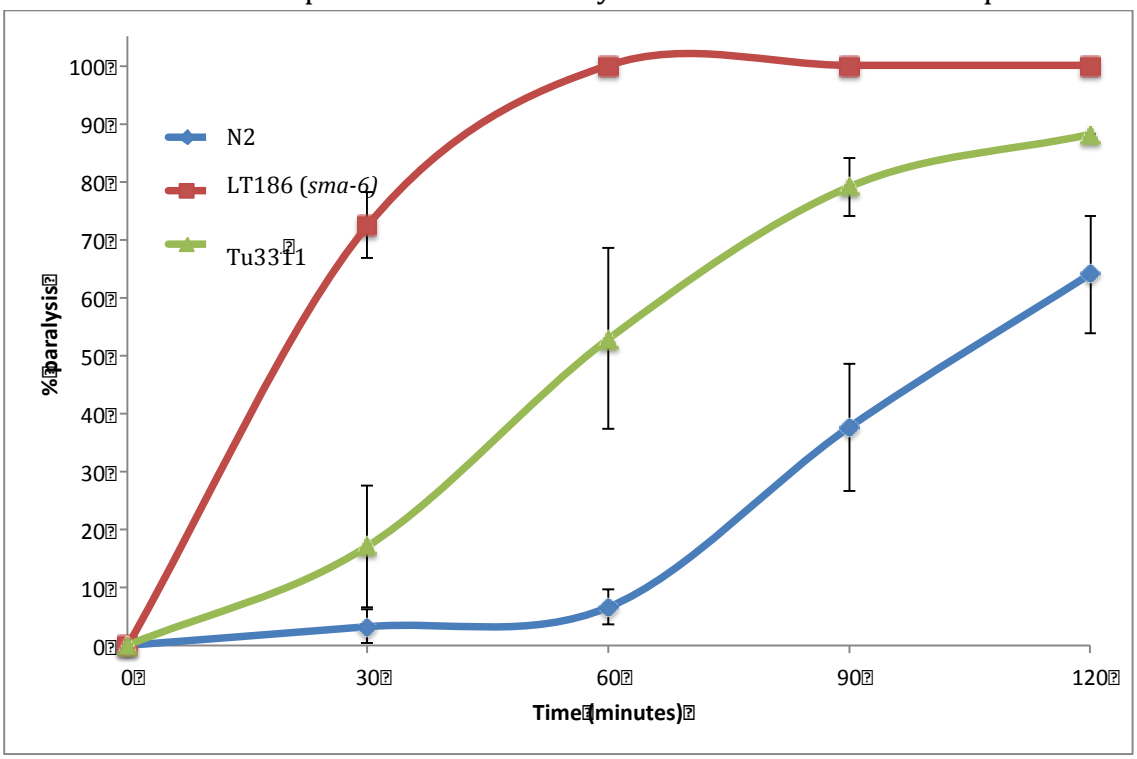

Figure 5.16 –**VPA induced changes in rate of paralysis for N2, Tu3311 and sma-6 (LT186) mutant worms**. In each case assays were performed in triplicate as described in materials and methods. Error bars represent standard deviation. n=3.

combined drug treatment were compared to those observed for wild type N2

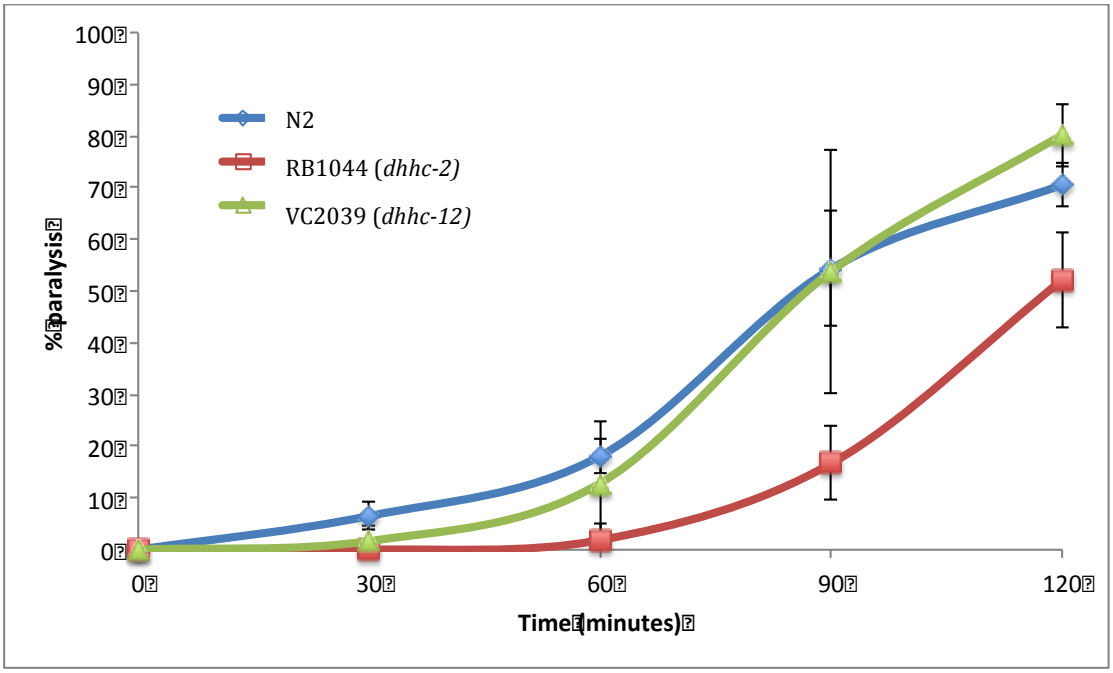

Figure 5.17 – **Relative changes in rate of paralysis following combined exposure to 1mM aldicarb and 15mM VPA for N2, *dhhc-2* (RB1044) and *dhhc-12* (VC2039) worms.** In each case assays were performed in triplicate as described in materials and methods. Error bars represent standard deviation. n=3.

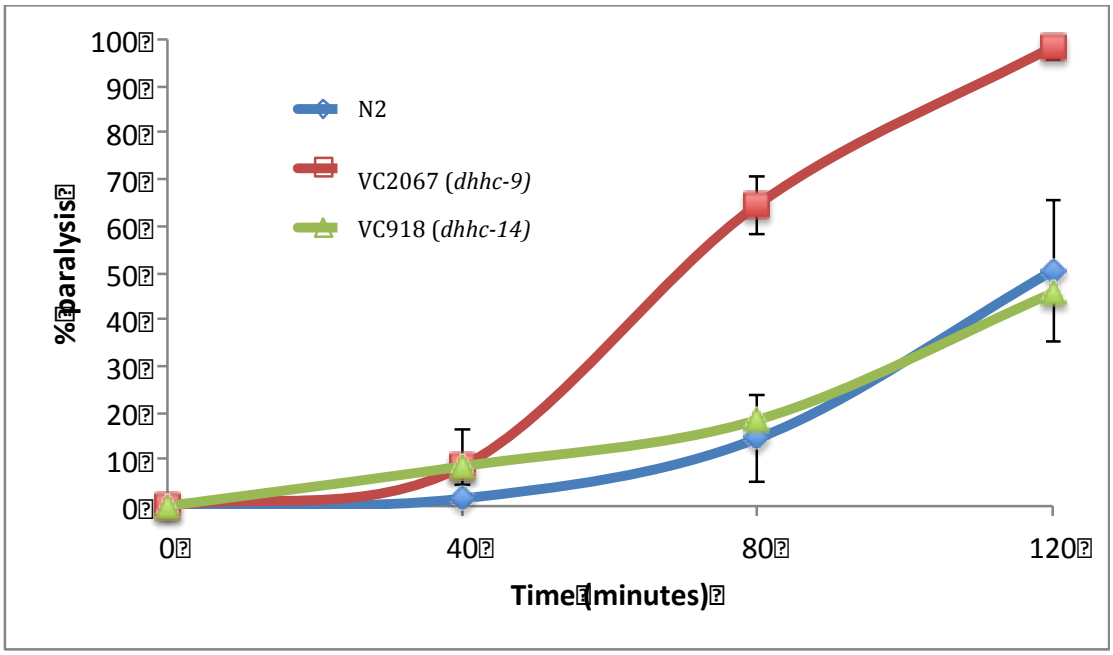

Figure 5.18 – **Relative changes in rate of paralysis following combined exposure to 1 mM aldicarb and 15 mM VPA for N2, *dhhc-9* (VC2067) and *dhhc-14* (VC918) worms**. In each case assays were performed in triplicate as described in materials and methods. Error bars represent standard deviation. n=3.

worms. In these assays significant deviation from the N2 responses indicates that

the gene in question has the ability to influence drug-induced paralysis, which in turn implies an involvement in the regulation or efficacy of synaptic function.

Initial analysis of genetically mutated PAT family worm strains showed that *dhhc-2* (RB1044) exhibited a slower rate of paralysis than N2 worms (Figure 5.17), while *dhhc-9* (VC2067) increased the rate of paralysis compared to control N2 worms (Figure 5.18). None of the other PAT family mutants caused a significant change in the rate of paralysis (Figures 5.17-5.19).

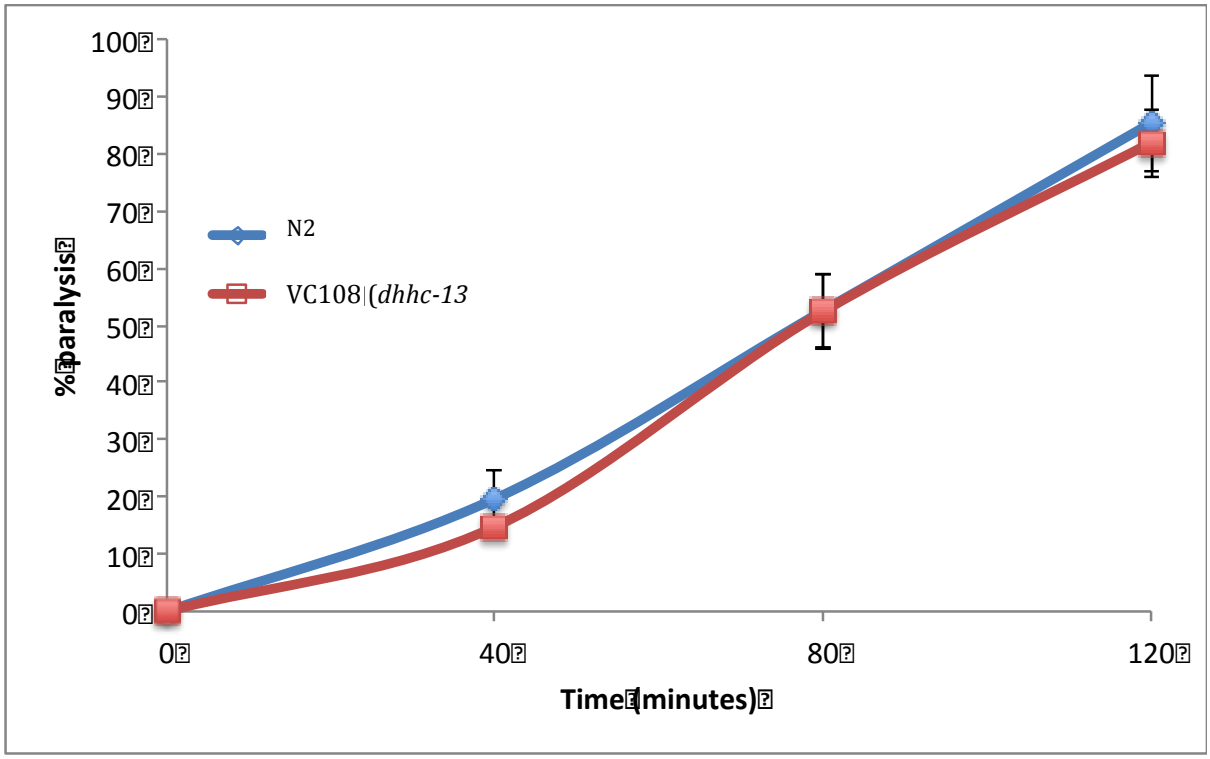

Figure 5.19 – **Relative changes in rate of paralysis following combined exposure to 1mM aldicarb and 15mM VPA for N2 and *dhhc-13* (VC108) worms.** In each case assays were performed in triplicate as described in materials and methods. Error bars represent standard deviation. n=3.

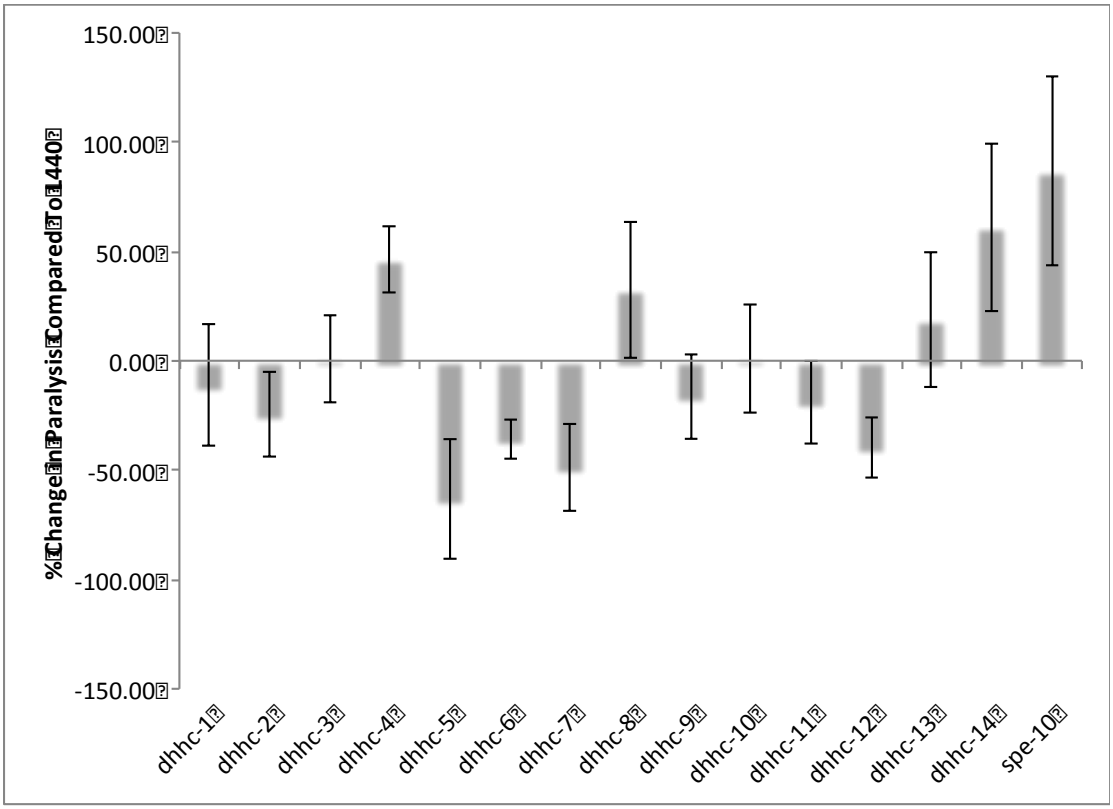

Figure 5.20 – **High-throughput analysis of the combined effect of 1mM aldicarb and 15mM VPA on *Tu3311* worms following RNAi mediated knockdown PAT family members**. All assays were performed in triplicate as described in materials and methods. Error bars represent standard deviation. n=3.

Gene Symbol	% Change in Paralysis Compared To L440	Standard Deviation	P Value	Significant?
dhhc-1	-11.34	27.68	0.522	No
dhhc-2	-24.59	19.33	0.103	No
dhhc-3	0.86	20.03	0.944	No
dhhc-4	46.46	15.22	0.002	Yes
dhhc-5	-63.14	27.72	0.020	Yes
dhhc-6	-35.94	9.20	0.006	Yes
dhhc-7	-49.09	19.93	0.036	Yes
dhhc-8	32.43	31.09	0.085	No
dhhc-9	-16.60	19.08	0.272	No
dhhc-10	0.91	24.61	0.952	No
dhhc-11	-19.04	19.01	0.223	No
dhhc-12	-39.59	13.79	0.037	Yes
dhhc-13	18.86	30.97	0.336	No
dhhc-14	61.14	38.53	0.039	Yes
spe-10	86.69	42.97	0.017	Yes

Table 5.7– Data relating to phenotypic trends shown in Figure 5.20.

When PAT family members were knocked down in *Tu3311*, *dhhc-2* and *dhhc-9* displayed no significant differences in paralysis as compared to the negative control when treated with aldicarb and VPA (Figure 5.20, Table 5.7). However, *dhhc-4* (46.5% change, P value = 0.023), *dhhc-14* (61.1% change, P value = 0.0394)

and *spe-10* (86.7% change, P value = 0.0171) all showed hypersensitivity in comparison to L440 knockdowns. Also, *dhhc-5* (-63.1% change, P value = 0.0195), *dhhc-6* (-35.9% change, P value = 0.0057) *dhhc-7* (-49.1% change, P value = 0.036) and *dhhc-12* (-39.6 % change, P value = 0.0365) showed a slower rate of a paralysis compared to the control. Tables 5.8 and 5.9 summarize the combined effects of drug treatment of PAT family mutants and corresponding

RNAi knock down studies.

5.3.6 Data mining of the PAT family

To better understand the possible conserved roles of PAT family members, the

Worm Gene Symbol	Aldicarb	VPA	Aldicarb + VPA
dhhc-1	HIC	No effect	No effect
dhhc-2	RIC	Paralysis	No effect
dhhc-3	RIC	No effect	No effect
dhhc-4	No effect	No effect	HIC
dhhc-5	HIC	No effect	RIC
dhhc-6	No effect	No effect	RIC
dhhc-7	No effect	No effect	RIC
dhhc-8	No effect	No effect	No effect
dhhc-9	No effect	Paralysis	No effect
dhhc-10	No effect	No effect	No effect
dhhc-11	No effect	No effect	No effect
dhhc-12	RIC	No effect	RIC
dhhc-13	No effect	Paralysis	No effect
dhhc-14	No effect	No effect	HIC
spe-10	RIC	No effect	HIC

Table 5.8 – Summary of RNAi phenotypes of each of the PAT family members. Green indicates an increased rate of paralysis was seen, and red indicates a decreased rate of paralysis was observed.

	dhhc-2	dhhc-9	dhhc-12	dhhc-13	dhhc-14
Mutant + Aldicarb	No effect	No effect	No effect	HIC	RIC
RNAi + Aldicarb	RIC	No effect	RIC	No effect	No effect
Mutant + Valproate	Paralysis	No effect	No effect	Paralysis	No effect
RNAi + Valproate	Paralysis	Paralysis	No effect	Paralysis	No effect
Mutant + Aldicarb + Valporate	RIC	HIC	No effect	No effect	No effect
RNAi + Aldicarb + Valproate	No effect	No effect	RIC	No effect	HIC

Table 5.9 – Summary of the aldicarb, VPA, and combinatorial drug treatments of PAT family members that had both mutants and dsRNA available. Green indicates an increased rate of paralysis was seen, and red indicates a decreased rate of paralysis was observed.

closest orthologs of each of *the C. elegans* PAT family of proteins were identified.

Although this phylogenetic analysis has been carried out before (Edmonds & Morgan, 2014), we decided to check the analyses, and found some differences. ITOL is a program used to create trees of life, dependent on sequence homology and identity (Letunic & Bork, 2016). We used this program to create a combined PAT family tree of life for worms, mouse, and human. This tree includes isoforms for each of the family members to ensure a whole representation of the family (Figure 5.21).

The sequence similarities between *C. elegans* PAT family members and their closest human orthologs were analyzed (Table 5.10). This data indicated that *dhhc-2*, the gene found in the earlier aldicarb screen, had the highest similarity to human *zDHHC9*, having 43 % identity, 61 % similarity and 8 % gaps. Although previous predictions identified isoform 2 of *zDHHC14* to be the closest ortholog (Edmonds & Morgan, 2014), this has a lower percentage identity to *C. elegans dhhc-2* (40% identity, 59% similarity, 10% gaps) than *zDHHC9*.

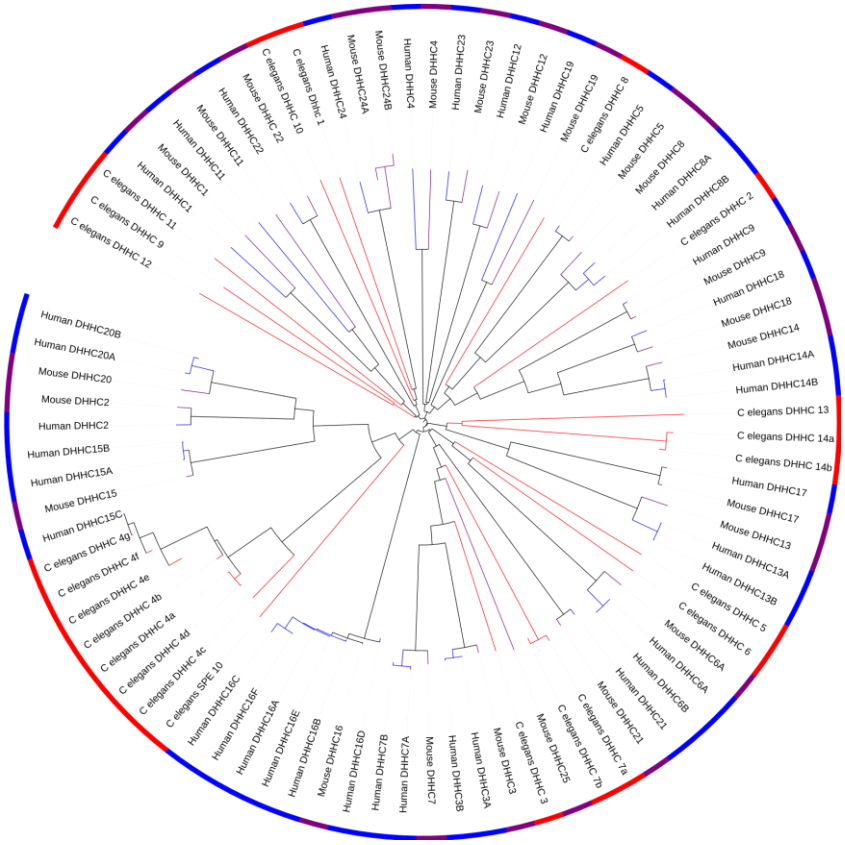

Figure 5.21 – **Tree of Life of the PAT family members, in humans, mice and worms.** This tree was generated by iTOL (Letunic & Bork, 2016).

C. elegans Gene Symbol	Closest Human Ortholog	% Identity	% Similarity	% Gaps
dhhc-1	ZDHHC24	31	43	16
dhhc-2	ZDHHC9	43	61	8
dhhc-3	ZDHHC3	51	62	13
dhhc-4	ZDHHC15	38	61	8
dhhc-5	ZDHHC23	31	43	23
dhhc-6	ZDHHC6	36	52	14
dhhc-7	ZDHHC21	31	43	19
dhhc-8	ZDHHC8	36	47	18
dhhc-9	ZDHHC16	30	43	19
dhhc-10	ZDHHC24	31	47	14
dhhc-11	ZDHHC11	27	46	14
dhhc-12	ZDHHC23	28	39	15
dhhc-13	ZDHHC13	26	43	17
dhhc-14	ZDHHC17	30	47	14
spe-10	ZDHHC15	34	48	17

Table 5.10 - Table to show the worm PAT family and their closest human orthologues. This was determined using DIOPT flyRNAi (Hu et al., 2011), and the percentage identity, similarity and gaps were calculated.

5.3.7 Construction of a PAT family PPI interactome

To better understand the potential role of PAT family members in synaptic function, a PAT family PPI network was assembled, which encompassed all known and predicted interactions involving PAT family members, including interolog data from human, mouse, worm and fly (Chapter 2, section 2.5). PAT family members and their closest neighbours were extracted to generate a PAT one-step network of 654 nodes and 852 edges (Figure 5.22).

The profile of the interaction partners for each PAT family member are shown in Table 5.11, which also specifies how many interactions are known to occur in humans. From this data it is clear that there is a large range in the number of known interaction partners for different PAT members. The only protein with a large number (>20) of human interaction partners was DHHC17 with 343 interaction partners, 240 of which were elucidated in humans.

5.3.8 Cloning the PAT family

In order to extrapolate phenotypic data from *C. elegans* to provide new insight into potential regulators of human synaptic function, as many human PAT family members were cloned as was technically possible. Genes that were successfully amplified from a human HeLa cDNA library (*zDHHC3*, *zDHHC4*, *zDHHC5*, *zDHHC7*, *zDHHC9, and zDHHC16*) were transferred into the pDONR223 Gateway compatible vector. The primers used to clone these genes are found in Chapter 2, Table 2.3.

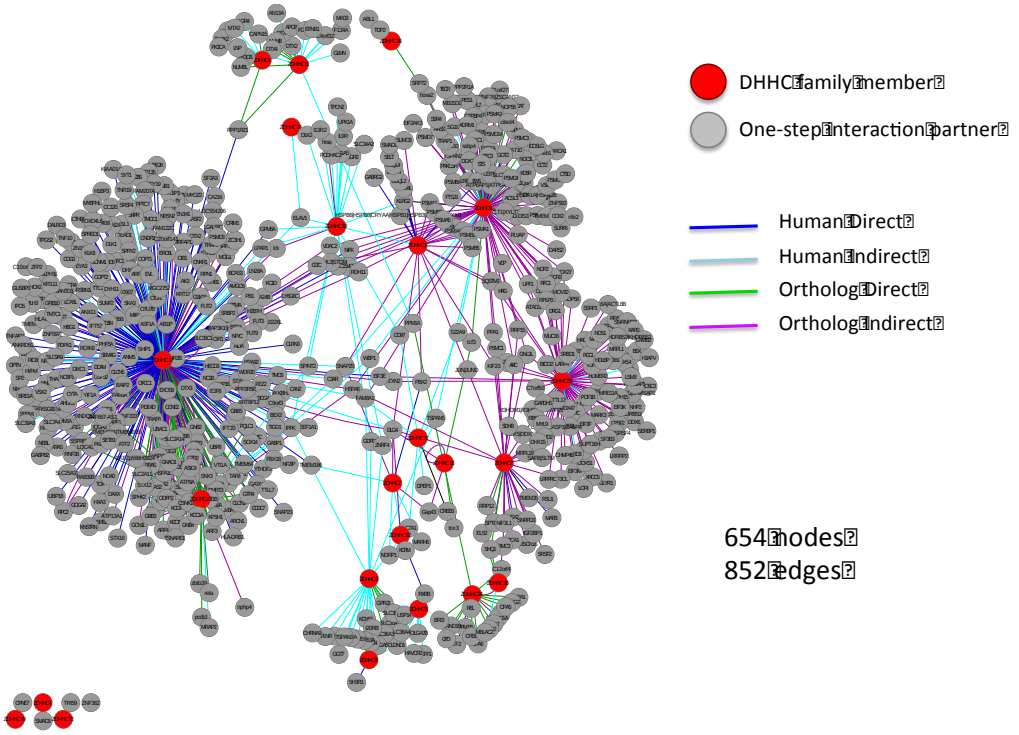

Figure 5.22 – **One-step network of the PAT family. Family members are shown in red, one-step interaction partners are shown in grey. The edge colour denotes the type of interaction**. Dark blue edges represent direct human interactions, light blue represent indirect human interactions, green are direct orthologous interactions and pink are orthologous indirect interactions. Cytoscape v3.2.1 was used to generate this network, using the spring-embedded display.

Although the remaining members of the human PAT family could not be cloned from the HeLa cell cDNA, the whole set of mouse PAT clones was also obtained from Masaki Fukata (National Institute for Physiological Sciences, Myodaiji), and Luke Chamberlain (Strathclyde Institute of Pharmacy and Biological Sciences). Table 5.12 shows the closest human orthologues of each mouse clone. Of note, mouse *zDHHC17* obtained from Fukata and Chamberlain contains a short N-terminal deletion of sixty nucleotides at the N-terminus.

Gene Symbol	Human and Ortholog Interactors	Human Interactors
zDHHC1	13	6
zDHHC2	31	2
zDHHC3	28	5
zDHHC4	1	1
zDHHC5	10	5
zDHHC6	117	13
zDHHC7	8	5
zDHHC8	7	2
zDHHC9	24	19
zDHHC11	17	10
zDHHC12	2	1
zDHHC13	68	6
zDHHC14	1	1
zDHHC15	5	0
zDHHC16	3	1
zDHHC17	373	240
zDHHC18	19	17
zDHHC19	1	1
zDHHC20	4	1
zDHHC21	6	6
zDHHC22	1	1
zDHHC23	94	5
zDHHC24	18	2

Table 5.11 – Number of interaction partners of the PAT family, according to the network generated in Figure 5.20. Interaction data was collected from several databases including Biogrid, CCSB, and Bioplex, as well as from literature curation.

Due to time constraints the PAT family members were prioritized based on structural features and known disease associations as indicated in DisGenet (Pinero et al., 2015) (Table 5.13).

Proteins that were found to have any association to neurological disorders were of particular interest. ZDHHC9 is the closest ortholog of dhhc-2, and mutations of ZDHHC9 have been linked to XLID (Mitchell et al., 2014). ZDHHC17 is linked to Huntington's disease (56. 57). Interestingly, HIP14L (encoded by zDHHC13) has 67.1 % similarity to DHHC17 and both proteins have N-Ankyrin repeat domains

at their N-terminus (Figure 5.21). Furthermore, this region of the two proteins is known to be responsible for the binding of some substrates.

Mouse Gene Symbol	Human Gene Symbol	% Identity	% Similarity	% Gaps
ZDHHC1	ZDHHC1	74	77	10
ZDHHC2	ZDHHC2	95	97	0
ZDHHC3	ZDHHC3	89	90	9
ZDHHC4	ZDHHC4	74	85	0
ZDHHC5	ZDHHC5	98	99	0
ZDHHC6	ZDHHC6	93	97	0
ZDHHC7	ZDHHC7	85	87	11
ZDHHC8	ZDHHC8	92	95	0.4
ZDHHC9	ZDHHC9	98	99	0
ZDHHC11	ZDHHC11	60	75	1
ZDHHC12	ZDHHC12	83	86	5
ZDHHC13	ZDHHC13	91	96	0
ZDHHC14	ZDHHC14	95	98	0
ZDHHC15	ZDHHC15	98	99	0
ZDHHC16	ZDHHC16	95	96	0
ZDHHC17	ZDHHC17	99	100	0
ZDHHC18	ZDHHC18	93	95	2
ZDHHC19	ZDHHC19	69	76	3
ZDHHC20	ZDHHC20	91	94	1
ZDHHC21	ZDHHC21	98	99	0
ZDHHC22	ZDHHC22	92	97	0
ZDHHC23	ZDHHC23	90	95	1
ZDHHC24	ZDHHC24	88	92	0
ZDHHC25	ZDHHC3	41	53	15

Table 5.12 – Conservation of human and mouse PAT family members. Sequences were compared using diopt FlyRNAI (Hu et al., 2011), and matches with the highest % identity, similarity and the lowest % gaps were chosen as the closest orthologs.

ZDHHC8 is implicated in schizophrenia, and DHHC5 is highly homologous to isoform 2 of DHHC8, having a 59.3 % similarity. Both have long C-termini (Figure 5.23), with DHHC5 and DHHC8 having 502 (70.2 % of the whole protein) and 553 (72.2 % of the whole protein) amino acids between their final trans-membrane domain and the C-terminus, respectively. Other PAT family members that have relevance to neurological disorders include zDHHC15, which plays a role in some forms of mental disability and Huntington's disease and zDHHC12, which is also linked to Huntington's disease (Bhattacharyya, Barren, & Kovacs, 2013).

Figure 5.23 shows topological diagrams of each of the PAT family members that were selected for the Y2H studies.

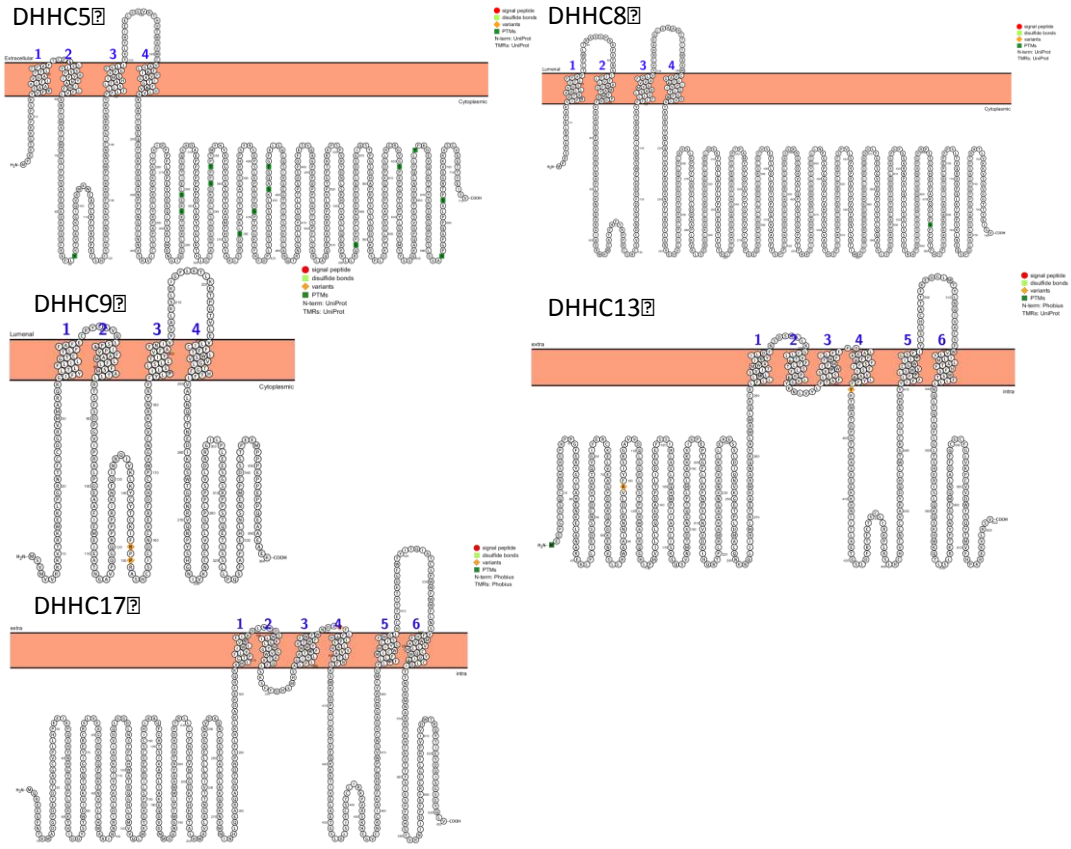

Figure 5.23 –**Visualizations of the topologies of the PAT proteins of interest DHHC5, 8, 9, 13 and 17**. (Adapted from Protter, (Omasits, Ahrens, Müller, & Wollscheid, 2014).

ID	Disease
ZDHHC1	Rheumatoid Arthritis, Crohn Disease, Diabetes Mellitus (insulin dependent and Independent), Herpes Simplex Infections, Coronary heart disease
zDHHC2	Rheumatoid Arthritis, Diabetic retinopathy, liver neoplasms, malignant neoplasm of stomach, Melanoma, Neoplasm metastasis, stomach neoplasms
	Tobacco Use disorder, Weight gain, Gastric adenocarcinoma, Secondary malignant neoplasm of lymph node, Stomach carcinoma, Liver carcinoma
zDHHC5	Non-Small Cell Lung Carcinoma
zDHHC6	Tobacco Use Disorder
zDHHC7	Breast carcinoma
zDHHC8	DiGeorge Syndrome, Mesothelioma, Parkinon's disease, schizophrenia, weight gain, shprintzen syndrome, malignant mesothelioma, 22q11 deletion syndrome
ZDHHC9	Adenocarcinoma, Colonic neoplasms, colorectal carcinoma, precancerous conditions, Lujan Fryns syndrome, Colorectal cancer, X-linked mental retaradation
zDHHC11	Bladder neoplasm, Tobacco Use Disorder, Disease Progression, Carcionoma of bladder
zDHHC12	Huntington's Disease
ZDHHC13	Alopecia, Amyloidosis, Huntington's disease, Osteoporosis
zDHHC14	Malignant neoplasm of prostate, Prostate carcinoma, Xenograft model, Fibrogen adverse event
zDHHC15	Huntington's disease, Neuronal Ceroid-Lipofuscinoses, Severe mental retardation, Mental retardation X-linked
zDHHC17	Huntington's disease, Paroxysmal artrial tachycardia
zDHHC20	Creatinine finding

Table 5.13 – Disease associations of the human PAT family according to DisGeNet (Piñero et al., 2015). Z in figure capital or not

Gene Symbol	Localization	N-terminus localization	C-terminus localization
zDHHC1	Endoplasmic Reticulum, Extracellular Exosome	Cytosol	Cytosol
zDHHC2	Endoplasmic Reticulum, Golgi Apparatus, Plasma Membrane	Cytosol	Cytosol
zDHHC3	Golgi Apparatus	Cytosol	Cytosol
zDHHC4	Golgi Apparatus	Cytosol	Cytosol
zDHHC5	Plasma Membrane, Dendrite	Cytosol	Cytosol
zDHHC6	Endoplasmic Reticulum	Cytosol	Cytosol
zDHHC7	Golgi Apparatus, Nucleus	Cytosol	Cytosol
zDHHC8	Golgi Apparatus, Mitochondria	Cytosol	Cytosol
zDHHC9	Endoplasmic Reticulum, Golgi Apparatus	Cytosol	Cytosol
zDHHC11	Endoplasmic Reticulum	Human: organelle, Mouse: cytosol	Human: organelle, Mouse: cytosol
zDHHC12	Endoplasmic Reticulum, Golgi Apparatus	Organelle	Organelle
zDHHC13	Endoplasmic Reticulum, Golgi Apparatus	Cytosol	Cytosol
zDHHC14	Endoplasmic Reticulum	Cytosol	Cytosol
zDHHC15	Golgi Apparatus, Extracellular Exosome	Cytosol	Cytosol
zDHHC16	Endoplasmic Reticulum, Golgi Apparatus	Cytosol	Cytosol
zDHHC17	Golgi Apparatus, Presynaptic Membrane	Cytosol	Cytosol
zDHHC18	Golgi Apparatus	Cytosol	Cytosol
zDHHC19	Endoplasmic Reticulum	Human: organelle, Mouse: cytosol	Human: organelle, Mouse: cytosol
zDHHC20	Plasma Membrane	Human: cytosol, Mouse: organelle	Human: cytosol, Mouse: organelle
zDHHC21	Golgi Apparatus, Plasma Membrane	Cytosol	Cytosol
zDHHC22	Endoplasmic Reticulum, Golgi Apparatus	Organelle	Organelle
zDHHC23	Integral component of membrane	Cytosol	Cytosol
zDHHC24	Integral component of membrane	Human: organelle, Mouse: cytosol	Human: cytosol, Mouse: organelle

Table 5.14 – Predicted subcellular localization of each of the human PAT proteins, determined by Protter (Omasits et al., 2014). N- and C- termini localizations were determined using Uniprot.

5.3.9 MYTH library screening of full-length DHHC family members

Unfortunately, classical yeast two hybrid systems are not ideal for studying full-length trans-membrane proteins. For this reason the trans-membrane yeast-two-hybrid technique known as split-ubiquitin membrane yeast two-hybrid (MYTH) assay was used in this study. In principle, the MYTH system should allow bait proteins that contain one or more trans-membrane domains, to be screened against a MYTH prey library in order to identify novel binary protein interaction partners as described in Chapters 1 and 2 (sections 1.16.2 and 2.8.9 to 2.8.11). Briefly, in the MYTH system if an interaction occurs between bait and prey, two fragments of ubiquitin (Nub and Cub) interact, leading to recognition and cleavage by deubiquitinating enzymes (DUBs) in the yeast, resulting in the release of a transcription factor, which then translocates into the nucleus to drive expression of the HIS2, ADE3 and lacZ reporter genes, which facilitate growth and blue colour development on selective plates.

As the MYTH system can only be used on transmembrane proteins that have N- or C- cytoplasmic domains, the predicted topology of each PAT family member was analyzed in order to select family members that were suitable for analysis using the MYTH system. Table 5.14 shows the predicted subcellular localization and membrane topology of each PAT family member. From this information human z*DHHC5* and z*DHHC9* and mouse z*DHHC8*, *13* and *17* were selected for analysis in MYTH protein interaction assays. Tables 2.3 and 2.20 (Chapter 2) show the gene-specific sequences used in the primer design.

Once the constructs had been cloned and sequenced, they were transformed into the yeast strain *NMY51*. Transformants were then checked for auto-activation, using the MYTH NubG/I test (Chapter 2, section 2.8.11). All constructs passed this bait auto-activation test. Figure 5.24 shows an example of a typical bait auto-activation test, using *zDHHC17* in the pAMBV vector as bait. However, when screened against the foetal brain MYTH cDNA library, no colonies appeared on plates where human z*DHHC5*, and mouse *zDHHC8*, *13* and *17* were used as baits.

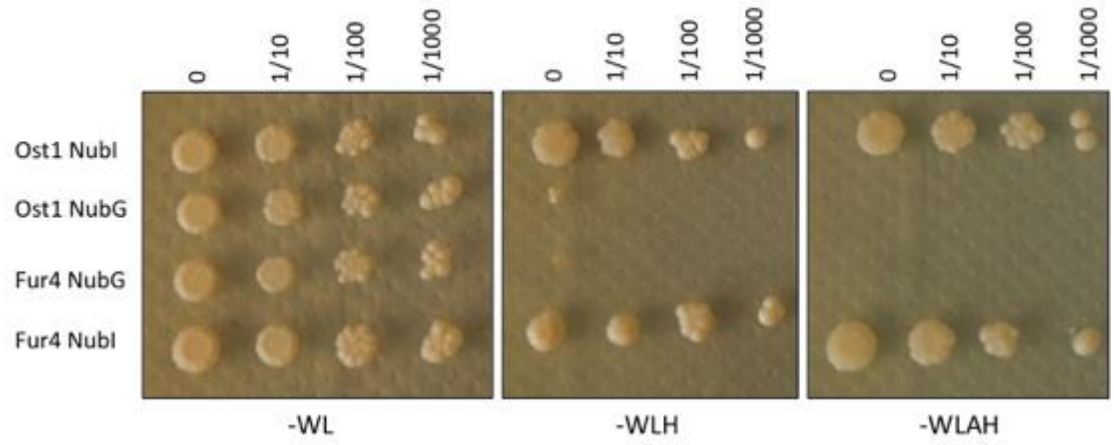

Figure 5.24 – **An example of a MYTH Bait auto-activation test. The bait of interest is transformed with Ost1/Fur4 NubG/NubI constructs**. If successful, growth of all constructs should occur on –WL, while only bait co-transformed with NubI constructs will grow on the –WLH and –WLAH plates. This example is of mouse *zDHHC17-pAMBV*.

ZDHHC9 was successfully screened with the help of lab members, Vanessa Pitz and Jennifer McNamee. Potential interaction partners were retested for specificity before being sequenced to reveal the identity of the binary interaction partner. This revealed twelve interaction partners (Table 5.15), as well as five interaction partners that have the potential to be non-specific partners (Table 5.16).

Gene Symbol	Brief Description	Localization
TECR	Encodes a multi-pass membrane protein residing in the endoplasmic reticulum, and belongs to the steroid 5-alpha reductase family.	Nucleus and ER
EMC4	ER membrane protein complex subunit 4. May mediate anti-apoptotic activity.	ER
ATP5G3	Encodes a subunit of mitochondrial ATP synthase.	Mitochondria
OST4	Oligosaccharyltransferase Complex Subunit 4, Non-Catalytic. May be involved in N-glycosylation with its association with N-oligosaccharyl transferase.	ER
SELK	Encodes a selenoprotein, which is localized to the endoplasmic reticulum and is highly expressed in the heart, where it may function as an antioxidant.	Golgi and ER
TMEM128	Transmembrane protein 128.	Membrane
SPCS1	Component of the microsomal signal peptidase complex, which removes signal peptides from nascent proteins as they are translocated into the lumen of the ER.	ER
TRO	Encodes a membrane protein that mediates cell adhesion between trophoblastic cells and the epithelial cells of the endometrium. Participates in cell signalling during embryo implantation, and may be involved in cancer formation.	Plasma membrane
FZD1	Member of the 'frizzled' gene family, which encodes 7-transmembrane domain proteins that are receptors for Wnt signaling proteins. Contains a signal peptide, a cysteine-rich domain in the N-terminal extracellular region, 7 transmembrane domains, and a C-terminal PDZ domain-binding motif.	Plasma membrane
RTN4	Belongs to the family of reticulon encoding genes. Associated with the ER, and are involved in neuroendocrine secretion or membrane trafficking in neuroendocrine cells. The gene product is a potent neurite outgrowth inhibitor which may also help block the regeneration of the central nervous system in higher vertebrates.	ER
GTF2F1	Endodes a general transcription factor, which binds to RNA polymerase II and helps to recruit the initiation complex with TFIIB.	Nucleus
ARV1	Encodes a transmembrane protein with a conserved zinc ribbon motif at the N-terminus. A similar protein in mouse is thought to function in fatty acid homeostasis. Mutations in this gene are associated with early infantile epileptic encephalopathy.	Golgi and ER

Table 5.15 – Brief description of interacting proteins found in the MYTH *ZDHHC9* screen. Descriptions were chelated from NCBI and Uniprot. Localizations were determined using the COMPARTMENTS database (Binder et al., 2014).

Gene Symbol	Brief Description	Localization
C14ORF1	Probable ergosterol biosynthetic protein 28	ER
TMEM14A	Protein coding gene. Associated with ovarian cystadenocarcinoma and generalized epilepsy type 5.	Membrane component
RNF41	E3 ubiquitin ligase. Controls the balance between JAK2-associated cytokine receptor degradation and ectodomain shedding.	Cytosol
C4ORF3	Protein coding gene.	Membrane component
TMEM230	Protein coding gene.	Recycling endosome, Synaptic vesicle

Table 5.16 – Brief description of the interacting proteins found in the MYTH *zDHHC9* screen, which were thought to be non-specific interaction partners. Descriptions were chelated from NCBI and Uniprot. Localizations were determined using the COMPARTMENTS database (Binder et al., 2014).

5.3.10 Cloning PAT fragments for use in classical Y2H library screens

Due to significant technical issues with our initial MYTH screens, the standard Y2H library system was also used to in an attempt to elucidate novel interaction partners of the PAT family members. In this system, proteins are truncated so that cytoplasmic domains can be investigated in isolation, although this approach will only be effective if truncated cytoplasmic domains continue to fold correctly even without the transmembrane domains.

Truncations of the same proteins used in the MYTH screens were cloned, as these were of more interest due to their known disease relations. Secondly, *DHHC5*, *8, 13* and *17* all have interesting cytoplasmic domains that could be studied in isolation. z*DHHC13* and *17* both have proposed N-Ankyrin repeat substrate binding domains in their N-terminus, while z*DHHC*5 and *8* have long C-terminal tails containing a type II PDZ ligand (Thomas, Hayashi, Chiu, Chen, & Huganir, 2012).

In total, six cytoplasmic regions of human DHHC proteins were successfully cloned (Table 5.17) and transferred into the Y2H bait vector pGBKT7, including N-terminal fragments of z*DHHC17* (DHHC17N) and zDHHC13 (DHHC13N), and C-terminal fragments of z*DHHC5* (DHHC5CT) and zDHHC8 (DHHC8CT), Following transformation into Y2HGold yeast all of the bait clones passed auto-activation and toxicity tests (Figure 5.25).

Gene Symbol	Organism	Fragment region (bp)	Primer	Primer Sequence
zDHHC9	Human	750-1092	Forward	atggtggctctcaaccagaca
			Reverse (+Stop)	ctacttctcagcttcagctgc
		1-568	Forward	ATGtctgtgatggtggtgaga
			Reverse (+Stop)	tcaaaggatgaagaggtagaagta
zDHHC5	Human	639-2147	Forward	ATGaggggacgcacaaccaat
			Reverse (+Stop)	tcacaccgaaatctcata
zDHHC8	Mouse	633-2288	Forward	ATGactggtcacgcggggccgcac
			Reverse (+Stop)	tcacaccgagatttcata
zDHHC13	Mouse	1-876	Forward	ATGgagggcccgggcctgggc
			Reverse (+Stop)	ctaggctctcatcttggc
zDHHC17	Mouse	1-912	Forward	ATGaccaagatggcggacggc
			Reverse (+Stop)	ctaatacccttcgcttg

Table 5.17 – Truncations generated for the Matchmaker Y2H library screens. Primer sequences shown are the gene-specific DNA regions used to generate the constructs.

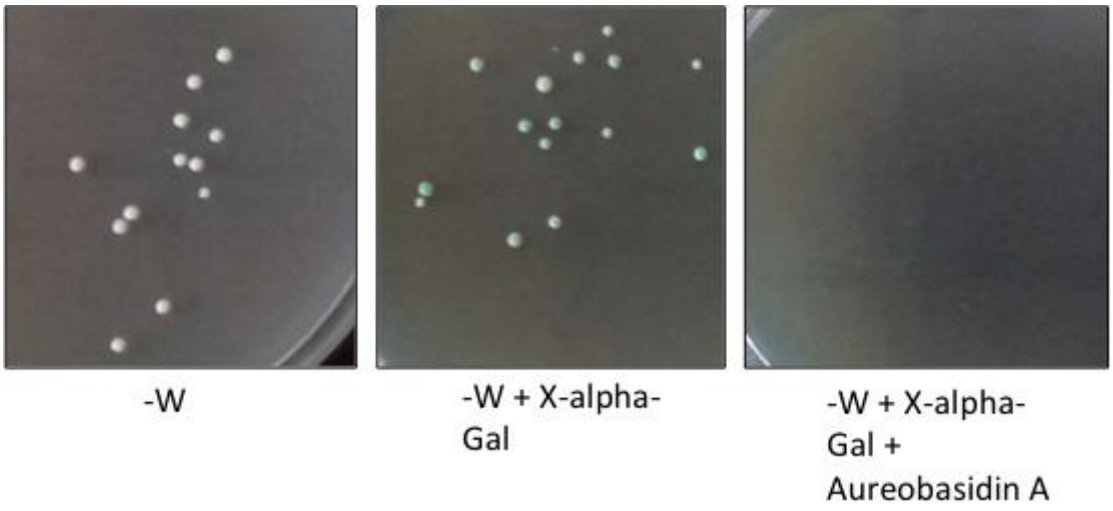

Figure 5.25 – **Example of bait auto-activation test for the Y2HGold system**. DHHC13N was transformed into Y2HGold and plated out onto –W, -W + X-alpha Gal, and –W + X-alpha Gal + Aureobasidin. To pass the auto-activation test, no growth should occur on plates containing the aureobasidin A.

Bait clones were then individually screened against a normalized brain pGADT7 library (Clontech). However, it should be noted that several aspects of the screening protocol had to be optimized, due to the facilities available in the lab. These differences are described in Chapter 2, section 2.8. As well as optimizing the protocol itself, the original library was also amplified to allow the screening of multiple baits (Chapter 2, section 2.8.4). Figure 5.26 and 5.27 show an example

plate following the screening process, on the double selection (-WL and Aureobasidin A) and quadruple selection (–WLAH, X-Alpha-Gal and Aureobasidin A plates), respectively.

The screening of DHHC8CT against the normalized brain library did give rise to a few colonies, but none of these had prey inserts. DHHC5CT, 13N and 17N all showed good transformation efficiencies (18.5 %, 11 % and 19.2 %), and many bands of different sizes were seen on a gel following yeast colony PCR amplification of prey.

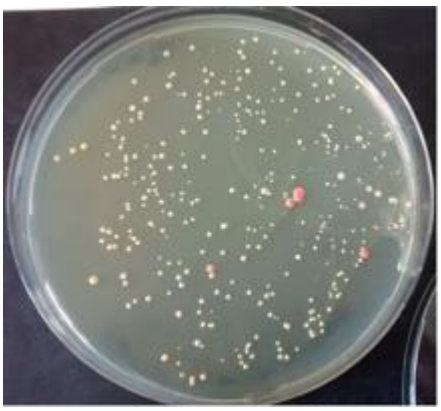

Figure 5.26 – **Example –WL + Aureobasidin A plate following screening of DHHC17N against the normalized brain library**. Colonies picked were more than 1 mm wide. Pink colonies were not picked.

The yeast colony PCR reaction is performed to amplify prey insert sequences of interacting proteins, which then need to be gap repaired back into the prey (pGADT7) vector. An example result is shown in Figure 5.28. The preys in this case were interaction partners of DHHC5CT. If the prey YCPCR fragment recombines with the cut pGADT7 prey vector, multiple colonies grow per spot (Chapter 2). Colonies were then picked and mated against the original bait construct in the reconfirmation test. Multiple spots failed the reconfirmation test, as the prey showed growth on selective plates when combined with both test bait and the

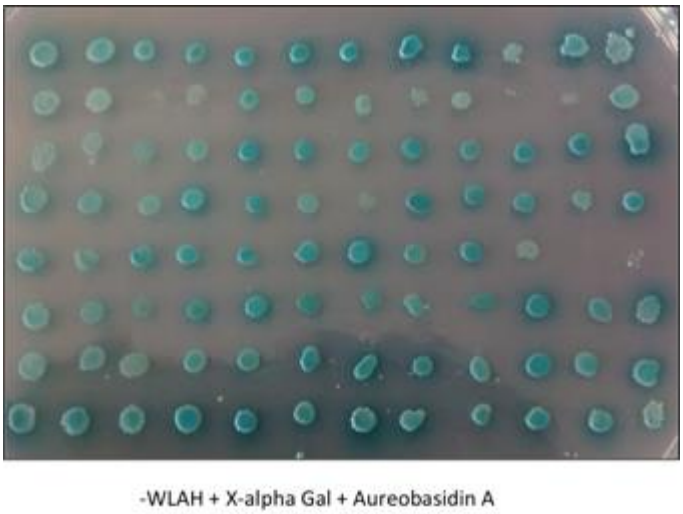

Figure 5.27 – **Example of bait screened against the normalized human brain library, when picked onto –WLAH + X-alpha-Gal + Aureobasidin A plates**. Colonies that displayed robust growth and turned blue were picked for further analysis.

negative control (empty-pGBKT7 vector). An example reconfirmation is shown in Figure 5.29. However, following the screens, 48 prey YCPCR fragments were elucidated from the zDHHC5CT, 27 from the zDHHC13N, and 39 from the zDHHC17N screens to send for sequencing. These were sent with the pGADT7.F sequencing vector.

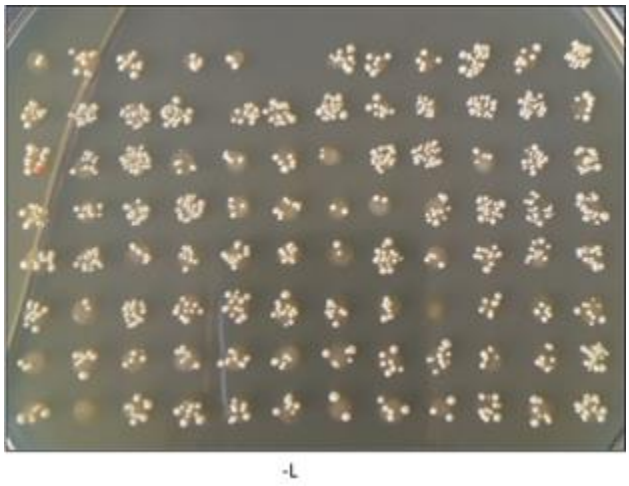

Figure 5.28 – **An example of a library gap repair reaction for the Y2HGold library screening**. Prey fragments are transformed with the cut pGADT7 vector into Y187 yeast. Image shows results from the zDHHC5CT library screen.

Results from this screen are shown in Tables 5.18, 5.19 and 5.20. The subcellular localization of these hits were also elucidated using the COMPARTMENTS web resource, to better understand whether the hits were logical (Binder et al., 2014). The localization of the interacting proteins is shown in Table 5.21. From Table 5.14 it can be see that zDHHC5 is localized in the plasma membrane and dendrites, zDHHC13 and 17 are both localized in the Golgi apparatus, whereas zDHHC13 is also localized in the endoplasmic reticulum.

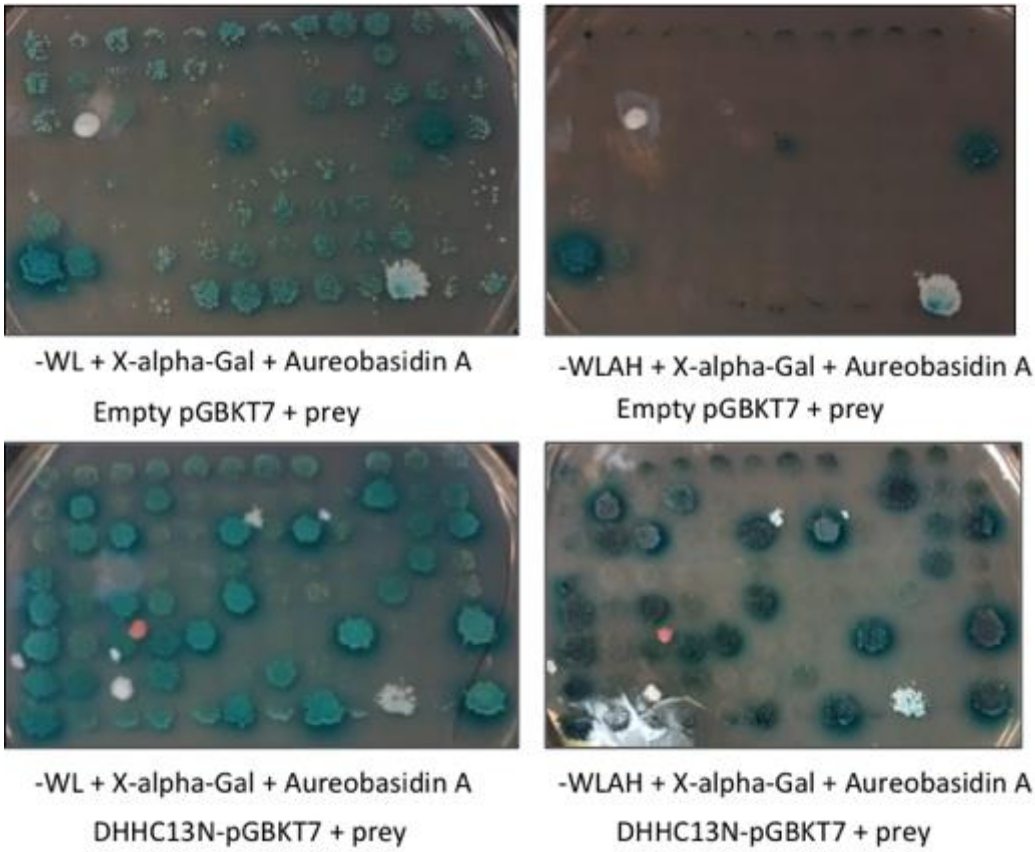

Figure 5.29 – **Example reconfirmation of preys against the bait of interest and the negative control.** Colonies that grew on the –WLAH + X-alpha-Gal + Aureobasidin plates, only in the presence of the bait vector, were considered positive hits and were sent for sequencing.

Gene Symbol	Brief Description
SNRPG	Core component of spliceosome U1, U2, U4 and U5 small nuclear ribonucleoproteins.
MFF	Mitochondrial fission factor. Promotes the recruitment and association of the fission mediator dynamin-related protein 1 (DNM1L) to the mitochondrial surface.
	May be involved in regulation of synaptic vesicle membrane dynamics by recruitment of DNM1L to clathrin-containing vesicles
PDE4DIP	Myomegalin. May function as an anchor sequestering components of cAMP-dependent pathway to Golgi and/or centrosomes
WDR61	Component of PAF1 complex. Functions during transcription by RNA polymerase II
RSL24D1	Involved in biogenesis of 60s ribosomal subunit
EFCAB7	EF-hand calcium-binding domain containing protein 7
NME7	Major role in the synthesis of nucleotide triphosphates other than ATP
RAB40B	May be a substrate-recognition component of a SCF-like ECS E3 ubiquitin ligase
CCNJ	Cyclin
ELAVL4	May play a role in neuron specific RNA processing
ZNF350	Transcriptional repressor

Table 5.18 - DHHC5CT interaction partners, elucidated from the normalized human brain library. Uniprot and NCBI were used to mine data about the interaction partners.

Gene Symbol	Brief Description
DCAF6	Ligand dependent co-factor of nuclear receptors
C19orf12	Small transmembrane protein. Mutations cause of a form of the hereditary spastic paraplegia (SPG43), and neurodegeneration with brain iron accumulation-4
EFEMP1	Binds EGFR, inducing EGFR autophosphorylation and activation of downstream signaling
EPRS	Glutamate/proline tRNA ligase
EIF1B	Translation factor
CCDC34	Chromosoal aberration involving CCDC34 found in patients with hamartoma of RPE and retina
NEMF	Component of ribosome quality control complex
MINA	Oxygenase that can act as both a histone lysine demethylase and ribosomal histidine hydroxylase
RAB7A	Key regulator in endolysosomal trafficking. Controls endosomal trafficking and neurite outgrowth. Charcot-marie-Tooth disease association
SAP18	Component of SIN3-repressing complex. Enhances SIN3-HDAC1 mediated transcriptional repression
CCDC65	May play role in motile cilia function.

Table 5.19 - Brief descriptions of the zDHHC13N interaction partners, elucidated from the normalized human brain library. Uniprot and NCBI were used to mine data about the interaction partners.

Gene Symbol	Brief Description
RAB7A	Key regulator in endolysosomal trafficking. Controls endosomal trafficking and neurite outgrowth. Charcot-marie-Tooth disease association
HNRNPL	Heterogeneous nuclear ribonucleoprotein L
APP	Amyloid Precursor Protein. Cell surface receptor/precursor protein cleaved to form a number of peptides, promoting transcriptional activation or amyloid plaques.
PICALM	Assembly protein recruiting clathrin and adapter protein complex 2 to the cell membrane. Involved in AP2-dependent clathrin mediated endocytosis at NMJ
RAB40B	May be a substrate-recognition component of a SCF-like ECS E3 ubiquitin ligase
ARHGAP21	Functions as GTPase activating protein for RhoA and CDC42.
PPIE	Accelerates protein folding, May be involved in pre-mRNA splicing
CCAR1	Cell division cycle and apoptosis regulator protein 1
CLIP3	Functions as cytoplasmic linker protein
NDUFA9	Accessory subunit of complex 1 in membrane respiratory chain. Associated with Alzheimers.
B2M	Component of MHC.
TAX1BP1	Inhibits TNF-induced apoptosis by mediating TNFAIP3 anti-apoptotic activity.
DHX9	Unwinds dsDNA and RNA in 3' to 5' direction.

Table 5.20 - DHHC17N interaction partners, elucidated from the normalized human brain library. Uniprot and NCBI were used to mine data about the interaction partners.

Gene Symbol	DHHC Interaction Partner	Localization (COMPARTMENTS)
C19orf12	DHHC13N	Mitochondrion, ER
CCDC34	DHHC13N	No evidence
CCDC65	DHHC13N	Cilium
DCAF6	DHHC13N	Cul4-Ring E3 ubiquitin ligase complex, nucleus, cytoplasm
EFEMP1	DHHC13N	Extracellular space
EIF1B	DHHC13N	No evidence
EPRS	DHHC13N	Cytoplasm
MINA	DHHC13N	Nucleus, Cytoplasm
NEMF	DHHC13N	Nucleus
SAP18	DHHC13N	Nuclear speck, ASAP complex, histone deacetylase complex
RAB7A	DHHC13N, DHHC17N	Lysosome, extracellular exosome, late endosome, phagocytic vesicle
APP	DHHC17N	membrane, dendritic spine, endosome, golgi, vesicle
ARHGAP21	DHHC17N	Cytoplasm
B2M	DHHC17N	Membrane, focal adhesion, extracellular exosome
CCAR1	DHHC17N	Nucleoplasm, perinuclear region of cytoplasm
CLIP3	DHHC17N	Recycling endosome membrane, early endosome membrane, trans-golgi network membrane
DHX9	DHHC17N	Nucleus
HNRNPL	DHHC17N	extracellular exosome, nucleoplasm
NDUFA9	DHHC17N	Mitochondrial matrix, mitochondrial membrane
PICALM	DHHC17N	golgi, clathrin-coated vesicle
PPIE	DHHC17N	Nucleus
TAX1BP1	DHHC17N	Extracellular exosome
CCNJ	DHHC5CT	nucleus
EFCAB7	DHHC5CT	primary cilium
ELAVL4	DHHC5CT	no evidence, could be ribonucleoprotein complex
MFF	DHHC5CT	mitochondrion outer membrane, tyep iv membrane protein, peroxisome, cytoplasmic vesicle,
		secretory vesicle, synaptic vesicle
NME7	DHHC5CT	centrosome, mitochondria
PDE4DIP	DHHC5CT	cytoskeleton, nucleus, golgi
RSL24D1	DHHC5CT	nucleus
SNRPG	DHHC5CT	spliceosome
WDR61	DHHC5CT	nucleus
ZNF350	DHHC5CT	nucleus
RAB40B	DHHC5CT, DHHC17N	plasma membrane

Table 5.21 - Subcellular localization of novel interaction partners of zDHHC5CT, zDHHC13N and zDHHC17N. Localization was determined using the COMPARTMENTS database (Binder et al., 2014).

5.3.11 Cloning fragments of zDHHC9

Fragments from zDHHC9 were also cloned. DHHC9 does not have a long cytoplasmic domain, or cytoplasmic regions with known interaction domains. For this reason, the C-terminal domain was first cloned (Table 5.17). Although this was successfully cloned into pGBKT7, only a few prey colonies grew on the double selection plates following library screening, and non of these passed the subsequent reconfirmation test. This may indicate that the C-terminal domain is not responsible for binding.

The N-terminal domain of zDHHC9 is very small, and so a fragment was cloned that extended from the N-terminus to the DHHC domain. Although this consisted of three trans-membrane domains, as mentioned previously, a similar *zDHHC17* truncation product had previously been used to identify hundreds of interaction partners (Butland et al., 2014). It is important to note however, that in the Butland et. al. study, several different DHHC17 baits were combined in one library screen.

In our hands, although the construct passed the bait auto-activation and toxicity testing, no colonies passed the reconfirmation stage. This indicates that interaction with zDHHC9 may require a co-factor, such as GCP16 (Swarthout et al., 2005a), or binding could in part require transmembrane domains. It is also possible that the fragments fold differently in comparison to the full-length protein.

The human PAT network was updated with the new interaction partners from both, the classical and MYTH screens performed in this study (Figure 5.30), with the novel interaction partners highlighted as yellow nodes. From this it can be seen that APP was previously known to interact with DHHC3, and SNRPG and RSL24D1 interacted with DHHC23.

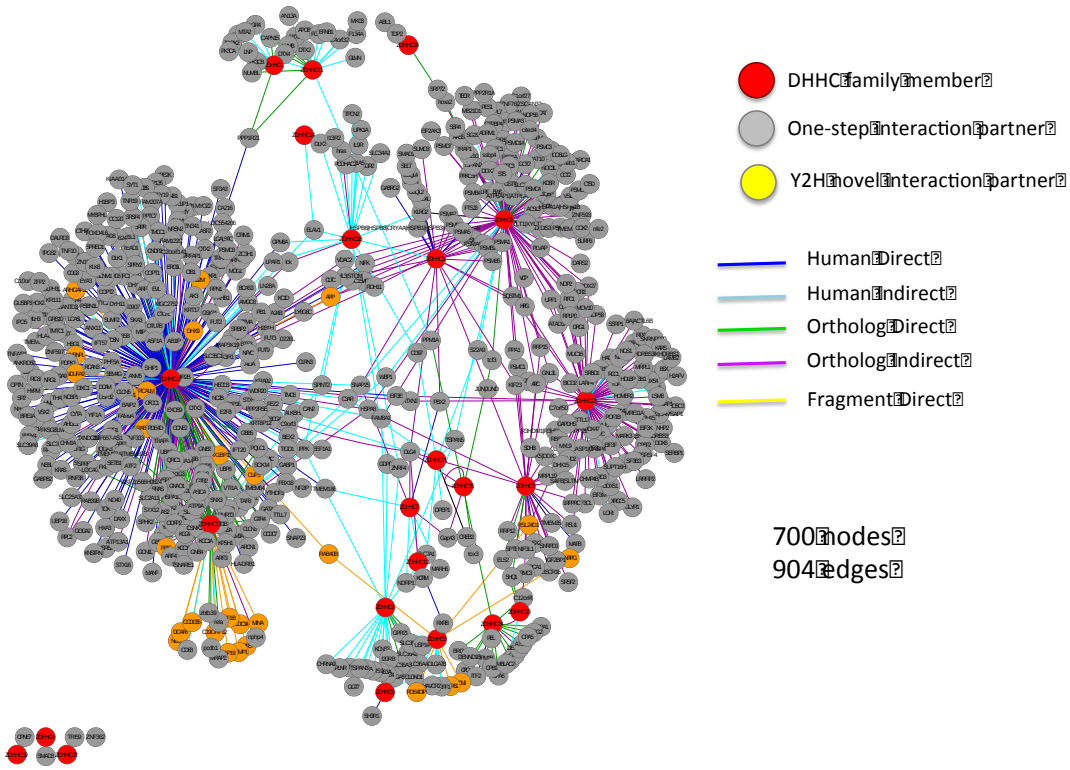

Figure 5.30 – **One step PAT network with updated novel yeast two-hybrid interaction partners.** Yellow nodes represent novel Y2H interaction partners, whereas yellow edges represent the novel interactions found in fragment Y2H library screens. PAT family members are shown as red nodes while grey nodes indicate non PAT one-step interaction partners. The edge colour denotes the type of interaction as indicated. Cytoscape v3.2.1 was used to generate this network, using the spring-embedded display.

5.4 Discussion

5.4.1 Elucidating a theory to explain the VPA phenotype

Many interesting phenotypes were observed in the *C. elegans* experiments, both when testing the mutants and neurosensitive RNAi mediated knockdowns. The discrepancies observed between the mutant and knockdown phenotypes could have occurred for several reasons. Firstly, RNAi is known to be less than 100 % efficient, and due to time limitations, no accurate measure to calculate knockdown efficiency was carried out. *Tu3335* has been reported to be more sensitive to neuronal RNAi but concerns remained with respect to the report of secondary *lin15-b* mutation in this strain (Calixto et al., 2010). Secondly, mutations are not targeted towards neurons, meaning that they occur throughout the worm. The RNAi, on the other hand, should be predominantly targeting neurons. This indicates that if an effect is observed in the mutant but not in the knockdown, the phenotype is due to defects at the muscular membrane, or even due to a secondary effect occurring in the worm.

It was previously suggested that as N2 is hypersensitive to aldicarb and VPA, in a similar way to the rate of paralysis of unc-25 mutants treated with aldicarb, the VPA might be inhibiting GABA neurotransmission in a similar manner (Munasinghe, 2015). Unc-25 encodes glutamic acid decarboxylase, which is involved in the biosynthesis of GABA (Jorgensen, 2005). By this theory, GABA biosynthesis is partially inhibited by VPA. Previously, VPA has been shown to increase GABA concentrations in the brain, possibly by inhibiting GABA catabolism (Lloyd, 2013). GABA is an inhibitory neurotransmitter in both *C. elegans* and mammalian brains. These opposing theories suggest that the role of VPA may either not be fully conserved between organisms, or its role is highly complex.

Multiple alternative mechanisms of VPA action have been proposed, making its molecular role very complex. For example, VPA has been reported to inhibit inositol-phosphate signaling in *C.* elegans (Yuan et al., 2001). It is important to note that the experiments in this paper revealed a resistance to paralysis when worms were treated with aldicarb and VPA. This could be due to differences in the assay methodology, as in their assay worms were picked onto plates containing VPA, then 2 hours later, picked onto plates containing aldicarb.

5.4.2 Decreased expression of PAT family members alters cholinergic and/or GABA signaling

If the previous theory that VPA partially inhibits GABA neurotransmission is correct, a mechanism to understand some of the phenotypes can be described. Nevertheless, it is vital to consider that VPA could instead be increasing excitatory neurotransmission, for example by moderately increasing acetylcholine secretion. This would lead to the same phenotype.

Under wild-type conditions the majority of worms do not paralyse following VPA treatment, as the change in GABA or acetylcholine levels may not be high enough to cause hypercontraction and paralysis. When aldicarb and VPA are combined, however, acetylcholine degradation is inhibited, meaning that there is a larger imbalance in the ratio of acetylcholine: GABA levels. This therefore leads to the increased rate of paralysis observed in the wild-type worms.

This theory can also be used to hypothesize why VPA induces paralysis in some mutants. When the expression of a gene involved in GABA and/or cholinergic neurotransmission is decreased, GABA neurotransmission may be further inhibited or cholinergic neurotransmission further excited, creating the large imbalance between the ratio of acetylcholine: GABA, which causes paralysis.

Both *dhhc-2* and *dhhc-13* mutants and knockdowns were paralyzed following treatment to VPA. This would lead to the suggestion that dhhc-2 and dhhc-13 play roles at the GABA synapse and/or the cholinergic synapse, thus have roles in excitatory and/or inhibitory neurotransmission. When added to the phenotypes seen when treated with aldicarb and levamisole, the role seems to be very complex.

Dhhc-2 mutants were resistant to levamisole, but showed no change in aldicarb-sensitivity. Knocking down *dhhc-2* in a neurosensitive strain however, lead to an increased resistance to aldicarb. This suggests that *dhhc-2* may be playing roles at both the pre- and post-synaptic terminals. For example, dhhc-2 may be involved in palmitoylating proteins required for GABA release, and also cholinergic receptors. When the mutant is treated with aldicarb, no phenotype is observed because a lower level of GABA has been secreted, but there are higher levels of cholinergic receptor. However, when *dhhc-2* is specifically knocked down in the neurons, the level of cholinergic receptors is not altered, thus resistance to aldicarb occurs. The reason for levamisole resistance could be that more nicotinic cholinergic receptors are produced/trafficked to the postsynaptic membrane, following *dhhc-2* mutation in comparison to levamisole-sensitive receptors.

When treated with both aldicarb and VPA, the *dhhc-2* mutants were less sensitive to paralysis than treated N2 worms. If mutating *dhhc-2* causes an increase in the number of cholinergic receptors and decreases GABA levels, this may explain this phenotype as the acetylcholine: GABA ratio is less skewed. However, it is necessary to point out that to elucidate the mechanism behind this phenotype, an experiment directly comparing *dhhc-2* mutants when treated with aldicarb and/or VPA is required.

Dhhc-13's closest human ortholog is DHHC13, which is a PAT family member associated to Huntington's disease, albeit not as strongly as DHHC17. Both the mutant and knocked down *dhhc-13* worms were paralyzed when treated with VPA. The *dhhc-1*3 mutant displayed hypersensitivity to aldicarb, but resistance to levamisole. This suggests that there may be an overall decrease in the number of cholinergic receptors, but that the proportion of receptors that are sensitive to levamisole has greatly decreased. Hence, both *dhhc-2* and *dhhc-13* may play a role in the trafficking or folding of subunits of the levamisole-sensitive cholinergic receptors.

When aldicarb and VPA treatments were combined, no difference was observed between dhhc-13 mutants (or knock downs) and wild type worms. However, it would be necessary to carry out an experiment to directly compare the *dhhc-13* mutant/knock down on aldicarb and/or VPA-treated plates, to elucidate the mechanism behind this phenotype. The phenotypes do suggest non-redundant

roles of at least these two PAT family members, and that both are vital for synaptic function.

Dhhc-14 also displayed some interesting phenotypes, and the closest human orthologs are DHHC17 (30 % identity, 47 % similarity, 14 % gaps) and DHHC13 (27 % identity, 48 % similarity, 12 % gaps). The *dhhc-14* mutant was resistant to aldicarb, but this was not observed in the neurosensitive knockdown, suggesting it may have a postsynaptic role. However, resistance to levamisole was only observed at one of the time points measured, indicating that *dhhc-14* does not play a significant role with regards to cholinergic signaling. *Dhhc-14* may instead play a role in GABA receptor subunit trafficking or folding. When mutated increased levels of GABA receptors may be functional at the postsynaptic membrane, leading to aldicarb resistance. However, when *dhhc-14* was knocked down, hypersensitivity was observed when treated with both aldicarb and VPA. In the knock down, the level of GABA receptors would not be altered, and therefore suggests that subtle changes in presynaptic cholinergic or GABA signaling may occur when the expression of dhhc-14 is decreased in neurons. This suggests that dhhc-14 is another interesting candidate for further study, and that it may be playing roles at both the pre- and post-synaptic terminals.

5.4.3 Novel interaction partners elucidated in the DHHC9 MYTH library screen

Many interesting proteins were elucidated in the DHHC9 screen. A paper published in 2014 chelated all known mammalian palmitoylated proteins from numerous high-throughput screens to create a palmitoylome (Sanders et al., 2015). If interacting proteins are found in this palmitoylome, the protein may be

a substrate of DHHC9. TECR and EMC4 were both shown to be palmitoylated in one and two studies, respectively. In addition, five studies found RTN4 to be palmitoylated, increasing the confidence of RTN4 being a novel substrate of DHHC9.

When analyzing the PAT network (Figure 5.20 and 5.30), TECR was found to interact with another PAT family member, DHHC6. SELK encodes selenoprotein K, and reports indicate that this protein acts as a cofactor of DHHC6 to palmitoylate inositol-1, 4, 5-triphosphate receptor (IP3R) in the endoplasmic reticulum (Hoffmann, 2016). The binding of SELK to DHHC6 is reported to be through its Src homology (SRC)-3 domain, which DHHC9 does not have. Therefore, it would be necessary to validate this interaction to understand where the interaction is occurring, and whether the interaction has a similar role to that of DHHC9's known cofactor, GCP16 (Swarthout et al., 2005b).

The COMPARTMENTS subcellular localization database was used to extract the predicted localization of the interaction partners (Binder et al., 2014). DHHC9 is localized in the ER and Golgi apparatus, and seven of the interaction partners and one non-specific partner co-localized in these organelles (Table 5.15 and 5.16). Nevertheless, proteins not localised in the ER, such as FZD1, may still require zDHHC9 interaction during their processing and thus should not be discounted at this stage.

The MYTH screening of zDHHC5, 8, 13 and 17 in the MYTH system was unsuccessful in our hands. All PAT family members have between four and six

trans-membrane domains, which may be the cause of the difficulty using these proteins in the MYTH system. It is plausible that the ER of the yeast has become oversaturated due to overexpression of these multiple trans-membrane proteins. This could prevent the proteins from being able to bind to their interaction partners. Matings of full-length PAT proteins have been carried out in a different membrane-based yeast-two-hybrid system (known as MBSUS, (Lemonidis et al., 2015)). This suggests a different system may be required to use the other PAT family members in a library.

5.4.4 Y2H screening of members of the mammalian PAT family

At the time of writing, no other Matchmaker Y2H screens had been carried out in the lab. This suggests that following future screens, some of the interaction partners may be found to be non-specific binding partners. To increase confidence in the interaction partners, the palmitoylome was used to elucidate interaction partners of the truncated PAT family members, which had been shown to be palmitoylated previously. None of the novel interaction partners of DHHC5CT were known to be palmitoylated. Five of the DHHC17N and three of DHHC13N

Gene Symbol	ID	DHHC Interactor	Source(s)
EFEMP1	2202	DHHC13N	wei 2014,
EPRS	2058	DHHC13N	kang 2008, martin 2009,
RAB7A	7879	DHHC13N, DHHC17N	kang 2008, martin 2012, wan 2014, wilson 2011
HNRNPL	3191	DHHC17N	wan 2014, wilson 2011
ARHGAP21	57584	DHHC17N	kang 2008, wan 2014,
NDUFA9	4704	DHHC17N	wan 2014
DHX9	1660	DHHC17N	wan 2014, wilson 2011

Table 5.22 - The palmitoylome database was used to determine which of the interaction partners from the yeast two-hybrid screen had been predicted to be palmitoylated.

partners had previously shown to be palmitoylated, including Rab7a, which was shared between these screens (Table 5.22).

Using the COMPARTMENTS website, we analysed the subcellular localizations of the interaction partners of the PAT family members and the interaction partners (Binder et al., 2014). Many were not annotated to have the same localization as the PAT proteins. For example, CSL and RSL24D1 are localized in the nucleus, yet zDHHC5 is localized at the plasma membrane and dendrites. This does not necessarily rule out an interaction, but does require further testing. One possible experiment would be to analyse the subcellular localization of the full length zDHHC5 in cells, and carry out co-localization studies with interaction partners.

Some proteins were found to co-localize with their interacting PAT family member. Rab40B is localized on the plasma membrane, which is the predominant localization of DHHC5. DHHC13 and DHHC17 localize in the ER and Golgi. C19orf12 was found to interact with DHHC13N and is localized in the ER. APP, PICALM and CLIP3 all have Golgi localizations and interacted with DHHC17. Due to the localization of DHHC13 and DHHC17, these enzymes may play a role in protein folding and assembly, rather than their final folded form.

Of note, CLIP3 has previously been shown to be both S-acylated as well as be an interaction partner of both DHHC13 and DHHC17. This protein therefore is acting as a positive control, demonstrating that the optimized Y2H screen is valid in determining physiologically relevant interaction partners. A paper published in 2015, described a novel sequence motif of substrate proteins binding to DHHC17 and DHHC13 – ΨβXXQP – where Ψ is an aliphatic amino acid (Valine, Isoleucine,

Alanine or Proline), β is a C-beta branched amino acid (Valine, Isoleucine or Threonine) and X is any amino acid (Lemonidis et al., 2015). The results of this paper indicate that CLIP3 had this consensus motif (VTMTQP). Of the novel zDHHC17 interaction partners, as well as CLIP3, PICALM (PVMTQP), ARHGAP21 (PVLTQP), B2M (VTLSQP), TAX1BP1 (VVCSQP) and DHX9 (IVVTQP) all had this consensus sequence. With respect to the zDHHC13 interaction partners, CCDC34 (PVISQP) and NEMF (PVKKQP) had this sequence. This suggests these proteins may be substrates of zDHHC13/17, although it is vital to check this via mutagenesis of these regions and carrying out Y2H matings with the full-length proteins.

One interesting cluster of proteins was found to interact with DHHC17N. Three genes; APP, NDUFA9 and PICALM are all associated with Alzheimer's disease. APP encodes amyloid-precursor protein and is vital in the development of Alzheimer's disease, as it cleaved to form the A_β peptides, which are found in amyloid plaques in the brains of patients. Interestingly, although APP has not been found in the palmitoylome database (Sanders et al., 2015), there are studies to demonstrate palmitoylation of APP by DHHC15, which has been suggested to target APP to lipid rafts and increase the processing of APP to the pathogenic A_β peptide via BACE1 cleavage (Bhattacharyya et al., 2013).

NDUFA9 is expressed in the hippocampus and also plays a role in Alzheimer's disease (L. Zhang et al., 2015). NDUFA9 plays a role in oxidative phosphorylation by acting as an accessory subunit to complex 1. Following KEGG analysis, NDUFA9 is also linked to Parkinson's and Huntington's disease. Furthermore it has been

shown to be palmitoylated (Sanders et al., 2015), suggesting it may be a substrate of zDHHC17.

PICALM has been elucidated as part of a susceptibility locus of late onset Alzheimer's disease through GWAS studies. Other data suggests that it plays a role in Alzheimer's disease by regulating the A_{β} peptide; through its production, trafficking and clearance (W. Xu, Tan, & Yu, 2015).

C19orf12 was found as a novel interaction partner of DHHC13N in our study, and would co-localize with full-length zDHHC13. C19orf12 is mutated in one form of hereditary spastic paraplegia (HSP) type 43 (SPG43). This is an autosomal recessive form of HSP (Landouré et al., 2013). C19orf12 is also mutated in a condition known as neurodegeneration with associated brain iron accumulation (NIBA). Although it has not previously been found to be palmitoylated, and it does not contain the ΨβXXQP consensus sequence, its pathological role makes it an interesting candidate for further study. As there is an overlap between zDHHC13 and zDHHC17 interaction partners, it would also be of interest to test the interaction between c19orf12 and zDHHC17.

Rab7a was found in the palmitoylome in four independent studies (Sanders et al., 2015). This protein is implicated in Charcot-Marie-Tooth disease, type 2B (CMT2B) (BasuRay, Mukherjee, Romero, Seaman, & Wandinger-Ness, 2013). Charcot-Marie-Tooth disease affects the peripheral nervous system, and type 2 is classified as having primary peripheral axonal neuropathy without obvious sign of myelin degeneration. It has been suggested that mutated forms of Rab7 may lead to the peripheral neuropathy by reducing its rate of membrane cycling. As

palmitoylation is known to play key roles in the cycling of other proteins (such as Ras proteins) between the cytosol and plasma membrane, it is plausible that palmitoylation of Rab7a is affected in the mutations. L129F, K157N, N161T and V162M are mutations that have been associated to CMT2B (BasuRay et al., 2013). Our study suggests that Rab7a interacts with both DHHC13 and 17, possibly via the N-Ankyrin repeat domain. This domain contains several ankyrin repeats, which may not only play a role in binding substrates, but also have other functions such as the activation of JNK signaling and suppression of heterotrimeric G-protein signaling. This association between the two N-ankyrin repeat-containing PATs and Charcot-Marie-Tooth disease is an interesting one, and the role of palmitoylation in this disease requires further study.

The C-terminal fragment of mouse *zDHHC8* did not work in this Y2H system. As can be seen in Table 5.13, the mouse and human orthologues share 92 % identity for the full-length proteins. When comparing the C-terminal fragments specifically they share 89.2% identity, 93.1% similarity and 0.5% gaps. Any differences between these sequences may be causing the lack of interaction partners. To test this, it would be necessary to generate C-terminal fragments of human *zDHHC8*, and screen this against the normalized foetal brain library. Alternatively, a mouse brain library could be tested with the mouse zDHHC8 ortholog.

5.4.5 Conclusions

In this chapter *C. elegans* were tested for their sensitivity to aldicarb, VPA, levamisole and the combination of aldicarb and VPA. Where possible, PAT family

mutants were also tested as well as *Tu3311* that had been knocked down with dsRNA targeting each of the PATs individually. This revealed many interesting phenotypes that require further study to establish the molecular basis of this phenotype. This study demonstrates that many PATs play a role at NMJs in *C. elegans*, and that the molecular basis of VPA action is still not clear.

In the Y2H studies, many novel interaction partners of DHHC5, 13 and 17 were elucidated, increasing our understanding of the PAT family. Clusters of these proteins have links to neurological disease; again highlighting the potential role that PAT proteins may play in neuropathology. A total of 17 novel interaction partners of DHHC9 were discovered using the MYTH system, although eight of these are possibly non-specific interaction partners. In future it will be necessary to find other techniques to elucidate interaction partners of the whole PAT family, and to determine their relevance in synaptic function.

Chapter 6 – Summary and Future Work

6.1 Screening genes with high connectivity and betweenness values in a one-step aldicarb network

This work aimed to elucidate novel effectors of synaptic function in *C. elegans*. For this the aldicarb-sensitivity assay was optimized and used, as it is a well-characterized technique for studying the effect of altered gene expression at NMJs. In order to elucidate novel effectors, genes were extracted, which were known to cause a change in aldicarb-sensitivity when their expression was altered. At the time of the study, 240 genes were known to cause delayed paralysis in the presence of aldicarb, and 12 genes were shown to cause an increased rate of paralysis.

Using merged Wormnet (Cho et al., 2014) and CCSB (Simonis et al., 2009) networks, interaction partners of these genes were extracted and mapped. Connectivity to genes known to cause a significant change in aldicarb sensitivity were measured and ranked. The top hundred candidates were then tested where appropriate, through genetic knockdown in the neurosensitive *Tu3311* strain. After independent validation, 19 novel genes were found to cause a RIC phenotype. It is important to note that many other genes did not re-confirm when independent testing was carried out. This could be due to differences in the efficiency of RNAi, or in the choice of a time point. In the future, the candidates who showed a phenotype in one high-throughput screen but not another, should be tested using full time course assays to check for this phenotype.

For the betweenness analysis core genes were added, which was associated with synaptic transmission GO terms. Another future experiment would be to re-calculate the connectivity rankings in the aldicarb and GO term one-step synaptic network, in order to elucidate other genes for analysis. This testing revealed there was a large degree of overlap between the connectivity and betweenness data sets. 10 novel genes were found to cause a change in aldicarb sensitivity, which were solely in the betweenness data set. The overlap may indicate that proteins of importance have both high connectivity and betweenness centrality. An exception of this is *unc-37*, whose knockdown caused a significant RIC phenotype, but has low connectivity to known aldicarb-sensitivity genes. This highlights that when elucidating lists of candidates to test, multiple factors including GO terms should be taken into account, and different forms of centrality used.

Both lists of novel positive effectors of aldicarb sensitivity were converted into human orthologs, and the synaptome database (Pirooznia et al., 2012) was used to predict whether the proteins were localized at the pre- or post-synaptic terminal. Interestingly, of the genes whose human orthologs were found in the database, the majority was post-synaptically localized. This is of interest, as in principle, the *Tu3311* strain should only be knocking down genes in neurons, and hence pre-synaptically at neuromuscular junctions. This may indicate that the gene is localized in a different neuronal type, such as sensory or interneurons. If synaptic transmission is affected in these neurons, this could also cause a defect in the response to being pressed by a wire and paralysis.

Future work is required to elucidate why the genetic knockdown of these genes leads to delayed paralysis of worms on aldicarb plates. This could be carried out through the microinjection of fluorescent constructs of interest into the wild-type worms (under the control of a pan-neuronal promoter), and examining the localization of the protein under a fluorescent microscope. For a higher spatial and temporal resolution on free moving worms, optogenics could also be carried out, which has been used successfully to analyze mechanosensory and motor neural circuits in *C. elegans*. Specific mutants of the genes of interest could also be generated and tested (for example, through the use of CRISPR (Katic & Grosshans, 2013)). If an effect was observed in the mutants, levamisole could be used to determine if the effect is pre- or post-synaptic (and whether the effect is occurring at cholinergic NMJ) (Locke et al., 2008). Due to the neuronal sensitivity of *Tu3311*, this strain is not suitable to be tested with levamisole (Calixto et al., 2010).

In future experiments it would be wise to check the RNAi efficiency prior to high throughput assays, in order to have confidence that the RNAi knockdown has been successful. This could be carried out through the use of real time polymerase chain reactions (RT-PCR) and western blots (with specific antibodies) following worm genetic knockdown and lysis, in order to determine whether the gene expression and protein levels decreased following knockdown (Ahringer, 2006). However, the number of potential candidate to be studied may restrict this level of detailed analysis in large-scale screens.

In the high throughput experiments, standard T-tests were used to filter for high confidence changes in aldicarb sensitivity. This meant that many genes were

found to be insignificant due to variability between plates. For this reason, in the future a different statistical test such as the chi^2 test (for categorical data) could be used, which may elucidate borderline candidates that could be tested further.

6.2 Using the VPA microarray to elucidate novel effectors of synaptic function

Other methods of elucidating novel effectors of synaptic function were also investigated. VPA is a drug used to treat epilepsy, but its mechanism of action is unclear (Lloyd, 2013). A microarray was carried out on wild-type *C. elegans*, which had been treated with varying concentrations of VPA. Analysis was carried out, and genes showing expression level changes were clustered. If the expression of two genes changes to a similar extent, they are likely to be working together, for example in a signaling or metabolic pathway. This analysis was combined with a basic RIC one-step Wormnet (version 1) network, generating modules of genes known to cause a RIC phenotype, and genes that had not been tested for an aldicarb-sensitivity phenotype previously. The original microarray analysis and network generation were created prior to the work carried out here, and all networks used bar this one used the latest versions of Wormnet (Cho et al., 2014) and CCSB (Simonis et al., 2009). One piece of work that could be carried out in the future would be to re-generate the modules using the updated Wormnet, and the most up-date one-step RIC and HIC network. This may generate more leads to be tested by the aldicarb-sensitivity assay.

The hits found in this analysis should also be analyzed further. This is discussed in detail in Chapter 4.4. Sel-12 is a specifically interesting gene for further study

due to it being an ortholog of PSEN2. PSEN2, PSEN1 and APP are the three main genes linked to early onset Alzheimer's disease. PSEN2 mutations are the least common, with only 19 potentially pathogenic mutations having been discovered (Jayadev et al., 2010). As PSEN2 was not found in the SynaptomeDB to be localized in the pre- and post-synaptic terminals, it would be interesting to analyze the localization of PSEN2 in human or mouse neuronal cell lines. This would improve our understanding of whether it serves a conserved function between mammals and worms. Furthermore, in *C. elegans* further study could be carried out through the use of mutant strains and carrying out full time course pharmacological assays (such as aldicarb- and levamisole-sensitivity assays).

In the work leading up to the microarray analysis, VPA was shown to cause paralysis in specific *C. elegans* mutants, such as *sma*-6 (Munasinghe, 2015). Another interesting experiment could be to test these knockdowns with VPA, to elucidate whether the worms underwent VPA-induced paralysis. This may give a better insight into the role that VPA plays in both *C. elegans* and humans.

6.3 VPA as an effector of synaptic function

The focus of the research was then switched onto VPA itself, as it appears to be a drug that alters synaptic function from the worm microarray analysis as well as other literature. In order to understand the role VPA plays at the synapse, the VPA microarray data in *C. elegans* was re-analyzed, and information was extracted from other microarrays. When re-analyzing the microarray data, genes were listed if they significantly increased or decreased in expression following VPA treatment.

Other microarrays were then downloaded and analyzed using identical algorithms in R. After finding the *C. elegans* orthologs of the differentially expressed genes, the data was compared and many processes were shared, especially in neurodevelopment.

From this microarray data, many other interesting genes were found to be significantly up or down regulated in *C. elegans*. To further this work, genes of interest could be knocked down in a neurosensitive strain and tested for a change in aldicarb sensitivity. This would provide a link between the microarray analysis and phenotypic effects in *C. elegans,* and further link VPA to synaptic function. Examples of interesting genes would be lrx-1, asp-12 and zmp-2, which all are reported to be part of the presenilin pathway, and were down regulated in response to VPA. The closest ortholog of asp-12 is Beta-site amyloid precursor protein-cleaving enzyme (BACE2). Increased BACE2 protein and mRNA levels have been found in the frontal lobe of patients with Down's syndrome and Alzheimer's disease (Barbiero et al., 2003).

In research carried out in this study as well as from previous work (Munasinghe, 2015), VPA-induced paralysis was observed in some worm mutants and RNAi strains. Given that VPA has been shown to extend *C. elegans* lifespan, other phenotypes could also be studied, such as morphology and behavioural assays. An example of a behavioural assay is thrashing, as decreased thrashing can be a sign of neurodegeneration (Edmonds & Morgan, 2014).

Conserved genes and pathways could also be tested using different experimental techniques. One example of an interesting gene to investigate further is *C. elegans* fpn-1.2, whose mouse ortholog is SLC40A1 and whose human ortholog is ferroportin. As this protein has been described to be involved in neural tube closure (Mao et al., 2010), it could be an important gene modified by VPA. To test whether such genes are of importance, they could be knocked down in neurologically relevant cell lines and phenotypic characteristics elucidated. These cells could also be treated with a physiologically relevant concentration of VPA, and QPCRs carried out to validate whether these genes are up and down regulated as expected. Microarrays could also be carried out on these cells, as to date, there are no published microarrays following the treatment of human neuronal cell lines with VPA. It would be necessary to use a therapeutically relevant dosage for these experiments.

Two distinct groups of microarrays were analyzed or extracted in this work – those that were related to development, for example mouse embryo brain cultures, and those that were found in the adult, for example rat brain. This revealed distinct patterns of gene expression changes. The key process shared between the majority of the data sets were changes in genes related to neuronal differentiation and development. Given the teratogenicity of VPA, these changes may help to explain the molecular basis of the defects. In the adult rat brain, changes in genes related to synaptic transmission, learning and memory were also elucidated, confirming VPA's possible role at the synapse outside of development.

The analysis of microarray data carried out in Chapter 4 links VPA treatment to several neurodegenerative diseases, namely Alzheimer's and Huntington's disease. VPA has been shown to have beneficial motor, behavioural and lifespan effects in both cellular and mouse models of Huntington's disease. Treatment in humans however has been controversial (Scheuing, Chiu, Liao, Linares, & Chuang, 2014). In addition, few theories have been proposed to explain this beneficial effect. The human or mouse orthologs of these genes would be ideal choices for the QPCR analysis mentioned previously. Y18D10.22 was down regulated in response to VPA, whose closest human ortholog is HIP1. HIP1 is one of the most widely studied interactors of huntingtin, and from this, could provide a link between the proposed beneficial roles of VPA. Huntingtin levels itself could also be checked following cell treatment with VPA to elucidate which pathways are being affected by VPA. From the KEGG analysis of the adult rat brain data a further seven genes were linked to Huntington's disease, and eight to Alzheimer's disease. These therefore add to the theory that VPA affects processes linked to these two diseases.

6.4 Understanding the role of PAT family members at the NMJ

When dhhc-2 was knocked down in *Tu3311*, a significant resistance to paralysis was seen when the knocked down worms were picked onto aldicarb plates. For this reason the rest of the PAT family were tested, as these experiments had not been previously carried out and published, and the family were an interesting family to study, given their links to intellectual disability and neurodegenerative diseases.

The results from chapter 5 require much further study. Firstly, from the worm work, full time course assays should be carried out on *Tu3311* knocked down with each PAT. Previously, few phenotypes were elucidated from the PAT worm family. These phenotypes could be re-analyzed following the knockdown of the PAT family in the neurosensitive *Tu3311* or *Tu3335* strain, and then analyzing the morphological and behavioural phenotypes carried out previously (Edmonds & Morgan, 2014). Wild type and *rrf-3* worms could also be knocked down with each PAT family member. Aldicarb-sensitivity assays would then reveal the strains that an effect was seen in, and allow hypotheses to be generated to explain the reasoning behind this. Double knockdowns of the PAT family could also be carried out.

In the Y2H work, many interesting interaction partners of certain fragments of human and mouse PAT family members were identified. The N-terminal fragment of DHHC17 provided the greatest number of interesting hits, as three proteins were linked to Alzheimer's disease, one of which was APP. The N-terminal fragment of DHHC13 was shown to bind to c19orf12, whose mutations are known to cause hereditary spastic paraplegia type 43.

The first experiment to be carried out following this work would be the validation of interactions through the use of Y2H matings. As c19orf12 is mutated in SPG43, one experiment would be to clone c19orf12, and then specifically mutate the gene to the form found in SPG43. The interaction of DHHC13 against the mutated c19orf12 could then be tested. Co-localization of the full length PATs and

proposed interaction partners could also be determined in neuronal cell lines. Co-immunoprecipitation experiments could also be carried out as a validation technique. Another interesting area to explore would be to discover whether the interaction partners are palmitoylated by the PAT of interest, for example DHHC17. For example, acyl resin assisted capture (acyl-RAC) coupled to mass spectrometry could be used to determine endogenous palmitoylation sites of specific proteins (Forrester et al., 2011).

In the time frame available, the only construct that functioned in the MYTH library system was DHHC9. There is a variation of MYTH that has been used to carry out matings with PAT family members previously, known as MbSUS (Grefen, Obrdlik, & Harter, 2009). This could be used in the future, as well as re-testing the MYTH constructs in the four other recommended vectors (two of which are N-terminal, three are C-terminal) (Lemonidis, Gorleku, Sanchez-Perez, Grefen, & Chamberlain, 2014; Stagljar & Fields, 2002). Constructs could also be sent to companies that specialize in high throughput Y2H assays, such as Dualsystems.

Nevertheless the Y2H work elucidated interaction partners that provide new links between PATs and neurological processes, which in the future may help in the better understanding of diseases such as Alzheimer's disease, and may provide clues as to novel therapeutics.

References

Ahringer, J. (2006). Reverse genetics. *WormBook*. http://doi.org/10.1895/wormbook.1.47.1

Alkema, M. J., Hunter-Ensor, M., Ringstad, N., & Horvitz, H. R. (2005). Tyramine functions independently of octopamine in the Caenorhabditis elegans nervous system. *Neuron*, *46*(2), 247–260. http://doi.org/10.1016/j.neuron.2005.02.024

Allache, R., De Marco, P., Merello, E., Capra, V., & Kibar, Z. (2012). Role of the planar cell polarity gene CELSR1 in neural tube defects and caudal agenesis. *Birth Defects Research Part A - Clinical and Molecular Teratology*, *94*(3), 176–181. http://doi.org/10.1002/bdra.23002

Alsdorf, R., & Wyszynski, D. F. (2005). Teratogenicity of sodium valproate. *Expert Opinion on Drug Safety*, *4*(2), 345–53. http://doi.org/10.1517/14740338.4.2.345

Barbiero, L., Benussi, L., Ghidoni, R., Alberici, A., Russo, C., Schettini, G., … Binetti, G. (2003). BACE-2 is overexpressed in Down's syndrome. *Experimental Neurology*, *182*(2), 335–345. http://doi.org/10.1016/S0014-4886(03)00049-9

BasuRay, S., Mukherjee, S., Romero, E. G., Seaman, M. N. J., & Wandinger-Ness, A. (2013). Rab7 mutants associated with Charcot-Marie-Tooth disease cause delayed growth factor receptor transport and altered endosomal and nuclear signaling. *Journal of Biological Chemistry*, *288*(2), 1135–1149. http://doi.org/10.1074/jbc.M112.417766

Bates, G. (2003). Huntingtin aggregation and toxicity in Huntington's disease. *Lancet*. http://doi.org/10.1016/S0140-6736(03)13304-1

Beadle, G. W., & Tatum, E. L. (1941). Genetic Control of Biochemical Reactions in Neurospora. *Proceedings of the National Academy of Sciences of the United States of America*, *27*(11), 499–506. http://doi.org/10.1086/281267

Ben-Salem, S., Al-Shamsi, A. M., John, A., Ali, B. R., & Al-Gazali, L. (2015). A Novel Whole Exon Deletion in WWOX Gene Causes Early Epilepsy, Intellectual Disability and Optic Atrophy. *Journal of Molecular Neuroscience*, *56*(1), 17–23. http://doi.org/10.1007/s12031-014-0463-8

Bhattacharyya, R., Barren, C., & Kovacs, D. M. (2013). Palmitoylation of Amyloid Precursor Protein Regulates Amyloidogenic Processing in Lipid Rafts. *The Journal of Neuroscience*, *33*(27), 11169–83. http://doi.org/10.1523/JNEUROSCI.4704-12.2013

Binder, J. X., Pletscher-Frankild, S., Tsafou, K., Stolte, C., O'Donoghue, S. I., Schneider, R., & Jensen, L. J. (2014). COMPARTMENTS: unification and visualization of protein subcellular localization evidence. *Database : The Journal of Biological Databases and Curation*, *2014*. http://doi.org/10.1093/database/bau012

Blaskovic, S., Blanc, M., & Van Der Goot, F. G. (2013). What does S-palmitoylation do to membrane proteins? *FEBS Journal*. http://doi.org/10.1111/febs.12263

Bosetti, F., Bell, J. M., & Manickam, P. (2005). Microarray analysis of rat brain gene expression after chronic administration of sodium valproate. *Brain Research Bulletin*, *65*(4), 331–338. http://doi.org/10.1016/j.brainresbull.2005.01.004

Boutin, C., Goffinet, A. M., & Tissir, F. (2012). Celsr1-3 Cadherins in PCP and Brain Development.

Current Topics in Developmental Biology, *101*, 161–183. http://doi.org/10.1016/B978-0-12-394592-1.00010-7

Brenner, S. (1974). The genetics of Caenorhabditis elegans. *Genetics*, *77*, 71–94. http://doi.org/10.1002/cbic.200300625

Brigidi, G. S., Santyr, B., Shimell, J., Jovellar, B., & Bamji, S. X. (2015). Activity-regulated trafficking of the palmitoyl-acyl transferase DHHC5. *Nature Communications*, *6*, 8200. http://doi.org/10.1038/ncomms9200

Brigidi, G. S., Sun, Y., Beccano-Kelly, D., Pitman, K., Mobasser, M., Borgland, S. L., … Bamji, S. X. (2014). Palmitoylation of δ-catenin by DHHC5 mediates activity-induced synapse plasticity. *Nature Neuroscience*, *17*(4), 522–32. http://doi.org/10.1038/nn.3657

Brockie, P. J., & Maricq, A. V. (2006). Ionotropic glutamate receptors: genetics, behavior and electrophysiology. *WormBook : The Online Review of C. Elegans Biology*, 1–16. http://doi.org/10.1895/wormbook.1.61.1

Bullitt, E. (1990). Expression of c-fos-like protein as a marker for neuronal activity following noxious stimulation in the rat. *The Journal of Comparative Neurology*, *296*(4), 517–530. http://doi.org/10.1002/cne.902960402

Butland, S. L., Sanders, S. S., Schmidt, M. E., Riechers, S. P., Lin, D. T. S., Martin, D. D. O., … Hayden, M. R. (2014). The palmitoyl acyltransferase HIP14 shares a high proportion of interactors with huntingtin: Implications for a role in the pathogenesis of Huntington's disease. *Human Molecular Genetics*, *23*(15), 4142–4160. http://doi.org/10.1093/hmg/ddu137

Calixto, A., Chelur, D., Topalidou, I., Chen, X., & Chalfie, M. (2010). Enhanced neuronal RNAi in C. elegans using SID-1. *Nat Methods*, *7*(7), 554–559. http://doi.org/10.1038/nmeth.1463

Cassada, R. C., & Russell, R. L. (1975). The dauerlarva, a post-embryonic developmental variant of the nematode Caenorhabditis elegans. *Developmental Biology*, *46*(2), 326–342. http://doi.org/10.1016/0012-1606(75)90109-8

Chase, D. L., & Koelle, M. R. (2007). Biogenic amine neurotransmitters in C. elegans. *WormBook : The Online Review of C. Elegans Biology*, 1–15. http://doi.org/10.1895/wormbook.1.132.1

Chen, X., Barclay, J. W., Burgoyne, R. D., & Morgan, A. (2015). Using C. elegans to discover therapeutic compounds for ageing-associated neurodegenerative diseases. *Chemistry Central Journal*, *9*, 65. http://doi.org/10.1186/s13065-015-0143-y

Cho, A., Shin, J., Hwang, S., Kim, C., Shim, H., Kim, H., … Lee, I. (2014). WormNet v3: A network-assisted hypothesis-generating server for Caenorhabditis elegans. *Nucleic Acids Research*, *42*(W1). http://doi.org/10.1093/nar/gku367

Christensen, J., Grønborg, T. K., Sørensen, M. J., Schendel, D., Parner, E. T., Pedersen, L. H., & Vestergaard, M. (2013). Prenatal valproate exposure and risk of autism spectrum disorders and childhood autism. *Jama*, *309*(16), 1696–703. http://doi.org/10.1001/jama.2013.2270

Christian, J., Ximenes, M., Crisóstomo, E., Verde, L., Da, M., Naffah-Mazzacoratti, G., & Socorro De Barros Viana, G. (2012). Valproic Acid, a Drug with Multiple Molecular Targets Related to Its Potential Neuroprotective Action. *Neuroscience & Medicine*, *3*, 107–123. http://doi.org/10.4236/nm.2012.31016

Combes, D., Fedon, Y., Toutant, J. P., & Arpagaus, M. (2003). Multiple ace genes encoding acetylcholinesterases of Caenorhabditis elegans have distinct tissue expression. *European Journal of Neuroscience*, *18*(3), 497–512. http://doi.org/10.1046/j.1460-9568.2003.02749.x

Corominas, R., Yang, X., Lin, G. N., Kang, S., Shen, Y., Ghamsari, L., … Iakoucheva, L. M. (2014). Protein interaction network of alternatively spliced isoforms from brain links genetic risk factors for autism. *Nature Communications*, *5*, 3650. http://doi.org/10.1038/ncomms4650

Corsi, A. K., Wightman, B., & Chalfie, M. (2015). A transparent window into biology: A primer on Caenorhabditis elegans. *Genetics*, *200*(2), 387–407. http://doi.org/10.1534/genetics.115.176099

Danbolt, N. C. (2001). Glutamate uptake. *Progress in Neurobiology*. http://doi.org/10.1016/S0301-0082(00)00067-8

Dawidowski, D., & Cafiso, D. S. (2016). Munc18-1 and the Syntaxin-1 N Terminus Regulate Open-Closed States in a t-SNARE Complex. *Structure*, *24*(3), 392–400. http://doi.org/10.1016/j.str.2016.01.005

del Castillo, J., De Mello, W. C., & Morales, T. (1963). The physiological role of acetylcholine in the neuromuscular system of *ascaris lumbricoides*. *Archives Internationales de Physiologie et de Biochimie*, *71*(5), 741–757. http://doi.org/10.3109/13813456309092194

Drisdel, R. C., & Green, W. N. (2004). Labeling and quantifying sites of protein palmitoylation. *BioTechniques*, *36*(2), 276–85. Retrieved from http://www.ncbi.nlm.nih.gov/pubmed/14989092

Du, W., Bautista, J. F., Yang, H., Diez-Sampedro, A., You, S.-A., Wang, L., … Wang, Q. K. (2005). Calcium-sensitive potassium channelopathy in human epilepsy and paroxysmal movement disorder. *Nature Genetics*, *37*(7), 733–738. http://doi.org/10.1038/ng1585

Edmonds, M. J., & Morgan, A. (2014). A systematic analysis of protein palmitoylation in Caenorhabditis elegans. *BMC Genomics*, *15*(1), 841. http://doi.org/10.1186/1471-2164-15-841

Eisenberg, S., Laude, A. J., Beckett, A. J., Mageean, C. J., Aran, V., Hernandez-Valladares, M., … Prior, I. A. (2013). The role of palmitoylation in regulating Ras localization and function. *Biochemical Society Transactions*, *41*(1), 79–83. http://doi.org/10.1042/BST20120268

El-Husseini, A. E. D., Schnell, E., Dakoji, S., Sweeney, N., Zhou, Q., Prange, O., … Bredt, D. S. (2002). Synaptic strength regulated by palmitate cycling on PSD-95. *Cell*, *108*(6), 849–863. http://doi.org/10.1016/S0092-8674(02)00683-9

Evason, K., Collins, J. J., Huang, C., Hughes, S., & Kornfeld, K. (2008). Valproic acid extends Caenorhabditis elegans lifespan. *Aging Cell*, *7*, 305–317. http://doi.org/10.1111/j.1474-9726.2008.00375.x

Feinberg, E. H., VanHoven, M. K., Bendesky, A., Wang, G., Fetter, R. D., Shen, K., & Bargmann, C. I. (2008). GFP Reconstitution Across Synaptic Partners (GRASP) Defines Cell Contacts and Synapses in Living Nervous Systems. *Neuron*, *57*(3), 353–363. http://doi.org/10.1016/j.neuron.2007.11.030

Fields, S., & Song, O. (1989). A novel genetic system to detect protein-protein interactions. *Nature*, *340*(6230), 245–6. http://doi.org/10.1038/340245a0

Forrester, M. T., Hess, D. T., Thompson, J. W., Hultman, R. C., Moseley, M. A., Stamler, J. S., & Casey, P. J. (2011). Site-specific analysis of protein S-acylation by resin-assisted capture (Acyl-RAC). *J Lipid Res*, *52*, 393–398. http://doi.org/10.1194/jlr.D011106

Fraser, A. G., Kamath, R. S., Zipperlen, P., Martinez-Campos, M., Sohrmann, M., & Ahringer, J. (2000). Functional genomic analysis of C. elegans chromosome I by systematic RNA interference. *Nature*, *408*(6810), 325–330. http://doi.org/10.1038/35042517

Frøkjær-Jensen, C. (2013). Exciting prospects for precise engineering of Caenorhabditis elegans genomes with CRISPR/Cas9. *Genetics*, *195*(3), 635–42. http://doi.org/10.1534/genetics.113.156521

Fromer, M., Pocklington, A. J., Kavanagh, D. H., Williams, H. J., Dwyer, S., Gormley, P., … O'Donovan, M. C. (2014). De novo mutations in schizophrenia implicate synaptic networks. *Nature*, *506*(7487), 179–184. http://doi.org/10.1038/nature12929

Fujiki, R., Sato, A., Fujitani, M., & Yamashita, T. (2013). A proapoptotic effect of valproic acid on progenitors of embryonic stem cell-derived glutamatergic neurons. *Cell Death and Disease*, *4*(6), e677. http://doi.org/10.1038/cddis.2013.205

Fukata, Y., & Fukata, M. (2010). Protein palmitoylation in neuronal development and synaptic plasticity. *Nature Reviews. Neuroscience*, *11*(3), 161–175. http://doi.org/10.1038/nrn2788

Fukuchi, M., Nii, T., Ishimaru, N., Minamino, A., Hara, D., Takasaki, I., … Tsuda, M. (2009). Valproic acid induces up- or down-regulation of gene expression responsible for the neuronal excitation and inhibition in rat cortical neurons through its epigenetic actions. *Neuroscience Research*, *65*(1), 35–43. http://doi.org/10.1016/j.neures.2009.05.002

Girgenti, M. J., LoTurco, J. J., & Maher, B. J. (2012). ZNF804a regulates expression of the schizophrenia-associated genes PRSS16, COMT, PDE4B, and DRD2. *PLoS ONE*, *7*(2). http://doi.org/10.1371/journal.pone.0032404

Göttlicher, M., Minucci, S., Zhu, P., Krämer, O. H., Schimpf, A., Giavara, S., … Heinzel, T. (2002). Valproic acid defines a novel class of HDAC inhibitors inducing differentiation of transformed cells. *EMBO Journal*, *20*(24), 6969–6978. http://doi.org/10.1093/emboj/20.24.6969

Greaves, J., Carmichael, J. a, & Chamberlain, L. H. (2011). The palmitoyl transferase DHHC2 targets a dynamic membrane cycling pathway: regulation by a C-terminal domain. *Molecular Biology of the Cell*, *22*(11), 1887–1895. http://doi.org/10.1091/mbc.E10-11-0924

Greaves, J., Gorleku, O. A., Salaun, C., & Chamberlain, L. H. (2010). Palmitoylation of the SNAP25 protein family: Specificity and regulation by DHHC palmitoyl transferases. *Journal of Biological Chemistry*, *285*(32), 24629–24638. http://doi.org/10.1074/jbc.M110.119289

Greaves, J., Lemonidis, K., Gorleku, O. A., Cruchaga, C., Grefen, C., & Chamberlain, L. H. (2012). Palmitoylation-induced aggregation of cysteine-string protein mutants that cause neuronal ceroid lipofuscinosis. *Journal of Biological Chemistry*, *287*(44), 37330–37339.

http://doi.org/10.1074/jbc.M112.389098

Greaves, J., Prescott, G. R., Gorleku, O. a, & Chamberlain, L. H. (2010). Regulation of SNAP-25 trafficking and function by palmitoylation. *Biochemical Society Transactions*, *38*(April 2009), 163–166. http://doi.org/10.1042/BST0380163

Grefen, C., Obrdlik, P., & Harter, K. (2009). The determination of protein-protein interactions by the mating-based split-ubiquitin system (mbSUS). *Methods in Molecular Biology*, *479*, 217–233. http://doi.org/10.1007/978-1-59745-289-2-14

Grishok, A. (2005). RNAi mechanisms in Caenorhabditis elegans. *FEBS Letters*. http://doi.org/10.1016/j.febslet.2005.08.001

Guan, X., & Fierke, C. A. (2011). Understanding protein palmitoylation: Biological significance and enzymology. *Science China Chemistry*. http://doi.org/10.1007/s11426-011-4428-2

Hansen, J., Corydon, T. J., Palmfeldt, J., Dürr, A., Fontaine, B., Nielsen, M. N., … Bross, P. (2008). Decreased expression of the mitochondrial matrix proteases Lon and ClpP in cells from a patient with hereditary spastic paraplegia (SPG13). *Neuroscience*, *153*(2), 474–482. http://doi.org/10.1016/j.neuroscience.2008.01.070

Hekman, K. E., Yu, G. Y., Brown, C. D., Zhu, H., Du, X., Gervin, K., … Gomez, C. M. (2012). A conserved eEF2 coding variant in SCA26 leads to loss of translational fidelity and increased susceptibility to proteostatic insult. *Human Molecular Genetics*, *21*(26), 5472–5483. http://doi.org/10.1093/hmg/dds392

Henderson, M. X., Wirak, G. S., Zhang, Y.-Q., Dai, F., Ginsberg, S. D., Dolzhanskaya, N., … Chandra, S. S. (2016). Neuronal ceroid lipofuscinosis with DNAJC5/CSPα mutation has PPT1 pathology and exhibit aberrant protein palmitoylation. *Acta Neuropathologica*, *131*(4), 621–37. http://doi.org/10.1007/s00401-015-1512-2

Herrero-Mendez, A., Almeida, A., Fernández, E., Maestre, C., Moncada, S., & Bolaños, J. P. (2009). The bioenergetic and antioxidant status of neurons is controlled by continuous degradation of a key glycolytic enzyme by APC/C-Cdh1. *Nature Cell Biology*, *11*(6), 747–52. http://doi.org/10.1038/ncb1881

Heuser, J. E., & Reese, T. S. (1973). Evidence for recycling of synaptic vesicle membrane during transmitter release at the frog neuromuscular junction. *The Journal of Cell Biology*, *57*(2), 315–44. Retrieved from http://www.ncbi.nlm.nih.gov/pubmed/4348786

Heuser, J. E., Reese, T. S., Dennis, M. J., Jan, Y., Jan, L., & Evans, L. (1979). Synaptic vesicle exocytosis captured by quick freezing and correlated with quantal transmitter release. *The Journal of Cell Biology*, *81*(2), 275–300. Retrieved from http://www.ncbi.nlm.nih.gov/pubmed/38256

Hill, E. J., Nagel, D. A., O'Neil, J. D., Torr, E., Woehrling, E. K., Devitt, A., & Coleman, M. D. (2013). Effects of Lithium and Valproic Acid on Gene Expression and Phenotypic Markers in an NT2 Neurosphere Model of Neural Development. *PLoS ONE*, *8*(3). http://doi.org/10.1371/journal.pone.0058822

Hoffmann, P. R. (2016). Selenoprotein K and Protein Palmitoylation in Regulating Immune Cell Functions. In *Selenium* (pp. 245–252). Cham: Springer International Publishing.

http://doi.org/10.1007/978-3-319-41283-2_20

Hortsch, M., Burmeister, M., Ren, Q., Makris, G. ., Samson, D., Bennett, V., … Siu, C.-H. (1996). The L1 family of neural cell adhesion molecules: old proteins performing new tricks. *Neuron*, *17*(4), 587–93. http://doi.org/10.1016/S0896-6273(00)80192-0

Hu, Y., Flockhart, I., Vinayagam, A., Bergwitz, C., Berger, B., Perrimon, N., … Wang, H. (2011). An integrative approach to ortholog prediction for disease-focused and other functional studies. *BMC Bioinformatics*, *12*(1), 357. http://doi.org/10.1186/1471-2105-12-357

Huang, K., Sanders, S. S., Kang, R., Carroll, J. B., Sutton, L., Wan, J., … Hayden, M. R. (2011). Wild-type HTT modulates the enzymatic activity of the neuronal palmitoyl transferase HIP14. *Human Molecular Genetics*, *20*(17), 3356–3365. http://doi.org/10.1093/hmg/ddr242

Huang, K., Sanders, S., Singaraja, R., Orban, P., Cijsouw, T., Arstikaitis, P., … El-Husseini, A. (2009). Neuronal palmitoyl acyl transferases exhibit distinct substrate specificity. *The FASEB Journal*, *23*(8), 2605–2615. http://doi.org/10.1096/fj.08-127399

Huttlin, E. L., Ting, L., Bruckner, R. J., Gebreab, F., Gygi, M. P., Szpyt, J., … Gygi, S. P. (2015). The BioPlex Network: A Systematic Exploration of the Human Interactome. *Cell*, *162*(2), 425–440. http://doi.org/10.1016/j.cell.2015.06.043

Iivonen, S., Helisalmi, S., Mannermaa, A., Alafuzoff, I., Lehtovirta, M., Soininen, H., & Hiltunen, M. (2003). *Heparan sulfate proteoglycan 2 polymorphism in Alzheimer's disease and correlation with neuropathology*. *Neuroscience Letters* (Vol. 352).

Iwasa, H., Maimaiti, S., Kuroyanagi, H., Kawano, S., Inami, K., Timalsina, S., … Hata, Y. (2013). Yes-associated protein homolog, YAP-1, is involved in the thermotolerance and aging in the nematode Caenorhabditis elegans. *Experimental Cell Research*, *319*(7), 931–45. http://doi.org/10.1016/j.yexcr.2013.01.020

Jayadev, S., Leverenz, J. B., Steinbart, E., Stahl, J., Klunk, W., Yu, C. E., & Bird, T. D. (2010). Alzheimer's disease phenotypes and genotypes associated with mutations in presenilin 2. *Brain*, *133*(4), 1143–1154. http://doi.org/10.1093/brain/awq033

Jensen, O. N. (2006). Interpreting the protein language using proteomics. *Nature Reviews Molecular Cell Biology*, *7*(6), 391–403. http://doi.org/10.1038/nrm1939

Jorgensen, E. M. (2005). Gaba. *WormBook : The Online Review of C. Elegans Biology*, *1*, 1–13. http://doi.org/10.1895/wormbook.1.14.1

Joseph, M., & Nagaraj, R. (1995). Interaction of Peptides Corresponding to Fatty Acylation Sites in Proteins with Model Membranes. *Journal of Biological Chemistry*, *270*(28), 16749–16755. http://doi.org/10.1074/jbc.270.28.16749

Joy, M. P., Brock, A., Ingber, D. E., & Huang, S. (2005). High-betweenness proteins in the yeast protein interaction network. *Journal of Biomedicine & Biotechnology*, *2005*(2), 96–103. http://doi.org/10.1155/JBB.2005.96

Kabouridis, P. S., Magee, A. I., & Ley, S. C. (1997). S-acylation of LCK protein tyrosine kinase is essential for its signalling function in T lymphocytes. *The EMBO Journal*, *Akinleye,*(16), 4983–98. http://doi.org/10.1093/emboj/16.16.4983

Kamath, R. S., & Ahringer, J. (2003). Genome-wide RNAi screening in Caenorhabditis elegans.

Methods, *30*, 313–321. http://doi.org/10.1016/S1046-2023(03)00050-1

Kamath, R. S., Fraser, A. G., Dong, Y., Poulin, G., Durbin, R., Gotta, M., … Ahringer, J. (2003). Systematic functional analysis of the Caenorhabditis elegans genome using RNAi. *Nature*, *421*, 231–237. http://doi.org/10.1038/nature01278

Kang, R., Wan, J., Arstikaitis, P., Takahashi, H., Huang, K., Bailey, A. O., … El-Husseini, A. (2008). Neural palmitoyl-proteomics reveals dynamic synaptic palmitoylation. *Nature*, *456*(7224), 904–9. http://doi.org/10.1038/nature07605

Katic, I., & Grosshans, H. (2013). Targeted Heritable Mutation and Gene Conversion by Cas9-CRISPR in Caenorhabditis elegans. *Genetics*. http://doi.org/10.1534/genetics.113.155754

Katz, B. (1970). Quantal mechanism of neural transmitter release. In *Nobel Lectures, Physiology or Medicine 1963-1970* (Vol. 173, pp. 485–492). http://doi.org/10.1126/science.173.3992.123

Kautu, B. B., Carrasquilla, A., Hicks, M. L., Caldwell, K. A., & Caldwell, G. A. (2013). Valproic acid ameliorates C. elegans dopaminergic neurodegeneration with implications for ERK-MAPK signaling. *Neuroscience Letters*, *541*, 116–119. http://doi.org/10.1016/j.neulet.2013.02.026

Keller, C. A., Yuan, X., Panzanelli, P., Martin, M. L., Alldred, M., Sassoè-Pognetto, M., & Lüscher, B. (2004). The gamma2 subunit of GABA(A) receptors is a substrate for palmitoylation by GODZ. *The Journal of Neuroscience : The Official Journal of the Society for Neuroscience*, *24*(26), 5881–91. http://doi.org/10.1523/JNEUROSCI.1037-04.2004

Kerrien, S., Alam-Faruque, Y., Aranda, B., Bancarz, I., Bridge, A., Derow, C., … Hermjakob, H. (2007). IntAct--open source resource for molecular interaction data. *Nucleic Acids Res*, *35*(Database issue), D561-5. http://doi.org/10.1093/nar/gkl958

Keshava Prasad, T. S., Goel, R., Kandasamy, K., Keerthikumar, S., Kumar, S., Mathivanan, S., … Pandey, A. (2009). Human Protein Reference Database--2009 update. *Nucleic Acids Research*, *37*(Database), D767–D772. http://doi.org/10.1093/nar/gkn892

Khabirova, E., Moloney, A., Marciniak, S. J., Williams, J., Lomas, D. A., Oliver, S. G., … Crowther, D. C. (2014). The TRiC/CCT chaperone is implicated in Alzheimer's disease based on patient GWAS and an RNAi screen in Aβ-expressing Caenorhabditis elegans. *PloS One*, *9*(7), e102985. http://doi.org/10.1371/journal.pone.0102985

Kowalski, J. R., Dube, H., Touroutine, D., Rush, K. M., Goodwin, P. R., Carozza, M., … Juo, P. (2014). The Anaphase-Promoting Complex (APC) ubiquitin ligase regulates GABA transmission at the C. elegans neuromuscular junction. *Molecular and Cellular Neuroscience*, *58*, 62–75. http://doi.org/10.1016/j.mcn.2013.12.001

Kramer, O. H., Zhu, P., Ostendorff, H. P., Golebiewski, M., Tiefenbach, J., Peters, M. A., … G??ttlicher, M. (2003). The histone deacetylase inhibitor valproic acid selectively induces proteasomal degradation of HDAC2. *EMBO Journal*, *22*(13), 3411–3420. http://doi.org/10.1093/emboj/cdg315

Kuan, C. Y., Yang, D. D., Samanta Roy, D. R., Davis, R. J., Rakic, P., & Flavell, R. A. (1999). The Jnk1 and Jnk2 protein kinases are required for regional specific apoptosis during early brain development. *Neuron*, *22*(4), 667–676. http://doi.org/10.1016/S0896-6273(00)80727-8

Kutscher, L. M., & Shaham, S. (2014). Forward and reverse mutagenesis in C. elegans. *WormBook*,

1–26. http://doi.org/10.1895/wormbook.1.167.1

Landouré, G., Zhu, P. P., Lourenço, C. M., Johnson, J. O., Toro, C., Bricceno, K. V., … Burnett, B. G. (2013). Hereditary spastic paraplegia Type 43 (SPG43) is caused by mutation in C19orf12. *Human Mutation*, *34*(10), 1357–1360. http://doi.org/10.1002/humu.22378

Lee, S.-F., Shah, S., Li, H., Yu, C., Han, W., & Yu, G. (2002). Mammalian APH-1 interacts with presenilin and nicastrin and is required for intramembrane proteolysis of amyloid-beta precursor protein and Notch. *The Journal of Biological Chemistry*, *277*(47), 45013–9. http://doi.org/10.1074/jbc.M208164200

Lehner, B., Calixto, A., Crombie, C., Tischler, J., Fortunato, A., Chalfie, M., & Fraser, A. G. (2006). Loss of LIN-35, the Caenorhabditis elegans ortholog of the tumor suppressor p105Rb, results in enhanced RNA interference. *Genome Biology*, *7*(1), R4. http://doi.org/10.1186/gb-2006-7-1-r4

Lehtovirta, M., Kyttälä, A., Eskelinen, E. L., Hess, M., Heinonen, O., & Jalanko, A. (2001). Palmitoyl protein thioesterase (PPT) localizes into synaptosomes and synaptic vesicles in neurons: implications for infantile neuronal ceroid lipofuscinosis (INCL). *Human Molecular Genetics*, *10*(1), 69–75. Retrieved from http://www.ncbi.nlm.nih.gov/pubmed/11136716

Lemonidis, K., Gorleku, O. A., Sanchez-Perez, M. C., Grefen, C., & Chamberlain, L. H. (2014). The Golgi S-acylation machinery comprises zDHHC enzymes with major differences in substrate affinity and S-acylation activity. *Molecular Biology of the Cell*, *25*(24), 3870–83. http://doi.org/10.1091/mbc.E14-06-1169

Lemonidis, K., Sanchez-Perez, M. C., & Chamberlain, L. H. (2015). Identification of a Novel Sequence Motif Recognized by the Ankyrin Repeat Domain of zDHHC17/13 S-Acyltransferases. *The Journal of Biological Chemistry*, *290*(36), 21939–50. http://doi.org/10.1074/jbc.M115.657668

Letunic, I., & Bork, P. (2016). Interactive tree of life (iTOL) v3: an online tool for the display and annotation of phylogenetic and other trees. *Nucleic Acids Research*, *44*(W1), W242-5. http://doi.org/10.1093/nar/gkw290

Lewis, J. A., Gehman, E. A., Baer, C. E., & Jackson, D. A. (2013). Alterations in gene expression in Caenorhabditis elegans associated with organophosphate pesticide intoxication and recovery. *BMC Genomics*, *14*, 291. http://doi.org/10.1186/1471-2164-14-291

Li, C., & Kim, K. (2008). Neuropeptides. *WormBook : The Online Review of C. Elegans Biology*, (212), 1–36. http://doi.org/10.1895/wormbook.1.142.1

Li, Y., Hu, J., Höfer, K., Wong, A. M. S., Cooper, J. D., Birnbaum, S. G., … Hofmann, S. L. (2010). DHHC5 interacts with PDZ domain 3 of post-synaptic density-95 (PSD-95) protein and plays a role in learning and memory. *Journal of Biological Chemistry*, *285*(17), 13022–13031. http://doi.org/10.1074/jbc.M109.079426

Licata, L., Briganti, L., Peluso, D., Perfetto, L., Iannuccelli, M., Galeota, E., … Cesareni, G. (2012). MINT, the molecular interaction database: 2012 Update. *Nucleic Acids Research*, *40*(D1). http://doi.org/10.1093/nar/gkr930

Lin, S. H., Lee, L. T., & Yang, Y. K. (2014). Serotonin and mental disorders: A concise review on

molecular neuroimaging evidence. *Clinical Psychopharmacology and Neuroscience*, *12*(3), 196–202. http://doi.org/10.9758/cpn.2014.12.3.196

Liu, L., Dudler, T., & Gelb, M. H. (1996). Purification of a protein palmitoyltransferase that acts on H-Ras protein and on a C-terminal N-Ras peptide. *The Journal of Biological Chemistry*, *271*(38), 23269–76. http://doi.org/10.1074/JBC.271.38.23269

Lloyd, K. a. (2013). A scientific review: mechanisms of valproate-mediated teratogenesis. *Bioscience Horizons*, *6*, hzt003-hzt003. http://doi.org/10.1093/biohorizons/hzt003

Lobo, S., Greentree, W. K., Linder, M. E., & Deschenes, R. J. (2002). Identification of a Ras palmitoyltransferase in Saccharomyces cerevisiae. *Journal of Biological Chemistry*, *277*(43), 41268–41273. http://doi.org/10.1074/jbc.M206573200

Locke, C., Berry, K., Kautu, B., Lee, K., Caldwell, K., & Caldwell, G. (2008). Paradigms for pharmacological characterization of C. elegans synaptic transmission mutants. *Journal of Visualized Experiments : JoVE*, (18), 3–5. http://doi.org/10.3791/837

López-Muñoz, F., & Alamo, C. (2009). Historical evolution of the neurotransmission concept. *Journal of Neural Transmission*. http://doi.org/10.1007/s00702-009-0213-1

Ma, X., Fei, E., Fu, C., Ren, H., & Wang, G. (2011). Dysbindin-1, a schizophrenia-related protein, facilitates neurite outgrowth by promoting the transcriptional activity of p53. *Molecular Psychiatry*, *16*(11), 1105–1116. http://doi.org/10.1038/mp.2011.43

Mah, A. L., Perry, G., Smith, M. A., & Monteiro, M. J. (2000). Identification of ubiquilin, a novel presenilin interactor that increases presenilin protein accumulation. *Journal of Cell Biology*, *151*(4), 847–862. http://doi.org/10.1083/jcb.151.4.847

Mahoney, T. R., Luo, S., & Nonet, M. L. (2006). Analysis of synaptic transmission in Caenorhabditis elegans using an aldicarb-sensitivity assay. *Nature Protocols*, *1*(4), 1772–1777. http://doi.org/Doi 10.1038/Nprot.2006.281

Mao, J., McKean, D. M., Warrier, S., Corbin, J. G., Niswander, L., & Zohn, I. E. (2010). The iron exporter ferroportin 1 is essential for development of the mouse embryo, forebrain patterning and neural tube closure. *Development*, *137*(18), 3079–3088. http://doi.org/10.1242/dev.048744

Markson, G., Kiel, C., Hyde, R., Brown, S., Charalabous, P., Bremm, A., … Sanderson, C. M. (2009). Analysis of the human E2 ubiquitin conjugating enzyme protein interaction network. *Genome Research*, *19*(10), 1905–1911. http://doi.org/10.1101/gr.093963.109

Marui, T., Funatogawa, I., Koishi, S., Yamamoto, K., Matsumoto, H., Hashimoto, O., … Kato, N. (2009). Association of the neuronal cell adhesion molecule (NRCAM) gene variants with autism. *The International Journal of Neuropsychopharmacology / Official Scientific Journal of the Collegium Internationale Neuropsychopharmacologicum (CINP)*, *12*(1), 1–10. http://doi.org/10.1017/S1461145708009413

Matthies, D. S., Fleming, P. A., Wilkes, D. M., & Blakely, R. D. (2006). The Caenorhabditis elegans choline transporter CHO-1 sustains acetylcholine synthesis and motor function in an activity-dependent manner. *The Journal of Neuroscience : The Official Journal of the Society for Neuroscience*, *26*(23), 6200–12. http://doi.org/10.1523/JNEUROSCI.5036-05.2006

McColl, G., Roberts, B. R., Pukala, T. L., Kenche, V. B., Roberts, C. M., Link, C. D., … Cherny, R. A. (2012). Utility of an improved model of amyloid-beta ($A\beta_{1-42}$) toxicity in Caenorhabditis elegans for drug screening for Alzheimer's disease. *Molecular Neurodegeneration*, *7*, 57. http://doi.org/10.1186/1750-1326-7-57

Menegon, A., Bonanomi, D., Albertinazzi, C., Lotti, F., Ferrari, G., Kao, H.-T., … Valtorta, F. (2006). Protein Kinase A-Mediated Synapsin I Phosphorylation Is a Central Modulator of Ca2+-Dependent Synaptic Activity. *Journal of Neuroscience*, *26*(45).

Mitchell, D. A., Hamel, L. D., Reddy, K. D., Farh, L., Rettew, L. M., Sanchez, P. R., & Deschenes, R. J. (2014). Mutations in the X-linked intellectual disability gene, zDHHC9, alter autopalmitoylation activity by distinct mechanisms. *Journal of Biological Chemistry*, *289*, 18582–18592. http://doi.org/10.1074/jbc.M114.567420

Mitchell, D. A., Mitchell, G., Ling, Y., Budde, C., & Deschenes, R. J. (2010). Mutational analysis of Saccharomyces cerevisiae Erf2 reveals a two-step reaction mechanism for protein palmitoylation by DHHC enzymes. *The Journal of Biological Chemistry*, *285*(49), 38104–14. http://doi.org/10.1074/jbc.M110.169102

Mitchell, D. A., Vasudevan, A., Linder, M. E., & Deschenes, R. J. (2006). Protein palmitoylation by a family of DHHC protein S-acyltransferases. *J Lipid Res*, *47*(6), 1118–1127. http://doi.org/R600007-JLR200 [pii]\n10.1194/jlr.R600007-JLR200

Miyoshi, K., Honda, A., Baba, K., Taniguchi, M., Oono, K., Fujita, T., … Tohyama, M. (2003). Disrupted-In-Schizophrenia 1, a candidate gene for schizophrenia, participates in neurite outgrowth. *Molecular Psychiatry*, *8*(7), 685–94. http://doi.org/10.1038/sj.mp.4001352

Morland, C., Nordengen, K., & Gundersen, V. (2012). Valproate causes reduction of the excitatory amino acid aspartate in nerve terminals. *Neuroscience Letters*, *527*(2), 100–104. http://doi.org/10.1016/j.neulet.2012.08.042

Morotti, A., Cilloni, D., Messa, F., Arruga, F., Defilippi, I., Carturan, S., … Saglio, G. (2006). Valproate enhances imatinib-induced growth arrest and apoptosis in chronic myeloid leukemia cells. *Cancer*, *106*(5), 1188–96. http://doi.org/10.1002/cncr.21725

Motohashi, K. (2015). A simple and efficient seamless DNA cloning method using SLiCE from Escherichia coli laboratory strains and its application to SLiP site-directed mutagenesis. *BMC Biotechnology*, *15*(1), 47. http://doi.org/10.1186/s12896-015-0162-8

Moy, S. S., Nonneman, R. J., Young, N. B., Demyanenko, G. P., & Maness, P. F. (2009). Impaired sociability and cognitive function in Nrcam-null mice. *Behavioural Brain Research*, *205*(1), 123–131. http://doi.org/10.1016/j.bbr.2009.06.021

Mukai, J., Dhilla, A., Drew, L. J., Stark, K. L., Cao, L., Macdermott, A. B., … Gogos, J. A. (2008). Palmitoylation-dependent neurodevelopmental deficits in a mouse model of 22q11 microdeletion. *Nature Neuroscience*, *11*(11), 1302–1310. http://doi.org/10.1038/nn.2204

Mukai, J., Liu, H., Burt, R. A., Swor, D. E., Lai, W.-S., Karayiorgou, M., & Gogos, J. A. (2004). Evidence that the gene encoding ZDHHC8 contributes to the risk of schizophrenia. *Nature Genetics*, *36*(7), 725–731. http://doi.org/10.1038/ng1375

Munasinghe, D. H. (2015). An integrative approach to understanding effects of valproate in C.

elegans.

Nakayama, K. I., & Nakayama, K. (2006). Ubiquitin ligases: cell-cycle control and cancer. *Nature Reviews Cancer*, *6*(5), 369–381. http://doi.org/10.1038/nrc1881

Natunen, T., Takalo, M., Kemppainen, S., Leskelä, S., Marttinen, M., Kurkinen, K. M. A., … Hiltunen, M. (2016). Relationship between ubiquilin-1 and BACE1 in human Alzheimer's disease and APdE9 transgenic mouse brain and cell-based models. *Neurobiology of Disease*, *85*, 187–205. http://doi.org/10.1016/j.nbd.2015.11.005

Nava-Mesa, M. O., Jiménez-Díaz, L., Yajeya, J., & Navarro-Lopez, J. D. (2014). GABAergic neurotransmission and new strategies of neuromodulation to compensate synaptic dysfunction in early stages of Alzheimer's disease. *Frontiers in Cellular Neuroscience*, *8*, 167. http://doi.org/10.3389/fncel.2014.00167

Ngo, J. K., Pomatto, L. C. D., & Davies, K. J. A. (2013). Upregulation of the mitochondrial Lon Protease allows adaptation to acute oxidative stress but dysregulation is associated with chronic stress, disease, and aging. *Redox Biology*, *1*(1), 258–264. http://doi.org/10.1016/j.redox.2013.01.015

Nguyen, P. V., & Woo, N. H. (2003). Regulation of hippocampal synaptic plasticity by cyclic AMP-dependent protein kinases. *Progress in Neurobiology*. http://doi.org/10.1016/j.pneurobio.2003.12.003

Noble, T., Stieglitz, J., & Srinivasan, S. (2013). An integrated serotonin and octopamine neuronal circuit directs the release of an endocrine signal to control C. Elegans body fat. *Cell Metabolism*, *18*(5), 672–684. http://doi.org/10.1016/j.cmet.2013.09.007

Noritake, J., Fukata, Y., Iwanaga, T., Hosomi, N., Tsutsumi, R., Matsuda, N., … Fukata, M. (2009). Mobile DHHC palmitoylating enzyme mediates activity-sensitive synaptic targeting of PSD-95. *Journal of Cell Biology*, *186*(1), 147–160. http://doi.org/10.1083/jcb.200903101

Oliver, S. (2000). Guilt-by-association goes global. *Nature*, *403*(6770), 601–603. http://doi.org/10.1038/35001165

Omasits, U., Ahrens, C. H., Müller, S., & Wollscheid, B. (2014). Protter: Interactive protein feature visualization and integration with experimental proteomic data. *Bioinformatics*, *30*(6), 884–886. http://doi.org/10.1093/bioinformatics/btt607

Pflugrad, A., Meir, J. Y., Barnes, T. M., & Miller 3rd, D. M. (1997). The Groucho-like transcription factor UNC-37 functions with the neural specificity gene unc-4 to govern motor neuron identity in C. elegans. *Development*, *124*(9), 1699–1709. Retrieved from http://www.ncbi.nlm.nih.gov/pubmed/9165118

Picciotto, M. R., Higley, M. J., & Mineur, Y. S. (2012). Acetylcholine as a Neuromodulator: Cholinergic Signaling Shapes Nervous System Function and Behavior. *Neuron*. http://doi.org/10.1016/j.neuron.2012.08.036

Pinero, J., Queralt-Rosinach, N., Bravo, A., Deu-Pons, J., Bauer-Mehren, A., Baron, M., … V., M. (2015). DisGeNET: a discovery platform for the dynamical exploration of human diseases and their genes. *Database*, *2015*(0), bav028-bav028. http://doi.org/10.1093/database/bav028

Pinner, A. L., Tucholski, J., Haroutunian, V., McCullumsmith, R. E., & Meador-Woodruff, J. H. (2015). Decreased protein S-palmitoylation in dorsolateral prefrontal cortex in schizophrenia. *Schizophrenia Research*. http://doi.org/10.1016/j.schres.2016.01.054

Pirooznia, M., Wang, T., Avramopoulos, D., Valle, D., Thomas, G., Huganir, R. L., … Zandi, P. P. (2012). SynaptomeDB: an ontology-based knowledgebase for synaptic genes. *Bioinformatics*, *28*(6), 897–899. http://doi.org/10.1093/bioinformatics/bts040

Rand, J. B. (2007). Acetylcholine. *WormBook : The Online Review of C. Elegans Biology*, 1–21. http://doi.org/10.1895/wormbook.1.131.1

Rauch, S. M., Huen, K., Miller, M. C., Chaudry, H., Lau, M., Sanes, J. R., … Burgess, R. W. (2011). Changes in brain β-amyloid deposition and aquaporin 4 levels in response to altered agrin expression in mice. *Journal of Neuropathology and Experimental Neurology*, *70*(12), 1124–37. http://doi.org/10.1097/NEN.0b013e31823b0b12

Ren, M., Leng, Y., Jeong, M., Leeds, P. R., & Chuang, D. M. (2004). Valproic acid reduces brain damage induced by transient focal cerebral ischemia in rats: Potential roles of histone deacetylase inhibition and heat shock protein induction. *Journal of Neurochemistry*, *89*(6), 1358–1367. http://doi.org/10.1111/j.1471-4159.2004.02406.x

Rinetti, G. V, & Schweizer, F. E. (2010). Ubiquitination acutely regulates presynaptic neurotransmitter release in mammalian neurons. *The Journal of Neuroscience : The Official Journal of the Society for Neuroscience*, *30*(9), 3157–66. http://doi.org/10.1523/JNEUROSCI.3712-09.2010

Robertson, J. D. (1953). Ultrastructure of Two Invertebrate Synapses. *Experimental Biology and Medicine*, *82*(2), 219–223. http://doi.org/10.3181/00379727-82-20071

Rolland, T., Taşan, M., Charloteaux, B., Pevzner, S. J., Zhong, Q., Sahni, N., … Vidal, M. (2014). A Proteome-Scale Map of the Human Interactome Network. *Cell*, *159*(5), 1212–1226. http://doi.org/10.1016/j.cell.2014.10.050

Rose, S., Malabarba, M. G., Krag, C., Schultz, A., Tsushima, H., Di Fiore, P. P., & Salcini, A. E. (2007). Caenorhabditis elegans intersectin: a synaptic protein regulating neurotransmission. *Molecular Biology of the Cell*, *18*, 5091–5099. http://doi.org/10.1091/mbc.E07-05-0460

Roth, A. F., Feng, Y., Chen, L., & Davis, N. G. (2002). The yeast DHHC cysteine-rich domain protein Akr1p is a palmitoyl transferase. *Journal of Cell Biology*, *159*(1), 23–28. http://doi.org/10.1083/jcb.200206120

Rual, J. F., Ceron, J., Koreth, J., Hao, T., Nicot, A. S., Hirozane-Kishikawa, T., … Vidal, M. (2004a). Toward improving Caenorhabditis elegans phenome mapping with an ORFeome-based RNAi library. *Genome Research*, *14*, 2162–2168. http://doi.org/10.1101/gr.2505604

Rual, J. F., Ceron, J., Koreth, J., Hao, T., Nicot, A. S., Hirozane-Kishikawa, T., … Vidal, M. (2004b). Toward improving Caenorhabditis elegans phenome mapping with an ORFeome-based RNAi library. *Genome Research*, *14*(10 B), 2162–2168. http://doi.org/10.1101/gr.2505604

Sabapathy, K., Jochum, W., Hochedlinger, K., Chang, L., Karin, M., & Wagner, E. F. (1999). Defective neural tube morphogenesis and altered apoptosis in the absence of both JNK1 and JNK2. *Mechanisms of Development*, *89*(1–2), 115–124. http://doi.org/10.1016/S0925-

4773(99)00213-0

Sanders, S. S., Martin, D. D. O., Butland, S. L., Lavallée-Adam, M., Calzolari, D., Kay, C., … Hayden, M. R. (2015). Curation of the Mammalian Palmitoylome Indicates a Pivotal Role for Palmitoylation in Diseases and Disorders of the Nervous System and Cancers. *PLoS Computational Biology*, *11*(8), e1004405. http://doi.org/10.1371/journal.pcbi.1004405

Schaefer, M. H., Fontaine, J.-F., Vinayagam, A., Porras, P., Wanker, E. E., Andrade-Navarro, M. A., … Huan, T. (2012). HIPPIE: Integrating Protein Interaction Networks with Experiment Based Quality Scores. *PLoS ONE*, *7*(2), e31826. http://doi.org/10.1371/journal.pone.0031826

Scheuing, L., Chiu, C. T., Liao, H. M., Linares, G. R., & Chuang, D. M. (2014). Preclinical and clinical investigations of mood stabilizers for Huntington's disease: what have we learned? *Int J Biol Sci*, *10*(9), 1024–1038. Retrieved from http://www.ncbi.nlm.nih.gov/entrez/query.fcgi?cmd=Retrieve&db=PubMed&dopt=Citation&list_uids=25285035

Schneider, J., Skelton, R. L., Von Stetina, S. E., Middelkoop, T. C., van Oudenaarden, A., Korswagen, H. C., & Miller, D. M. (2012). UNC-4 antagonizes Wnt signaling to regulate synaptic choice in the C. elegans motor circuit. *Development*, *139*(12), 2234–2245. http://doi.org/10.1242/dev.075184

Shah, R. D., Jagtap, J. C., Mruthyunjaya, S., Shelke, G. V, Pujari, R., Das, G., & Shastry, P. (2013). Sodium valproate potentiates staurosporine-induced apoptosis in neuroblastoma cells via Akt/survivin independently of HDAC inhibition. *Journal of Cellular Biochemistry*, *114*(4), 854–63. http://doi.org/10.1002/jcb.24422

Sharpe, H. J., Stevens, T. J., & Munro, S. (2010). A Comprehensive Comparison of Transmembrane Domains Reveals Organelle-Specific Properties. *Cell*, *142*(1), 158–169. http://doi.org/10.1016/j.cell.2010.05.037

Sieburth, D., Ch'ng, Q., Dybbs, M., Tavazoie, M., Kennedy, S., Wang, D., … Kaplan, J. M. (2005). Systematic analysis of genes required for synapse structure and function. *Nature*, *436*(7050), 510–7. http://doi.org/10.1038/nature03809

Simonis, N., Rual, J., Carvunis, A., Tasan, M., Lemmens, I., Hirozane-Kishikawa, T., … Vidal, M. (2009). Empirically controlled mapping of the Caenorhabditis elegans protein-protein interactome network. *Nature Methods*, *6*(1), 47–54. http://doi.org/10.1038/nmeth.1279

Singaraja, R. R., Huang, K., Sanders, S. S., Milnerwood, A. J., Hines, R., Lerch, J. P., … Hayden, M. R. (2011). Altered palmitoylation and neuropathological deficits in mice lacking HIP14. *Human Molecular Genetics*, *20*(20), 3899–3909. http://doi.org/10.1093/hmg/ddr308

Skorobogatko, Y., Landicho, A., Chalkley, R. J., Kossenkov, A. V, Gallo, G., & Vosseller, K. (2014). O-linked β-N-acetylglucosamine (O-GlcNAc) site thr-87 regulates synapsin I localization to synapses and size of the reserve pool of synaptic vesicles. *The Journal of Biological Chemistry*, *289*(6), 3602–12. http://doi.org/10.1074/jbc.M113.512814

Soares, D. C., & Abbott, C. M. (2013). Highly homologous eEF1A1 and eEF1A2 exhibit differential post-translational modification with significant enrichment around localised sites of sequence variation. *Biology Direct*, *8*, 29. http://doi.org/10.1186/1745-6150-8-29

Speese, S. D., Trotta, N., Rodesch, C. K., Aravamudan, B., & Broadie, K. (2003). The ubiquitin proteasome system acutely regulates presynaptic protein turnover and synaptic efficacy. *Current Biology*, *13*(11), 899–910. http://doi.org/10.1016/S0960-9822(03)00338-5

Stagljar, I., & Fields, S. (2002). Analysis of membrane protein interactions using yeast-based technologies. *Trends in Biochemical Sciences*. http://doi.org/10.1016/S0968-0004(02)02197-7

Stawicki, T. M., Takayanagi-Kiya, S., Zhou, K., & Jin, Y. (2013). Neuropeptides Function in a Homeostatic Manner to Modulate Excitation-Inhibition Imbalance in C. elegans. *PLoS Genetics*, *9*(5). http://doi.org/10.1371/journal.pgen.1003472

Stiernagle, T. (2006). Maintenance of C. elegans. *WormBook : The Online Review of C. Elegans Biology*, (1999), 1–11. http://doi.org/10.1895/wormbook.1.101.1

Sudhof. (2013). Neurotransmitter release: the last milisecond in the life of a synaptic vesicle. *Neuron.*, *80*(3), 675–690.

Sudhof, T. C., & Rizo, J. (2011). Synaptic Vesicle Exocytosis. *Cold Spring Harbor Perspectives in Biology*, *3*(12). http://doi.org/ARTN a005637DOI 10.1101/cshperspect.a005637

Suo, S., & Ishiura, S. (2013). Dopamine Modulates Acetylcholine Release via Octopamine and CREB Signaling in Caenorhabditis elegans. *PLoS One*, *8*(8), e72578. http://doi.org/10.1371/journal.pone.0072578

Sutton, L. M., Sanders, S. S., Butland, S. L., Singaraja, R. R., Franciosi, S., Southwell, A. L., … Hayden, M. R. (2013). Hip14l-deficient mice develop neuropathological and behavioural features of Huntington disease. *Human Molecular Genetics*, *22*(3), 452–465. http://doi.org/10.1093/hmg/dds441

Swarthout, J. T., Lobo, S., Farh, L., Croke, M. R., Greentree, W. K., Deschenes, R. J., & Linder, M. E. (2005a). DHHC9 and GCP16 constitute a human protein fatty acyltransferase with specificity for H- and N-Ras. *Journal of Biological Chemistry*, *280*(35), 31141–31148. http://doi.org/10.1074/jbc.M504113200

Tallent, M. K., Varghis, N., Skorobogatko, Y., Hernandez-Cuebas, L., Whelan, K., Vocadlo, D. J., & Vosseller, K. (2009). In vivo modulation of O-GlcNAc levels regulates hippocampal synaptic plasticity through interplay with phosphorylation. *J Biol Chem*, *284*(1), 174–181. http://doi.org/M807431200 [pii]\r10.1074/jbc.M807431200

Terbach, N., Shah, R., Kelemen, R., Klein, P. S., Gordienko, D., Brown, N. A., … Williams, R. S. B. (2011). Identifying an uptake mechanism for the antiepileptic and bipolar disorder treatment valproic acid using the simple biomedical model Dictyostelium. *Journal of Cell Science*, *124*(Pt 13), 2267–76. http://doi.org/10.1242/jcs.084285

Thomas, G. M., Hayashi, T., Chiu, S.-L., Chen, C.-M., & Huganir, R. L. (2012). Palmitoylation by DHHC5/8 targets GRIP1 to dendritic endosomes to regulate AMPA-R trafficking. *Neuron*, *73*(3), 482–96. http://doi.org/10.1016/j.neuron.2011.11.021

Thomas, G. M., Hayashi, T., Huganir, R. L., & Linden, D. J. (2013). DHHC8-dependent PICK1 palmitoylation is required for induction of cerebellar long-term synaptic depression. *The Journal of Neuroscience : The Official Journal of the Society for Neuroscience*, *33*(39), 15401–

7. http://doi.org/10.1523/JNEUROSCI.1283-13.2013

Tokuoka, S. M., Saiardi, A., & Nurrish, S. J. (2008). The mood stabilizer valproate inhibits both inositol- and diacylglycerol-signaling pathways in Caenorhabditis elegans. *Molecular Biology of the Cell*, *19*(5), 2241–50. http://doi.org/10.1091/mbc.E07-09-0982

Tomatis, V. M., Trenchi, A., Gomez, G. A., & Daniotti, J. L. (2010). Acyl-protein thioesterase 2 catalizes the deacylation of peripheral membrane-associated GAP-43. *PLoS ONE*, *5*(11). http://doi.org/10.1371/journal.pone.0015045

Tseng, P. T., Chen, Y. W., Chung, W., Tu, K. Y., Wang, H. Y., Wu, C. K., & Lin, P. Y. (2016). Significant Effect of Valproate Augmentation Therapy in Patients With Schizophrenia: A Meta-analysis Study. *Medicine (Baltimore)*, *95*(4), e2475. http://doi.org/10.1097/MD.0000000000002475

Van Horssen, J., Wesseling, P., Van Den Heuvel, L. P. W. J., De Waal, R. M. W., & Verbeek, M. M. (2003). Heparan sulphate proteoglycans in Alzheimer's disease and amyloid-related disorders. *Lancet Neurology*. http://doi.org/10.1016/S1474-4422(03)00484-8

Varshney, L. R., Chen, B. L., Paniagua, E., Hall, D. H., & Chklovskii, D. B. (2011). Structural properties of the Caenorhabditis elegans neuronal network. *PLoS Computational Biology*, *7*(2). http://doi.org/10.1371/journal.pcbi.1001066

Vashlishan, A. B., Madison, J. M., Dybbs, M., Bai, J., Sieburth, D., Ch'ng, Q., … Kaplan, J. M. (2008). An RNAi Screen Identifies Genes that Regulate GABA Synapses. *Neuron*, *58*(3), 346–361. http://doi.org/10.1016/j.neuron.2008.02.019

Veit, M., Becher, A., & Ahnert-Hilger, G. (2000). Synaptobrevin 2 Is Palmitoylated in Synaptic Vesicles Prepared from Adult, But Not from Embryonic Brain. *Molecular and Cellular Neuroscience*, *15*(4), 408–416. http://doi.org/10.1006/mcne.1999.0830

Vera, M., Pani, B., Griffiths, L. A., Muchardt, C., Abbott, C. M., Singer, R. H., & Nudler, E. (2014). The translation elongation factor eEF1A1 couples transcription to translation during heat shock response. *eLife*, *3*. Retrieved from http://elifesciences.org/content/3/e03164.abstract

Vidal, M., Cusick, M. E., & Barabási, A.-L. (2011). Interactome networks and human disease. *Cell*, *144*(6), 986–98. http://doi.org/10.1016/j.cell.2011.02.016

von Trotha, K. T., Heun, R., Schmitz, S., Lütjohann, D., Maier, W., & Kölsch, H. (2006). Influence of lysosomal acid lipase polymorphisms on chromosome 10 on the risk of Alzheimer's disease and cholesterol metabolism. *Neuroscience Letters*, *402*(3), 262–266. http://doi.org/10.1016/j.neulet.2006.04.009

Waltes, R., Gfesser, J., Haslinger, D., Schneider-Momm, K., Biscaldi, M., Voran, A., … Chiocchetti, A. G. (2014). Common EIF4E variants modulate risk for autism spectrum disorders in the high-functioning range. *Journal of Neural Transmission*, *121*(9), 1107–1116. http://doi.org/10.1007/s00702-014-1230-2

Wang, Z., Xu, L., Zhu, X., Cui, W., Sun, Y., Nishijo, H., … Li, R. (2010). Demethylation of specific Wnt/β-catenin pathway genes and its upregulation in rat brain induced by prenatal valproate exposure. *Anatomical Record (Hoboken, N.J. : 2007)*, *293*(11), 1947–53. http://doi.org/10.1002/ar.21232

White, J. G., Southgate, E., Thomson, J. N., & Brenner, S. (1986). The structure of the nervous system of the nematode Caenorhabditis elegans. *Philosophical Transactions of the Royal Society of London*, *314*(1165), 1–340. http://doi.org/10.1098/rstb.1986.0056

Willeumier, K., Pulst, S. M., & Schweizer, F. E. (2006). Proteasome inhibition triggers activity-dependent increase in the size of the recycling vesicle pool in cultured hippocampal neurons. *The Journal of Neuroscience : The Official Journal of the Society for Neuroscience*, *26*(44), 11333–41. http://doi.org/10.1523/JNEUROSCI.1684-06.2006

Winston, W. M., Molodowitch, C., & Hunter, C. P. (2002). Systemic RNAi in C-elegans requires the putative transmembrane protein SID-1. *Science*, *295*(5564), 2456–2459. http://doi.org/Doi 10.1126/Science.1068836

Wragg, R. T., Hapiak, V., Miller, S. B., Harris, G. P., Gray, J., Komuniecki, P. R., & Komuniecki, R. W. (2007). Tyramine and octopamine independently inhibit serotonin-stimulated aversive behaviors in Caenorhabditis elegans through two novel amine receptors. *The Journal of Neuroscience : The Official Journal of the Society for Neuroscience*, *27*(49), 13402–13412. http://doi.org/10.1523/JNEUROSCI.3495-07.2007

Wright, M. H., Heal, W. P., Mann, D. J., & Tate, E. W. (2010). Protein myristoylation in health and disease. *Journal of Chemical Biology*. http://doi.org/10.1007/s12154-009-0032-8

Xu, J., Mashimo, T., & Sudhof, T. C. (2007). Synaptotagmin-1,-2, and-9: Ca2+ sensors for fast release that specify distinct presynaptic properties in subsets of neurons. *Neuron*, *54*(4), 567–581. http://doi.org/Doi 10.1016/J.Neuron.2007.05.004

Xu, W., Tan, L., & Yu, J. T. (2015). The Role of PICALM in Alzheimer's Disease. *Molecular Neurobiology*. http://doi.org/10.1007/s12035-014-8878-3

Yokoi, N., Fukata, Y., Sekiya, A., Murakami, T., Kobayashi, K., & Fukata, M. (2016). Identification of PSD-95 Depalmitoylating Enzymes. *The Journal of Neuroscience : The Official Journal of the Society for Neuroscience*, *36*(24), 6431–44. http://doi.org/10.1523/JNEUROSCI.0419-16.2016

Yuan, P. X., Huang, L. D., Jiang, Y. M., Gutkind, J. S., Manji, H. K., & Chen, G. (2001). The Mood Stabilizer Valproic Acid Activates Mitogen-activated Protein Kinases and Promotes Neurite Growth. *Journal of Biological Chemistry*, *276*(34), 31674–31683. http://doi.org/10.1074/jbc.M104309200

Zhang, B., Kirov, S., & Snoddy, J. (2005). WebGestalt: An integrated system for exploring gene sets in various biological contexts. *Nucleic Acids Research*, *33*(SUPPL. 2). http://doi.org/10.1093/nar/gki475

Zhang, C., Browne, A., Kim, D. Y., & Tanzi, R. E. (2010). Familial Alzheimer's disease mutations in presenilin 1 do not alter levels of the secreted amyloid-beta protein precursor generated by beta-secretase cleavage. *Current Alzheimer Research*, *7*(1), 21–6. Retrieved from http://www.ncbi.nlm.nih.gov/pubmed/20205669

Zhang, C., Wu, B., Beglopoulos, V., Wines-Samuelson, M., Zhang, D. W., Dragatsis, I., … Shen, J. (2009). Presenilins are essential for regulating neurotransmitter release. *Nature*, *460*(7255), 632-U100. http://doi.org/Doi 10.1038/Nature08177

Zhang, F. L., & Casey, P. J. (1996). Protein prenylation: molecular mechanisms and functional consequences. *Annual Review of Biochemistry*, *65*, 241–269. http://doi.org/10.1146/annurev.bi.65.070196.001325

Zhang, L., Guo, X. Q., Chu, J. F., Zhang, X., Yan, Z. R., & Li, Y. Z. (2015). Potential hippocampal genes and pathways involved in Alzheimer's disease: a bioinformatic analysis. *Funpecrp.com.br Genetics and Molecular Research Genet. Mol. Res*, *14*(142), 7218–7232. http://doi.org/10.4238/

Zhang, X. Z., Li, X. J., & Zhang, H. Y. (2010). Valproic acid as a promising agent to combat Alzheimer's disease. *Brain Research Bulletin*. http://doi.org/10.1016/j.brainresbull.2009.09.003

Zhao, Y., Hegde, A. N., & Martin, K. C. (2003). The ubiquitin proteasome system functions as an inhibitory constraint on synaptic strengthening. *Current Biology*, *13*(11), 887–898. http://doi.org/10.1016/S0960-9822(03)00332-4

Zhou, F., Xue, Y., Yao, X., & Xu, Y. (2006). CSS-Palm: Palmitoylation site prediction with a clustering and scoring strategy (CSS). *Bioinformatics*, *22*(7), 894–896. http://doi.org/10.1093/bioinformatics/btl013

Zhu, Y.-C., Li, D., Wang, L., Lu, B., Zheng, J., Zhao, S.-L., … Xiong, Z.-Q. (2013). Palmitoylation-dependent CDKL5-PSD-95 interaction regulates synaptic targeting of CDKL5 and dendritic spine development. *Proceedings of the National Academy of Sciences of the United States of America*, *110*(22), 9118–23. http://doi.org/10.1073/pnas.1300003110